University of Alberta

Velocity variability of Devon Ice Cap tidewater glaciers

by

Bradley D. Danielson

A thesis submitted to the Faculty of Graduate Studies and Research
in partial fulfillment of the requirements for the degree of

Doctor of Philosophy

Department of Earth and Atmospheric Sciences

Spring 2014
Edmonton, Alberta

For my parents and grandparents,
who never discouraged the curious boy who asked too many questions.

And for Loyd,
who never got tired of all my photos and stories of the Arctic.

Abstract

Tidewater outlet glaciers drain approximately 47% of the ~105,000 km^2 covered by ice caps in the Queen Elizabeth Islands of Nunavut, Canada, suggesting that iceberg discharge may be an important process in the mass balance of these ice caps. Seasonal and inter-annual velocity changes of tidewater glaciers may result in the misestimation of annual or multi-year iceberg calving fluxes, if these are estimated on the basis of short-term ice velocity measurements derived from repeat satellite imagery. The aim of this study is to observe and quantify the variability of tidewater glacier velocity at a range of time scales, and to examine the processes driving these variations, with a focus on the impact of temporal and spatial variations in the delivery of surface meltwater to the glacier bed.

High-frequency ice surface velocity measurements were made at four tidewater outlet glaciers of the Devon Ice Cap. Observations over three summers on the Belcher Glacier revealed an annually consistent pattern of ice velocities higher than the annual mean during the 50-60 day long melt season. During this fast-flow period, surface meltwater entered the glacier via moulins and the rapid drainage of supra-glacial melt ponds and water filled crevasses. Rapid drainage events coincided with short-duration ice velocity fluctuations. Inter-annual variations in the magnitude of the enhanced velocity in summer and the velocity variability during the fast-flow period were linked to factors which affect the rate and timing of meltwater delivery to the subglacial drainage system, such as variations in spring snowpack thickness and the degree of variability in late

summer meltwater production. The effective contribution to the annual displacement resulting from enhanced velocities during the summer melt season was only ~5-8% at the glacier terminus, due to the relatively short duration of the fast-flow period.

On the lower 5-8 km of the Belcher Glacier and North Croker Glacier, multi-year changes in annual mean velocity were observed that were not clearly linked to inter-annual variations in the amplitude and/or timing of the seasonal velocity cycle. Because of their flow mechanics, these glaciers may be poised to respond extremely sensitively to even minor long-term changes in driving stress. For such glaciers, it may be extremely difficult to identify any obvious external forcing for relatively large, long-term changes in velocity and rates of iceberg discharge.

Overall, the results provide a demonstration of the seasonal bias that may be expected in different zones of the Devon Ice Cap if annual mean glacier velocities are estimated from velocity measurements made over periods less than a full annual cycle.

Acknowledgements

Many thanks to my supervisor Dr. Martin Sharp, who allowed me the freedom to explore questions that interested me, secured the resources that enabled me to turn those questions into a rewarding field research project, offered advice and direction, and provided me with numerous opportunities for training, travel and collaboration along the way. Thanks for being patient with me – it took me a long time to complete this PhD. thing – but the process has been very worthwhile.

Thanks to all of my field partners: to Dave, for teaching me how to farm a glacier and appreciate Scotch; to Alex for being an Arctic Cowboy; to Jamie for teaching me the finer points of ice cap carpentry; to Ben for his unique singing abilities; to Angus, for whom it was just another day in Scotland; to Gabrielle for never letting her cold feet get the better of her; and to Hannah for making oatmeal an everyday adventure. These and many other people helped make the months spent on Devon Island amongst the richest experiences of my life.

Thanks to all members of the Arctic and Alpine Research Group, whom I came to consider friends more than co-workers. Many good discussions over the cubicle wall were initiated by Faye Wyatt; although we used very different approaches, our research looked at very similar issues. I think we frequently reminded each other that we weren't working in isolation, and were actually making progress.

Dr. David Burgess has been a friend and mentor throughout my research program. I'm particularly grateful for his contribution of field data, and review comments, on Chapter 4. Dr. Shad O'Neel provided enthusiastic discussion and some clever Matlab code that allowed me to pursue my ideas on time-lapse photography in Chapter 2. Dr. Osmar Zaiane introduced me to Computing Science, and a whole new set of tools. Thanks to all members of my examination committee, who volunteered their time and experience to make sure my work was up to standard.

I sincerely appreciate the feedback from Dr. Gordon Hamilton, whose critical appraisal of my writing helped to improve the final draft of this thesis.

I am extremely grateful to the Government and people of Canada for the opportunity to conduct my research, which was funded by the Natural Sciences and Engineering Research Council of Canada, the University of Alberta, the Dr. SM Blair Research Graduate Scholarship, the Steve and Elaine Antoniuk Graduate Scholarship in Arctic Research, the Queen Elizabeth II Graduate Scholarship, the Canadian Circumpolar Institute and the Northern Scientific Training Program. Logistical support for fieldwork was provided by the Polar Continental Shelf Project (all Canadians should be proud of this tiny group of people who do the real heavy lifting of Canadian Arctic Science).

With greath respect, I thank the Nunavut Research Institute and the communities of Grise Fjord and Resolute Bay for permitting me to work on the Devon Ice Cap. I've grown very attached to that place after spending nearly a year of my life there, but it's their backyard.

Thanks to my Mom & Dad, Loyd & Mara, and my Grandparents, for their unending proud support, even though they probably questioned my decision to spend years (and years) studying glaciers.

Finally, thanks to my wife Brita, not only for being my 'sugar-momma', but also for her ongoing encouragement and moral support throughout this project (especially when I got to the "I hate this" phase of thesis writing). True story: it was Brita who found Martin's UofA web profile and said "Maybe you should go talk to this guy. He does some interesting research." Without her, I would never have seriously considered embarking on a PhD. – which has been a stranger and more interesting adventure than I ever expected.

Table of Contents

List of Tables

List of Figures and Illustrations

Chapter One: Introduction

1.1 Purpose

The central aim of this thesis is to observe and quantify the time-varying nature of tidewater glacier velocity at a range of scales (hourly to daily, seasonal, and inter-annual), and to examine the processes driving these variations, with a particular focus on the impact of temporal and spatial variations in the delivery of meltwater from the glacier surface to the glacier bed Velocity variability has direct bearing on efforts to both quantify rates of ice mass loss due to iceberg calving, and develop a capability to predict future changes in glacier dynamics. Several recent efforts to quantify the mass balance of Arctic glaciers and ice caps (GIC) (Burgess and others, 2005; Williamson and others, 2008; Mair and others, 2009; Moholdt and others, 2012; Van Wychen and others, 2012) have stressed that their estimates of iceberg calving fluxes are uncertain because of the unquantified influence of seasonal and inter-annual velocity changes. This thesis uses detailed studies of velocity variations on a small number of tidewater outlet glaciers of the Devon Ice Cap in the Canadian Arctic Archipelago to determine whether short-term ice displacement measurements, frequently extrapolated to annual velocities for the purpose of calculating calving fluxes, over or under-estimate true annual velocity if they do not account for seasonal meltwater-driven velocity variations, and to determine whether inter-annual velocity variations are likely to affect multi-year calving flux estimates.

1.2 Motivation

Flooding due to Sea Level Rise (SLR) is one of the most significant threats to human life and infrastructure in the world's densely populated, low-lying coastal regions. Approximately 200 million people and one trillion dollars of assets are located in areas less than 1m above current mean sea level (Stern, 2006; Milne and others, 2009). The mean rate of global SLR over the 20th century was 1.7 mm a^{-1}, but this increased in the late-20th to early-21st century, reaching

3.2 mm a^{-1} for the 1993-2010 period (Nerem and others, 2010; Nicholls and Cazenave, 2010; Alexander, 2013). Forecasting how much SLR should be anticipated over the next 50 to 100 years is of critical importance for the development of risk mitigation strategies. Unfortunately, making such predictions is extremely complex (Milne and others, 2009), and uncertainties in the physical processes causing SLR mean that the best estimates of SLR by the year 2100 have an uncertainty range of nearly ±30% (Alexander, 2013). The largest source of SLR is currently the transfer of meltwater from land-based ice to the oceans. According to the Fifth Assessment Report of the Intergovernmental Panel on Climate Change (IPCC AR5), the primary contributors to SLR during the 1993–2010 period were: the thermal expansion of ocean water (~1.1 mm a^{-1}), mass loss from GIC (~0.76 mm a^{-1}), mass loss from the Greenland ice sheet (~0.33mm a^{-1}), mass loss from the Antarctic ice sheet (~0.27 mm a^{-1}), and changes in land water storage (~0.38 mm a^{-1}).

The term GIC encompasses all the mountain glaciers, ice fields, and ice caps outside of the polar ice sheets. The total area of GIC is 0.729 Mm^2, and the combined volume is equivalent to 0.41 m SLR (Gardner and others, 2013; Radic and others, 2013), while the Greenland ice sheet covers 1.711 Mm^2 (volume equivalent to 7.36 m SLR) (Kargel and others, 2012; Bamber and others, 2013; Gardner and others, 2013) and the Antarctic ice sheets cover 12.295 Mm^2 (volume equivalent to 58m SLR) (Fretwell and others, 2013). The combined GIC are orders of magnitude smaller than the Greenland and Antarctic ice sheets, yet are far more sensitive to atmospheric changes than the large ice sheets because of their generally lower mean elevations. Under contemporary warming trends they are undergoing rapid mass loss (ACIA, 2013; Gardner and others, 2013; Radic and others, 2013), and are likely to dominate SLR through the 21st century (Meier and others, 2007).

Until very recently, the global inventory of GIC was incomplete, leading to uncertainty and inconsistencies in estimates of their mass change and SLR contribution (Pfeffer, 2011; Kerr, 2013). Because it was becoming clear that

mass loss from GIC was having a strong impact on SLR, a significant amount of effort has recently been invested in establishing a global database of glacier outlines, and area/volume estimates (Arendt and others, 2012).

The GIC of the northern and southern Canadian Arctic Archipelago, two of the 19 glaciated regions identified in the Randolph Glacier Inventory (Arendt and others, 2012), together form the largest assemblage of land ice (~145,800 km^2) outside the polar ice sheets. The larger northern portion (~104,900 km^2), is composed primarily of the large ice caps and ice fields of the Queen Elizabeth Islands. Approximately 47% of this area is drained by tidewater outlet glaciers (Gardner and others, 2013), which implies that the mechanical discharge of icebergs to the ocean is potentially an important term in the mass balance of these ice caps.

Glacier mass balance is the total annual change in ice mass resulting from the climatic mass balance (CMB; the difference between snow accumulation and mass loss by sublimation, evaporation and meltwater runoff), the discharge of icebergs, and subaqueous melting of the termini of tidewater glaciers. The mass balance of GIC in the Queen Elizabeth Islands has undergone dramatic changes over the past ~50 years. Between 1960 and ~2000, the CMB was only slightly negative but trending towards more negative values by the end of the period (Koerner, 2005). During this period, the mass loss due to iceberg discharge was of a similar magnitude to the net mass balance (Lenaerts and others, 2013). A strong warming trend began in the early 2000s as a result of changing summer atmospheric circulation patterns which increased advection of warm air from the North Atlantic towards the Queen Elizabeth Islands. Relative to 2000-2004, the 2005-2009 period saw summer ice surface temperatures increase by 0.8 to 2.2^{o}C and melt season durations increase by 4.7 to 11.9 d a^{-1} (Sharp and others, 2011). The ice masses in this region demonstrated an extreme sensitivity to these changes, with modelled net mass loss increasing from 7±18 Gt a^{-1} (2004 to 2006), to 61±18 Gt a^{-1} (2007 to 2009) (Gardner and others, 2011). Calving fluxes were estimated to be a constant 4.6±1.9 Gt a^{-1} over the 2004 to 2009 period, comprising

a small contribution of the overall mass balance relative to meltwater runoff (Gardner and others, 2011).

Gardner and others (2011) provide the most comprehensive assessment to date of the total mass balance of the GIC of the Queen Elizabeth Islands, but they were forced to estimate rates of iceberg discharge (with a large uncertainty) and to assume that this rate was constant throughout their study period due to the infrequency and scarcity of iceberg calving flux measurements in the region. Unfortunately, this assumption could potentially lead to the mis-estimation of iceberg discharge, which can change over time. For example, at the Academy of Sciences Ice Cap (5570 km^2) in the Russian High Arctic, rates of net mass loss varied from ~0.6 Gt a^{-1} in 1995 to ~3.0 Gt a^{-1} (2000-2002) to ~1.4 Gt a^{-1} (2003-2009), but the CMB was estimated to be near zero over the entire 1988 to 2009 period. These changes in the net mass loss were thus driven almost exclusively by changes in the dynamics of just a few of the major tidewater outlet glaciers (Moholdt and others, 2012). The magnitudes of these mass changes are small, but this demonstrates that multi-year velocity changes of tidewater outlet glaciers can have an impact on GIC mass loss rates, and that iceberg flux cannot be assumed to be constant when assessing regional mass balance. Furthermore, this assumption does not allow for the possibility that rates of dynamic ice discharge and iceberg calving may respond to the same climatic factors that are responsible for the current extreme negative trends in CMB. More refined regional estimates of iceberg discharge can be made by comprehensively measuring iceberg calving rates for all tidewater glaciers in the region and repeating the procedure at annual or multi-year intervals to identify mass flux changes related to changes in glacier dynamics.

Mass loss due to iceberg calving is the difference between the flux of ice through a flux gate defined near the glacier terminus, and any change in ice mass beyond the flux gate that results from an advance or retreat of the glacier terminus position. The volume of ice passing through the flux gate is the product of the depth-averaged glacier flow velocity and the cross-sectional area of the flux gate.

Ideally, the cross-sectional area of the flux gate is determined from ice thickness and surface elevation measurements made by radio echo sounding. Where such measurements are missing or incomplete, the cross-sectional area must be estimated using an assumed cross-sectional geometry, such as a parabolic cross section (Williamson and others, 2008), that reasonably represents the geometry of the glacial fjord. Recent airborne radar measurement campaigns such as NASA's Operation Icebridge and the Scott Polar Research Institute's Arctic campaign (Dowdeswell and others, 2004) have provided cross-terminus ice thickness measurements that were previously lacking for many major Arctic tidewater glaciers. However, the determination of ice flux through the terminus is also dependent on measurements of the ice velocity across the terminus. Surface velocity measurements of tidewater glaciers have been made on an ice cap by ice cap basis over different time periods (Burgess and others, 2005; Williamson and others, 2008; Mair and others, 2009; Van Wychen and others, 2012) but estimates for the entire Canadian Arctic have yet to be published (Van Wychen and others, submitted manuscript), and even then these are not measurements of mean annual velocities.

The most effective way to determine surface velocity with the spatial coverage and resolution required to estimate the terminus flux for many glaciers in a (large) region is to employ satellite remote sensing techniques such as synthetic aperture radar interferometry, speckle-tracking, or optical image correlation. These methods provide the ice surface displacement between two sequential images, which is commonly converted to an annually averaged velocity. Users of optical imagery can utilize carefully selected images that were collected close to a full year apart to determine true annual displacements (Wyatt, 2013), but cloud cover or unfavourable illumination may limit the number of suitable images. Radar imagery is unaffected by cloud cover or variations in natural lighting, potentially yielding a larger number of usable image pairs, but interferometric or speckle-tracking techniques have their own limitations. Significant between-image changes in the viewing geometry of the satellites, or

large changes to the surface caused by melt, heavy snowfall, drifting, or ice deformation, may result in the loss of image coherence and a failure to determine surface displacements. For this reason, image-pairs must be collected over a short time period (on the order of days to weeks), and images collected during the winter or early spring seem to have the best chances of achieving coherence (Short and Gray, 2005; Van Wychen, 2010; Van Wychen and others, 2012). However, an unquantified seasonal bias may be introduced when these short-interval winter displacement measurements are extrapolated to produce annual ice velocity estimates, because strong seasonal-scale velocity variations can occur on these glaciers.

Tidewater glaciers are, by definition, in contact with the ocean, and changes in ocean temperature, ocean currents, sea ice concentration and thickness, and the stability of floating ice shelves or glacier tongues are all known to affect their stability and behaviour (Carr and others, 2013). Observations from Greenland have shown that the retreat and acceleration of large marine-terminating glaciers beginning in the 1990s (including Jakobshavn Isbrae and Helheim Glacier) were preceded by oceanic warming along the Greenland coasts (Holland and others, 2008; Bevan and others, 2012; Rignot and others, 2012; Carr 2013). Several studies have shown that sub-surface currents brought warm Atlantic water into some of the deepest fjords occupied by large, thick glaciers, and the resulting submarine melting caused undercutting of the terminus ice cliff, and/or the thinning and destabilization of floating glacier tongues (Straneo and others, 2010, 2011; Murray and others, 2010; Motyka and others, 2011). It has been argued that this submarine thinning, in conjunction with surface thinning due to concurrent warm air temperatures, initiated a cycle of calving front retreat, decrease in resistive forces, and acceleration of the flow of these glaciers (Howat and others, 2005, 2008; Luckman and others 2006; Nick and others, 2009).

Two notable differences between the Greenland outlet glaciers and the ice cap outlet glaciers of the CAA may suggest why the CAA glaciers have not, so far, demonstrated similar oceanorgraphically-forced dynamic changes. The first

is that the eastern and western coasts of Greenland have a maritime climate, being bordered by the open waters of the North Atlantic and Baffin Bay, whereas the CAA has a more continental climate due to the persistence of sea ice cover through much of the year (Braithwaite, 2005; Koerner, 2005). The relative proximity to these open water moisture sources means that the glaciers of coastal Greenland receive much higher rates of precipitation, and consequently have generally higher rates of mass turnover and glacier flow than the CAA glaciers. The second major difference is that most of the Greenland tidewater glaciers that have undergone recent dynamic changes lie in deep fjords (600-900m) which allow sub-surface currents below 250m to bring warm water into contact with the glacier termini (Rignot and others, 2012). In contrast, the small amount of bathymetric mapping available in the CAA shows that the straights between islands and the fjords leading to tidewater glaciers are generally less deep (~100-300m) (Bell and others, 2006; Jakobsson and others, 2008), and it is less likely that warmer North Atlantic currents infiltrate these fjords. Eventually, the warm waters that first affected the glaciers of southeast and southwest Greenland may spread from northern Baffin Bay into the Canadian Arctic, but there is no evidence that this has yet occurred. Measurements of sea water temperature, salinity, or the structure of deepwater currents throughout the CAA are still rare, and the effects on the glaciers in this region are largely unknown. Velocity variations that have been observed on CAA outlet glaciers have often been attributed to surge events or seasonal variations driven by meltwater lubrication (Short and Gray, 2005; Williamson and others, 2008; Van Wychen and others, 2012).

1.3 Hydrologic controls on glacier velocity variability

The goals of this thesis are to determine the magnitude of velocity variations on High Arctic tidewater glaciers at a range of time scales, and to explore the relationships between these velocity variations and potential hydrologic drivers. We focus on the potential hydrologic processes as opposed to

other potential drivers of flow change, due to an interest in determining whether the recent changes in summer synoptic weather patterns (Sharp and others, 2011; Gascon and others, 2013) and related increases in summer meltwater generation, might have an impact on glacier dynamics. It is important to consider velocity variations at different time-scales because:

1. Seasonal velocity variability makes it difficult to determine the annual mean velocity from short-term measurements.
2. Year-to-year changes in the magnitude of seasonal velocity fluctuations may drive changes in the annual mean velocity, making it difficult to estimate an appropriate multi-year mean velocity from a single year of measurements.

Glacier surface velocity is the sum of internal ice deformation and basal motion. Rates of internal deformation will change whenever the driving stress, forces resisting flow, or ice viscosity change (Paterson, 1994), but these changes usually occur over relatively long time scales. More rapid changes in velocity are possible when the glacier flows, at least in part, by basal sliding or the deformation of subglacial sediments. Water under high pressure at the glacier bed can reduce the friction between the ice and the underlying bedrock by forming water-filled cavities that lead to ice-bed separation (Iken, 1981), or by reducing the strength of subglacial sediments and promoting deformation of the bed itself (Paterson, 1994). Either of these effects can lead to higher glacier velocities. A reduction in water pressure can have the opposite effect, leading to reduced flow velocity.

The liquid water required to drive variations in basal motion may be sourced from the subglacial environment by geothermal or frictional heating, so long as the ice in contact with the bed is at the pressure melting point. However, much higher volumes of water can be delivered to the bed from the glacier surface during the summer melt season (Paterson, 1994). Conduits linking the supra-glacial and subglacial drainage systems may exist in the form of moulins (Iken, 1972), and new pathways may form by the downwards propagation of water-filled

crevasses by hydrofracture (Boon and Sharp, 2003), which occurs when the weight of water in a crevasse causes the tip of the fracture to propagate through the full thickness of the ice (Van der Veen, 2007). The initiation of this mechanism relies on either the availability of large volumes of water overlying a pre-existing fracture, or a crevasse filling rate of ~1 m hr^{-1} (van der Veen, 2007). Observations of the drainage of supra-glacial lakes via fractures in their beds (Boon and Sharp, 2003; Das and others, 2008; Doyle and others, 2013), and of supra-glacial meltwater streams sinking within crevasse fields (Skidmore and Sharp, 1999; Colgan and others, 2011) indicate that this is likely a widespread phenomenon.

Rapid velocity variations associated with the drainage of supra-glacial meltwater into glaciers are well documented (Willis, 1995). A rapid increase in surface velocity early in the melt season, sometimes referred to as a 'spring event', which follows the onset of meltwater drainage into englacial conduits, has been interpreted as the result of meltwater reaching the glacier bed, raising basal water pressures in an inefficient subglacial drainage system and reducing basal friction so that the rate of basal sliding increases (Iken and others, 1983; Röthlisberger and Lang, 1987). The spring event is often defined by a spike in surface velocity lasting a few days, and it is typically followed by a period of variable but elevated velocity (relative to the lower, steady winter velocity) that declines to lower over-winter values towards the end of the melt season. Some variant of this pattern of velocity variability has been observed at temperate valley glaciers (Iken and Bindschadler, 1986; Mair and others, 2002; Bartholomaus and others, 2008), High Arctic polythermal glaciers (Iken, 1972; Copland and others, 2003), and at the margins of the Greenland ice sheet (Zwally and others, 2002; Bartholomew and others, 2010; Bartholomew and others, 2011b; Hoffman and others, 2011). The examples cited above all provide coincident observations of surface meltwater production, meltwater drainage, and glacier surface velocity, which reveal clear links between velocity increases and drainage events involving large volumes of water. These observations confirm that, at short time scales, variations in surface

meltwater availability, and even specific drainage events such as the emptying of supra-glacial lakes, can result in variations in glacier velocity.

One topic of recent investigation has been to determine why glacier velocity becomes gradually less responsive to sustained meltwater inputs over the course of a melt season. Some early studies argued that future climate warming could result in more widespread or greater seasonal acceleration of ice flow due to basal sliding (Zwally and others, 2002; Parizek and Alley, 2004) if surface melting directly (and proportionately) impacted mean annual ice velocity. However, the subglacial drainage system may react to continuous inputs of meltwater by evolving into an increasingly efficient system that can evacuate large volumes of meltwater, leading to a progressive reduction of basal water pressure over time (Müller and Iken, 1973; Fountain and Walder, 1998; Schoof, 2010). This interpretation has been supported by observations of ice velocity, melt rates, and drainage system evolution along land-terminating sections of the GrIS (Bartholomew and others, 2010; Bartholomew and others, 2011a; Hoffman and others, 2011; Sundal and others, 2011; Cowton and others, 2013), and by many previous studies of alpine and Arctic valley glaciers (i.e. Fountain and Walder, 1998). An alternative hypothesis suggests that high variability in both the rate and total volume of meltwater delivery can force a subglacial drainage system into a constant state of adaptation, leading to effective pressure changes that facilitate accelerated sliding (Bartholomaus and others, 2008; Schoof, 2010). Some recent observations from Greenland suggest that this hypothesis may be correct (Hoffman and others, 2011), but multi-year observations that could demonstrate whether inter-annual differences in seasonal velocity variations might be the result of differences in summer melt conditions, drainage system development, or the timing and volume of meltwater drainage throughout the summer are lacking.

Few field investigations of High Arctic tidewater outlet glaciers have addressed the issue of meltwater driven velocity variations and their impact on

annual ice displacement. At Hansbreen (southern Spitsbergen, Svalbard), two velocity events in 1999, each lasting 1-2 days, were associated with periods of enhanced surface melt or rainfall, but Hansbreen's velocity was relatively constant at seasonal to annual timescales (Vieli and others, 2004). GPS measurements over two years along the centerlines of two tidewater outlets of the Austfonna ice cap showed seasonal velocity patterns that generally corresponded to the seasonal melt cycle (Dunse, 2012), which suggested that the seasonal velocity changes were impacted by variations in surface meltwater availability. However, it was difficult to determine how sensitive seasonal and inter-annual velocity variations were to differences in the time of onset, intensity, and duration of the summer melt season.

This leads to some of the key questions investigated in this thesis:

1. Do individual supra-glacial drainage events have a measurable impact on tidewater glacier flow velocity? How do these events contribute to the overall pattern of seasonal velocity variability, and do they have a quantifiable impact on total seasonal/annual displacement?
2. Is there a pattern of seasonal velocity variability that is consistent over multiple years? Is there interannual variability in this pattern that can be explained by differences in melt season characteristics, the seasonal evolution of the surface drainage system, or the occurrence of distinct meltwater drainage events? How does the glacier velocity response to meltwater inputs evolve over a melt season?
3. Do hydrologically-driven seasonal variations in velocity significantly affect the estimation of annual mean velocity from short-term measurements?

1.4 Field Program

A field program was devised to address the questions identified above. The Devon Ice Cap was chosen as a study site due, in part, to the 50 year history of glaciological work (see (Boon and others, 2010)), but also due to previous observations of ice dynamics on some of the tidewater outlet glaciers, which

invited further investigation into the role of time-varying dynamics in glacier mass balance.

With an area of ~14,000 km^2, the Devon Ice Cap is among the largest ice caps in the Canadian Arctic (Burgess and Sharp, 2004). It covers the eastern portion of Devon Island (part of the Queen Elizabeth Islands archipelago), and has a relatively simple single-dome shape that reaches an elevation of ~1900 m above sea level at its centre. Tidewater outlet glaciers drain from the interior of the ice cap to its northern, eastern, and southern margins. Between 1960 and 1999, iceberg calving from these glaciers is estimated to have accounted for ~30% of the total mass loss from the ice cap, with the Belcher Glacier alone responsible for ~50% of the total iceberg discharge (Burgess and others, 2005). Burgess and others, (2005) used speckle-tracking of satellite radar data to determine ice surface velocities of 180-300 (±10%) m a^{-1} in the terminus region of the Belcher Glacier, but recommended future seasonal measurements of glacier surface velocity and the inland extent of seasonally enhanced glacier flow to better constrain their estimates of iceberg calving rates.

Belcher Glacier was chosen as a target for further study because it appeared to be the fastest flowing and most significant iceberg producing glacier draining the Devon Ice Cap. It seems to be common that a single glacier, occupying a large drainage basin, dominates the iceberg calving losses from ice caps in the Queen Elizabeth Islands (Short and Gray, 2005). Approximately 80% of the iceberg mass calved from the Prince of Wales Icefield is from the Trinity-Wykeham Glacier (Mair and others, 2009), while ~54% of the calving from the Agassiz Ice Cap occurs via the Eugenie Glacier (Williamson and others, 2008). The Mittie Glacier (Manson Icefield), Otto Glacier (Northern Ellesmere Icefield) and Iceberg Glacier (Müller Ice Cap) are three large surge-type glaciers that are very likely the dominant sources of calving from their respective ice caps (Short and Gray, 2005). The potential impact of calving from these few glaciers on the mass balance of their parent ice caps suggests that it makes sense to focus detailed monitoring efforts on them.

In 2007 we therefore initiated a program to determine glacier surface velocities on the Belcher Glacier using high-frequency GPS measurements. Additional instrumentation, including time-lapse cameras and meteorological sensors, was added to monitor changes in environmental conditions and glacier surface hydrological processes that might influence glacier flow. These observations were made as part of the Canadian contribution to the GLACIODYN (IPY) project, an extensive field, remote sensing, and modelling study designed to understand the links between climate, hydrology, and glacier flow dynamics. Later, the GPS measurement program was extended to include three other outlet glaciers in different quadrants of the Devon Ice Cap, to determine whether the observations of Belcher Glacier were representative of the dynamics of other outlet glaciers in the region.

1.4.1 Core Observational Dataset

The primary accomplishment of this project was the detailed monitoring of glacier flow in regions where such measurements are scarce and difficult to acquire. Similar field measurements have been collected before (or were collected concurrently with ours) at a variety of locations, including: Greenland (Zwally and others, 2002; Nettles and others, 2008; Bartholomew and others, 2011b; Sole and others, 2011), Antarctica (Murray and others, 2007; Scott and others, 2009), Svalbard (Vieli and others, 2004; Dunse, 2012), and Alaska (Bartholomaus and others, 2008), among others. However, these are the first multi-year GPS measurements of displacement from tidewater outlet glaciers in the Canadian Arctic. They provide a unique look at the dynamic processes occurring in this region.

The GPS-based methods we used to derive ice velocity estimates provide high accuracy and high-temporal resolution, but they also have some drawbacks. Each GPS instrument repeatedly measures the position of a single point, from which we can derive ice displacement over time. To acquire information about the spatial variation in ice flow, multiple systems must be deployed across a glacier.

The GPS receivers and supporting power supply systems are expensive, and despite their durable design, occasionally fail in the harsh environmental conditions of the High Arctic. The logistics required for installing and servicing these systems are considerable, and the measurements are not sustainable in the long-term without a large fieldwork budget. Therefore the objective in deploying these systems was to collect as much high-quality data as possible over 3-5 years, and to use the knowledge gained to assist in the analysis and interpretation of results from ongoing remote sensing-based programs for determining glacier velocity.

1.5 Progression of Chapters

The chapters of this thesis follow a progression towards larger temporal and spatial scales, in terms of the processes examined. In Chapter 2, which has been published in the Journal of Glaciology, we focus on specific regions of the Belcher Glacier to study the impact of supra-glacial lake drainage events on short-term ice velocity changes over a period during the 2009 summer. We use time-lapse photography to monitor the development and drainage of a set of supra-glacial lakes and water-filled crevasses, and develop a method to estimate both the area and the rate of area change of these lakes. This allows us to characterize modes of lake drainage. By examining ice velocity derived from GPS measurements during the same time period, we are able to determine which lake drainage events had the most significant short-term and seasonal impacts on the rate of glacier flow. In Chapter 3, we examine seasonal and inter-annual changes in flow of the glacier over three years. We explore how inter-annual variations in factors such as spring snowpack, supra-glacial drainage development, melt intensity, and total ablation can impact the characteristics of the seasonally enhanced flow observed in the upper, mid, and lower regions of the glacier. Our observations suggest that this glacier behaves as a bi-modal system: the mid- and upper-glacier regions behave like a typical alpine glacier system, while the behaviour of the lower glacier is heavily influenced by its marine-based setting.

These observations also indicate that the terminus region was undergoing a multi-year increase in velocity, while the mid- and upper-glacier regions were not. We suggest four possible reasons for the differences in dynamics between these regions, including differences in the bed geometry, bed composition, distribution of sink-points for supra-glacial meltwater, and the impact of lateral (valley-wall) friction on glacier flow.

Although the first two chapters explore the varying dynamics of the Belcher Glacier on multiple time scales, they left open the question of whether the behaviour observed is characteristic of other outlet glaciers of the Devon Ice Cap. In Chapter 4, we examine GPS records from the Sverdrup, North Croker, and Southeast Glaciers, and compare these to our multi-year measurements from Belcher Glacier to determine whether similar processes influence seasonal and annual scale velocity variations at all four of these large, rapidly flowing, tidewater outlet glaciers. The flow regimes model proposed by Burgess and others (2005) provides a useful framework for making this comparison. This model allows mapping of regions where basal sliding probably contributes to glacier flow, and thus the identification of areas of the ice cap that might be subject to hydrologically driven changes in flow dynamics. We find that the different flow regimes were characterised by different degrees of annual, seasonal, and shorter-term flow variability. In this respect, our findings corroborate those of recent work by Wyatt (2013) that demonstrated linkages between the magnitude of inter-annual velocity variability and the structure of supra-glacial drainage systems in different parts of Devon Ice Cap. A key result from this study is the approximate quantification of the seasonal bias that may be expected if annual mean flow velocities are estimated from short-term displacement measurements in different zones of the Devon Ice Cap.

Chapter 5 provides a summary of our findings, proposes answers to the questions we set out to solve, and suggests some directions for further work on this topic.

1.6 Bibliography

ACIA, 2013. Arctic Climate Impact Assessment Chapter 6: Cryosphere and Hydrology (pp. 183-242). Cambridge University Press.

Alexander, L. S. A., N.L. Bindoff, F.-M. Bréon, J. Church, U. Cubasch, S. Emori, P. Forster, P. Friedlingstein, N. Gillett, Jonathan Gregory, D. Hartmann, E. Jansen, B. Kirtman, R. Knutti, K.K. Kanikicharla, P. Lemke, J. Marotzke, V. Masson-Delmotte, G. Meehl, I. Mokhov, S. Piao, G.-K. Plattner, Q.Dahe, V. Ramaswamy, D. Randall, M. Rhein, M. Rojas, C. Sabine, D. Shindell, T. F. Stocker, L. Talley, D. Vaughan, S.-P. Xie 2013. Working Group I Contribution to the IPCC Fifth Assessment Report Climate Change 2013: The Physical Science Basis Summary for Policymakers.

Arendt, A., T Bolch, JG Cogley, A Gardner, JO Hagen, R Hock, G Kaser, WT Pfeffer, G Moholdt, F Paul, V Radić, L Andreassen, S Bajracharya, M Beedle, E Berthier, R Bhambri, A Bliss, I Brown, E Burgess, D Burgess, F Cawkwell, T Chinn, L Copland, B Davies, E Dolgova, K Filbert, R Forester, A Fountain, H Frey, B Giffen, N Glasser, S Gurney, W Hagg, D Hall, UK Haritashya, G Hartmann, C Helm, S Herreid, I Howat, G Kapustin, T Khromova, M Kienholz, M Koenig, J Kohler, D Kriegel, S Kutuzov, I Lavrentiev, R LeBris, J Lund, W Manley, C Mayer, X Li, B Menounos, A Mercer, N Moelg, P Mool, G Nosenko, A Negrete, C Nuth, R Pettersson, A Racoviteanu, R Ranzi, P Rastner, F Rau, J Rich, H Rott, C Schneider, Y Seliverstov, M Sharp, O Sigurðsson, C Stokes, R Wheate, S Winsvold, G Wolken, F Wyatt, N Zheltyhina 2012. Randolph Glacier Inventory [v2.0]: A Dataset of Global Glacier Outlines. *Global Land Ice Measurements from Space, Boulder, CO, USA* **Digital Media**.

Bamber, J. L., J. A. Griggs, R. T. W. L. Hurkmans, J. A. Dowdeswell, S. P. Gogineni, I. Howat, J. Mouginot, J. Paden, S. Palmer, E. Rignot and D. Steinhage 2013. A new bed elevation dataset for Greenland. *The Cryosphere* **7**(2), 499-510.

Bartholomaus, T. C., R. S. Anderson and S. P. Anderson 2008. Response of glacier basal motion to transient water storage. *Nature Geoscience* **Vol 1**(Number 1), 33-37.

Bartholomew, I., P. Nienow, D. Mair, A. Hubbard, M. A. King and A. Sole 2010. Seasonal evolution of subglacial drainage and acceleration in a Greenland outlet glacier. *Nature Geoscience* **3**(6), 408-411.

Bartholomew, I., P. Nienow, A. Sole, D. Mair, T. Cowton, S. Palmer and J. Wadham 2011a. Supraglacial forcing of subglacial drainage in the ablation zone of the Greenland ice sheet. *Geophysical Research Letters* **38**(8), L08502.

Bartholomew, I. D., P. Nienow, A. Sole, D. Mair, T. Cowton, M. A. King and S. Palmer 2011b. Seasonal variations in Greenland Ice Sheet motion: Inland extent and behaviour at higher elevations. *Earth and Planetary Science Letters* **307**(3-4), 271-278.

Bevan, S. L., A. J. Luckman and T. Murray 2012. Glacier dynamics over the last quarter of a century at Helheim, Kangerdlugssuaq and 14 other major Greenland outlet glaciers. *The Cryosphere* **6**(5), 923-937.

Boon, S., D. Burgess, R. M. Koerner and M. J. Sharp 2010. Forty-seven years of research on the Devon Island Ice Cap, Arctic Canada. *Arctic* **63**(1), 13-29.

Boon, S. and M. Sharp 2003. The role of hydrologically-driven ice fracture in drainage system evolution on an Arctic glacier. *Geophysical Research Letters* **30**(18).

Braithwaite, R. J. 2005. Mass-balance characteristics of arctic glaciers. *Annals of Glaciology* **42**(1), 225-229.

Burgess, D. O. and M. J. Sharp 2004. Recent changes in areal extent of the Devon Ice Cap, Nunavut, Canada. *Arctic, Antarctic, and Alpine Research* **36**(2), 261-271.

Burgess, D. O., M. J. Sharp, D. W. F. Mair, J. A. Dowdeswell and T. J. Benham 2005. Flow dynamics and iceberg calving rates of Devon Ice Cap, Nunavut, Canada. *Journal of Glaciology* **51**(173), 219-230.

Carr, J. R., C. R. Stokes and A. Vieli 2013. Recent progress in understanding marine-terminating Arctic outlet glacier response to climatic and oceanic forcing: Twenty years of rapid change. *Progress in Physical Geography*, 1-32.

Colgan, W., K. Steffen, W. S. McLamb, W. Abdalati, H. Rajaram, R. Motyka, T. Phillips and R. Anderson 2011. An increase in crevasse extent, West Greenland: Hydrologic implications. *Geophysical Research Letters* **38**(18).

Copland, L., M. J. Sharp and P. W. Nienow 2003. Links between short-term velocity variations and the subglacial hydrology of a predominantly cold polythermal glacier. *Journal of Glaciology* **49**(166), 337-348.

Cowton, T., P. Nienow, A. Sole, J. Wadham, G. Lis, I. Bartholomew, D. Mair and D. Chandler 2013. Evolution of drainage system morphology at a land-terminating Greenlandic outlet glacier. *Journal of Geophysical Research: Earth Surface* **118**, 1-13.

Das, S. B., I. Joughin, M. D. Behn, I. M. Howat, M. A. King, D. Lizarralde and M. P. Bhatia 2008. Fracture propagation to the base of the Greenland Ice Sheet during supraglacial lake drainage. *Science* **320**(5877), 778-781.

Dowdeswell, J. A., T. J. Benham, M. R. Gorman, D. Burgess and M. J. Sharp 2004. Form and flow of the Devon Island Ice Cap, Canadian Arctic. *Journal of Geophysical Research-Earth Surface* **109**(F2).

Doyle, S. H., A. L. Hubbard, C. F. Dow, G. A. Jones, A. Fitzpatrick, A. Gusmeroli, B. Kulessa, K. Lindback, R. Pettersson and J. E. Box 2013. Ice tectonic deformation during the rapid in situ drainage of a supraglacial lake on the Greenland Ice Sheet. *The Cryosphere* **7**(1), 129-140.

Dunse, T., Schuler, T. V., Hagen, J. O., and Reijmer, C. H. 2012. Seasonal speed-up of two outlet glaciers of Austfonna, Svalbard, inferred from continuous GPS measurements. *The Cryosphere* **6**, 453-466.

Fountain, A. G. and J. S. Walder 1998. Water flow through temperate glaciers. *Reviews of Geophysics* **36**(3), 299-328.

Fretwell, P., H. D. Pritchard, D. G. Vaughan, J. L. Bamber, N. E. Barrand, R. Bell, C. Bianchi, R. G. Bingham, D. D. Blankenship, G. Casassa, G. Catania, D. Callens, H. Conway, A. J. Cook, H. F. J. Corr, D. Damaske, V. Damm, F. Ferraccioli, R. Forsberg, S. Fujita, Y. Gim, P. Gogineni, J. A. Griggs, R. C. A. Hindmarsh, P. Holmlund, J. W. Holt, R. W. Jacobel, A. Jenkins, W. Jokat, T. Jordan, E. C. King, J. Kohler, W. Krabill, M. Riger-Kusk, K. A. Langley, G. Leitchenkov, C. Leuschen, B. P. Luyendyk, K. Matsuoka, J. Mouginot, F. O. Nitsche, Y. Nogi, O. A. Nost, S. V. Popov, E. Rignot, D. M. Rippin, A. Rivera, J. Roberts, N. Ross, M. J. Siegert, A. M. Smith, D. Steinhage, M. Studinger, B. Sun, B. K. Tinto, B. C. Welch, D. Wilson, D. A. Young, C. Xiangbin and A. Zirizzotti 2013. Bedmap2: improved ice bed, surface and thickness datasets for Antarctica. *The Cryosphere* **7**(1), 375-393.

Gardner, A. S., G. Moholdt, J. G. Cogley, B. Wouters, A. A. Arendt, J. Wahr, E. Berthier, R. Hock, W. T. Pfeffer, G. Kaser, S. R. M. Ligtenberg, T. Bolch, M. J. Sharp, J. O. Hagen, M. R. van den Broeke and F. Paul 2013. A

reconciled estimate of glacier contributions to Sea Level Rise: 2003 to 2009. *Science* **340**(6134), 852-857.

Gardner, A. S., G. Moholdt, B. Wouters, G. J. Wolken, D. O. Burgess, M. J. Sharp, J. G. Cogley, C. Braun and C. Labine 2011. Sharply increased mass loss from glaciers and ice caps in the Canadian Arctic Archipelago. *Nature* **473**(7347), 357-360.

Gascon, G., M. Sharp and A. Bush 2013. Changes in melt season characteristics on Devon Ice Cap, Canada, and their association with the Arctic atmospheric circulation. *Annals of Glaciology* **54**(63), 101-110.

Hoffman, M. J., G. A. Catania, T. A. Neumann, L. C. Andrews and J. A. Rumrill 2011. Links between acceleration, melting, and supraglacial lake drainage of the western Greenland Ice Sheet. *J. Geophysical Research* **116**(F4), F04035.

Holland, D. M., R. H. Thomas, B. de Young, M. H. Ribergaard and B. Lyberth 2008. Acceleration of Jakobshavn Isbrae triggered by warm subsurface ocean waters. *Nature Geoscience* **1**(10), 659-664.

Howat, I. M., I. Joughin, M. Fahnestock, B. E. Smith and T. A. Scambos 2008. Synchronous retreat and acceleration of southeast Greenland outlet glaciers 2000-2006: ice dynamics and coupling to climate. *Journal of Glaciology* **54**(187), 646-660.

Howat, I. M., I. Joughin, S. Tulaczyk and S. Gogineni 2005. Rapid retreat and acceleration of Helheim Glacier, east Greenland. *Geophysical Research Letters* **32**(22).

Iken, A. 1972. Measurements of water pressure in moulins as part of a movement study of the White Glacier, Axel Heiberg Island, Northwest Territories, Canada. *Journal of Glaciology* **11**(61), 53-58.

Iken, A. 1981. The effect of the subglacial water pressure on the sliding velocity of a glacier in an idealized numerical model. *Journal of Glaciology* **27**(97), 407-421.

Iken, A. and R. A. Bindschadler 1986. Combined measurements of subglacial water pressure and surface velocity of Findelengletscher, Switzerland: conclusions about drainage system and sliding mechanism. *Journal of Glaciology* **32**(110), 101-119.

Iken, A., H. Rothlisberger, A. Flotron and W. Haeberli 1983. The uplift of Unteraargletscher at the beginning of the melt season — a consequence of water storage at the bed? *Journal of Glaciology* **29**(101), 28-47.

Jakobsson, M., R. Macnab, L. Mayer, R. Anderson, M. Edwards, J. Hatzky, H. W. Schenke and P. Johnson 2008. An improved bathymetric portrayal of the Arctic Ocean: Implications for ocean modeling and geological, geophysical and oceanographic analyses. *Geophysical Research Letters* **35**(7), L07602.

Kargel, J. S., A. P. Ahlstrom, R. B. Alley, J. L. Bamber, T. J. Benham, J. E. Box, C. Chen, P. Christoffersen, M. Citterio, J. G. Cogley, H. Jiskoot, G. J. Leonard, P. Morin, T. Scambos, T. Sheldon and I. Willis 2012. Brief communication Greenland's shrinking ice cover: "fast times" but not that fast. *The Cryosphere* **6**(3), 533-537.

Kerr, R. A. 2013. Melting Glaciers, Not Just Ice Sheets, Stoking Sea-Level Rise. *Science* **340**(6134), 798.

Koerner, R. M. 2005. Mass balance of glaciers in the Queen Elizabeth Islands, Nunavut, Canada. *Annals of Glaciology* **42**(1), 417-423.

Lenaerts, J. T. M., J. H. van Angelen, M. R. van den Broeke, A. S. Gardner, B. Wouters and E. van Meijgaard 2013. Irreversible mass loss of Canadian Arctic Archipelago glaciers. *Geophysical Research Letters* **40**(5), 870-874.

Luckman, A., T. Murray, R. de Lange and E. Hanna 2006. Rapid and synchronous ice-dynamic changes in East Greenland. *Geophysical Research Letters* **33**(L03503).

Mair, D., D. Burgess, M. Sharp, J. A. Dowdeswell, T. Benham, S. Marshall and F. Cawkwell 2009. Mass balance of the Prince of Wales Icefield, Ellesmere Island, Nunavut, Canada. *Journal of Geophysical Research: Earth Surface* **114**(F2), F02011.

Mair, D., P. Nienow, M. J. Sharp, T. Wohlleben and I. Willis 2002. Influence of subglacial drainage system evolution on glacier surface motion: Haut Glacier d'Arolla, Switzerland. *Journal of Geophysical Research-Solid Earth* **107**(B8).

Meier, M. F., M. B. Dyurgerov, U. K. Rick, S. O'Neel, W. T. Pfeffer, R. S. Anderson, S. P. Anderson and A. F. Glazovsky 2007. Glaciers Dominate Eustatic Sea-Level Rise in the 21st Century. *Science* **317**(5841), 1064-1067.

Milne, G. A., W. R. Gehrels, C. W. Hughes and M. E. Tamisiea 2009. Identifying the causes of sea-level change. *Nature Geoscience* **2**(7), 471-478.

Moholdt, G., T. Heid, T. Benham and J. A. Dowdeswell 2012. Dynamic instability of marine-terminating glacier basins of academy of sciences ice cap, russian high arctic. *Annals of Glaciology* **53**(60), 193-201.

Motyka, R. J., M. Truffer, M. Fahnestock, J. Mortensen, S. Rysgaard and I. Howat 2011. Submarine melting of the 1985 Jakobshavn Isbræ floating tongue and the triggering of the current retreat. *Journal of Geophysical Research: Earth Surface* **116**(F1), F01007.

Müller, F. and A. Iken 1973. Velocity fluctuations and water regime of Artic valley glaciers. Symposium on the Hydrology of Glaciers. Cambridge, IASH.

Murray, T., A. M. Smith, M. A. King and G. P. Weedon 2007. Ice flow modulated by tides at up to annual periods at Rutford Ice Stream, West Antarctica. *Geophysical Research Letters* **34**(L18503).

Murray, T., K. Scharrer, T. D. James, S. R. Dye, E. Hanna, A. D. Booth, N. Selmes, A. Luckman, A. L. C. Hughes, S. Cook and P. Huybrechts 2010. Ocean regulation hypothesis for glacier dynamics in southeast Greenland and implications for ice sheet mass changes. *Journal of Geophysical Research: Earth Surface* **115**(F3), F03026.

Nerem, R. S., D. P. Chambers, C. Choe and G. T. Mitchum 2010. Estimating Mean Sea Level Change from the TOPEX and Jason Altimeter Missions. *Marine Geodesy* **33**(sup1), 435-446.

Nettles, M., Larsen, T. B., Elósegui, P., Hamilton, G. S., Stern, L. A., Ahlstrøm, A. P., Davis, J. L., Andersen, M. L., de Juan, J., Khan, S. A., Stenseng, L., Ekström, G., & Forsberg, R. (2008). Step-wise changes in glacier flow speed coincide with calving and glacial earthquakes at Helheim Glacier, Greenland. *Geophysical Research Letters*, *35*(24), L24503. doi: 10.1029/2008GL036127

Nicholls, R. J. and A. Cazenave 2010. Sea-Level Rise and Its Impact on Coastal Zones. *Science* **328**(5985), 1517-1520.

Nick, F. M., A. Vieli, I. M. Howat and I. Joughin 2009. Large-scale changes in Greenland outlet glacier dynamics triggered at the terminus. *Nature Geoscience* **2**(2), 110-114.

Parizek, B. R. and R. B. Alley 2004. Implications of increased Greenland surface melt under global-warming scenarios: ice-sheet simulations. *Quaternary Science Reviews* **23**(9-10), 1013-1027.

Paterson, W. S. B. 1994. *The Physics of Glaciers*. Oxford, Butterworth-Heinemann.

Pfeffer, W. T. 2011. Land ice and sea level rise: A thirty-year perspective. *Oceanography* **24**(2), 94-111.

Radic, V., A. Bliss, A. C. Beedlow, R. Hock, E. Miles and J. G. Cogley 2013. Regional and global projections of twenty-first century glacier mass changes in response to climate scenarios from global climate models. *Climate Dynamics*, 1-22.

Rignot, E., I. Fenty, D. Menemenlis and Y. Xu 2012. Spreading of warm ocean waters around Greenland as a possible cause for glacier acceleration. *Annals of Glaciology* **53**(60), 257-266.

Röthlisberger, H. and H. Lang 1987. Glacial Hydrology.In A. M. G. a. M. J. Clark, *ed. Glacio-fluvial sediment transfer: an alpine perspective*. Chichester, John Wiley and Sons**:** 207-284.

Schoof, C. 2010. Ice-sheet acceleration driven by melt supply variability. *Nature* **468**(7325), 803-806.

Scott, J. B. T., G. H. Gudmundsson, A. M. Smith, R. G. Bingham, H. D. Pritchard and D. G. Vaughan 2009. Increased rate of acceleration on Pine Island Glacier strongly coupled to changes in gravitational driving stress. *The Cryosphere* **3**(1), 125-131.

Sharp, M., D. O. Burgess, J. G. Cogley, M. Ecclestone, C. Labine and G. J. Wolken 2011. Extreme melt on Canada's Arctic ice caps in the 21st century. *Geophysical Research Letters* **38**(11), L11501.

Short, N. H. and A. L. Gray 2005. Glacier dynamics in the Canadian High Arctic from RADARSAT-1 speckle tracking. *Canadian Journal of Remote Sensing* **31**(3), 225-239.

Skidmore, M. L. and M. J. Sharp 1999. Drainage system behaviour of a High-Arctic polythermal glacier. *Annals of Glaciology* **28**, 209-215.

Sole, A. J., D. W. F. Mair, P. W. Nienow, I. D. Bartholomew, M. A. King, M. J. Burke and I. Joughin 2011. Seasonal speedup of a Greenland marine-terminating outlet glacier forced by surface melt–induced changes in subglacial hydrology. *Journal of Geophysical Research* **116**(F3), F03014.

Straneo, F., R. G. Curry, D. A. Sutherland, G. S. Hamilton, C. Cenedese, K. Vage and L. A. Stearns 2011. Impact of fjord dynamics and glacial runoff on the circulation near Helheim Glacier. *Nature Geoscience* **4**(5), 322-327.

Straneo, F., G. S. Hamilton, D. A. Sutherland, L. A. Stearns, F. Davidson, M. O. Hammill, G. B. Stenson and A. Rosing-Asvid 2010. Rapid circulation of

warm subtropical waters in a major glacial fjord in East Greenland. *Nature Geoscience* **3**(3), 182-186.

Stern, N. 2006. The Economics of Climate Change: The Stern Review, Cambridge University Press.

Sundal, A. V., A. Shepherd, P. Nienow, E. Hanna, S. Palmer and P. Huybrechts 2011. Melt-induced speed-up of Greenland ice sheet offset by efficient subglacial drainage. *Nature* **469**(7331), 521-524.

Van der Veen, C. J. 2007. Fracture propagation as means of rapidly transferring surface meltwater to the base of glaciers. *Geophysical Research Letters* **34**(1), L01501.

Van Wychen, W. 2010. Spatial and Temporal Variations in Ice Motion, Belcher Glacier, Devon Island, Nunavut, Canada. (*MSc. Thesis,* University of Ottawa.)

Van Wychen, W., D. Burgess, L. Gray, L. Copland, M. Sharp, J. A. Dowdeswell and T. Benham submitted manuscript. Glacier velocities and dynamic ice discharge from the Queen Elizabeth Islands, Nunavut, Canada. *Geophysical Research Letters*.

Van Wychen, W., L. Copland, L. Gray, D. Burgess, B. Danielson and M. Sharp 2012. Spatial and temporal variation of ice motion and ice flux from Devon Ice Cap, Nunavut, Canada. *Journal of Glaciology* **58**(210), 657-664.

Vieli, A., J. Jania, H. Blatter and M. Funk 2004. Short-term velocity variations on Hansbreen, a tidewater glacier in Spitsbergen. *Journal of Glaciology* **50**(170), 389-398.

Williamson, S., M. Sharp, J. Dowdeswell and T. Benham 2008. Iceberg calving rates from northern Ellesmere Island ice caps, Canadian Arctic, 19992003. *Journal of Glaciology* **54**, 391-400.

Willis, I. C. 1995. Intra-annual variations in glacier motion: a review. *Progress in Physical Geography* **19**(1), 61-106.

Wyatt, F. 2013. The spatial structure and temporal development of supraglacial drainage systems, and their influence on the flow dynamics of High Arctic ice caps. (*Doctoral Thesis*, University of Alberta.)

Zwally, H. J., W. Abdalati, T. Herring, K. Larson, J. Saba and K. Steffen 2002. Surface melt-induced acceleration of Greenland ice-sheet flow. *Science* **297**(5579), 218-222.

Chapter Two: Development and application of a time-lapse photo analysis method to investigate the link between tidewater glacier flow variations and supra-glacial lake drainage events [*]

2.1 Introduction

Tidewater glaciers - glaciers terminating at a marine interface – undergo both melting and iceberg calving, and both mechanisms transfer significant land-ice mass to the oceans. Ice loss from a tidewater glacier can be generally expressed as the water equivalent sum of surface runoff, submarine melt, volume loss due to retreat of the glacier terminus, and volume loss due to iceberg calving flux. The iceberg calving flux is strongly dependent on the glacier flow rate, which is often assumed to be constant for estimates of regional total mass balance (Dowdeswell and others, 2002; Burgess and others, 2005; Dowdeswell and others, 2008; Gardner and others, 2011). However, tidewater glaciers may experience significant flow variability at seasonal and annual timescales, and this may introduce uncertainty in estimates of ice mass discharge to the oceans. Reducing this uncertainty requires that the flow variability of tidewater glaciers be quantified.

Some tidewater glaciers exhibit seasonal flow variability (Vieli and others, 2004) similar to that exhibited by High Arctic and alpine valley glaciers (Iken, 1972; Copland and others, 2003; Sugiyama and Gudmundsson, 2004; Bartholomaus and others, 2008). This variability may be missed by some methods of determining glacier ice displacement due to seasonal biases in their temporal sampling. For example, while feature tracking methods applied to optical satellite imagery can measure average annual ice displacements

[*] A version of this chapter has been published as: Danielson, B. D. and M. J. Sharp 2013. Development and application of a time-lapse photograph analysis method to investigate the link

(Williamson and others, 2008), interferometric synthetic aperture radar (InSAR) and speckle tracking methods (Burgess and others, 2005; Van Wychen and others, 2012) can determine ~ monthly displacements during fall, winter and spring. InSAR methods have also been used successfully in summer (Joughin and others, 2008), but in some cases are less effective during the melt period because of loss of coherence between radar images (Van Wychen and others, 2012). Therefore it is important to have an estimate of the magnitude of seasonal flow variability when evaluating errors associated with ice flux estimates from sub-annual measurements.

Glacier flow variations may include a 'spring event' - a sudden increase in horizontal ice velocity and simultaneous vertical ice motion that coincides with meltwater flow into moulins early in the melt season, initiating a supra-glacial to sub-glacial drainage connection (Iken and others, 1983; Röthlisberger and Lang, 1987; Bingham and others, 2006). Additional ice uplift and fast-flow events later in the melt season have been associated with periods of enhanced meltwater production and increased runoff into moulins. Faster glacier flow during these events is usually interpreted as a result of hydrologically enhanced basal sliding, which occurs when water inputs exceed the capacity of the existing sub-glacial drainage network and increase sub-glacial water pressure to the point where water-filled cavities grow and ice-bed separation increases (Iken and Bindschadler, 1986).

Velocity variations have also been observed on High Arctic glaciers and parts of the Greenland Ice Sheet in association with the rapid drainage of supra-glacial lakes via crevasses opened by hydro-fracture (Boon and Sharp, 2003; van der Veen, 2007; Das and others, 2008; Sole and others, 2011). Lakes accumulate meltwater over a period of days to weeks and may deliver some or all of that water to the subglacial drainage system in an event lasting a few hours. This

---

between tidewater glacier flow variations and supraglacial lake drainage events. Journal of Glaciology **59**(214), 287-301.

mechanism has the potential to rapidly perturb a slowly evolving subglacial drainage system. Both rates of meltwater production and supra-glacial lake drainage events must therefore be considered when attempting to assess the causes of glacier flow variability.

Supra-glacial lake drainage events have been observed directly and by remote sensing methods. Individual lakes have been instrumented with pressure transducers and monitored in detail to determine fill and drainage rates (Boon and Sharp, 2003; Bartholomaus and others, 2008; Das and others, 2008). However, on larger glaciers or regions of the Greenland Ice Sheet where many lakes exist over a large area, it is difficult to monitor multiple lakes in this way. Satellite imagery has been used to document the spatial distribution of lakes on the Greenland Ice Sheet, and methods of estimating lake depth and volume have been proposed (Box and Ski, 2007; Sneed and Hamilton, 2007; Tedesco and Steiner, 2011). Only very recently have MODIS images been used to determine the fill and drainage rates of these lakes at sub-daily temporal resolution (Selmes and others, 2011). The temporal and spatial resolution is still insufficient to reveal details of the drainage mechanism.

Terrestrial time-lapse photography may present a way to observe lakes on large outlet glaciers at higher spatial and temporal resolution. While it may not be ideally suited for some locations where elevated vantage points are unavailable (such as flatter parts of the Greenland Ice Sheet), time-lapse photography has been used with success at many alpine and outlet glacier settings. An early prototype of automatic time-lapse camera was deployed to observe the advance of an alpine glacier on Mt. Rainier (Miller and Crandell, 1959). Other glacial features or processes that have been monitored with time-lapse photography include pro-glacial streams (Humphrey and Raymond, 1994), snow surface albedo changes (Corripio, 2004), ice mélange interactions at the front of Jakobshavn Isbræ (Amundson and others, 2010), iceberg plume discharge events (Herdes and others, 2012), and meltwater plume discharge (Milne, 2011). The combination of time-lapse photography, digital image matching techniques, and

photogrammetric methods has been used to determine glacier terminus velocity (Krimmel and Rasmussen, 1986), detect calving terminus position and area change at Alaskan and Svalbard marine terminating glaciers (Motyka and others, 2003; O'Neel, 2003; Chapuis and others, 2010), and calculate surface velocity fields on Greenland outlet glaciers (Ahn and Box, 2010). Boon and Sharp (2003) used a time-lapse camera to monitor lake development on John Evans Glacier (Ellesmere Island) but, to our knowledge, photogrammetric methods have not been applied to time-lapse imagery of supra-glacial lakes to quantify the size or rate of change of these reservoirs.

In this study, we combine photogrammetric methods with automated digital image processing of time-lapse photographs to study the impact of supra-glacial lake drainage events on the flow variability of Belcher Glacier, a tidewater outlet glacier of the Devon Ice cap in Nunavut, Canada. Time-lapse cameras were used to observe several of the most significant supra-glacial lakes on the glacier over an entire melt season. We describe how the sequence of images from each camera was used to produce a time series of supra-glacial lake area, which we use to estimate rates of water delivery to the subglacial drainage system. Comparing this dataset with multiple time series of glacier flow velocity derived from GPS measurements allows the identification of ice acceleration events that correspond in time with lake drainages. These short duration events are part of a broader pattern of seasonal flow acceleration that occurs on this glacier. After isolating these events and measuring the corresponding ice displacement at the glacier terminus, we discuss the significance of the flow enhancement driven by lake drainage events for the total seasonal and annual ice displacement.

2.2 Study Site

Devon Ice Cap is among the largest ice caps in the Canadian Arctic; it has an area of ~14,000 km^2 and contains ~ 4110 km^3 of ice (Burgess and Sharp, 2004). Numerous outlet glaciers, many of which have marine termini, punctuate the north, east, and southern boundaries of the ice cap (Figure 2-1).

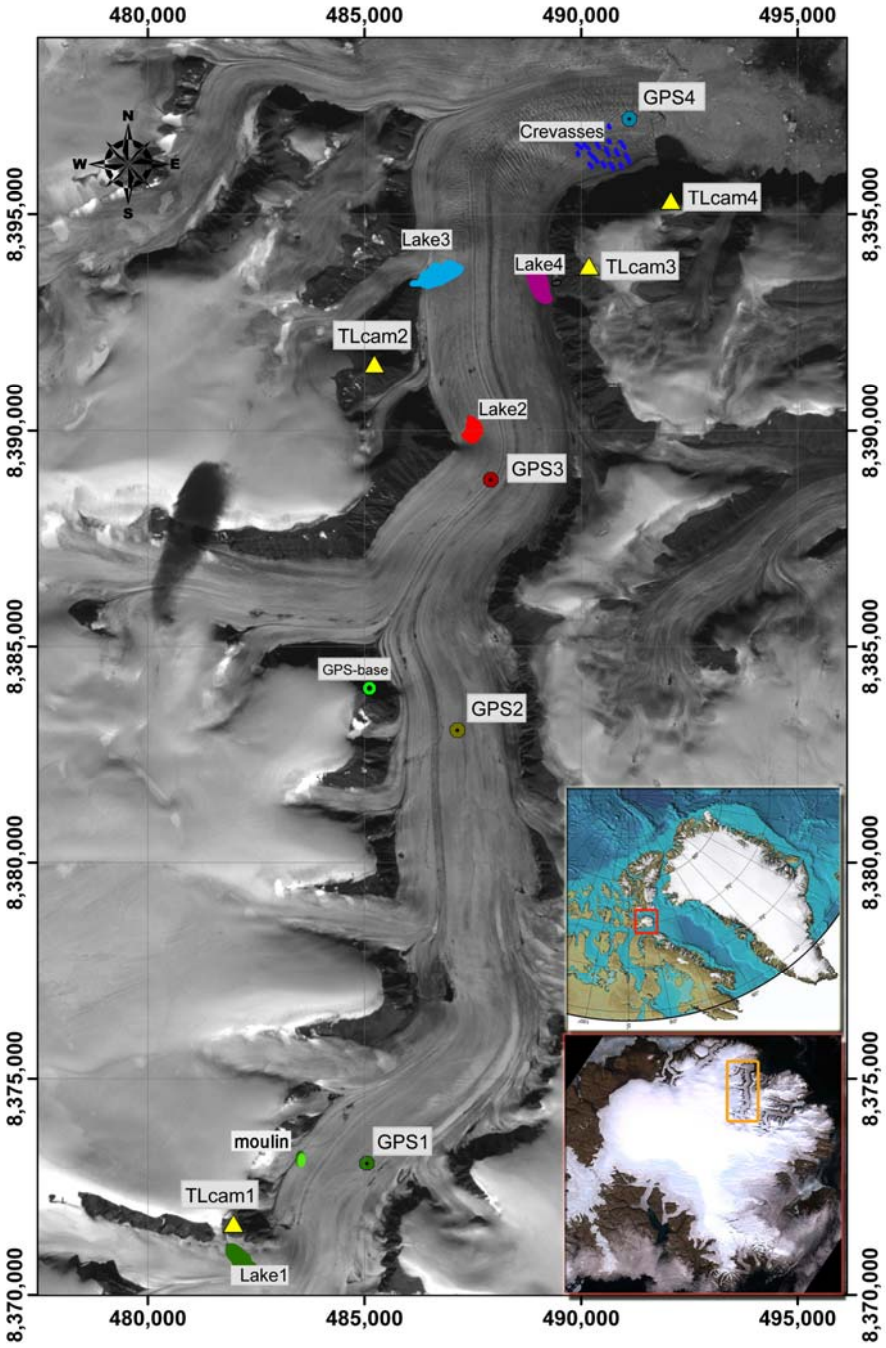

Figure 2-1: Landsat7 image of the Belcher Glacier, showing locations of Time-lapse cameras, GPS stations, and lakes described in the Data section. Grid coordinates are in UTM zone 17X.
(Upper Inset Map) Devon Island is part of the Canadian Arctic Archipelago. The Devon Ice Cap (red box) is located at 75° N, between 80° and 90° W. Map selected from the International Bathymetric Chart of the Arctic Ocean (Jakobsson and others, 2008).
(Lower Inset Map) Landsat 7 image of the Devon Ice Cap, with location of Belcher Glacier outlined in the orange box. ***(Both Landsat7 images are from August, 2000)***

Belcher Glacier is a ~40 km long tidewater outlet glacier that flows through a steep-walled fjord and is fed by multiple tributaries. Flow rates are fastest in the terminus region, up to ~300 m a^{-1}. Airborne radar data show the grounded terminus ice is ~250m thick, and the glacier remains grounded below sea level 15 km up-glacier from the terminus (Dowdeswell and others, 2004). The glacier is a large source of icebergs, accounting for ~17% of the net mass loss from the Devon Ice Cap between 1960-1999 (Burgess and others, 2005). The majority of this calving loss is due to the glacier's high rate of ice flux rather than to retreat of its terminus, which has remained relatively stable for the past 50 years (Burgess and Sharp, 2004; Burgess and others, 2005).

2.3 Data

2.3.1 Lake Observations

We examined July and August imagery from Landsat 7 (1999, 2000), SPOT5 (2007) and Government of Canada aerial photographs (1959, 1960) to identify locations where lakes form on the surface of Belcher Glacier. Comparison of 1959-60 and contemporary imagery confirms that many of these lakes have formed repeatedly over decades.

Photographs taken on the glacier and from light aircraft during May and August fieldwork campaigns in 2006-2009 provided further evidence that many lakes form annually in the same basins. During spring fieldwork, we explored the topographic basins in which the lakes form, and looked for signs of moulins or incised drainage channels leading into and out of lake basins. These can be difficult to find and map accurately due to snow cover. We also noted that some basins were ringed with stranded lake ice, while others were not, which suggested that some lakes persist until after freeze up while others drained before then. Return trips in mid- to late-August confirmed that some lake basins were empty by the end of the melt season, while others still contained water.

2.3.2 Time-lapse Photography

The aforementioned imagery was used to identify potential cliff-top locations that offered viewing positions for several of the largest supra-glacial lakes. In May 2007, we reconnoitred these sites by snowmobile and helicopter and began installing time-lapse camera systems. We used Harbortronics time-lapse kits, Pentax K110D 6M pixel DSLR cameras, Pentax 18-55mm lenses, and 4Gb SD memory cards. Each camera recorded high-quality 3008x2000 JPEG files (using the in-camera Pentax RAW to JPEG convertor). Each camera system was housed in a weather-proof enclosure with a glass window, a lithium battery with solar panel and charging regulator, an adjustable camera mount, and a DigiSnap2000 intervalometer/shutter controller. At each installation, the camera lens was set to the desired focal length and manually focused on the scene. Auto-exposure and shutter speed were selected, so that the camera could adjust to changing lighting conditions, but a pre-programmed "daylight' white balance was selected to provide consistent color cast through the resulting image series. A 2-m steel tripod and guy-wires were anchored to exposed rock using expansion bolts to provide a solid foundation for the camera system.

In 2007 and 2008 we had mixed success with the time-lapse systems and our chosen viewing locations. After replacing some of the intervalometers and moving the cameras to more suitable locations, we successfully operated four time-lapse systems at a 1-hour image capture rate over the entire spring and summer of 2009. These cameras observed the four lakes and crevasse field labelled in Figure 2-1. This study focuses on the 2009 observations.

2.3.3 Ice Velocity Time Series

We deployed five Trimble dual-frequency GPS receivers that acquired observations at a 15 second sampling rate continuously from May through August of 2009. One receiver was used as a base station, and was installed on a steel tripod anchored to bedrock at a cliff-top site. The other four were installed on the glacier surface along the centerline (referred to as GPS1 through GPS4 in the rest

of this paper). Data from these four stations were used to examine variations in the flow speed of the ice. The GPS antennae were fixed to the tops of steel poles drilled 2-3m into the glacier ice. Antennae heights were typically ~1 m above the ice surface in May, and were between 2-3 m above the surface by the end of August.

Table 2-1: On-Ice GPS Site Details

GPS ID	Centerline Distance from Terminus (km)	Surface Elevation (m. a.s.l.)	Ice Thickness (m) *
GPS1	0.5	50	290
GPS2	9.6	500	450
GPS3	18.0	700	570
GPS4	25.7	880	130

* Estimated from airborne radar survey (Dowdeswell and others, 2004).

We used TRACK, the kinematic processing module associated with the GAMIT software (Herring and others, 2006; McClusky, 2010), to post-process our GPS observations differentially in kinematic mode. For each set of raw GPS observations, TRACK produces a kinematic position estimate, with 1-sigma uncertainties stated for each coordinate dimension. These datasets were filtered to remove any positions with 2D 1-sigma distance root mean square (DRMS) errors greater than 0.05 m, or vertical 1-sigma uncertainties greater than 0.1 m. All remaining position estimates produced from each GPS station were concatenated into individual long time series. These time series were then sampled uniformly to produce position estimates every 1-hour. Horizontal ice velocity time series were produced for each site by estimating the horizontal displacement between position estimates, then dividing by the intervening time-step. A 4-hour moving average was used to remove the effects of high-frequency noise.

2.3.4 Air Temperature Time Series

Automatic air temperature loggers, installed in radiation shrouds, were co-located with the GPS stations to measure the local air temperature every hour over

the duration of the summer. The GPS station nearest the glacier terminus (GPS4) did not have a co-located temperature logger, so we used the air temperature observations from the nearest available logger (located 5 km southwest and +300 m elevation) adjusted by an altitude dependent lapse rate of 4.9 ^{o}C km^{-1} (Gardner and Sharp, 2009), to estimate the air temperature in the terminus area.

2.3.5 Ice Surface Elevation

A Digital Elevation Model (DEM) of the Devon Ice Cap was produced using SPOT5 satellite imagery collected in summer 2007, as part of the Spot 5 stereoscopic survey of Polar Ice: Reference Images and Topographies (SPIRIT) project. The SPIRIT DEM shows good agreement with ICESat laser altimetry in the ablation zone (Korona and others, 2009), which includes the Belcher Glacier region. We found that this DEM has sufficient spatial resolution (~30 m) to resolve supra-glacial lake basin geometry, which we used to assess the accuracy of the position and size of lakes identified via our time-lapse photography analysis methods.

2.4 Methods

We deployed four time-lapse cameras between 27 May and 15 August 2009, and each acquired ~2000 images. With such a high volume of imagery, it was desirable to automate the process of finding lakes and measuring the area covered by water. A strict method is needed to quantify the size of the lake in each image, and produce a time series of lake sizes from which filling and drainage rates can be derived. We developed a set of image analysis procedures that involved the following steps:

1) Image pre-filtering and masking: data cleaning
2) Automated image classification: find the lakes
3) Image-space to Real-space Conversion: measure the lake areas
4) Time series production: compare the lake areas over time

2.4.1 Image Pre-filtering and Masking

Fog cover was a persistent problem at all camera locations due to the close proximity to the open water of Baffin Bay. As our image classification procedure was unable to produce usable results from images partially or wholly obscured by fog, we required a pre-filtering algorithm to identify and remove fog-filled images from each set of time-lapse photographs. As a result of JPEG compression, uniformly grey, fog-filled images require much less memory storage than images containing a variety of colors. Any image with a file size below a tuneable threshold was omitted from further processing.

Some of our time-lapse cameras observed multiple lakes or water-covered areas, but we were interested in monitoring and measuring individual lakes. For example, TLCam3 observed both Lake3 and Lake4, but we wanted to observe them individually. Likewise, TLCam4 observed a field of water-filled crevasses which we were interested in, but also a small lake far across the glacier and melt water or marine water beyond the glacier terminus, in which we were not interested. For this reason we applied a digital mask or cropped the images (preserving the original image coordinates) before applying our procedures, so that individual regions of interest could be monitored.

2.4.2 Automated Image Classification

A systematic way to identify a lake in an image is to employ an image pattern recognition function that examines each pixel in an image relative to a set of criteria to determine whether the pixel fits in the target class (e.g., water) or in one or more non-target classes (e.g., snow, ice, rock, other). We used color information to provide the criteria for determining pixel class membership. Human vision also uses characteristics such as roughness or edge detection to identify transitions between snow/ice and water, but such criteria are highly variable and more challenging to implement on a pixel-by-pixel basis.

A digital image can be manipulated as an X-by-Y-by-3 data array; X and Y being the pixel dimensions of the image, with 3 dimensions or layers of color

information. The default RGB color pallete divides red, green and blue reflectance values into the 3 color layers. Unfortunately, lake water is not simply "blue" and the reflectance values of water change as depth changes, or as lighting conditions change with weather and time of day. The significant limitation of the RGB color representation is that lighting and saturation information are mixed into each color layer, making it a poor choice for pixel classification criteria in a natural scene. Instead, we converted each photograph into two alternative color representation systems (called HSV and L*a*b* color spaces) that define color along continuous spectra of hue and chromaticity, and separate brightness and saturation information into different layers. These conversions allowed us to ignore most of the brightness variation, and focus on the hue and chromaticity layers as pixel classification criteria. (*For additional information on color spaces, see Endnote 1*).

We performed pixel classification using a software routine developed around the K-means algorithm (MacQueen, 1967) in MATLAB. K-means is technically not a classification technique, but a data clustering method. The user defines the number of clusters (defined by the parameter 'k') that the data should be sorted into. The choice of 'k' depends partly on how many groups within the data the user desires to find, but also on the nature and modality of the dataset itself. Some amount of reiterative testing may be required to find an appropriate choice of 'k' (MacQueen, 1967).

The K-means algorithm begins by randomly selecting 'k' pixels from an image, and uses these pixel attributes (the hue and chromaticity layer values) as the initial 'means', or the definition of the cluster centers. Next, all the remaining pixels from that image are assigned to the cluster with the closest mean attribute set. The cluster means are updated (becoming the average of all pixels in the cluster), and then the process is repeated until the algorithm converges on a solution where the cluster means do not change after the update step (MacKay, 2003).

The MATLAB implementation of the K-means algorithm includes numerous refinements and options for optimizing clustering results. One optimization we employed involved running multiple replicates of the clustering process on each image, using new random starting pixels. Variations in the tightness of the clusters (minimum sum of distances between all pixels and their cluster mean) can occur by using different starting points; we kept the tightest result of 5 replicates.

After the K-means algorithm was run on an image, all pixels in the image were labelled with their cluster identification. Using the cluster associated with 'blue' band values, a binary mask was created to isolate the 'Lake' feature in the image. A subsequent algorithm then drew an outline around the lake perimeter and created a list of the image-space coordinates of the lake perimeter. Finally, a rapid quality control procedure allowed us to reject any erroneous lake outlines that resulted from fog, shadow, reflections, or floating lake ice obscuring parts of the lake.

2.4.3 Image-space to Real-space Conversion

The points comprising the lake perimeter were then converted from pixel coordinates to UTM coordinates. The real-space area of the lake (m^2) in each image could then be calculated using the georectified perimeter.

The UTM coordinates of the lake perimeter were determined using a monophotogrammetric (MPG) technique implemented in MATLAB by M. Truffer at the University of Alaska Fairbanks. This technique adapts the methods of Krimmel and Rasmussen (1986) for use with digital photography. A detailed description of the technique and associated error analysis can be found in O'Neel, 2000.

This MPG technique has been utilized at several study sites in Alaska (O'Neel, 2003; O'Neel and others, 2007), and Svalbard (Chapuis and others, 2010) to measure temporal changes in the calving line position of tidewater glaciers. In these cases, the points where the glacier terminus ice cliff meets the marine water

surface form an intersection line along a plane of known elevation: 0 m.a.s.l. (± tidal fluctuation). Utilizing this constraint on elevation, the horizontal coordinates of any point along this intersection line may be estimated if the position and orientation of the camera, and geographic locations of several Ground Control Points (GCPs) in the scene, are known. For our scenario, we assumed that all points along the surface of a lake were at the same elevation, thus the lake shoreline intersects a plane. We were therefore able to apply the same code, with minor modifications, to solve for the horizontal UTM coordinates of the lake perimeter.

Our time-lapse cameras were initially installed only to perform a monitoring role and no photogrammetric campaign was planned; therefore, we did not survey GCPs in any of the scenes except for the terminus scene imaged by TLCam4. GCPs were therefore selected from high resolution orthorectified imagery. An example time-lapse scene and a SPOT5 HRS image (captured August 20, 2007) of the same area were examined together to locate sharp rock outcrops, nunatak edges, or incised drainage channels that appeared to be persistent features that could be seen in both images. These were selected as potential GCPs. The pixel coordinates from the time-lapse image and the geographic coordinates from the SPOT image for each GCP were co-registered. Elevation values for the GCPs, lake surface, and camera position were extracted from the SPIRIT DEM of the region.

The required camera parameters include the 3-dimensional camera rotation angles (which were measured in the field, estimated from photographs of the camera installation, or calculated based on scene geometry), and the image enlargement factor (a function of image size, sensor size, and focal length).

Testing the quality of the GCPs and camera orientation parameters involved an iterative trial and error process: all the parameters were entered into the input settings file used by the MPG program, and the program was run using a training image of the scene that included the lake at or near maximum size, with the outline drawn around it. The output of the MPG program (UTM coordinate

outline of the lake perimeter, and relative position of GCPs) was examined after each run to determine whether the relative positions of GCPs and lake appeared correct, and the shape of the lake outline appeared true. This was verified by plotting the GCP points and lake outline on the SPOT image with the original GCP points. If fit was not good (this process was quite subjective), then the program was run again after one parameter in the MPG input settings file was modified. Subtle variations in any of these parameters could produce large changes in the correspondence between the lake outline and GCP points from the TL image and their projection on the SPOT image. A set of GCPs and other input parameters was settled upon when it was determined that the overall fit of the solution was as good as possible.

2.4.4 Time Series Production

The above three steps were applied to all the images from the time-lapse cameras. The date and time were stored with the lake area calculated from each photograph to produce a time series of lake area change, beginning when the lake was first detected, and ending sometime after the lake had drained or when the camera was retrieved. A time series was produced for each of the four major lakes and the water-filled crevasse area in the glacier terminus region. To produce an approximation of the net drainage rates of each lake, we calculated the first derivative of the lake area time series and plotted the negative values, which represent reduction in lake area in square meters per hour.

These time series of lake areas and net drainage rates were plotted on the same time axis as our GPS-based ice velocity time series and our measurements of air temperature. We examined each individual time series, noting significant changes in surface melt conditions (inferred from air temperature), instances when lakes switched from filling to draining, and rapid variations in ice velocity. We then combined these observations to evaluate the potential relationships between melt events, lake drainage events and specific glacier acceleration events.

2.4.5 Lake Area Validation

We compared the maximum area of each lake found in the time-lapse images with the area of the same lake as seen in orthorectified aerial or satellite imagery, where available. We also used the SPIRIT DEM, which has sufficient accuracy and spatial detail (i.e. 30 m resolution) to resolve the lake basins, to validate the area of the lakes. We used the Quick Terrain Modeler (QTM) software (www.appliedimagery.com) to draw a contour line (using QTM's Flood Analysis tool) at the elevations of the maximum lake surface levels on the DEM (see Figure 2-3, right column). We found the maximum lake surface level by adjusting a hypothetical 'flood level' such that water filled the basin of interest without connecting to adjacent basins or flooded down-glacier areas. The Flood Analysis tool uses a simple "Bathtub" model of flooding, and reports both an area and volume estimate for inundated regions of the DEM. By progressively lowering the flood level until the basin of interest was 'dry', we determined the basin floor elevation, and thus the lake depth. Unfortunately the DEM did not have sufficient spatial detail to resolve the terminus area crevasses, and thus we were unable to determine the area or volume of water-filled crevasses in the same manner.

2.5 Results

2.5.1 Image Classification Results

Using our automated lake detection method, we were able to identify and delineate lakes faster than was possible in trials using manual digitization methods. The K-means clustering technique enabled the identification of water-covered pixels in a variety of different lighting conditions and challenging viewing situations. The segmented groups of water-filled crevasses provided the most challenging scenario (a sample of the results is shown in Figure 2-2). Ambiguity between water-filled crevasses and strongly shadowed crevasses often occurred, which required many of the results from the TLCam4 time series to be discarded in the quality control procedure.

Figure 2-2: Single image acquired by TLCam4 on June 30, 2009 showing the results of our automated image classification technique. In this case our technique has successfully picked out water-filled crevasses (outlined in red).

2.5.2 Classification Challenges

One challenge we encountered was due to the changing appearance of water on the glacier surface as the melt season progressed and the surface changed from snow, to slush, to ice, to dirty ice. The number of surface types, and therefore colors recognized, increased with time. K-means clustering could not converge on a stable solution if the choice of 'k' was inappropriate for the data. For instance, when the image was dominated by only two features (e.g., pure white snow and blue water), and we attempted to find five clusters ('k' = 5), then K-means either failed to converge on a solution and reported an error, or attempted to divide the two logical clusters into inappropriate fractions. Conversely, if 'k' was set too low for an image with high variability (i.e., 'k' = 2 for a scene composed of snow, ice, dirt, rocks, water, shadow, etc.) then the algorithm was forced to merge clusters and produced unusable results.

To mitigate the effect of changing surface appearance over time, we divided the time-lapse images into sub-seasons (i.e., early, mid-, and late-summer) so that the number of clusters could be changed to optimize the clustering results for the conditions. We found that k = 2 effectively clustered snow and water early in the summer and that clustering was more effective when 'k' was increased to 3 or 4 later in the summer.

2.5.3 Coordinate Conversion Results

Due to the non-ideal methods used for GCP registration, absolute errors in the coordinate projections produced by the MPG program were quite high. The magnitude of error differed for each time-lapse camera scene, but we noted mis-registration of up to ~150 m for some projected lake perimeters. However, the relative position quality was satisfactory: some lake outlines were slightly distorted, but the general shape and area of each lake outline produced by the MPG program corresponded to what can be seen in orthorectified imagery or the SPIRIT DEM.

The center column of Figure 2-3 shows a comparison of lake outlines produced by our automated method (red outline) and manually drawn outlines of the same lakes visible in a variety of orthorectified imagery (blue outline). The top row shows Lake1 at ~25% filled state in a 1999 Landsat7 image; the red outline represents Lake1 at a similar fill-state in 2009. The second row shows Lake2 at or near its maximum fill level in a 1959 aerial photograph. Noticeable changes to shoreline geometry have occurred in the intervening 50 years, but the 2009 maximum lake area is very similar. The third row shows the red outline of Lake3 at maximum fill-state in 2009, and a blue outline of the lake at ~70% fill state, as seen in a georeferenced DigitalGlobe (WorldView-2) quick-look image captured June 24, 2011. Note that this comparison shows a large shift between lake outlines, which is perpendicular to the viewing direction of the camera. This may be due to an error in one of the camera rotation parameters. The fourth row shows Lake4 at maximum size in a 2007 SPOT5 image, compared to the red

outline of Lake4 at maximum size in 2009. Comparisons of lake areas based on these red and blue lake outlines are presented in Table 2-2.

Table 2-2: Lake Area Comparisons

Lake	Time-lapse Image	Ortho- Imagery Source	Time-lapse Calculated Area (m^2)	Ortho-Image Calculated Area (m^2)	SPIRIT DEM Lake Area (m^2)	Area Difference TL – Ortho	Area Difference TL - DEM
Lake 1 (1/4 filled stage)	12-07-09 16:59:29	Landsat7 1999 Orthomosaic.	33,980.5	34,544.5	29,600 *	-563.5 (1.7%)	4,380.5 (13%)
Lake 1 (Max. size)	18-07-09 12:59:32	Lake not found at max. size	129,793.5	N/A	131,200	N/A**	-1,406.5 (1%)
Lake 2 (Max. size)	12-07-09 13:00:56	1959 Orthophoto	113,330.3	125,106.3	128,000	-11,776 (10%)	-14,669.7 (13%)
Lake 3 (Max. size)	16-07-09 13:01:01	DigitalGlobe 11-06-2011 Lake not found at max. size	271,389.0	198,900 (~70% full)	241,600	N/A**	29,789 (11%)
Lake 4 (Max. size)	19-07-09 21:01:04	SPOT HR5 20-08-2007	160,836.3	183,537.5	153,600	-22,701.2 (14%)	7,236.3 (4%)

* Average of two lake sizes: for small lake basins in the DEM, very small increments in depth produced large step changes in lake area.
** Area Differences not available because comparably sized lakes were not found in available imagery.

Since we could not always find the lakes at fill-states useful for comparison in the available orthorectified imagery, we used a second method to validate the area of the four lakes. As described above in the Methods section, we used QTM's Flood Analysis tool and the SPIRIT DEM to estimate the area, volume, and depth of our selected lake basins.

The lake basins found via this method are shown as blue areas outlined in black in the right column of Figure 2-3. Areas for each lake found via this method are shown in Table 2-2. Lake volume and depth estimates are given in Table 2-3. Comparison of the maximum lake areas found via the DEM method and our photogrammetry method show good agreement; the maximum area difference is 13%. As we are only interested in areal changes of the lakes, and not in absolute positions, we consider our lake outline coordinate conversion results acceptable.

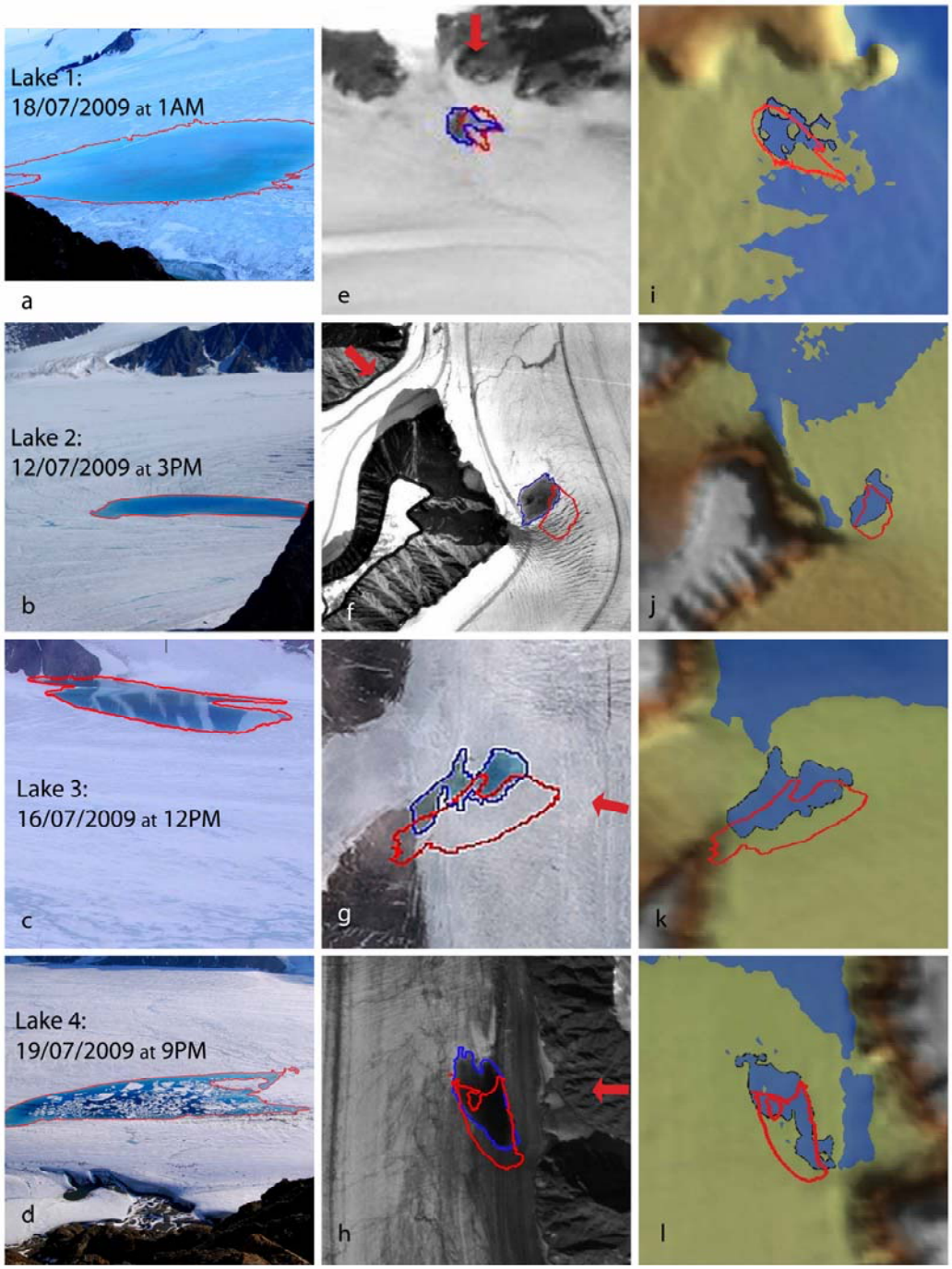

Figure 2-3: Lake Area Validation. The left column shows each lake at maximum size in the original time-lapse photo. The red outline was drawn by our classification procedure, and corresponds to the points converted from image-space to UTM coordinates. The center column compares our method's lake outlines (red) to manually drawn outlines of the same lakes visible in orthorectified imagery (blue). Since these images are not coincident in time, some differences are expected. The red arrow represents the view angle of the time-lapse camera. The right column compares the lake outlines from the time lapse images (red) with the lake basins found in the SPIRIT DEM.

Table 2-3: Lake Volume Estimates. Each volume and depth estimate is reported with an uncertainty found by raising and lowering the lake surface elevation by 0.25m, which is the limit of resolution of the DEM.

Lake	Lake Surface Elevation (m.a.s.l.)	Lake Bottom Elevation (Lake Depth) (m)	Lake Volume ± variance (m^3)
Lake 1	1031.5 ± 0.25	1027 (3.5 ±0.25)	247,900 ± 36100
Lake 2	354.5 ± 0.25	348 (6.5 ±0.25)	366,400 ± 32000
Lake 3	310 ± 0.25	300 (10 ±0.25)	989,200 ± 65600
Lake 4	309 ± 0.25	302 (7 ±0.25)	434,200 ± 43800
Total			2,037,700 ± 43800

2.6 Observations

2.6.1 Ice Velocity and Air Temperature Events

The air temperature time series in Figure 2-4(e) can be divided into two periods: Spring from day 170 – 190 (June 19 – July 9), and Summer from day 190 – 217 (July 9 – August 5). This division corresponds closely to the pattern observed in the horizontal ice velocity timeseries; the glacier exhibited different flow characteristics before and after day 190. Below we describe several of the distinct events observed during these two time periods.

During the Spring period, time-lapse imagery showed that snow melt and water begin to accumulate in supra-glacial storage. The horizontal ice velocity at stations GPS1, GPS2, and GPS3 (Figure 2-4c) remained consistently at or near the mean winter flow rates recorded at these locations, and there was little to no variability in vertical ice motion. However, ice near the terminus began to accelerate during this period, as seen in the GPS4 horizontal velocity time series.

Acceleration event A1, day 172.5 – 174.3 (June 21 – 23), marks the first departure from the relatively stable winter flow rate of 0.6 m d^{-1} in the terminus region. This event was composed of two pulses of high flow speed, and simultaneous abrupt jumps in vertical ice motion (up to 0.2 m). The end of this event was followed by a gradual increase in ice velocity leading up to event A2.

Acceleration event A2, day 181.0 – 185.5 (June 30 – July 4), began with a rapid acceleration of ice flow to ~1 m d^{-1}, which was sustained for 19 hrs, followed by a 24 hr deceleration to 0.85 m d^{-1}. Event A2 culminated with a rapid return to ice flow above 1 m d^{-1}, after which flow speeds return to rates seen prior to day 181. A slight 'bulge' can be seen in the vertical motion of GPS4 during this event, though it is less distinct than the rapid uplift seen during event A1. The dual peaks in ice velocity seen during event A2 correspond closely in time to twin peaks in air temperature recorded in this region. Similar air temperature fluctuations were recorded at the measurement sites up-glacier, but the ice velocities at stations GPS1, GPS2, and GPS3 did not vary in the same way as at GPS4.

In the Summer period, air temperature remained consistently above $0^{o}C$, apart from two short negative excursions in the higher elevation regions of the glacier. The air temperature generally ranged between $0^{o}C$ and $+6^{o}C$, with the exception of one particularly warm day during which a peak temperature of $+13^{o}C$ was reached in the lowest elevation regions of the glacier. Horizontal ice velocity became much more variable during this period, and several specific events are described below. In addition, between days 200 – 204 (July 19-23), ice flow at GPS2 and GPS3 exhibited distinct diurnal variations that were coincident in time with diurnal temperature variations.

Acceleration event A3 was a wave of increased ice velocity that was recorded along most of the glacier between day 191 – 197 (July 10-16). It initiated on day 191 in the mid-upper glacier, when ice velocity at GPS2 rapidly increased from a background rate of ~0.18 m d^{-1} to 0.64 m d^{-1}, in 24 hours. Rapid vertical motion of the ice lagged the onset of horizontal acceleration by ~16 hrs. The ice surface at GPS2 rose 0.15 m, then up to 0.2 m, and remained near this elevation for the duration of event A3. Acceleration at GPS3 began as the first peak in velocity was reached at GPS2, at the beginning of day 192. Velocity at GPS3 peaked and began to slow down at the beginning of day 193, at which point GPS4 began to accelerate. Near the end of day 193, GPS2 and GPS3

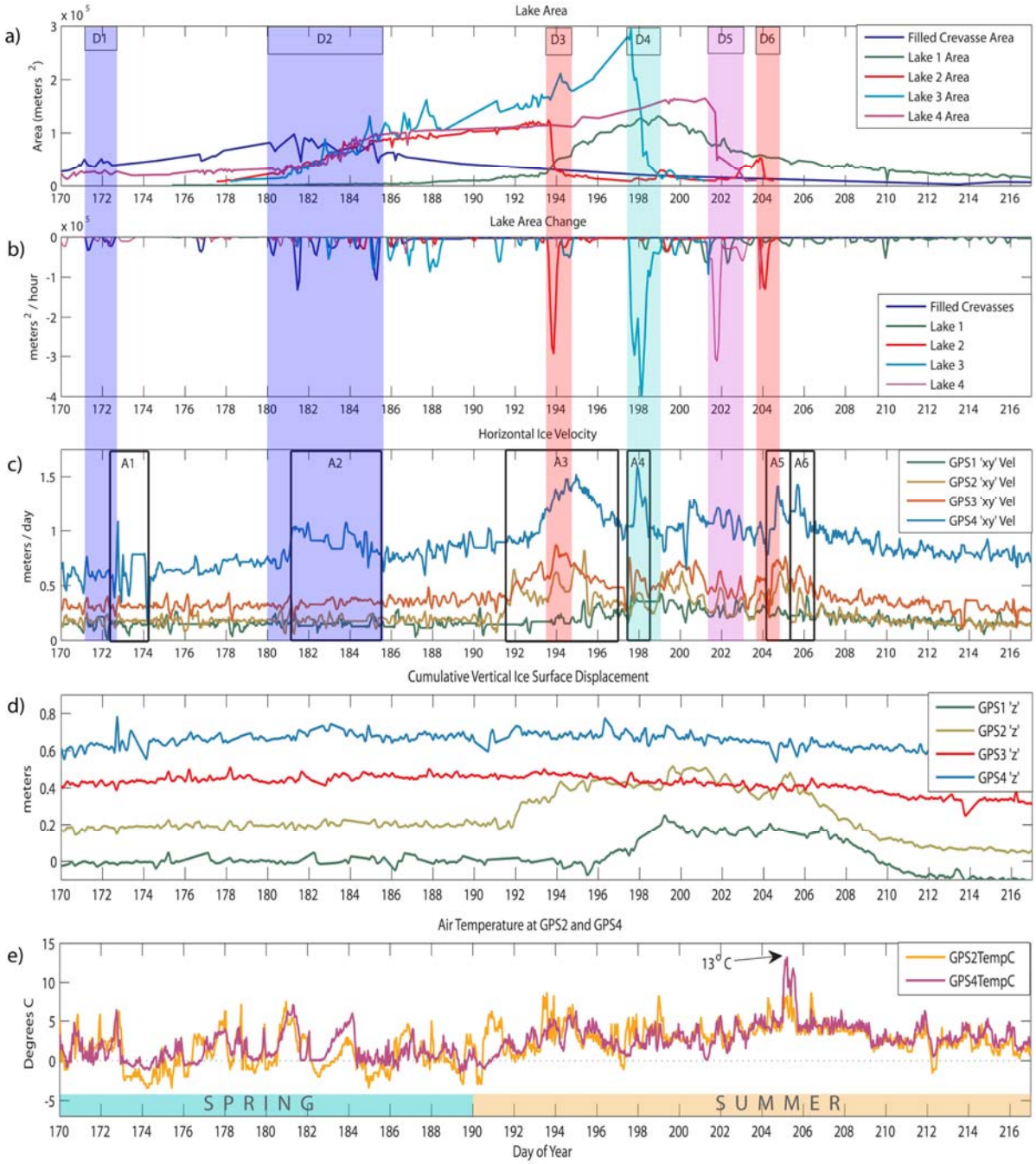

Figure 2-4: Lake Area, GPS, and Temperature time series, plotted on the same time axis. a) Area of four lakes and water-filled crevasse region, measured from time lapse photography. b) Lake Area Change Rate – our proxy for net drainage rate. Vertical shaded boxes delimit Drainage Events (D1-D6) and are color coded to corresponding lakes. c) Horizontal (xy) ice velocity measurements from four GPS stations. See Figure 2-1 for GPS locations. Black-outlined boxes delimit Acceleration Events (A1-A6), which are referred to in the text. d) Cumulative change in ice surface elevation, relative to day 170, after correction for down-slope motion. The GPS2, GPS3, and GPS4 time series have been offset by 0.2, 0.4, and 0.6 m, respectively, to improve viewing. e) Air temperature measurements co-located with two of the above GPS stations.

simultaneously accelerated again, and velocity at GPS4 continued to climb. During this second episode of acceleration, GPS3 recorded its highest velocities in 2009 (0.87 m d^{-1}) and GPS4 its second highest (1.52 m d^{-1}). Velocity peaked at GPS2 (0.82 m d^{-1}) on day 195. Event A3 concluded at the beginning of day 197, when the velocities at GPS2, GPS3 and GPS4 returned to pre-A3 velocity. GPS3 and GPS4 did not show significant variation in vertical ice motion during this event.

Near the end of event A3, day 195.5 (July 14), when GPS2 velocity fell rapidly, horizontal and vertical velocities at GPS1 began to vary. Vertical uplift of ice at GPS1 increased gradually from day 195.5 to peak at day 199.2 (July 18). During this 88 hr period, GPS1 horizontal velocity accelerated above its pre-summer mean, and fluctuated several times, often broadly coincident in time with velocity at GPS2. Between day 201 and 204 (July 20-23) both GPS1 and GPS2 exhibited distinct diurnal velocity fluctuations, accompanied by vertical motion undulations, that coincided with diurnal air temperature variations in the same area. The ice remained elevated until the surface at GPS2 began to fall on day 205.5. Lowering followed at GPS1 on day 206.8. The ice surface elevation at both stations returned to the pre-uplift elevation by day 210. These events can be seen in Figure 2-4, and are enlarged in Figure 2-5.

Acceleration event A4 (day 197.3 – 198.5 (July 16-17)) was rapid and led to the fastest ice flow rates measured in the 2009 GPS4 time series (1.59 m d^{-1}). Acceleration also occurred at GPS3 at this time, though ice velocity did not exceed the peak reached during event A3. This short duration event concluded when the velocities at GPS3 and GPS4 returned to pre-A4 values. Air temperature was cooling slightly at the initiation of event A4.

Acceleration event A5 (day 204.3 – 205.3 (July 23-24)) involved rapid and near-simultaneous acceleration of ice at GPS4 and GPS3, followed by acceleration at GPS2 ~1 hour later. Velocities at GPS4 and GPS2 peaked rapidly and then began to fall, while velocity at GPS3 remained elevated for nearly the

full duration of the event. This event began ~12 hours before the onset of an extreme positive temperature anomaly (up to 13 ^{o}C) on day 205 (July 24).

Acceleration event A6 (day 205.3 – 206.1 (July 25-26)) immediately followed event A5. At GPS4, the peak velocities recorded during events A5 and A6 were roughly the same, while GPS3 and GPS2 recorded lower velocities during event A6.

2.6.2 Melt Water Storage and Drainage Events

The collection of water-filled crevasses near the glacier terminus was the first supra-glacial reservoir to fill and drain. This area of the glacier (the lower ~5 km) is very heavily crevassed, with crevasses running roughly perpendicular to the glacier flow direction. However they are not long, straight fissures; these crevasses have been curved and contorted by ice flow, such that the crevasse mouths form openings of various widths (up to ten meters across), and lengths (tens to hundreds of meters). Available satellite and photographic imagery shows that the network of drainage channels visible on the ice surface in the upper- and mid-glacier regions is progressively destroyed as the ice is advected into the terminus region and becomes more crevassed. This makes surface drainage inefficient in this region of the glacier, and we observed meltwater collecting in crevasse mouths over a wide area (see Figure 2-2), with no obvious routes for evacuation over the surface.

Although it is plotted in Figure 2-4(a) as a single aggregated melt water storage reservoir, the 'Filled Crevasse Area' is actually a collection of many small, unconnected ponds that fill and drain independently of each other. None of these crevasse ponds individually formed a large lake, but they covered a total area comparable to that of Lake1. As described in the Methods section, it is not possible to estimate the volume using the SPIRIT DEM.

The two most active phases of crevasse pond drainage (D1 and D2), occurred from day 171.2 – 172.6 (June 20-21) and day 180.1 – 185.4 (June 29 – July 4). D1 consisted of two pulses of drainage over ~34 hours, and D2 consisted

of six drainage pulses over five days. (These drainage pulses are bounded within the blue boxes marking events D1 & D2 in the Lake Area Change plot of Figure 2-4.) During each of these periods, the time-lapse imagery showed multiple individual crevasses fill with water and then drain rapidly. Because the total area of these crevasse ponds was aggregated, the rapid changes that occurred at individual crevasses appear as a few discrete drainage pulses in the plot of Lake Area Change.

Drainage event D3 occurred between day 193.5 – 194.7 (July 12-13) when Lake 2 became the first of the large lakes to drain. The majority of the lake drained in the first 4 hours of the event, leaving a small remnant lake which continued to decrease in size over several more hours. It is difficult to identify a single crevasse or moulin that may have been responsible for draining the lake. The lake basin lay directly below an icefall and numerous large crevasses were visible in the area. The only visible surface drainage channels lead into the lake basin from up-glacier, and none appear to flow out, probably because there is a slight topographic rise just down-glacier of the lake basin.

Drainage event D4, on day 197.3 – 199.1 (July 16-18), involved the rapid, complete drainage of Lake 3, the largest of the lakes observed in this study. The timeseries of Lake 3 Area Change shows that drainage of this lake began very rapidly, slowed briefly, and then continued rapidly, emptying most of the lake within 14 hours. The time-lapse photography revealed several large, deep crevasses within the lake basin immediately after drainage.

Drainage event D5 occurred from day 201.4 – 203.2 (July 20-22), when Lake 4 drained rapidly, leaving water in only the deepest part of its basin. The time-lapse imagery shows that this lake did not drain across the glacier surface. This lake is very close to the lateral margin of the glacier, and its down-glacier end lies in a deep trench formed along a medial moraine. A large crevasse extending from the edge of the glacier intersects this trench, and provides the only indication visible on the surface of a potential englacial drainage route.

Drainage event D6 occurred after Lake 2 partially refilled around day 202 (July 21) and then drained rapidly between day 203.9 – 204.6 (July 22-23). This second drainage of Lake 2 left no remnant lake behind.

The drainage of Lake 1 was not identified as a specific event, as it is very different from the crevasse pond drainages (D1 & D2) and the rapid lake drainages (D3 - D6) described above. This lake filled in approximately 18 days, and drained slowly over a similar time period. Maximum size was reached on day 198 (July 17). We examined the time-lapse imagery from this date, and noticed that water in the lake drained through a snow-dam that had filled a pre-existing, incised drainage channel that intersected the southern margin of the lake basin. The breach of this snow-dam resulted in the first significant drainage pulse that can be seen in the Lake 1 area change timeseries on day 198 (see Figure 2-5). The next day, a second parallel channel developed, and the flow of water leaving the lake increased slowly as water flow progressively enlarged and deepened the supra-glacial channels. However, these channels did not become deep enough to rapidly or completely drain the entire basin. The Lake 1 area change timeseries demonstrates that the lake decreased in size during the coldest parts of the day, and grew during the warmest parts of the day, when the rate of meltwater influx matched or exceeded the rate of outflow from the drainage channels. For this reason, the drainage of Lake 1 appears as a series of small drainage pulses, the first 8 of which occur with approximately 24 hour periodicity.

Observations of the glacier's surface drainage system, from satellite imagery, field photography (from aircraft and from cliffs overlooking the glacier) and ground survey during the 2008 melt season (Duncan, 2011) show that the outflow from Lake 1 drains into a large moulin roughly 5 km from the lake, and 1.5 km west of GPS1 (moulin location shown on Figure 2-1).

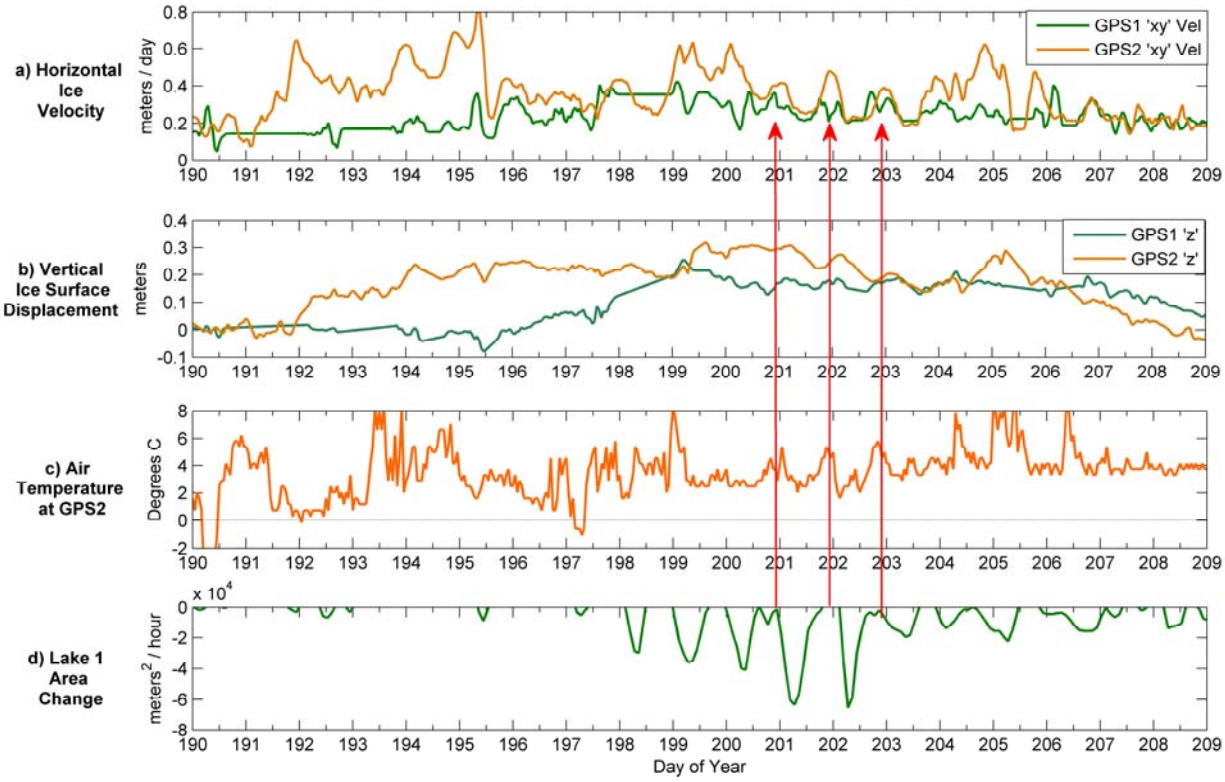

Figure 2-5: Enlarged view of events from day 190 to 209. a) Horizontal Ice Velocity at GPS1 and GPS2. b) Vertical Ice Surface Displacement at GPS1 and GPS2, corrected for down-slope motion. c) Air Temperature at GPS2. d) Lake 1 Area Change. The red arrows highlight the apparent synchronization of events in all four timeseries.

2.7 Discussion

Examination of the summer 2009 horizontal ice velocity time series and air temperature measurements supports the hypothesis that variations in meltwater production and delivery drive ice flow variability. During the 'summer' period, air temperature demonstrates general covariance with ice velocity and, in some instances, short-term variations in ice velocity were generally coincident with diurnal temperature variations. However, some of the ice velocity variations (including the most rapid acceleration events observed) cannot be explained as a simple function of variable surface meltwater production. Instead, we suggest that several of these ice acceleration events are driven by supra-glacial lake drainage.

2.7.1 Lake Drainage Typology

Based on the results presented above, we identify three mechanisms for the drainage of supra-glacially stored water:

Type 1 (Crevasse Pond Drainage): Large crevasses fill with water forming a region of small, discontinuous ponds. Lack of visible surface drainage routes and rapid, asynchronous drainage of individual crevasse ponds suggests the crevasses empty via their bottoms.

Type 2 (Slow Lake Drainage): Supra-glacial lake overfills its basin. Net storage ceases and net drainage occurs as water spilling out of the lake progressively erodes larger surface channels. Drainage rate is similar to filling rate (on the order of $10^2 – 10^3$ m^3 hr^{-1}, over multiple days), and incomplete drainage may leave a remnant lake in the deepest part of the basin.

Type 3 (Fast Lake Drainage): Supra-glacial lake drains via a crevasse or moulin opening within the lake basin. Drainage is complete and rapid (on the order of 10^4 m^3 hr^{-1}, for less than 2 days).

To clarify, our use of the term 'slow drainage' here does not indicate an insignificant rate of meltwater drainage. The slow and fast drainage rates may be one or two orders of magnitude apart, but either drainage rates would be sufficient to sustain crevasse fracture propagation to the glacier bed, and/or overcome rates of refreezing in cold-ice conduits, according to the findings of van der Veen (2007).

In the sections below, we describe how the observed drainage events and associated ice acceleration events fit within this typology.

2.7.2 Type 1: Crevasse Pond Drainage

Drainage of the crevasse ponds (events D1 and D2) was associated with localized acceleration of the terminus area of the glacier (events A1 and A2), well

before any of the ice up-glacier had accelerated beyond the stable late-winter/early-spring flow velocity.

2.7.2.1 Events D1 & A1

Approximately 26 hrs after initiation of crevasse pond drainage event D1, ice acceleration and uplift (event A1) are seen in the GPS4 timeseries. The ice velocity during this event has a multi-peak pattern, similar to that of pond area change rate during event D1. The delay between the onset of drainage and ice acceleration could suggest that these are unrelated events. However, since this is the first drainage event of the year, the delay may instead indicate that water draining from crevasse ponds required some time to establish drainage routes through the thick ice in this region.

A previous investigation of the Belcher Glacier terminus region (Milne, 2011), utilized bathymetric mapping of the bay in front of the glacier and an ice thickness profile parallel to the terminus measured by airborne radio echo sounding, to assess whether the glacier front was floating. The bathymetry data revealed that the glacier encountered deep water (~220 m) along a ~1000 m wide medial segment of the terminus. Milne (2011) showed that the hydrostatic pressure exerted by the sea water across this section of the terminus would likely generate negative subglacial effective pressure in an area extending less than 500m up-glacier from the margin. As GPS4 was placed along the glacier centerline ~500m from the ice margin, it would have been located on the edge of this narrow band of ice that is potentially at or near the floating point. Because of the very low (close to negative) effective pressure at the glacier bed in this region, relatively small inputs of meltwater drainage could potentially increase ice-bed separation and cause measureable changes in basal sliding.

The ice uplift and speed-up at GPS4 following event D1 is consistent with the assertion that a hydraulic connection was made to the glacier bed and a brief spike in water pressure resulted in temporary ice-bed separation. Immediately after this acceleration event, both the ice velocity and ice surface elevation briefly decreased, and then returned to pre-event velocity and elevation. This rapid

reorganization of flow speed and surface elevation suggests that ice encountered momentary friction at the bed as the water supplied from the crevasse ponds was evacuated from the region, and subglacial water pressure renormalized. If evacuated water formed a meltwater plume at the front of the glacier at this time, we were unable to see it because of remaining sea ice cover.

Vertical ice surface motion could also have been caused by ice flowing over an obstacle at the glacier bed. We do not have sufficiently detailed information on bed topography to rule out the existence of bedrock undulations; however, it seems unlikely that roughness at the glacier bed could be expressed on the glacier surface over the horizontal distance of ~1.18 m traversed by GPS4 during event A1. Alternatively, the observed uplift and subsidence could have been due in part to varying rates of longitudinal strain and associated vertical extension of the ice, caused by the rapid localized velocity anomalies at GPS4 in relation to the surrounding ice.

2.7.2.2 Events D2 & A2

The second sequence of crevasse pond drainage, event D2, began on day 180, and a clear acceleration of ice flow (event A2) is apparent in the GPS4 time series within ~18 hrs. Ice velocity dropped to near the pre-acceleration velocity within hours of the cessation of the last drainage pulse in D2. (See Figure 2-4)

D2 involved many crevasse ponds distributed over a ~1.5 km^2 area. Some of these crevasses drained for the first time during D2, though some may have drained during D1 and refilled if their exit conduits resealed. Several periods of freezing temperatures occurred between events D1 and D2, which would have reduced meltwater production and flux into established drainage conduits, perhaps allowing them to close via creep closure and refreezing. At the beginning of D2, the shorter delay (relative to event D1) between the initiation of drainage and ice acceleration suggests that the englacial drainage routes between the surface and subglacial drainage systems in this region were quickly re-established. Alternatively, the shorter delay may have been the result of the greater number of

water-filled crevasses (and thus higher water volume) that drained during event D2.

Compared to event A1, very little vertical motion was observed at GPS4 during event A2, which is superimposed on a longer term gradual acceleration at GPS4 that began after A1 and continued through A3. This gradual speedup of already fast-flowing ice in the lower glacier region would have increased longitudinal extension and the associated ice thinning and may have obscured transient vertical uplift. In general, neither GPS4 nor GPS3 demonstrate significant vertical surface motion during any of the subsequent horizontal acceleration events, while GPS2 and GPS1 show clear vertical uplift during the period of peak meltwater production and runoff (as indicated by air temperature). Both GPS3 and GPS4 are located on areas of the glacier with very steep surface gradients, as compared to the nearly flat surfaces at GPS1 and GPS2. It is possible that subtle vertical ice motion superimposed on the steep down-slope flow of ice is harder to detect at GPS3 and GPS4 than at the other GPS sites.

2.7.3 Type 2: Slow Lake Drainage

Type 2 drainage is exemplified by the drainage of Lake 1, which transitioned from a state of net storage to net drainage when drainage channels developed the capacity to remove water from the lake faster than influx from local melt production. The drainage channels emptying the lake connected to the existing supra-glacial drainage network, and the released lake water augmented the daily runoff into the nearest sink point.

During the initial drainage period of this lake (day 198 – 199 (July 17-18)), the ice in the vicinity of the moulin exhibited its maximum seasonal uplift and flow velocity (See GPS1 in Figure 2-5). Over the next 72 hours there appear to be coherent variations in lake area change, diurnal temperature, ice velocity, and glacier uplift rates at GPS1 and GPS2. (These events are marked by arrows in Figure 2-5.) However, although these events seem to be linked, it is not possible to separate the relative contributions to enhanced ice flow made by lake outflow

and runoff of daily meltwater production. The direct impact on ice velocity is not known.

2.7.4 Type 3: Fast Lake Drainage

Type 3 drainage is exemplified by Lakes 2, 3, and 4, which fill gradually over a period of many days to weeks and then drain in a few hours when a drainage conduit opens, leaving an empty basin or tiny remnant of the original lake. The drainage of Lake 3 and the secondary drainage of Lake 2 (events D4, and D6) had the most pronounced impacts on ice velocity, most notably in the terminus area, but also at GPS3. The drainage of these lakes appears to accelerate the ice to short-lived velocity peaks. However, the fast drainage of Lake 4 (event D5) made no apparent impact on ice flow, and during event D3, there was a complex relationship between the drainage of Lake 2 and the ongoing evolution of supra- and sub-glacial drainage connections.

2.7.4.1 Events D4 & A4

Event D4, the drainage of Lake 3, coincided with rapid ice acceleration at GPS3, followed by acceleration at GPS4. The fastest flow rates at GPS4 in 2009 (1.59 m d^{-1}) were recorded during this event, but peak velocity at GPS3 did not exceed the value reached during A3. Air temperature was decreasing at the beginning of event A4, so this acceleration event was probably not coincident with a sudden increase in meltwater production.

2.7.4.2 Event D6, A5 & A6

The extreme air temperature anomaly (+13 ^{o}C) on day 205 would have caused high rates of meltwater production. This meltwater would have been quickly routed to moulins via the surface drainage system that existed at this late stage in the melt season. Rapid delivery of runoff to the subglacial drainage system was the likely cause of acceleration event A6, but cannot explain event A5, which began 12 hours before the rise in air temperature. It is more likely that event A5 was triggered by D6, the final drainage of Lake 2. The peak rate of D6

lake area change coincided with the near-simultaneous acceleration of ice at GPS4 and GPS3 on day 204.

2.7.4.3 Event D5

Though event D5 was the second largest drainage event observed, drainage of Lake 4 did not cause noticeable flow acceleration at either of the nearest GPS stations (GPS3 and GPS4). Indeed, ice velocity was decreasing gradually during event D5. We have been unable to determine how water drains from this lake. However, a large crevasse that connects to the down-glacier end of the lake basin presents the possibility that this lake may drain towards the glacier margin, and may not deliver water to the central region of the glacier.

2.7.4.4 Events D3 & A3

Acceleration event A3 began before drainage event D3, but velocities recorded at GPS2, GPS3, and GPS4 peaked after D3. The following evidence suggests that the lake drainage did not trigger this acceleration event, but may have enhanced it. Day 190 marked the beginning of a one week warm period when air temperatures remained consistently above freezing. Snowpack diminished progressively, revealing bare glacier ice, and the resulting reduction in surface albedo would have contributed to higher melt rates. Time-lapse imagery shows the occurrence of a slush-flow in the vicinity of GPS3, and the development of surface drainage channels along the entire mid- and upper-glacier. All lakes observed on the glacier, except the crevasse ponds, grew during this period. Event A3 began at GPS2 on day 191.1, and then spread progressively down-glacier; GPS3 began to accelerate at day 191.6, and GPS4 at day 193.2. We interpret this period of flow acceleration as a 'spring event' (Röthlisberger and Lang, 1987), brought on by high rates of melt water production and the connection of many surface drainage channels to moulins and crevasses.

The ice surface uplift recorded at GPS2 early on day 192 may have been caused partly by longitudinal compression and vertical extension, since at that time, velocity at GPS2 was temporarily higher than velocity down-glacier at GPS3. (See Figure 2-4 c & d) However this cannot explain why the surface

remained elevated and continued to rise when the down-stream ice began flowing faster later in the day. Thus the ice uplift associated with acceleration at GPS2 more likely indicates ice-bed separation in response to the injection of surface melt water into the subglacial drainage system.

At day 193.3, GPS3 decelerated to ~0.6 m d^{-1}, while GPS4 continued to accelerate (See Figure 2-4). The ice between GPS3 and GPS4, already undergoing extensional strain, would have temporarily experienced increased rates of longitudinal strain. Lake 2 is located in the zone between GPS3 and GPS4, and it is plausible that increased longitudinal stretching of the ice in this region caused the opening of crevasses, leading to the drainage of Lake 2. Lake 2 began draining on day 193.5, and peak lake area change rate (our proxy for net drainage rate) occurred at day 193.9. Peak velocity was recorded at GPS3 two hours later, at day 194.0, and at GPS4 on day 195.0, seven hours after Lake 2 ceased draining at day 194.7. Following these peaks, velocity fell gradually at both GPS3 and GPS4 , returning to pre-A3 values by day 197. Air temperature also began decreasing after day 195, briefly returning to 0^{o}C in the mid-glacier region on day 197, which would have decreased meltwater production rates.

The enhanced ice velocity recorded during event A3 seems to be a response to the combined influence of increased surface runoff and stored meltwater gaining access to the subglacial drainage system. While the event began as a 'spring event', the rapid injection of water from Lake 2 (~366,400 ± 32000 m^3) into the subglacial drainage system likely contributed to the peak velocities and/or duration of acceleration event A3.

2.7.5 Impact on Seasonal and Annual Ice Displacement

To understand how the lake drainage induced acceleration events affect the total flow of the glacier, we focus further attention on the terminus region. Ice displacement measured in the terminus region provides a good indication of the dynamic flux of a tidewater glacier. Our GPS4 measured ice displacement along the centerline and within ~500 m of the glacier margin – the fastest flowing region of the glacier.

The locations of the lakes and the relative timing of their drainage likely influenced the impact that drainage events had on the subglacial drainage system and in stimulating accelerated ice flow in the terminus region. The crevasse pond drainage events that we observed occurred very close to the glacier terminus, a region potentially close to flotation, and occurred very early in the melt season, before highly developed drainage routes had evolved. This combination of factors allowed a relatively small volume of meltwater drainage to perturb a poorly developed subglacial drainage system, resulting in a measurable response in ice flow localized to the terminus region. In extreme contrast, the slow drainage of Lake 1 occurred far up-glacier, late in the melt season when a highly developed subglacial drainage system was efficiently evacuating high volumes of ongoing melt. While there may have been some localized effect, there was negligible impact on ice flow acceleration in the terminus region. By comparison, the fast lake drainages that we observed occurred in the mid- or late melt season, when some form of subglacial drainage system was already in place, and occurred in the lower-mid glacier. Only some of these events (i.e. D4 and D6) were sufficiently rapid and appropriately located to generate short-term hydrologic perturbations and stimulate measureable ice acceleration near the terminus.

The total ice displacement at GPS4 during the high velocity events (A1, A2, A4, A5) that we believe were driven by drainage events (D1, D2, D4 and D6), was 7.98 ± 0.14 m. However, the displacement resulting from ice velocity in excess of the background rate (i.e. the mean pre- and post-event velocity) during these events was only 1.34 ± 0.14 m. For comparison, the excess displacement resulting from the 'spring event' (event A3) was 1.08 ± 0.14 m. The summer displacement (in excess of the mean winter flow rate of ~0.6 m d^{-1} at GPS4) that occurred between days 172 – 217, was 14.70 ± 0.14 m. The total annual ice displacement was 239.2 ± 0.1 m [†] (May 2009 – May 2010).

[†] This figure has been updated from the published version of this paper to reflect the correction of an error in the total annual displacement calculation.

In summary, the additional ice displacements produced by the lake events, the spring event, and the total summer accelerated flow represent, respectively, 0.6%, 0.5%, and 6.1% [‡]of the annual ice displacement near the glacier margin. However, it is difficult to meaningfully isolate these events, which are all part of the larger pattern of seasonal melt-enhanced ice flow. The drainage of crevasse ponds early in the melt season and of larger lakes in the mid-melt season, likely served to initiate and enhance the overall seasonal melt-water induced acceleration by opening connections between the surface and subglacial drainage networks. The prime example was event D3: while it was difficult to determine the immediate ice response to this single perturbation, it almost certainly played a role in enhancing the spring event that was observed along the entire glacier.

2.8 Conclusion

We have presented a new method for determining and monitoring the morphology of a supra-glacial lake from time-lapse photography of a glacier surface. This has allowed us to estimate the area change rates (a proxy for net filling and drainage rates) of several lakes for which we have no other hydrological measurements. The photogrammetric methods we have employed are somewhat coarse and the results could be improved if ground control points were collected within the area covered by each camera view during the period of measurement. Lake areas derived using our lake identification and photogrammetry procedures are within 14% of those found by manually digitizing the outline of the same lake in remotely sensed imagery. These results are acceptable for the purpose of determining the timing and relative magnitude of supra-glacial lake drainage events, and demonstrate what can easily be accomplished using oblique terrestrial photography.

[‡] These figures have been updated from the published version of this paper to reflect the correction of an error in the total annual displacement calculation.

A typology of lake filling/drainage styles has been defined, and can be linked to modes of ice velocity variability. Type 3 rapid lake drainages contribute to rapid, short duration increases in glacier velocity. The observed link between these events is consistent with the hypothesis that drainage of some supra-glacial lakes can quickly inject large volumes of water into the subglacial drainage system, raising subglacial water pressure and promoting ice flow acceleration.

The lake driven rapid ice flow events observed here constitute approximately 10% of the summer enhanced ice displacement, or 0.6% of the total annual ice displacement, as measured near the glacier terminus. This figure may understate the significant impact that lake drainages, particularly those early in the melt season, may have on driving open conduits, priming the subglacial drainage system, and initiating seasonally enhanced velocity.

2.9 Endnotes

[1]Additional notes on alternative color spaces

We converted all time lapse images from RGB color space into the following alternative color spaces.

HSV Color Space

Hue (H): contains the "color" information. Hue values (0.0 – 1.0) map to a color wheel ranging through ROYGBIV.

Saturation (S): represents the intensity or purity of a color. 0 would produce a grey pixel, while 1.0 pure, unmixed colors.

Value (V): contains the Brightness information of each pixel. 0 is no-brightness (Black) and 1.0 is full brightness.

L*a*b* Color Space

L* dimension: Luminance on a black-to-diffuse white axis.

a* dimension: chromaticity, indicating where color falls along the red-green axis.

b* dimension: chromaticity, indicating where color falls along the blue-yellow axis.

These conversions allowed brightness information to be isolated in the 'V' and 'L*' layers while 'H', 'a*' and 'b*' (and optionally 'S') layers were used as criteria for assessing class membership.

Documentation on the above color space definitions is available in the following electronic articles by G. Hoffmann, available online:

"CIELab Color Space." (http://www.fho-emden.de/~hoffmann/cielab03022003.pdf)

"Color Models: RGB / HLS / HSB." (http://www.fho-emden.de/~hoffmann/hlscone03052001.pdf)

Bibliography

Ahn, Y. and J. E. Box 2010. Glacier velocities from time-lapse photos: technique development and first results from the Extreme Ice Survey (EIS) in Greenland. *Journal of Glaciology* **56**(198), 723-734.

Amundson, J. M., M. Fahnestock, M. Truffer, J. Brown, M. P. Lüthi and R. J. Motyka 2010. Ice mélange dynamics and implications for terminus stability, Jakobshavn Isbræ, Greenland. *J. Geophys. Res.* **115**(F1), F01005.

Bartholomaus, T. C., R. S. Anderson and S. P. Anderson 2008. Response of glacier basal motion to transient water storage. *Nature Geoscience* **Vol 1**(Number 1), 33-37.

Bingham, R. G., P. W. Nienow, M. J. Sharp and L. Copland 2006. Hydrology and dynamics of a polythermal (mostly-cold) High Arctic glacier. *Earth Surface Processes and Landforms* **31**, 1463-1479.

Boon, S. and M. Sharp 2003. The role of hydrologically-driven ice fracture in drainage system evolution on an Arctic glacier. *Geophysical Research Letters* **30**(18).

Box, J. E. and K. Ski 2007. Remote sounding of Greenland supraglacial melt lakes: implications for subglacial hydraulics. *Journal of Glaciology* **53**(181), 257-265.

Burgess, D. O. and M. J. Sharp 2004. Recent changes in areal extent of the Devon Ice Cap, Nunavut, Canada. *Arctic, Antarctic, and Alpine Research* **36**(2), 261-271.

Burgess, D. O., M. J. Sharp, D. W. F. Mair, J. A. Dowdeswell and T. J. Benham 2005. Flow dynamics and iceberg calving rates of Devon Ice Cap, Nunavut, Canada. *Journal of Glaciology* **51**(173), 219-230.

Chapuis, A., C. Rolstad and R. Norland 2010. Interpretation of amplitude data from a ground-based radar in combination with terrestrial photogrammetry and visual observations for calving monitoring of Kronebreen, Svalbard. *Annals of Glaciology* **51**, 34-40.

Copland, L., M. J. Sharp and P. W. Nienow 2003. Links between short-term velocity variations and the subglacial hydrology of a predominantly cold polythermal glacier. *Journal of Glaciology* **49**(166), 337-348.

Corripio, J. G. 2004. Snow surface albedo estimation using terrestrial photography. *International Journal of Remote Sensing* **25**(24), 5705-5729.

Das, S. B., I. Joughin, M. D. Behn, I. M. Howat, M. A. King, D. Lizarralde and M. P. Bhatia 2008. Fracture propagation to the base of the Greenland Ice Sheet during supraglacial lake drainage. *Science* **320**(5877), 778-781.

Dowdeswell, J. A., R. P. Bassford, M. R. Gorman, M. Williams, A. F. Glazovsky, Y. Y. Macheret, A. P. Shepherd, Y. V. Vasilenko, L. M. Savatyuguin, H. W. Hubberten and H. Miller 2002. Form and flow of the Academy of Sciences Ice Cap, Severnaya Zemlya, Russian High Arctic. *Journal of Geophysical Research-Solid Earth* **107**(B4).

Dowdeswell, J. A., T. J. Benham, M. R. Gorman, D. Burgess and M. J. Sharp 2004. Form and flow of the Devon Island Ice Cap, Canadian Arctic. *Journal of Geophysical Research-Earth Surface* **109**(F2).

Dowdeswell, J. A., T. J. Benham, T. Strozzi and J. O. Hagen 2008. Iceberg calving flux and mass balance of the Austfonna ice cap on Nordaustlandet, Svalbard. *Journal of Geophysical Research* **113**(F3), F03022.

Duncan, A. 2011. Spatial and Temporal Variations of the Surface Energy Balance and Ablation on the Belcher Glacier, Devon Island, Nunavut, Canada. (*MSc. Thesis*, University of Alberta.)

Gardner, A. and M. Sharp 2009. Sensitivity of net mass-balance estimates to near-surface temperature lapse rates when employing the degree-day method to estimate glacier melt. *Annals of Glaciology* **50,** 80-86.

Gardner, A. S., G. Moholdt, B. Wouters, G. J. Wolken, D. O. Burgess, M. J. Sharp, J. G. Cogley, C. Braun and C. Labine 2011. Sharply increased mass loss from glaciers and ice caps in the Canadian Arctic Archipelago. *Nature* **473**(7347), 357-360.

Herdes, E., L. Copland, B. Danielson and M. Sharp 2012. Relationships between iceberg plumes and sea-ice conditions on northeast Devon Ice Cap, Nunavut, Canada. *Annals of Glaciology* **53**(60) 1-9.

Herring, T. A., R. W. King and S. C. McClusky 2006. Documentation of the GAMIT GPS Analysis Software (Release 10.3), Massachusetts Institute of Technology. **:** 182.

Humphrey, N. and C. F. Raymond 1994. Hydrology, erosion and sediment production in a surging glacier; Variegated Glacier, Alaska, 1982-83 *Journal of Glaciology* **40**(136), 539-552.

Iken, A. 1972. Measurements of water pressure in moulins as part of a movement study of the White Glacier, Axel Heiberg Island, Northwest Territories, Canada. *Journal of Glaciology* **11**(61), 53-58.

Iken, A. and R. A. Bindschadler 1986. Combined measurements of subglacial water pressure and surface velocity of Findelengletscher, Switzerland: conclusions about drainage system and sliding mechanism. *Journal of Glaciology* **32**(110), 101-119.

Iken, A., H. Rothlisberger, A. Flotron and W. Haeberli 1983. The uplift of Unteraargletscher at the beginning of the melt season — a consequence of water storage at the bed? *Journal of Glaciology* **29**(101), 28-47.

Jakobsson, M., R. Macnab, L. Mayer, R. Anderson, M. Edwards, J. Hatzky, H. W. Schenke and P. Johnson 2008. An improved bathymetric portrayal of the Arctic Ocean: Implications for ocean modeling and geological, geophysical and oceanographic analyses. *Geophys. Res. Lett.* **35**(7), L07602.

Joughin, I., S. B. Das, M. A. King, B. E. Smith, I. M. Howat and T. Moon 2008. Seasonal speedup along the western flank of the Greenland Ice Sheet. *Science* **320**(5877), 781-783.

Korona J., Berthier E., Bernard M., Rémy F. & Thouvenot E. SPIRIT. SPOT 5 stereoscopic survey of Polar Ice: Reference Images and Topographies during the fourth International Polar Year (2007-2009). *ISPRS Journal of Photogrammetry and Remote Sensing*, 64, 204-212, doi:10.1016/j.isprsjprs.2008.10.005, 2009

Krimmel, R. M. and L. A. Rasmussen 1986. Using sequential photography to estimate ice velocity at the terminus of Columbia Glacier, Alaska. *Annals of Glaciology* **8**, 117-123.

MacKay, D. 2003. Chapter 20. An example inference task: clustering, *ed. Information Theory, Inference and Learning Algorithms*, Cambridge University Press**:** 284-292.

MacQueen, J. (1967). Some methods for classification and analysis of multivariate observations. Fifth Berkeley Symposium on Mathematical Statistics and Probability, Berkley, California, University of California Press.

McClusky, S. 2010. GAMIT-GLOBK Home Page, http://www-gpsg.mit.edu/~simon/gtgk/.

Miller, R. D. and D. R. Crandell 1959. Time-lapse motion picture technique applied to the study of geological processes. *Science* **130**(3378), 795-796.

Milne, H. 2011. Iceberg calving from a Canadian Arctic tidewater glacier. (*MSc. Thesis*, University of Alberta.)

Motyka, R. J., L. Hunter, K. A. Echelmeyer and C. Connor 2003. Submarine melting at the terminus of a temperate tidewater glacier, LeConte Glacier, Alaska, U.S.A. *Annals of Glaciology* **36**(1), 57-65.

O'Neel, S. 2000. Motion and calving at LeConte Glacier, Alaska. (*MSc. Thesis*, University of Alaska.)

O'Neel, S., H. P. Marshall, D. E. McNamara and W. T. Pfeffer 2007. Seismic detection and analysis of icequakes at Columbia Glacier, Alaska. *J. Geophys. Res.* **112**(F3), F03S23.

O'Neel, S. E., Keith A.; Motyka, Roman J. 2003. Short-term variations in calving of a tidewater glacier: LeConte Glacier, Alaska, U. S. A. *Journal of Glaciology* **49**, 587-598.

Röthlisberger, H. and H. Lang 1987. Glacial Hydrology. In *Glacio-fluvial sediment transfer: an alpine perspective*. A. M. Gurnell and M. J. Clark, *ed.* Chichester, John Wiley and Sons**:** 207-284.

Selmes, N., T. Murray and T. D. James 2011. Fast draining lakes on the Greenland Ice Sheet. *Geophysical Research Letters* **38**(15), L15501.

Sneed, W. A. and G. S. Hamilton 2007. Evolution of melt pond volume on the surface of the Greenland Ice Sheet. *Geophysical Research Letters* **34**(3), L03501.

Sole, A. J., D. W. F. Mair, P. W. Nienow, I. D. Bartholomew, M. A. King, M. J. Burke and I. Joughin 2011. Seasonal speedup of a Greenland marine-terminating outlet glacier forced by surface melt induced changes in subglacial hydrology. *Journal of Geophysical Research* **116**(F3), F03014.

Sugiyama, S. and H. G. Gudmundsson 2004. Short-term variations in glacier flow controlled by subglacial water pressure at Lauteraargletscher, Bernese Alps, Switzerland. *Journal of Glaciology* **50**, 353-362.

Tedesco, M. and N. Steiner 2011. In-situ multispectral and bathymetric measurements over a supraglacial lake in western Greenland using a remotely controlled watercraft. *Cryosphere* **5**(2), 445-452.

van der Veen, C. J. 2007. Fracture propagation as means of rapidly transferring surface meltwater to the base of glaciers. *Geophysical Research Letters* **34**(1), L01501.

Van Wychen, W., L. Copland, L. Gray, D. Burgess, B. Danielson and M. Sharp 2012. Spatial and temporal variation of ice motion and ice flux from Devon Ice Cap, Nunavut, Canada. *Journal of Glaciology* **58**(210), 657-664.

Vieli, A., J. Jania, H. Blatter and M. Funk 2004. Short-term velocity variations on Hansbreen, a tidewater glacier in Spitsbergen. *Journal of Glaciology* **50**(170), 389-398.

Williamson, S., M. Sharp, J. Dowdeswell and T. Benham 2008. Iceberg calving rates from northern Ellesmere Island ice caps, Canadian Arctic, 19992003. *Journal of Glaciology* **54**, 391-400.

Chapter Three: Seasonal and inter-annual variations in ice flow of the Belcher Glacier, a High Arctic tidewater outlet glacier [§]

3.1 Introduction

Tidewater terminating glaciers comprise 47% (by area) of the 104,900km^2 of glaciers in the Canadian Queen Elizabeth Islands (QEI) (Gardner and others, 2013) . These glaciers have a dynamic mechanical mass loss component that is difficult to quantify accurately at regional scales. Mass loss due to iceberg calving can only be estimated for the small number of glaciers for which flow speed and ice thickness have been measured. The infrequency and scarcity of these measurements often necessitates that glacier flow rates and iceberg calving rates are assumed constant over multi-year time-scales when estimating regional total mass balance (Dowdeswell and others, 2002; Burgess and others, 2005; Dowdeswell and others, 2008; Gardner and others, 2011). However, a growing body of work has demonstrated that rates of mass loss from tidewater glaciers are non-constant through the year (Williamson and others, 2008; Howat and others, 2010) and that there can be year to year variability in glacier flow and iceberg calving flux (Williamson and others, 2008). To produce more refined estimates of net mass balance and assess the contribution to sea level change made by large glaciated regions such as the QEI, we need to account for the variability in iceberg calving discharge, which involves understanding tidewater glacier flow variability. The work described here is an investigation of ice cap outlet-glacier flow variability at seasonal and annual timescales using high temporal resolution field measurements of glacier velocity and supporting observations of local meteorology. The goal is to determine whether seasonal variations in flow

[§] A version of this chapter will be submitted for publication to the Journal of Glaciology as: Danielson, B.D., and M.J. Sharp. Seasonal and inter-annual variations in ice flow of a High Arctic tidewater outlet glacier.

contribute to changes in annual mean displacement, especially at the glacier terminus where these changes must be factored into calving flux estimates.

There are numerous observations of intra-annual ice velocity variations that follow the onset of strong melt conditions (Willis, 1995). Spring events (Iken and others, 1983; Röthlisberger and Lang, 1987) and more general summer velocity increases associated with the lubricating effect of surface meltwater penetrating to the ice-bed interface have been observed at temperate valley glaciers (Iken and Bindschadler, 1986; Mair and others, 2002), polythermal Arctic glaciers (Iken, 1972; Copland and others, 2003), and the margins of the GrIS, extending to and above the equilibrium line (Zwally and others, 2002; Andersen and others, 2011; Bartholomew and others, 2011b; Hoffman and others, 2011). Some studies have hypothesized that future climate warming will result in more widespread or greater seasonal acceleration of ice flow due to basal sliding (Zwally and others, 2002) leading to, for example, rapid down-wastage of the Greenland Ice Sheet (Parizek and Alley, 2004) if surface melting directly (and proportionately) impacts mean annual ice velocity.

However, an increase in mean surface melt alone is unlikely to cause a corresponding positive feedback on glacier velocity (Müller and Iken, 1973; Schoof, 2010). In a climate regime in which summers may be warmer and melt may begin earlier, much higher volumes of meltwater may be directed to the subglacial drainage system. While this would initially raise subglacial water pressure and lead to a spring event, the rapid, high-volume drainage may cause the correspondingly rapid development of an efficient channelized drainage system which could evacuate high volumes of meltwater, effectively lowering the subglacial water pressure over wide areas of the glacier bed, even if runoff rates remained consistently high (Fountain and Walder, 1998; Schoof, 2010). Reduced water pressure in sediments or cavities distributed across the glacier bed increases basal friction, resulting in lowered basal sliding rates as long as the drainage channels are able to keep pace with rates of meltwater drainage inputs. This concept has been supported by observations of ice velocity, melt rates, and

drainage system evolution along land-terminating sections of the GrIS (Bartholomew and others, 2010; Bartholomew and others, 2011a; Hoffman and others, 2011; Sundal and others, 2011; Cowton and others, 2013).

An alternative hypothesis is that meltwater drainage variability may have a greater impact on seasonally enhanced ice flow than a simple increase in mean runoff. This hypothesis suggests that high variability in both the rate and total volume of meltwater delivery can force a subglacial drainage system into a constant state of adaptation, leading to effective pressure changes that facilitate accelerated sliding (Bartholomaus and others, 2008; Schoof, 2010). While some recent studies employing high temporal-resolution GPS measurements of glacier flow speed have supported this hypothesis (Hoffman and others, 2011), most have not presented multiple years of observations to demonstrate inter-annual differences in seasonal acceleration patterns that might be the result of different summer melt conditions or patterns of meltwater drainage variability.

Tidewater glaciers may respond somewhat differently to seasonal fluctuations in meltwater inputs than land terminating glaciers. A comparison between flow speeds observed on land-terminating glaciers and fast-flowing tidewater glaciers along the south-western margins of the GrIS found that the seasonal melt induced speedup effect was relatively small on the tidewater glaciers (<10% to 15% change) compared to the speedups of land-terminating portions of the ice sheet (>50% change), and that this amounted to a very small percentage of the annual displacement of the outlet glaciers (Joughin and others, 2008). Instead, the velocity variations observed on the outlet glaciers were driven mainly by changes in the back-stress at the ice front and/or the stability of the floating glacier tongue. However, the outlet glaciers included in that study were all very fast flowing (>1000 m a^{-1}), and may be dynamically very different from the tidewater outlet glaciers found on the perimeters of smaller Arctic ice caps which typically flow an order of magnitude less rapidly (Williamson and others, 2008; Blaszczyk and others, 2009). Glacier mass turnover rates at QEI outlet glaciers are much lower than Greenland outlet glaciers, due in part to the more

continental climate setting and lower annual precipitation rates of the Canadian Arctic islands versus coastal Greenland. Ice cap outlet glaciers may be less sensitive to changes in the floating glacier tongue, and many of the slower glaciers (<100 m a^{-1}) have no floating tongue at all (Williamson and others, 2008). It is therefore possible that seasonal flow variations could comprise a relatively larger percentage of the annual ice displacement of ice cap outlet glaciers. Furthermore, even though the percentage of displacement change may be smaller for tidewater glaciers than land-terminating glaciers, the resulting ice flux produced at the terminus of tidewater glaciers will be large due to their generally high flow speeds.

A few recent studies have explored whether High Arctic ice cap outlet glaciers undergo seasonal velocity variations, whether these variations follow the alpine- or tidewater-style patterns observed elsewhere, and whether these variations are significant to annual ice displacement. At Hansbreen (southern Spitsbergen, Svalbard), short-term flow variations were observed using continuously operating GPS from the end of June to the end of July, 1999 (Vieli and others, 2004), and repeat optical surveys during the summer of 1998 (Vieli and others, 2000). Two short-term speedup events were observed in 1999, and were related to periods of enhanced surface melt or rainfall, during which increased water pressure was measured in a moulin. These speedups, each lasting 1-2 days, convinced the authors that Hansbreen acts much like a land-based alpine valley glacier in its response to short-term hydrologic inputs to the subglacial drainage system. At seasonal to annual scales, however, its flow speed was relatively constant. However, in northern Svalbard, velocity measurements from May 2008 to May 2010 along the centerlines of two tidewater outlets of the Austfonna ice cap showed different seasonal velocity patterns (Dunse, 2012). One of these glaciers doubled its flow speed between July and August, and then gradually slowed back down to a minimum flow speed that it reached the following June. The other glacier experienced multiple short-duration speedup events during the summer months, but continued flowing at a relatively constant

background velocity throughout the rest of the year. Dunse and others (2012) interpreted the differences in the observed velocity responses as products of the different geometries and bed properties of these two glaciers.

Here we report velocity observations from a fast-flowing ice cap outlet tidewater glacier, with a view to documenting the form of its annual velocity cycle. Specifically, we seek to answer the following questions:

1) Is there an annually consistent pattern of summer ice velocity change at this glacier?

2) How much interannual variability is there in the pattern of summer ice velocity changes, and can this variability be explained by differences in melt season characteristics?

3) Does the additional summer displacement (relative to what would be expected from mean annual velocity) constitute a significant fraction of the total annual ice displacement? Do variations in summer velocity translate into equivalent variations in annual velocity?

4) Are the summer velocity variations exhibited by this tidewater glacier similar to those seen on alpine or other land terminating glaciers, or does the unique geometry and hydrological regime of a tidewater glacier modulate the influence of meltwater drainage on seasonal velocity variations?

To answer these questions, we examined three years of velocity observations from a tidewater glacier in the Canadian High Arctic (see Figure 3-1). We used high-rate GPS methods to monitor the glacier flow velocity through the summers of 2008, 2009, and 2010. We also used automatic weather stations, air temperature loggers, and ablation stake measurements to estimate meltwater production on the glacier surface. The three melt seasons had distinctly different characteristics and we find that variations in initial spring conditions and the subsequent variability in summer air temperatures elicited different dynamic responses in glacier flow.

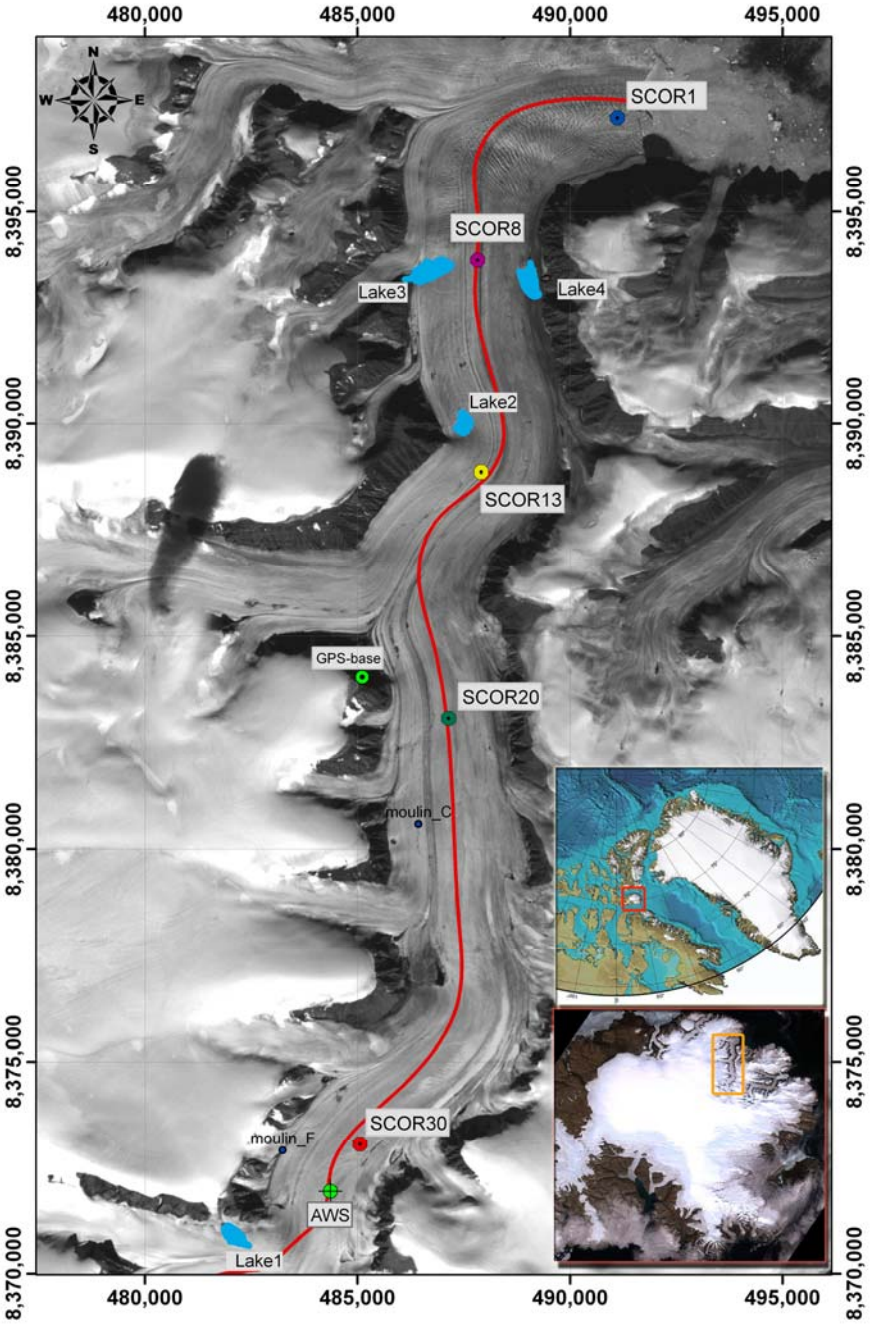

Figure 3-1: Landsat-7 image (August, 2000) of Belcher Glacier showing the SCOR GPS stations, AWS site, as well as Lakes and moulins noted in the text. The red line shows the transect where ice thickness and surface elevation were measured. Grid coordinates are in UTM zone 17X. Upper inset map shows Devon Island, which is part of the Canadian Arctic Archipelago. Devon Ice Cap (red box) is located at 75^{o} N, between 80^{o} and 90^{o} W. Map selected from the International Bathymetric Chart of the Arctic Ocean (Jakobsson and others, 2008). Lower inset image (also Landsat-7, August 2000) shows the location of Belcher Glacier in the NE quadrant of Devon Ice Cap.

3.2 Study Site

The study was conducted on Belcher Glacier, a ~40 km long tidewater outlet glacier that drains the north-east quadrant of the Devon Ice Cap, Nunavut, Canada. Two independent radar remote sensing assessments of iceberg calving rates estimated that Belcher Glacier accounted for ~42-50% of the total calving mass loss from the Devon Ice Cap (Burgess and others, 2005; Van Wychen and others, 2012).

Due in part to its significant role in the dynamic mass loss of the ice cap, Belcher Glacier has been the focus of the Canadian component of the GLACIODYN (IPY) project, an extensive field, remote sensing, and modelling study designed to understand the links between climate, hydrology and glacier flow dynamics. This study makes a contribution to that effort.

Figure 3-2 shows ice thickness and surface elevation measurements collected along the glacier centerline in 2005 by a NASA aircraft equipped with the University of Kansas Coherent Radar Depth Sounder Instrument (provided by S.P. Gogenini at the Center for Remote Sensing of Ice Sheets, University of Kansas) and NASA's Airborne Topographic Mapper (ATM) laser altimeter (provided by W. Krabill of NASA Wallops Flight Facility, Virginia, U.S.A.).

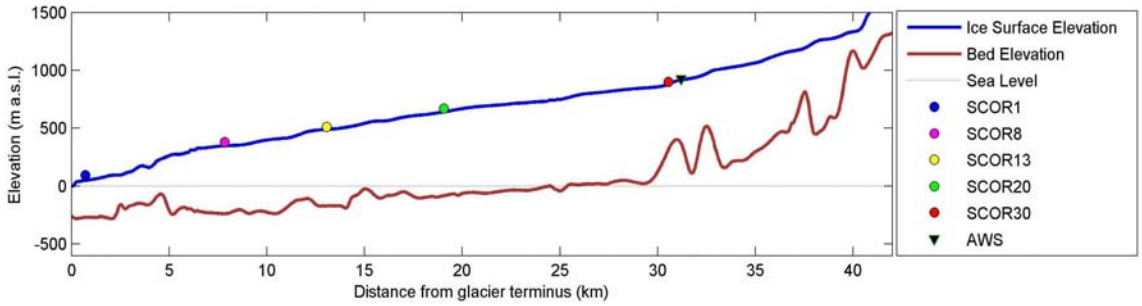

Figure 3-2: Profiles of the ice surface and bed elevations along the centerline of the Belcher Glacier (location of transect plotted in Figure 3-1). Data collected by NASA in 2005 as part of the IceBridge mission: Ice surface elevation (±10 cm) was measured with the Airborne Topographic Mapper (laser altimeter) and Ice thickness (±10 m) (which was used to calculate bed elevation) was measured with the University of Kansas Coherent Depth Sounder Instrument.

These measurements show that ice near the terminus is ~250 m thick, the ice is up to ~800 m thick in the mid-glacier region, and the glacier bed lies below sea level for up to ~20 km from the terminus. The glacier terminus is grounded, but close to flotation (Milne, 2011). As on many tidewater glaciers, ice flow rates increase towards the glacier terminus. Both satellite interferometric synthetic aperture radar (InSAR) (Burgess and others, 2005) and speckle tracking measurements (Van Wychen and others, 2012) show ice flow rates up to 250 m a^{-1} in the fast flowing terminus region, which are the highest rates anywhere on the glacier.

The ~5 km long region of fast flowing ice near the glacier terminus is extensively fractured by wide, deep crevasses that are easily visible in Landsat imagery (Figure 3-1). The damage sustained by ice advecting through this region likely plays a role in determining the types of icebergs produced by this glacier. Analysis of time lapse photography from the spring and summer of 2008 and 2009 revealed that the glacier produced predominantly small bergs at irregular intervals (Milne, 2011). Larger tabular icebergs were infrequently produced from a protruding bulge of ice that occasionally developed in the vicinity of the thickest ice at the glacier centreline (Milne, 2011). Icebergs produced throughout the winter formed a melange with sea ice at the glacier front, which was typically purged in a large plume around the time of sea ice breakup each year (within a week of July 15) (Herdes and others, 2012). Digital Globe imagery from June 2011 shows that the sea ice immediately in front of the terminus and ice melange was folded and fractured in response to the force exerted on it by the glacier (Milne, 2011). This suggests that the sea ice contributes to flow resistance of the glacier in winter, and may be an influence on summer flow velocity after breakup, though the magnitude of this effect has yet to be determined.

Individual fast flow events, such as those following lake drainage events (Danielson and Sharp, 2013), do not correlate strongly in time with distinct calving events (Milne, 2011). However, at annual time scales, variations in ice flow velocity must translate into variations in calving flux because the overall

position of Belcher Glacier's terminus is stable from year to year (Milne, 2011), and seems to have been so for as long as 50 years (Burgess and Sharp, 2004). This potential for dynamic variability in calving flux is the primary motivation for studying the seasonal and annual velocity variations of this glacier.

3.3 Data

3.3.1 Glacier Velocity Timeseries

We operated multiple Trimble dual-frequency (L1+L2) GPS receivers on Belcher Glacier from 2008 through 2010. One receiver was used as a differential base station and was installed on bedrock adjacent to the glacier, and the remainder were installed on the glacier surface along the centerline. GPS antennas were mounted on steel poles drilled into the glacier ice, while the receivers and power supplies were placed in enclosures at ice level. The antennae were typically installed 1 m above the ice surface in May, and due to surface melt were ~2-3 m above the surface by the end of August.

As a power saving strategy, we operated the GPS receivers in a continuous recording mode during 'summer' (May - August 2008 & 2009), and at a reduced duty cycle mode when we could not make return visits to maintain the power supplies (September – April 2008 & 2009, and all of 2010). In both cases, raw GPS observations were collected at a 15 second sampling rate. In the reduced duty-cycle mode, observations were collected in 1-hour long sessions every six hours, which allowed some of the stations to operate through the fall and early spring, though none operated during mid-winter (December – February). For this reason, we refer to these stations as Semi-Continuously Operating Receivers (SCOR). The locations of these stations are shown in Figures 1 and 2. The numeric identifier of each station indicates its approximate position along the centerline in kilometres up-glacier of the terminus. SCOR1, 20 and 30 were installed in 2008; SCOR13 and SCOR8 were added in 2009 and 2010 to increase the density of measurements in the lower glacier region.

We attempted to position SCOR1 within ~500 m of the glacier terminus to measure the ice velocity as close to the calving front as prudently possible. This required the station to be repositioned each year to ensure it would not be lost in a calving event. Due to the difficulty in finding a suitable installation site amongst the crevasses, the survey location is slightly different each year. In 2008, SCOR1 was closest to the terminus, but ~750 m south of the glacier centerline; in 2009 and 2010, we repositioned SCOR1 300-500 m further back from the terminus and closer to the centerline. Moving the station to a different area of ice could potentially impact the comparison of velocity results, as we would expect the ice closest to the centerline to flow fastest. However, examination of ice velocity fields across the terminus region (determined by InSAR and speckle tracking methods (Burgess and others, 2005; Van Wychen and others, 2012)) indicates that the whole ~1 km^2 zone of ice occupied by SCOR1 over these three years is fast-flowing, with no discernible longitudinal or transverse velocity gradient.

The data collected from summers 2008 and 2009 were differentially post-processed in kinematic mode using TRACK, the kinematic processing module associated with the GAMIT software (Herring and others, 2006; McClusky, 2010). All position estimates were filtered to remove any points with 2D horizontal 1-sigma distance root mean square (DRMS) errors greater than 0.05 m, or vertical 1-sigma errors greater than ±0.1 m.

The kinematic position estimates from each SCOR station were concatenated into time series which spanned each of the two summer melt seasons. Horizontal ice displacement was calculated as the Euclidean distance between sequential coordinates; horizontal ice velocity was calculated at each time-step using the average displacement over a 6-hour moving window to remove the effects of high-frequency noise. (The high-frequency component of the displacement signal may have included information about real ice motion events. We attempted to use frequency-domain analysis to detect small, semi-diurnal motion variations due to tidal forcing at the glacier terminus, but were unable to confidently resolve such motion from the background noise.) The

resulting time series were reduced to hourly-sampled series to facilitate comparison with our other time series datasets. We calculated the uncertainty (sum of squared DRMS errors) for all velocities in the summer 2008 and 2009 timeseries: the maximum 1-sigma uncertainty was ±0.07 m a^{-1} (the mean was ±0.036 m a^{-1}).

The shorter duration of each data file recorded by the SCOR stations during the reduced duty-cycle operation (i.e. Summer 2010) made it impossible to use the kinematic processing approach described above. Instead, we used a "segmented static" approach. Each 1-hour long file was post-processed to a single static point using Precise Point Positioning (PPP) methods (Kouba, 2000), that utilize corrected satellite clock and ephemeris data to derive centimetre-accuracy coordinates (we used the Canadian Spatial Reference System (CSRS) PPP online service operated by Natural Resources Canada). All position estimates generated by the PPP software were filtered such that points with 2D 1-sigma (DRMS) errors greater than 0.12m were discarded. This filtering resulted in a mean DRMS of 0.10 m for horizontal positions.

The resulting position timeseries were resampled at uniform 1-hour sampling rates for the purpose of time series analysis. Horizontal ice displacements and velocities were calculated as described above, except that a 12-hour moving average was used to reduce noise effects. We calculated the uncertainty (sum of squared DRMS errors) for all displacements in the summer 2010 timeseries: the maximum 1-sigma uncertainty was ±0.165 m (the mean was ±0.141 m).

CSRS analysis of PPP processing results from 24-hour long datasets demonstrate that ~7 cm accuracy in horizontal position can be expected with 1-hour of observations (Canada, 2004; Canada, 2007). To assess the horizontal accuracy of our dataset, we analyzed the long-term repeatability of position solutions from 1-hour observations collected at our bedrock reference station: 696 PPP solutions produced a dense point cloud with 92% of the points falling within ±0.05 m of the median position. This represents the best case scenario. However,

each 1-hour observation from our SCOR stations actually includes 1-hour of glacier motion; therefore the PPP "static" solution effectively averages this motion into the final position solution. This "quasi-static approach" (King, 2004) has been shown to incorporate erroneous motion signals into a position timeseries. King (2004) demonstrated that employing this approach where the GPS antenna is moving $\geq$1 m d^{-1} can result in periodic motion signals of magnitude 0.05-0.1 m in the Easting and Vertical coordinate components. Horizontal ice motion at the Belcher Glacier was typically less than 0.75 m d^{-1} (0.03 m hr^{-1}), and greater than 1.0 m d^{-1} (0.04 m hr^{-1}) only in the terminus area during peak flow events. In our dataset we note that there is some quasi-periodic noise in the velocity timeseries, roughly double the sampling frequency, with an amplitude that lies within our stated measurement uncertainty. We therefore refrain from attempting interpretations of any ice velocity variations with a period <12 hours in the summer 2010 datasets.

3.3.2 Air Temperature

We installed an automatic air temperature logger at each SCOR site to measure the spatial and temporal variation in the onset, duration, and intensity of local melt conditions, and estimate local ablation rates using a Positive Degree Day (PDD) model. The air temperature for the SCOR station nearest the terminus was estimated using a temperature sensor located 5 km to the southwest and 300 m higher in elevation. We adjusted this temperature record using an altitude dependent lapse rate (4.9 ^{o}C km^{-1}, as suggested for the summer near surface lapse rate on Devon Ice Cap (Gardner and Sharp, 2009)).

Air temperature was also measured at an Automatic Weather Station (AWS) which was located on the glacier centerline at ~900 m elevation. A second AWS at lower altitude was repeatedly damaged by wildlife, and thus we only use results from the 900 m station, which provides a nearly complete record of 2008-2010 summer air temperatures, and of other parameters discussed below.

3.3.3 Snow Thickness and Ablation Measurements

We measured snow depth at 10 ablation stakes (see Figure 3-3) along the glacier centerline at the beginning of each May from 2008-2010. We also collected full thickness samples of the snowpack using a 4 cm diameter snow coring tube, weighed the samples using a spring-scale, and then calculated the depth-averaged snow density. In 2008, we only collected single-point snow core samples at 5 of our ablation stakes. In 2009 and 2010 we collected samples at all 10 ablation stakes as well as 3 cross-glacier profiles; in some cases the values shown in Figure 3-3 for these years represent average density measurements at multiple points (see Table 3-1). These measurements were used to determine the water equivalent (w.e.) snowpack depth at each SCOR site, each spring.

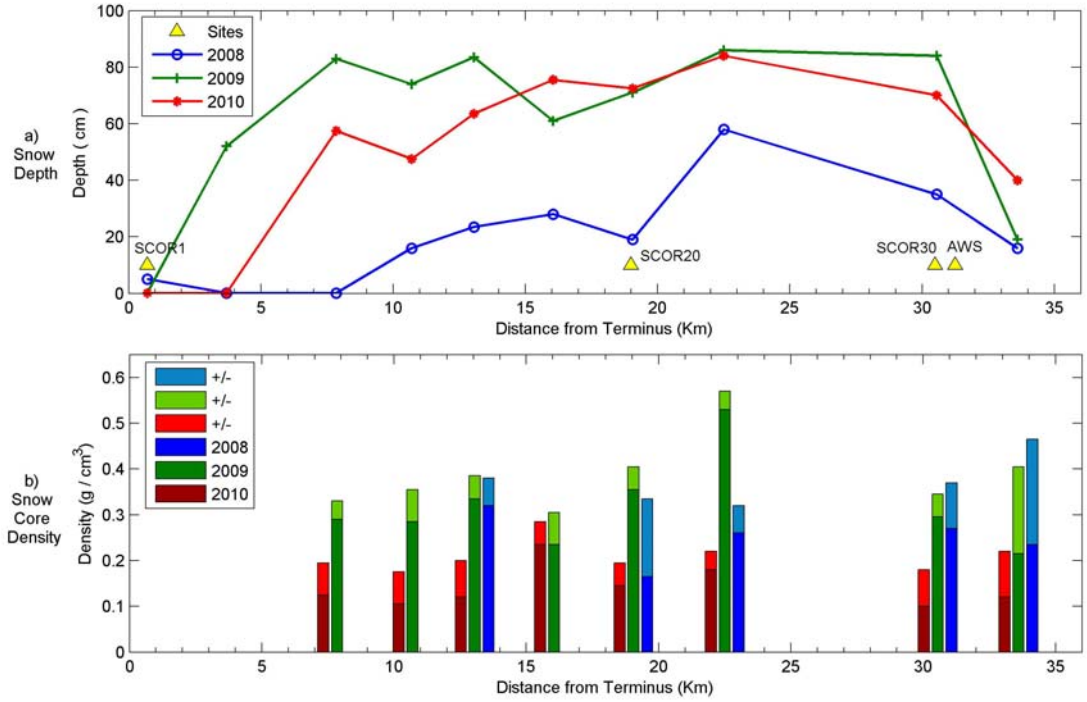

Figure 3-3: (Top) Repeat snow depth measurements at ablation stakes positioned along the glacier. Measurement points are plotted by distance up-glacier from the terminus. Yellow triangles show relative positions of SCOR stations and AWS along glacier centerline. (Bottom) Snow density values derived from snow core samples collected at ablation stakes along glacier centerline. The lighter color at the top of each bar represents the range of uncertainty for each density measurement.

One problem with this method of snow sampling is that weaker layers within the snowpack can be compressed by the insertion of the snow tube. We found this especially true when the bottom layer of the snowpack was composed of fragile hoar crystals. In this case, the snow tube would often crush the snow and then 'drop' the bottom part of the sample back into the hole. For this reason we had to double-check the length of the sample against the depth of the hole to ensure we had retrieved the entire sample, and repeat the sample if a discrepancy was found. These density measurements have a relatively high degree of uncertainty (±40%), but taken as a whole, they allow us to see annual variations in spring snowpack density.

Table 3-1: Mean snow depth and density

	2008 Depth (cm)	2008 Density (g/cm^3)	2009 Depth (cm)	2009 Density (g/cm^3)	2010 Depth (cm)	2010 Density (g/cm^3)
Mean	20.0 ± 0.5	0.31 ± 0.13	67.0 ± 0.5	0.35 ± 0.07	63.0 ± 0.5	0.17 ± 0.07
Standard Deviation	17.6	0.04	25.6	0.08	26.3	0.04
N	10	5	34	32	35	34

At the AWS, an SR50 sonic Snow Depth Gauge (SDG) was used to measure snow pack and ice ablation through the melt seasons of 2008 – 2010. We measured the instrument height above snow surface, and the distance between the surface and the snow-ice interface, while conducting maintenance at the AWS each May. The SDG made hourly soundings of the sensor-to-surface distance (from which we could estimate ablation) throughout the spring and summer. These measurements were used to determine when the snow pack was removed in each melt season, allowing us to establish the date of bare ice exposure (DBI). The DBI marks the important transition from high-albedo snow to lower albedo bare ice, which results in a notable change in ablation rate.

The distance soundings were generally reliable until the very end of each melt season, when melt-out of the station mast caused the AWS to lean over (or fall over, in 2010), and thus decrease the SDG to surface distance. We have identified and removed these sections of the measurement record. For this reason

we were not always able to use the SDG to measure maximum ice ablation each year.

Figure 3-4 shows the snow and ice ablation measurements made by the SDG, as well as the corresponding water equivalent ablation. We used the snow depth and density measurements taken in the vicinity of the AWS to calculate the SWE depth of the snowpack each spring. Using the same snow density value, we estimated SWE depth for each of the hourly SDG measurements, until the snowpack was removed. (While we recognize that some of the snowpack lowering was due to increased densification, this was the closest estimate we could make with the available data.) After the DBI, we used the published mean density for glacier ice (873.5 Kg m^{-3}) from Table 2.1 in Paterson, (1994) to calculate the water equivalent ablation for the remaining SDG measurements.

3.3.4 Surface Albedo

A CNR1 Net Radiometer mounted on the AWS measured incoming and outgoing short-wave and long-wave radiation, from which we estimated surface albedo. We used the albedo time series to confirm the timing of the removal of the annual snowpack.

The albedo measurements show a lot of variability, and even suggest that the surface albedo increases late in the melt season. One explanation for such an increase in albedo may be that fresh snowfall covered the darker ice surface; in some cases (noted in Figure 3-4), coincident positive changes in the surface height measured by the SDG confirm that snow was added to the surface. In the absence of corroborating surface height changes, these albedo increases may also be attributed to the drainage of water from within the weathered surface layer of ice, which can make the ice appear 'whiter' due to reduced absorption and increased scattering of light between crystals. Another possible explanation for the increased albedo measurements is that, under extremely foggy conditions (which occur frequently at this location due to the proximity to the open water of Baffin Bay), the net radiometer may not reliably measure light reflected from the

glacier surface and may instead measure the diffuse bright light scattered by the fog. However, we are only concerned with snowfall events, and interpret these to have occurred only when indicated by both an albedo increase and net increase in surface height.

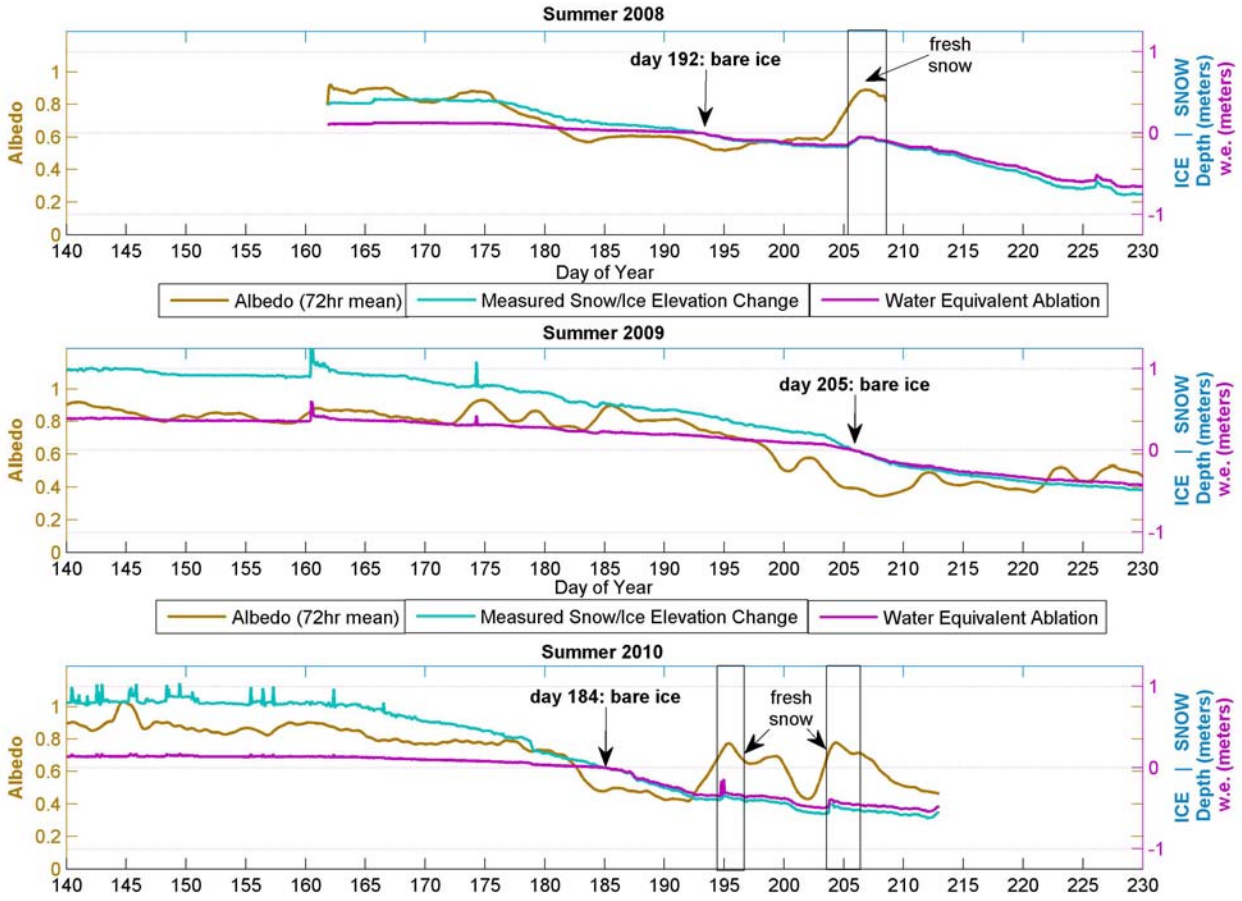

Figure 3-4: Albedo and Ablation measurements at the Belcher Glacier 900 m.a.s.l. AWS, day 140-230 (May 20 – Aug 18); 2008 (top), 2009 (middle), and 2010 (bottom). Surface albedo measured by net radiometer is high in spring when surface is covered with snow, and transitions to a lower value as bare glacier ice is exposed. Subsequent summer snowfall events temporarily raise albedo.
Snow/Ice depth change measured by sonic snow depth gauge; the date of bare ice exposure is marked each summer. Measured snow density and an average ice density value were used to calculate the water equivalent ablation.

3.4 Methods

3.4.1 Positive Degree Days and Surface Ablation

A common method of relating air temperature to glacier surface ablation is via the use of a temperature index model (Hock, 2003). In such a model, Positive Degree Days (PDD), the sum of positive daily air temperatures, are used to compute snow or ice melt at a specific point in time using a Degree Day Factor (DDF). The DDF is a proportionality factor, which is derived by dividing the total measured melt by the total PDD of the model time domain (see Hock (2003) for a summary of DDF values for snow and ice from a variety of glacier locations). The temperature index model is a simplification of the melt process described by full energy balance modeling (Braithwaite, 1995); air temperature alone cannot account for all of the variation exhibited in meltwater production. However, a strong correlation exists between melt and air temperature (Braithwaite, 1995), and for the purposes of this study, a general indication of melt intensity and variability is sufficient.

We computed PDD as:

$$PDD = \sum_{i=a}^{i=b} \alpha i \cdot Ti$$

where

Ti is the daily averaged Air Temperature (^{o}C) on day i

α is a threshold value;

$\alpha i = 1$ where $Ti \geq 0^{o}$C

$\alpha i = 0$ where $Ti < 0^{o}$C

a and b denote the beginning and end dates of the time period of interest.

For each SCOR site (and the AWS), we produced a time-series of cumulative PDD (cPDD) based on the hourly air temperature time series, and then found the first derivative of PDD with respect to time (dPDD/dt) which is useful for identifying major melt events. By applying a DDF appropriate to the surface type, these time-series can be expressed in terms of ablation:

cPDD (^{o}C d) x DDF (mm $^{o}C^{-1}$ d^{-1}) = total Ablation (mm w.e.)

*d*PDD/*dt* (^{o}C) x DDF (mm $^{o}C^{-1}$ d^{-1}) = Ablation rate (mm w.e. d^{-1})

Where ^{o}C is degrees Celsius and d represents time in days.

Ice absorbs more radiant energy and melts faster at a given temperature than snow due to its lower albedo, and this requires us to use different DDFs for snow and ice. We used our field measurements of snow depth, density and relative surface height change (change in distance from SDG to surface) taken at the AWS, to determine values for DDF_{snow} and DDF_{ice} for each year of our study. DDF_{snow} was found by dividing the water equivalent depth of the spring snowpack by the sum of PDDs that occurred between the first day of melt and the DBI. Total ice ablation was taken as the total change in SDG to surface distance that occurred between the DBI and the end of the AWS record. DDF_{ice} was found by dividing the water equivalent depth of ice removed by the sum of PDDs that occurred over the same time period. However, any PDDs that occurred during periods where fresh snow had fallen on the ice (based on the albedo and SDG measurements (see Figure 3-4)) were subtracted from the ice-melt PDDs.

We then modeled the summer cumulative ablation and the ablation rate at hourly resolution for each SCOR site, using the PDD time series derived from the local air temperature time series, and the local measurements of snow depth and snow density. For each summer period, the model calculated ablation at each time step using DDF_{snow} until ablation equalled the initial spring snowpack depth, and then used DDF_{ice} at each subsequent time step except during periods when the SDG and albedo measurements indicated that fresh snow had fallen on the glacier. (We assumed that all regions of the glacier experienced roughly the same snowfall during these events.)

3.4.2 Enhanced Velocity Days

To quantify the seasonally enhanced velocity and make inter-annual comparisons, we used a method analogous to PDD: we calculated Enhanced Velocity Days (EVD) by summing the ice velocity on days when the glacier's

flow rate exceeded the Spring Pre-Speedup Velocity (SPSV or "spring velocity" hereafter) by more than one standard deviation of the SPSV. The spring velocity was calculated as the average velocity from day 140 to 160 (May 20 - June 9) of each year's velocity time series. The spring velocity reasonably represents the "steady-state" flow rate of ice, prior to the onset of seasonal hydraulically driven basal sliding. The one standard deviation threshold (1σ) was chosen to eliminate artefacts associated with high frequency noise in the velocity timeseries.

$$EVD = \sum_{i=a}^{i=b} \alpha i \cdot Vi$$

where

Vi is the daily averaged ice flow velocity (m/day) on day i

α is a threshold value;

$\alpha i = 1$ where $Vi \geq \text{SPSV} + 1\sigma_{\text{SPSV}}$

$\alpha i = 0$ where $Vi < \text{SPSV} + 1\sigma_{\text{SPSV}}$

a and b denote the beginning and end dates of the time period of interest.

For each SCOR site, we produced time series of cumulative EVD, and the first derivative of EVD (*d*EVD).

cEVD (m) = Cumulative Enhanced Displacement

*d*EVD (m d^{-1}) = Daily Enhanced Displacement

3.5 Results & Observations

We focus most of our comparison of results on the period for which we have unbroken time series of glacier motion from our three main SCOR sites: SCOR1 in the terminus region, SCOR20 in the mid-glacier, and SCOR30 in the upper-glacier. These three stations have complete and comparable data records from days 140 – 227 (May 20 to August 15), of 2008, 2009, and 2010.

3.5.1 Summer Melt Characteristics

We characterized each summer (indicating the entire melt season) in terms of the onset, duration, intensity, and variance of the melt season, and summarized

these in Table 3-2. Melt onset was taken as the date of the first recorded PDD, and duration as the difference between the first and last day on which PDDs were recorded in each year (ignoring days where PDD < 0). To characterize melt intensity, we divided the cumulative PDDs at each SCOR station by the local melt season duration. The total water equivalent melt at each station is the degree-day modeled total ablation, which is shown in Figure 3-5. To get a sense of the melt season temperature variance, we computed the standard deviation of the daily mean air temperature time series from each SCOR station. Variance at this level of smoothing effectively captures temperature swings between melting and freezing, without incorporating hourly-resolution noise.

Table 3-2: Melt season characteristics for each summer 2008-2010

	2008			2009			2010		
Characteristic	SCOR1	SCOR20	SCOR30	SCOR1	SCOR20	SCOR30	SCOR1	SCOR20	SCOR30
Onset: First PDD (doy)	158	171	176	146	146	146	160	161	165
End: Last PDD (doy)	227	227	227	227	227	227	227	227	227
Duration: Length of melt season (days)	69	56	51	81	81	81	67	66	62
Total cPDD	166.45	105.90	110.78	240.23	129.58	128.20	245.81	148.81	147.28
Total ablation (m w.e.) at SCOR	1.08	0.61	0.49	1.41	0.55	0.55	1.81	1.11	1.11
Intensity: cPDD/Duration	2.412	1.891	2.172	2.966	1.600	1.583	3.669	2.255	2.375
Variance: *d*PDD/*dt* Standard Dev.	0.07	0.06	0.07	0.08	0.06	0.08	0.09	0.06	0.07
Variance: 24hr avg Air Temp Standard Dev.	2.72	3.83	4.19	2.48	2.94	3.30	3.62	4.00	4.28
mean variance		3.58			2.91			3.96	

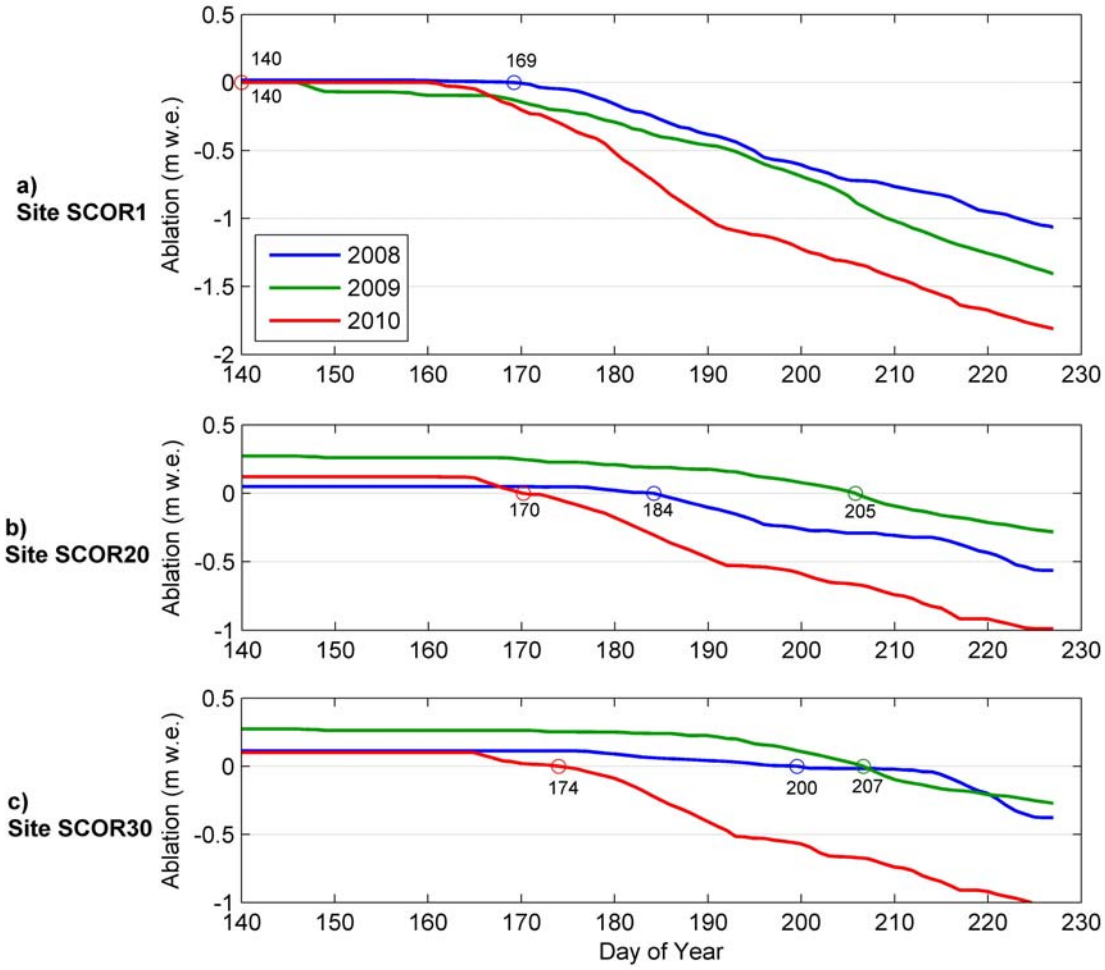

Figure 3-5: Calculated total water equivalent ablation at three SCOR sites, for each year of study. 0 meters marks the transition between snow and ice. The Date of Bare Ice exposure is marked by a coloured circle with the day number above or below.

A noteworthy feature of the temperature time series (Figure 3-6b and 3-6c) is the mid-summer cool period that occurred between days 200 and 210 (July 18-28) of 2008. This cool period coincided with a windstorm on July 18-20, followed by snowfall on July 23-24, events which were recorded by the AWS and observed by colleagues conducting fieldwork at the time (Duncan, 2011). This mid-summer storm and prolonged cool period halted melt on the mid- and upper-glacier for much of this 10 day period, and was a unique event in the three years of observations.

3.5.2 Ice Velocity Variations

The continuous ice velocity records from SCOR1, SCOR20, and SCOR30 are displayed in Figures 3-6, 3-7, and 3-8 (2008, 2009, and 2010, respectively). These plots demonstrate the ice velocity variations that occurred on Belcher Glacier during each melt season.

In Table 3-3 we quantify the velocity enhancement experienced at the three SCOR sites in each summer. The spring velocity is the mean ice velocity from day 140 to 160. The mean summer enhanced velocity is the mean velocity on all days on which flow was faster than the spring velocity, and the Total EVD is the total ice displacement that occurred during this period. The ratio of EV: SPSV expresses the mean summer enhanced velocity as a percentage of the spring background velocity. We determined the total annual ice displacement (TAD) at each SCOR site as the difference between static DGPS surveys of the SCOR antenna positions, which were repeated each May during our site maintenance visits (as close as possible to one calendar year apart, but expressed here as (displacement/interval)*365). Finally, we expressed the summer enhanced displacement as a percentage of the total ice displacement (EVD/TAD).

As noted earlier**,** comparisons of the velocity at SCOR1 in successive years must take into consideration the fact that the station was repositioned progressively closer to the glacier centerline each year. We observe that the spring velocity and total annual displacement were greater at SCOR1 in successive years. This may be partially due to repositioning of the station or due to the station advecting into regions of faster flow, but we consider it equally possible that the changes in spring velocity and total annual displacement reflect real annual variations in ice flow.

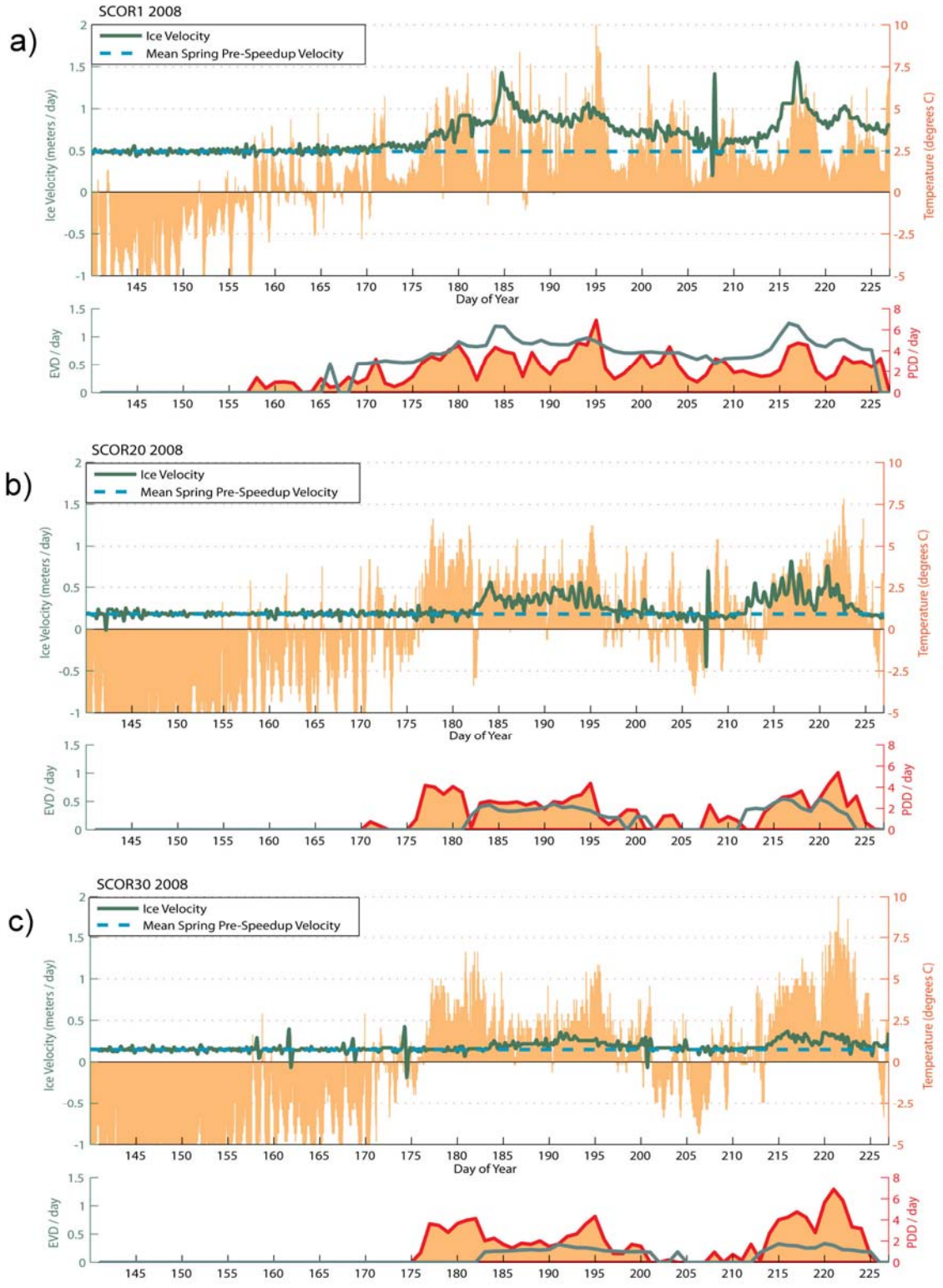

Figure 3-6: Ice velocity, air temperature, *d*EVD, and *d*PDD/*dt* at each SCOR site, 2008

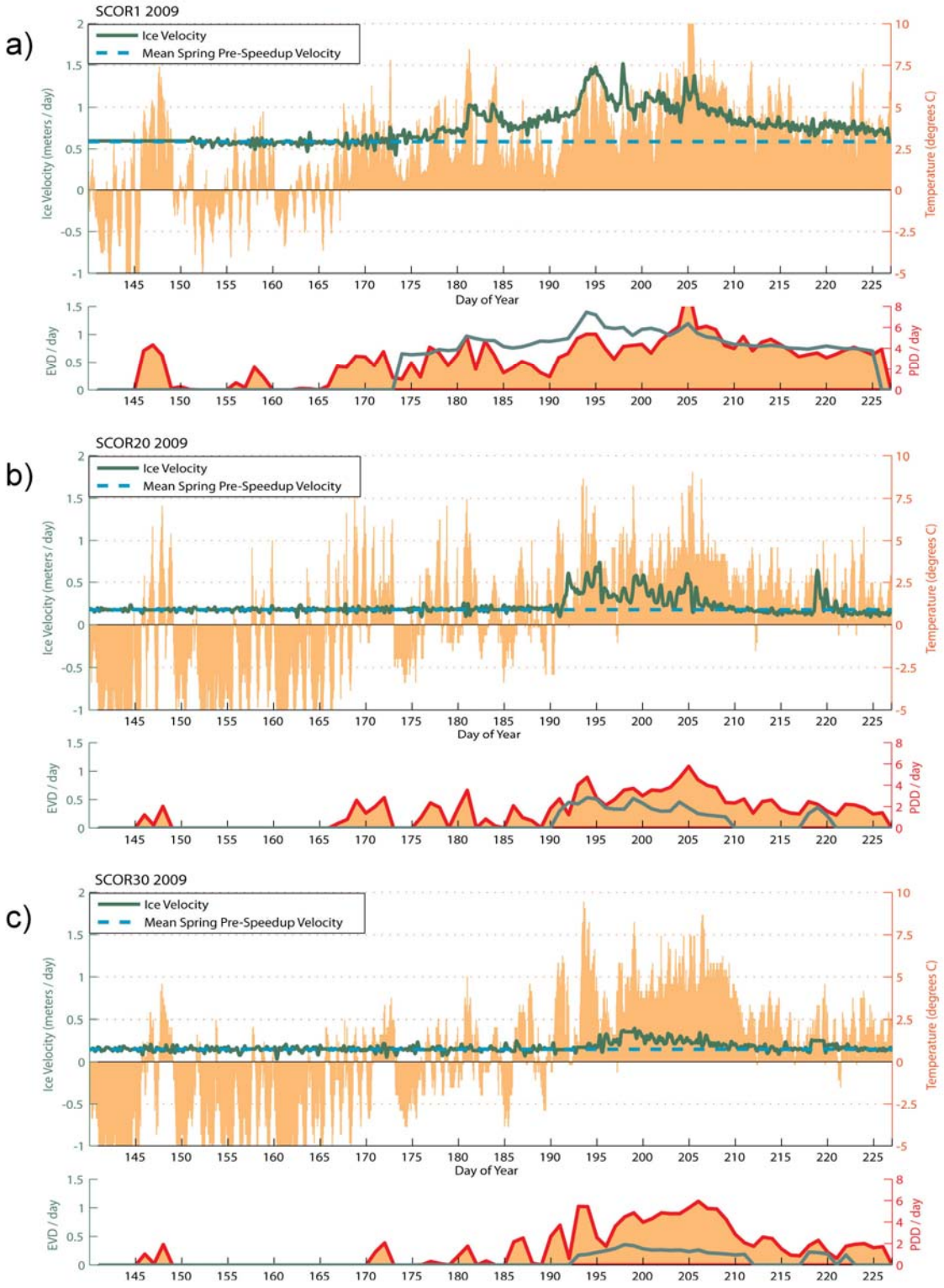

Figure 3-7: Ice velocity, air temperature, *d*EVD, and *d*PDD/*dt* at each SCOR site, 2009.

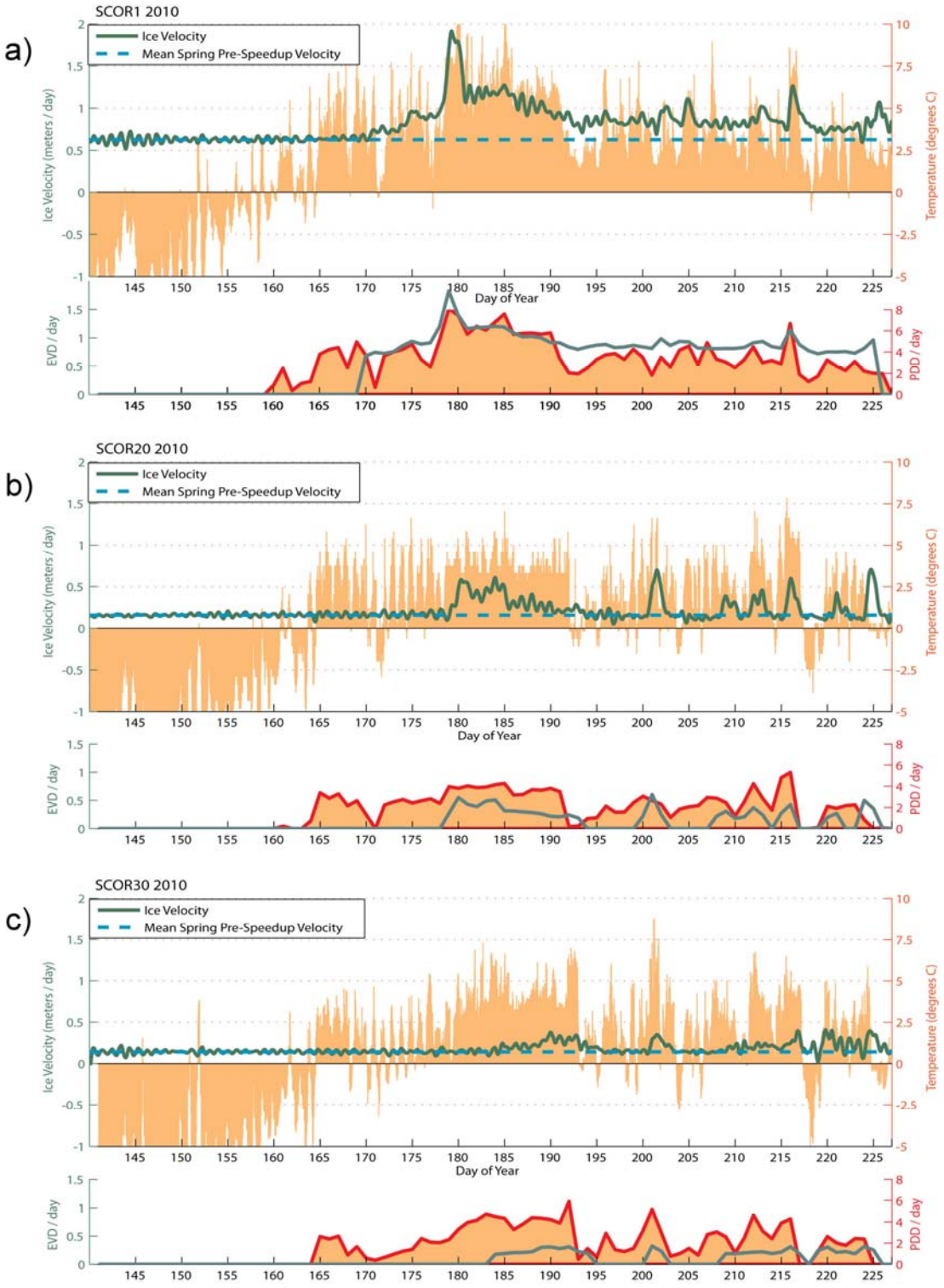

Figure 3-8: Ice velocity, air temperature, *d*EVD, and *d*PDD/*dt* at each SCOR site, 2010.

Table 3-3: Ice flow velocity enhancements at three SCOR sites for each summer 2008-2010

	2008			2009			2010		
	SCOR1	SCOR20	SCOR30	SCOR1	SCOR20	SCOR30	SCOR1	SCOR20	SCOR30
Spring Velocity (doy 140-160) (m/day)	0.49	0.18	0.15	0.59	0.18	0.15	0.63	0.16	0.14
Mean Summer Enhanced Velocity (m/day)	0.78	0.36	0.23	0.89	0.35	0.23	0.92	0.32	0.24
Total EVD (m)	45.41	11.26	7.66	46.06	7.61	5.39	51.61	9.57	6.86
Velocity increase: EV over SPSV	59%	101%	57%	51%	97%	58%	47%	104%	67%
Surveyed Total Annual Displacement (m)	206.45	65.22	56.29	239.20	59.73	54.47	239.35	58.00	54.6
EVD / TAD	22%	17%	14%	19%	13%	10%	22%	17%	12%

Measurements from the SCOR stations outside of the spring-summer time-frame (day 140-227) are available, but are much more sporadic due to the reduced measurement duty-cycle, winter power system failures, and occasional wildlife damage or damage due to the antenna mast melting out of the ice at the end of summer. We have used whatever data we could recover to compute the mean velocity during the fall and winter periods so that comparisons can be made with the mean spring and summer velocity values shown above. To determine the fall velocity, we compute the displacement from day 227 (our last day of summer) to the latest available GPS measurement of the year (which typically ranged from mid-September to late-November) and divided by the intervening time span. For the winter velocity, we used the same late-fall GPS measurement, and the first available measurement in the following year when the GPS system came back on-line (which ranged from late-February to late-April). In the cases where a station did not come back on-line after winter, our earliest spring dates coincided with our site maintenance visits in May. We also calculate the total displacement between the end of the summer and the following spring to provide a "summer vs. non-summer" velocity comparison. These results are presented in Table 3-4.

Table 3-4: Mean Fall and Winter velocities at three SCOR sites, 2008-2010.

		2008			2009			2010	
	SCOR1	SCOR20	SCOR30	SCOR1	SCOR20	SCOR30	SCOR1	SCOR20	SCOR30
Fall Date Span	14/08/08 to 08/09/08	14/08/08 to 15/10/08	14/08/08 to 15/10/08	14/08/09 to 09/09/09	15/08/09 to 27/11/09	15/08/09 to 27/11/09	15/08/10 to 01/12/10		
Fall Velocity m / yr *(m /day)*	213.02 ± 0.15 *(0.58)*	50.36 ± 0.14 *(0.14)*	51.58 ± 0.19 *(0.14)*	251.28 ± 0.19 *(0.69)*	49.37 ± 0.11 *(0.14)*	50.18 ± 0.22 *(0.14)*	226.36 ± 0.16 *(0.62)*	N/A*	N/A**
Winter Date Span	08/09/08 to 28/05/09	15/10/08 to 26/02/09	15/10/08 to 28/02/09	09/09/09 to 08/05/10	27/11/09 to 26/02/10	27/11/09 to 26/02/10	01/12/10 to 31/03/11	16/08/10 to 26/04/11	15/08/10 to 28/04/11
Winter Velocity m / yr *(m /day)*	192.70 ± 0.18 *(0.53)*	57.89 ± 0.13 *(0.16)*	53.12 ± 0.20 *(0.15)*	224.47 ± 0.13 *(0.61)*	53.70 ± 0.12 *(0.15)*	51.41 ± 0.22 *(0.14)*	215.07 ± 0.15 *(0.59)*	51.81 ± 0.06 *(0.14)*	51.79 ± 0.52 *(0.14)*
Mean non-Summer Velocity m / y	194.46 ± 0.19	57.11 ± 0.16	53.06 ± 0.20	227.05 ± 0.12	52.50 ± 0.13	50.95 ± 0.22	220.03 ± 0.16	51.81 ± 0.06	51.79 ± 0.52

*SCOR20 antenna cable damaged on 17/08/2010, and SCOR30 began slowly falling over in late August 2010 due to mast melt-out. Therefore these winter velocity estimates incorporate all displacement from late August to late April.

3.5.3 EVD : PDD Comparisons

We compared the timing and duration of PDD and EVD to explore the relationship between the episodes of enhanced velocity and melt water generation. These results are summarized in Table 3-5. We are particularly interested in comparing the dates of onset of PDD and EVD, as well as the ratio of EVD:PDD at each site.

Two observations stand out from the results shown in Table 3-5. First, there is no obvious 'threshold' number of PDDs between the onset of melt and the onset of the summer speedup. Second, the EVD:PDD ratio varies significantly between years, and between regions of the glacier. These observations are notable when contrasting the 2008 summer speedup with those in 2009 and 2010. In 2008, the onset of melt (first PDD) was generally later than in the other years, and the delay between the melt onset and speedup onset was shorter, especially when compared to 2009. Despite the fact that the fewest PDDs were recorded at all three sites in 2008, the EVD:PDD ratio was significantly lower than in the following years.

This suggests that in 2008, more enhanced displacement occurred per PDD than in 2009 or 2010.

Table 3-5: Comparisons between PDD and EVD at three SCOR sites, 2008-2010.

	2008			2009			2010		
	SCOR1	SCOR20	SCOR30	SCOR1	SCOR20	SCOR30	SCOR1	SCOR20	SCOR30
PDDs before first EVD (C d)	6.55	21.40	24.60	35.83	33.42	26.97	29. 60	38.28	44.99
First PDD (day#)	158	171	176	146	146	146	160	161	165
First EVD (day#)	166	182	183	174	191	193	170	179	184
Delay First PDD to First EVD (days)	8	11	7	28	45	47	10	18	19
Total PDD	166.45	105.90	110.78	240.23	129.58	128.20	245.81	148.81	147.28
Total EVD	45.41	11.26	7.66	46.06	7.61	5.39	51.61	9.57	6.86
EVD:PDD ratio	3.67	9.40	14.47	5.22	17.02	23.77	4.76	15.55	21.46

3.6 Discussion

A common pattern of seasonal velocity variation occurs each year at this glacier. However there are also some distinct differences in glacier flow variability that result from differences in the initial spring conditions and/or melt variability in the three years of observations. Below we discuss both the seasonal similarities and the inter-annual differences, and suggest potential causes for these differences.

3.6.1 Pattern of Seasonal Flow Variations

We observed a pattern of seasonal velocity changes which included five distinct phases. These phases are similar to those observed by Bartholomew and others (2010) at two sites on the margins of the Greenland Ice Sheet, but we distinguish additional features which may be unique to a tidewater glacier system. Below, we describe the surface observations that define each phase (as seen in Figure 3-9), followed by what we can infer about the state of the subglacial drainage system during each of these periods. The divisions between these phases

were chosen based on interpretation of the changes observed in the velocity time-series, but not necessarily on specific thresholds of $d\mathrm{V}/dt$.

Phase 1: Quiescence - In all regions of the glacier, the ice moved at a relatively uniform rate, which we refer to above as the spring velocity. During this phase, air temperature starts to reach a few degrees above 0^{o}C at mid-day, and returned to below-freezing temperatures at night. Field observations during this period (late May to early June) suggest that the small amount of meltwater produced during the day percolates into the snowpack and refreezes at night. Our ablation model and SDG measurements indicate that only minimal amounts of melt occurred on the glacier during this period, except in the terminus region in 2009 when this region had little to no snow cover, and above-freezing temperatures as early as day 145 resulted in ablation of the exposed ice. Time-lapse photography in 2009 showed that meltwater generated in the terminus region began to pond in crevasse depressions during this time period, but no drainage was observed (Danielson and Sharp, 2013). From these observations, we infer that there were no surface melt water inputs to the subglacial drainage system, no corresponding perturbations to basal friction, and thus no changes in ice velocity at the surface during the Quiescent Phase.

Phase 2: Terminus Zone Activation - The onset of seasonal velocity variations each year occurred first in the terminus zone, the lower ~5 km of the glacier. Our velocity measurements at SCOR1 (and to a lesser extent SCOR8 in 2010) show that the ice in this zone started to accelerate 10 to 20 days before there was any deviation from spring velocity in other regions of the glacier. During this period, positive mean daily air temperatures were frequent and freezing temperatures were infrequent, especially in the vicinity of SCOR1. Our modeled ablation shows melt occurring at all regions of the glacier, but melt rates were highest in the terminus region where bare ice was already exposed.

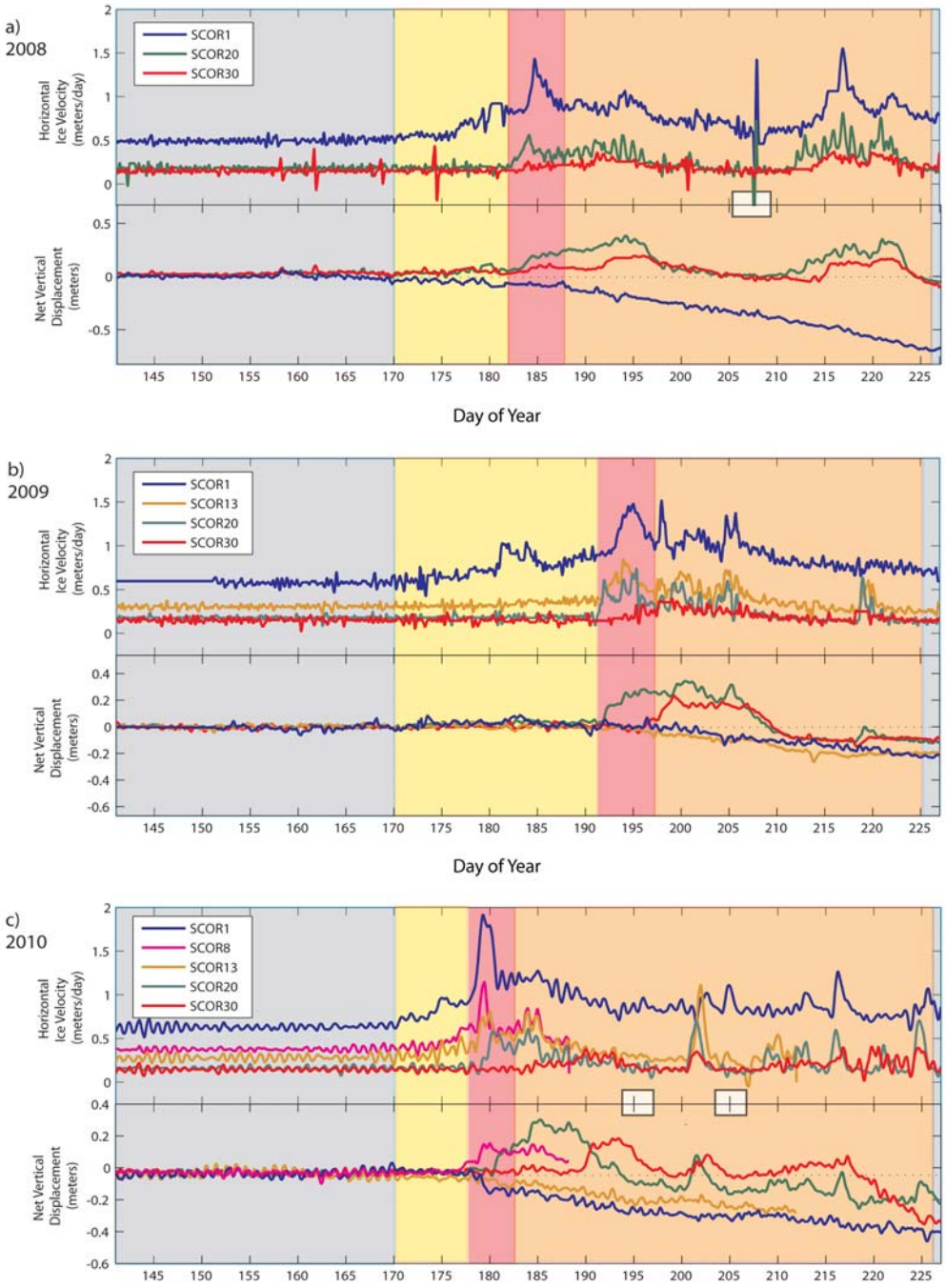

Figure 3-9: The phases of seasonal velocity variation marked by coloured boxes on plots of ice velocity and net vertical displacement. *Grey*, Phase 1 & 5 (Quiescence); *Yellow*, Phase 2 (Terminus Activation); *Red,* Phase 3 (Spring Event); *Orange*, Phase 4 (Hydro-Active).
Each plot [a) 2008 b) 2009 c) 2010] is composed to two sub-plots:
TOP: Horizontal (xy) ice velocity measurements from all available SCOR stations.
BOTTOM: Net change in ice surface elevation, relative to day 140, after correction for down-slope bed-parallel motion.
White boxes along x-axis show fresh snowfall events (corresponding to those shown in Figure 3-4).

The ice in the terminus zone is heavily fractured, with wide, deep crevasses covering most of the lower 5 km of the glacier. Large lakes tend not to form in this area, but supra-glacial water does pool in crevasses to form a spatially extensive collection of small ponds. Danielson and Sharp (2013) show that, in 2009, the cumulative area covered by these lakes reached a maximum during the time period we classify here as Phase 2, and that several abrupt acceleration events at SCOR1 were preceded by meltwater drainage into these crevasses (the rapid velocity changes seen on day 181, and 184 in Figure 3-9b). These observations suggest that water filled crevasses may drain through their bottoms via the hydrofracture propagation of cracks through the full thickness of the glacier ice, thereby delivering surface meltwater to the glacier bed. This mechanism has been proposed on the basis of both observations (Boon and Sharp, 2003; Das and others, 2008) and numerical modeling (Van der Veen, 2007) to be possible even for cold thick ice, if the influx rate of meltwater is high enough to overcome the tendency of the crack to close via refreezing and compressive strain. It is also reasonable to expect that multiple water-filled crevasses in a tightly spaced field of crevasses could penetrate to the bed, provided that the ice is in a state of tension (Van der Veen, 1998), which we expect is the case based on observations that surface velocity increases steadily towards the terminus in this region of the glacier (Van Wychen and others, 2012).

The gradually increasing ice velocity observed at SCOR1 and SCOR8 during this phase is consistent with other observations of increasing ice velocity in response to increasing subglacial water pressure or water storage (Iken and others, 1983; Bartholomaus and others, 2008). This increase in velocity over time could be partially explained by the fact that the GPS stations are advecting through a spatially varying velocity field, however, the coincident timing of meltwater drainage and the fact that the velocity decreases later in the melt season suggest that advection into a region of faster flowing ice cannot completely explain the velocity increase observed during Phase 2. We infer that, during Phase 2, multiple supra- to sub-glacial drainage connections were established in the

terminus zone, allowing runoff to raise subglacial water pressure. At this point in the melt season, the subglacial drainage system was likely inefficient and un-channelized, as it would not yet have been forced to accommodate very high volumes of melt water.

Phase 3: Spring Event - During this 2-5 day time period, at all GPS sites, we observe rapid changes in ice dynamics which coincided with an up-glacier progression of melt and the initiation of supra-glacial drainage into sink points at mid- and upper-glacier regions. Similar observations at a variety of other glaciers have been referred to as "spring events" (Iken and others, 1983; Röthlisberger and Lang, 1987; Bingham and others, 2003). We observed rapid acceleration to near-maximum annual velocity in the terminus region (SCOR1 and SCOR8). This is either slightly preceded (2008, 2009), or slightly lagged (2010) by rapid acceleration in the mid-glacier regions (SCOR20 and SCOR13), and followed, in 1 to 5 days, by similar but less pronounced acceleration at the upper-glacier (SCOR30). This was the first departure from the spring velocity in the mid- and upper-glacier regions.

We also observed upwards vertical motion at SCOR20 and SCOR30 that closely coincided with the initial horizontal acceleration, and we note that there was net upwards displacement of the ice surface at these sites in Phases 3 and 4 that was coincident with increased horizontal velocity. While total vertical motion measured at the ice surface is a combination of three components (Copland and others, 2003; Hoffman and others, 2011), the net vertical displacement shown in Figure 3-9 is indicative of vertical motion of the ice relative to the bed combined with vertical strain of the ice, since we have removed most of the effect of bed-parallel motion by subtracting the long-term downward-motion trend (which we assume represents the bed slope). If lateral strain is assumed constant, then upwards vertical ice motion due to longitudinal compression (or reduced extension) will occur when upstream ice accelerates more than downstream ice. Such events can be observed in our measurements of ice velocity, though they are transient and short-lived. Generally the ice is in

longitudinal tension (and thus thinning) since the velocity increases towards the terminus. We have not separated the effects of vertical strain from the net vertical displacement time series shown in Figure 3-9, and we use these as an indication of potential ice-bed separation, but not as absolute measurements of cavity growth. We infer that ice-bed separation occurs in response to increased water pressure at the bed if this interpretation is supported by observations of increased runoff and drainage to englacial conduits.

Significant increases in melt and supra-glacial drainage events were observed during Phase 3. While we noted earlier that there appears to be no consistent PDD threshold, the onset of Phase 3 was preceded by an average of 15 PDDs in the terminus zone, and 24 PDDs in the mid- and upper-glacier. Comparing Figure 3-9 with our ablation and albedo measurements (Figure 3-4) and calculated ablation (Figure 3-5), shows that the spring event occurred when all snow had melted from the lower glacier, and the little remaining snow on the mid- and upper-glacier had significantly reduced albedo, suggesting that the snow was either saturated with water, and/or patchy with sections of bare ice exposed. High melt rates resulting from bare ice exposure to sustained warm air temperatures and strong solar radiation led to increased rates of runoff into englacial conduits. Time-lapse photography from 2009 showed that lakes were beginning to form in at least 3 locations on the lower half of the glacier during Phase 3. This indicates that a substantial amount of runoff was being generated, and that it was no longer being stored in the snowpack but was flowing through supra-glacial channels and collecting in supra-glacial reservoirs. One of these lakes (Lake 2 in Figure 3-1) drained rapidly through its base during the 2009 spring event (Danielson and Sharp, 2013).

Based on these observations, we argue that the spring event marks the establishment of multiple, wide-spread, surface to subglacial hydrologic connections. The spring event may not occur simultaneously glacier-wide, but may be phase-shifted along the glacier. The upwards vertical motion of ice associated with horizontal acceleration at SCOR20 and SCOR30 suggests that

ice-bed separation occurred in response to high subglacial water pressures over a large region of the mid- and upper-glacier during this period. From this we infer that during Phase 3, the inefficient and non-channelized subglacial drainage system became inundated with sharply increased amounts of meltwater, and the inability of the drainage system to evacuate this water promoted the formation of water-filled cavities over extensive regions of the glacier bed. This allowed the observed rapid increase in ice velocity, which we infer was caused by basal sliding. Spring event sliding velocity peaked and then began to decrease, presumably when the evolving drainage system began to evacuate subglacial water at a rate approaching or exceeding the runoff input, so that water storage in basal cavities stabilized or decreased. The emergence of a turbid water plume in the fjord at the glacier terminus provides some evidence that sub-glacially stored water began to escape from the glacier drainage system around this time. In 2009, time lapse photographs of the Belcher terminus show the first visible signs of this turbid water plume on day 195 (July 14) (Milne, 2011), which corresponds to the date when velocity at SCOR1 reached its spring event peak and began to decrease.

Phase 4: Hydro-Active - Following the spring event, the mean ice velocity remained higher than the spring velocity during a 28-45 day period characterized by high velocity variability. In the terminus zone, the velocity generally decreased towards the spring velocity. Brief, irregular high-velocity events were superimposed on this trend, but regular diurnal variations were not typical. At SCOR13 and SCOR20, velocity fluctuated within a range from minima equal to the spring velocity to peaks ~200% above the spring velocity, and it sometimes varied diurnally. The velocity fluctuations at SCOR30 follow a similar pattern, but were more subdued.

The observed short-term fast flow events were frequently coincident with periods of warm air temperatures, which we infer increased runoff into existing drainage channels and englacial sink points. The warmer episodes were often interspersed with cooler low-melt periods, sometimes caused by storms that

brought fresh snowfall which further reduced surface melt rates (see Figure 3-4). These cooler periods were associated with decreased ice velocity. During prolonged periods of cool air temperatures and decreased runoff, ice velocity in the mid- and upper-glacier approached or decreased to below the spring velocity, and the net vertical ice displacement decreased to 0m or less. This can be seen particularly well at SCOR20 between day 200 and 210 in 2008 (Figures 3-6b and 3-9a) and between day 210 and 217 in 2009 (Figures 3-7b and 3-9b). SCOR30 exhibits similar patterns, but with lower amplitude changes in both velocity and vertical displacement.

Lake drainage events also contributed to rapid meltwater drainage fluctuations during this phase. In 2009, Lakes 3 and 2 drained on days 198 and 204 (July 17 and 23), coincident with the ice acceleration events seen at SCOR1 on these dates (Danielson and Sharp, 2013).

During this phase, we suggest that the subglacial drainage system must have developed the capacity to evacuate a high, steady-state volume of meltwater input. With sustained high rates of meltwater input, we expect that subglacial channels would grow in size and efficiency, and subglacial water pressure would decrease, thereby effectively raising basal resistance to sliding. This would account for the trend towards lower ice velocities, relative to the spring event, observed at all sites. However, we infer that during periods of sharply increased melt or lake drainage events, meltwater that entered the system exceeded the capacity of the drainage channels. This could have caused the pressure within these channels to increase and force water out into a more distributed drainage system. This state would last only until the channelized system grew to accommodate the increased meltwater flux, and/or the runoff rate decreased. The inability of the channelized drainage system to adapt to rapidly changing meltwater injection rates would explain the abrupt changes in ice velocity and temporary vertical uplift events observed during periods of high melt or lake drainages during Phase 4.

Phase 5: Return to Quiescence - As surface temperatures drop near the end of August, runoff rates decreased. In the terminus region we observed a continued gradual decrease in ice velocity. An annual minimum velocity was reached sometime in the winter or early spring of the following year (Table 3-4).

In the mid- and upper regions of the glacier, the net vertical ice displacement decreased to or below 0 m, and glacier velocity fell to or below the spring velocity. While these conditions occurred temporarily during low-runoff / slow-flow periods in Phase 4, they became the norm in Phase 5. Minimum annual velocities at SCOR20 and SCOR30 occurred in the fall - the period directly after the time frame we have plotted in Figure 3-9. Based on these observations, we infer that the subglacial conduits in the mid- and upper-glacier region were no longer filled with water. In the absence of runoff input, any water left in the system would continue flowing down the hydrologic gradient to lower regions of the glacier, and the subglacial water pressure would become very low (~atmospheric pressure, if moulins remained open).

3.6.2 Inter-annual Variations in Seasonal Flow

Variations in the seasonal pattern described above produced distinct differences in the enhanced ice displacement that occurred each year. Although Phase 3 may vary in timing, the glacier appears to experience a spring event each year. The most significant inter-annual variations in seasonal enhanced displacement occur before and after the spring event, during phases 2 and 4. The primary drivers of these differences appear to be spring snowpack thickness and late summer melt variability.

3.6.2.1 Pre-Spring Event Snowpack Variation

Our observations of annual snowpack depth, measured ablation at the AWS, and modeled ablation at each SCOR site (Figures 3-3, 3-4, and 3-5, respectively) help to reveal the influence of spring snow cover on the initiation of the flow variations characteristic of phases 2 and 3. In 2008 and 2010 a thin spring

snowpack melted away relatively quickly. In 2008, 0.120 m w.e. of snow at the AWS melted by day 192; this was the thinnest spring snowpack in the three years of observations. The slightly thicker snowpack in 2010 (0.210 m w.e. at the AWS) was removed eight days earlier, due to a slightly earlier and stronger onset of melt. As a result, phase 2 was relatively short (7-12 days) in 2008 and 2010, the spring event occurred earlier, and phase 4 was long (40-45 days). In contrast, the thick snowpack in 2009 (0.530 m w.e. at the AWS) resulted in later snowpack removal (day 205), and a relatively long phase 2 (20 days), despite the earliest onset of melt. The thicker 2009 snowpack delayed the start of the spring event and shortened phase 4 (28 days), the period during which the largest percentage of EVDs usually occur.

Thicker snowpack delays the onset of the spring event in three main ways:

1) It delays the transition from a high albedo (snow) to a low albedo (ice) surface, and keeps the melt rate low for a larger fraction of the summer.

2) It delays runoff of surface meltwater by acting as a storage medium via either refreezing, or water storage in its pore volume.

3) It delays the development of surface drainage channels and the opening of drainage linkages between the surface and sub-glacial drainage systems.

We suggest that these snowpack-induced delays partially explain the differences seen between years in the EVD:PDD ratios (Table 3-5). The EVD:PDD ratios at all sites were lower in 2008 and 2010 than in 2009, meaning that less enhanced displacement occurred per PDD in 2009. In 2009, a large proportion of the PDDs were expended in melting the thick snowpack.

3.6.2.2 Post-Spring Event Melt Variability

The Phase 4 periods exhibit very different degrees of variability in melt conditions, which would have affected variability in meltwater supply and runoff.

In 2008, Phase 4 included 2 strong melt periods, separated by a deep, unseasonal cold period – a large summer storm that caused surface melt to cease,

and deposited fresh snow on the surface. This produced variations between high and low rates of meltwater supply on a 20-30 day cycle. The mid-summer cool period temporarily halted melt and would have drastically reduced runoff into subglacial conduits (Duncan, 2011). Water would have continued to flow through the englacial drainage system, but very little new water entered the system for 2-3 days in the mid- and upper-glacier regions. Reduced flow rates in englacial and subglacial channels would have decreased the rate of channel growth by channel wall melt, and decreased water pressure in the channels would have allowed faster creep closure.

When the storm ended and warm temperatures returned, the thin layer of fresh snow melted away quickly, and the melting of ice resumed, leading to rapid rates of meltwater runoff. This runoff would have been routed quickly to sink-points via the well-developed supra-glacial drainage network, and would have encountered a constricted englacial and subglacial drainage network. Water pressure in these systems would therefore have risen, until the drainage system could adapt to accommodate the increased water flux. As a result, we saw what could be interpreted as a second spring event on the glacier, between days 212 to 217 in 2008. Figure 3-10 presents this alternative interpretation of the phases of velocity variation in 2008.

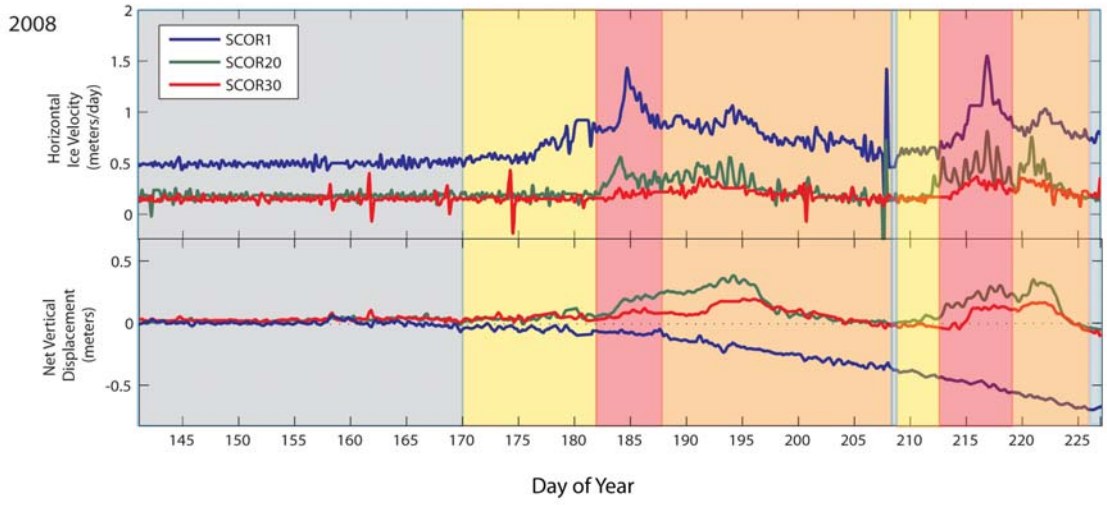

Figure 3-10: Alternative Interpretation of the velocity variation phases for 2008. *Grey*, Phase 1 & 5 (Quiescence); *Yellow*, Phase 2 (Terminus Activation); *Red,* Phase 3 (Spring Event); *Orange*, Phase 4 (Hydro-Active).

By contrast, the 2009 melt season was long and consistently warm. Sustained high melt rates followed the spring event, and the subglacial drainage system would have adapted to efficiently evacuate high volumes of meltwater. Only peak rates of runoff would inject enough water into the subglacial system to force water out of existing channels and across other areas of the bed, potentially driving uplift and flow acceleration. Three such events were observed during phase 4 in 2009: the rapid drainages of Lakes 3 and 2 (see Figure 3-1 for the lake locations) were coincident with high velocity events on days 197 and 204 (July 16 and 23), and an extreme melt event coincided with a high velocity event on day 205 (July 25) (Danielson and Sharp, 2013). Otherwise, air temperature variations during Phase 4 of 2009 were defined primarily by 24 hr periodicity and a gradual decrease in mean air temperature over the 27 day period. It appears that by late in the melt season, the subglacial drainage system had the capacity to absorb diurnal variations in runoff input without producing basal pressure changes sufficient to cause diurnal speed variations.

The 2010 summer was characterized by medium-scale variability in melt conditions. Whereas the Phase 4 period of 2008 was dominated by the 20-30 day cycle of intense melt interrupted by a storm, and 2009 was characterized by diurnal melt variability superimposed on a long-term trend of gradual cooling, melt during Phase 4 of 2010 was characterized by variability with 3-5 day periodicity. There were multiple days when air temperatures dipped significantly below freezing in the mid- and upper-glacier areas, and at least two incidences of fresh snowfall (shown in Figure 3-4 on days 195 and 204). Directly following both of these brief snowfall events, warm air temperatures allowed rapid melt of the fresh snow, and there were velocity peaks on days 201 and 209 at SCOR13, SCOR20, and SCOR30 that were likely a response to the rapid resumption of runoff production. While not as extreme as the hiatus in melt caused by the storm in 2008, these small interruptions and resumptions in meltwater generation and

runoff likely caused the subglacial drainage system to be in a constant state of adaptation to changing water fluxes throughout of Phase 4.

The relationship between short-duration high-velocity events and fluctuations in melt water supply during Phase 4 is described well by the modeling work of Schoof (2010): rates of meltwater supply can vary quickly (on timescales of hours), but sub-glacial conduits require days to adjust in size and develop the capacity to evacuate additional water volume. As a consequence, basal water pressure may increase if water is forced out of the channels, potentially leading to ice-bed decoupling and enhanced rates of sliding, until either the conduits enlarge or the meltwater supply decreases.

The underlying importance of this property of the drainage system, suggested by Schoof (2010) and observed here, is that there is not necessarily a direct positive feedback between mean annual surface melt and enhanced glacier flow. Rather, there is more likely a feedback between runoff variability and glacier flow enhancement. Therefore, a melt season characterized by multiple warm weather periods lasting two to three days, interspersed with cool periods of similar length that interrupt runoff, may produce sufficient high-frequency variations in meltwater supply to keep the subglacial drainage system in a constant state of adjustment. This would result in a series of multiple fast flow events during the hydro-active phase. In contrast, a monotonically warm melt season may result in glacier velocity showing less dynamic variation in the later part of summer, and possibly returning to a quiescent state earlier. We can see evidence for the first case, the highly variable melt and velocity profile, during phase 4 of 2010 (Figure 3-8, days 185 to 225), whereas phase 4 of 2009 (Figure 3-7, days 197 to 225), was characterized by consistently warm (above freezing) air temperatures, which resulted in very little velocity variability.

3.6.2.3 Links to Synoptic Weather Changes

Our observations may suggest that summer glacier velocity variability is positively correlated with variability in synoptic weather patterns. A recent

investigation of melt season characteristics over the Devon Ice Cap (Gascon and others, 2013) reported an increased frequency of 3-5 day long surface low-pressure systems in August during the later half of the 2000-2010 decade. These low pressure systems bring warm moist air to the Canadian Arctic from the south and result in a significant short-term shift in the surface energy balance. The associated increases in relative humidity and heavy cloud cover block incoming shortwave radiation but increase the absorption and re-emission of longwave radiation, producing a net increase in available melt energy. The timing and frequent occurrence of these low-pressure systems (and associated changes in net longwave radiation) identified by Gascon and others (2013) help to explain the 3-5 day variability in melt (and implied runoff) which we observed on Belcher Glacier in August 2010.

If Arctic atmospheric conditions favourable to the development of surface low pressure systems persist, we might expect to see the trend towards longer and more variable melt seasons continue. It has already been suggested that extended portions of Greenland may experience further flow acceleration if runoff rates are frequently amplified by rainfall (Schoof, 2010), since a northward shift in the North Atlantic storm track is predicted to increase precipitation over a large area of the ice sheet in the 21st century (Schuenemann and Cassano, 2010). The latter study indicates that Baffin and Devon islands, and to a lesser extent Ellesmere Island, will see an increase in precipitation and changes in synoptic patterns over the coming century. This could suggest that Belcher Glacier, and other outlet glaciers in the region, could continue to display highly variable late-summer flow rates, similar to that observed in 2010.

3.6.3 Impact of Summer Speedup on Annual Ice Displacement

One of our goals was to determine whether the summer speedup constituted a significant fraction of the total annual ice displacement. In Table 3-3 we compared the enhanced displacement that occurred during summer (the total EVD) with the total annual ice displacement (TAD) that was determined by repeat

dGPS stake survey in May of each year. These results show that the ice flow that occurred during the ~2 month mid-summer period (or 15% of the year) made up 19-22% of the total annual displacement in the terminus region, and 10-17% in the mid- and upper-glacier regions. But to determine whether year to year differences in summer velocity translate to proportional changes in total annual displacement we also need to examine these flow speed changes from the perspective of inter-annual variability.

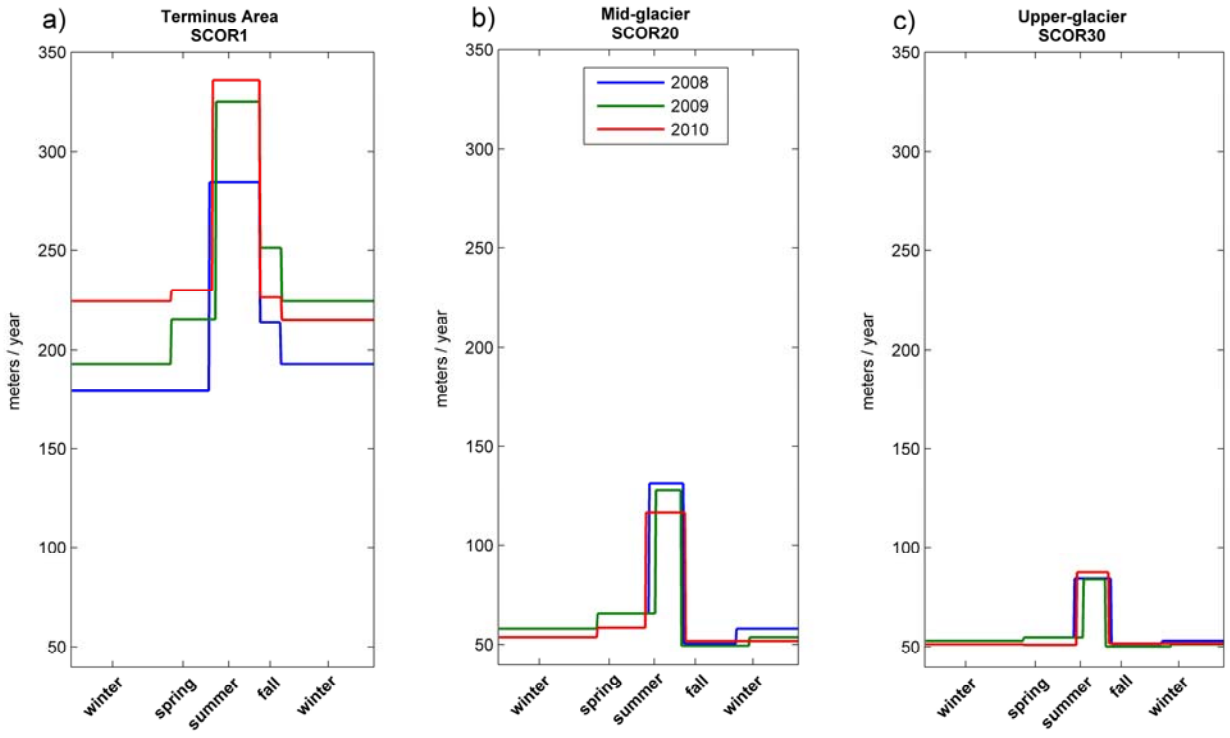

Figure 3-11: Inter-annual comparisons of seasonal mean ice velocity at the terminus, mid-glacier, and upper-glacier regions, 2008-2010. The seasonal ice velocities plotted here come from Table 3-3 and 3-4.

The three sub-plots of Figure 3-11 show the 2008-2010 spring, summer, fall and winter velocities at each of the SCOR sites. These plots reveal that the seasonal velocity cycles in the mid- and upper-glacier regions are highly consistent, while those in the terminus area are more variable between years. We interpret this to mean that there may be significant differences in the dynamic behaviour between these regions.

At SCOR20 and SCOR30 (Figure 3-11b and 3-11c), the summer velocity was 97-104% and 57-67% faster, respectively, than the spring velocity at these sites. At both of these sites, the minimum annual velocity occurred in the fall, and the velocity increased gradually over the course of the winter and following spring. The high summer velocity occurred for a much shorter fraction of the year than the slower fall and winter velocity, and as a result the annual mean velocity approximates the spring velocity.

The fall minimum velocity was remarkably consistent year to year, and we interpret this to mean that the annual minimum velocity in these regions represents ice flow dominated by internal deformation, with minimal contribution by hydrologically driven sliding. This assertion is consistent with the expected decrease in subglacial water pressure that would follow the rapid decrease in runoff inputs to the subglacial drainage system at the end of the melt season. Any remaining water stored at the bed would likely continue to drain down-glacier through the well developed channel system, and water pressure would become very low across most of the bed in these regions. Furthermore, if any moulins or englacial conduits remained open, then subglacial water pressure in the connected channel networks would approach atmospheric pressure (Willis, 1995). The slow increase in ice velocity through the winter and spring could be explained as the result of the progressive closure of these englacial and subglacial drainage channels; the vastly decreased volume of subglacial cavity space that would result from the downward pressure of thick ice in these regions would mean that even small amounts of stored water (or water generated by frictional heating) may result in progressively decreased effective pressure in an inefficient, non-channelized system composed of semi-isolated cavities (Weertman, 1972; Iken and Bindschadler, 1986).

Figure 3-11a shows us that the terminus region exhibits very different behaviour. At SCOR1, the change in velocity from spring to summer was relatively consistent each year, but the rate of slow-down in fall, the timing and magnitude of the annual velocity minimum, and the total annual displacement

were all variable. The variability in the annual velocity minimum and the generally high but variable total annual displacement suggest that there is always basal water present in the terminus region, but that the pressure is likely modulated by something other than just the availability of surface runoff. We hypothesize that subglacial water pressure in this region may be kept perennially high due to a connection between the subglacial drainage system and marine water and due to the fact that a large percentage of the ice in this region is grounded below mean sea level, meaning that some portion of this region may be close to flotation. Because of this, even relatively small additions of runoff to subglacial water storage (crevasse drainage, additional late-fall runoff), may potentially enhance glacial sliding in this region.

Unlike the mid- and upper-glacier regions, minimum velocity in the terminus region did not occur in the fall, but rather in the winter or spring. In the fall, the terminus-region velocity was still gradually decelerating from the summer maximum. Our interpretation of these observations is that water from up-glacier storage continued to pass through the subglacial drainage system, through and beyond the end of the melt season, and continued to sustain relatively high water pressures in the terminus region. We propose two potentially complementary reasons for the inter-annual difference in the rate of fall slow-down and the variable timing in annual minimum velocity: 1) The fall of 2009 was slightly warmer than that of either 2008 or 2010. Temperatures high enough to produce small amounts of melt may have persisted a little longer in 2009, especially at lower elevations. We have not shown the temperature time series past day 227 in Figures 3-6, 3-7, or 3-8 (and have not calculated PDD or ablation past this date). 2) Just as the thick snowpack may have delayed meltwater drainage in the spring of 2009, we suspect it may have played a similar role in the fall by slowly releasing stored meltwater from areas above the ELA. Observations of liquid water persisting in firn aquifers long past the end of fall freeze-up have been reported (Forster, 2013). It is conceivable that water within firn, insulated from sub-freezing surface air temperatures by lingering snow in the

accumulation area, could continue to flow through englacial drainage networks before these pathways became closed off in winter (Fountain and Walder, 1998).

We estimate the effective change in annual displacement attributable to the summer speedup (*Δds* hereafter) as the difference between the total annual displacement and the hypothetical displacement that would occur if the ice moved only at the non-summer flow speed for 365 days (i.e. without seasonal hydrological forcing). The *Δds* was expressed in three different ways:

1. The Absolute displacement change:

Absolute Δds = TAD – Dw

2. The Relative displacement change as a percentage of TAD:

Relative Δds = (TAD – Dw) / TAD x100%

3. The Deviation from the 3-year mean non-summer displacement:

Deviation Δds = TAD – $mDw_{2008:2010}$

where:

TAD is the total annual ice displacement at a given SCOR site for a given year.

Dw is the displacement at the non-summer velocity (from Table 3-4) for a given SCOR site in a given year.

$mDw_{2008:2010}$ is the displacement at the 2008-2010 mean non-summer velocity for a given SCOR site.

Figure 3-12 shows, for each SCOR site and year, a) the Absolute *Δds*, b) the Relative *Δds*, and c) the Deviation *Δds*, plotted against the annual ablation which was determined for each SCOR site. If we look at Figure 3-12a as a whole and consider all sites in all years, there is a roughly linear relationship between the Absolute *Δds* and local ablation. However, this in itself does not necessarily mean that the *Δds* always increases with greater ablation (and implied runoff / potential for hydrological forcing). Rather, we also note that the points cluster reasonably well by site (symbol shape), and together the trend and the site clusters indicate that the Absolute *Δds* increases towards the glacier terminus. This linear relationship breaks down in Figure 3-12b where we compare the Relative *Δds*.

Because ice velocity is generally much higher at SCOR1, *Δds* as a percentage of the TAD is lower than that at SCOR20, where the average summer velocity may be up to 100% higher than the background velocity, which is relatively lower.

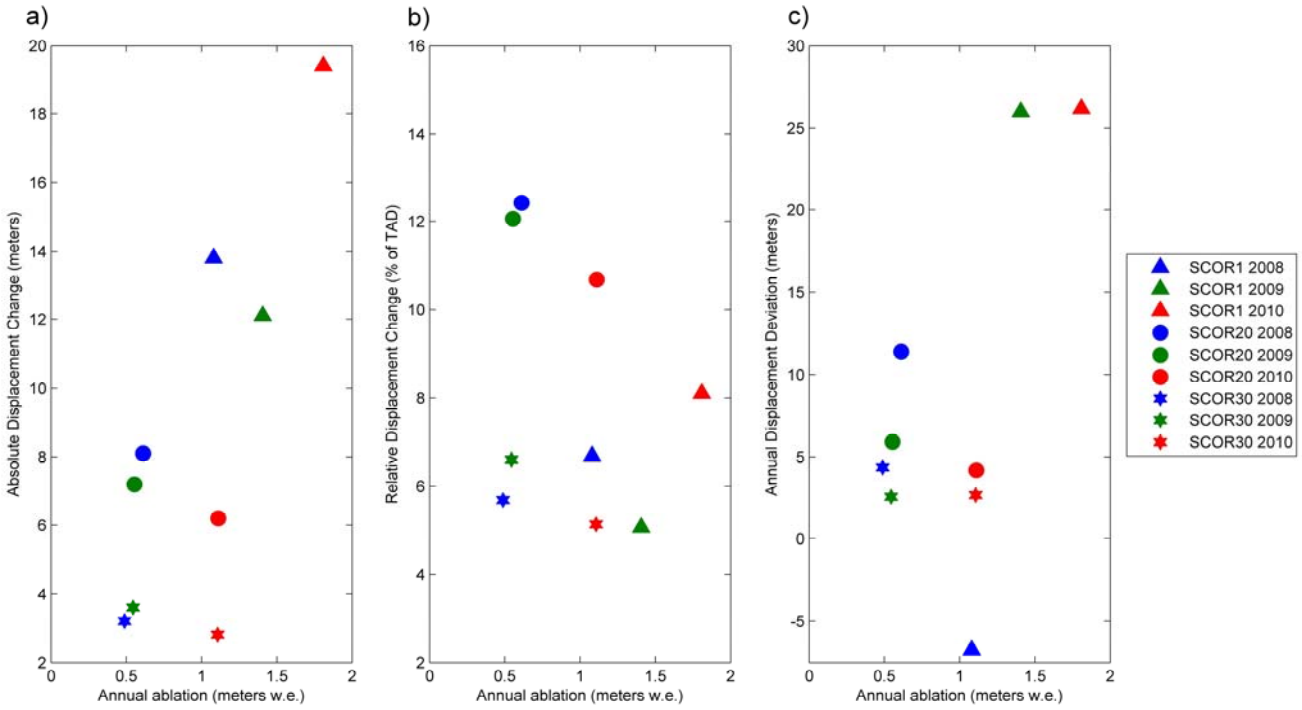

Figure 3-12: Comparisons of *Δds*, the effective change in annual displacement caused by the summer speedup vs. the summer surface ablation at each SCOR site: (a) Absolute value (meters) of *Δds*, (b) *Δds* Relative to TAD (%), and (c) *Δds* as a deviation from the mean non-summer velocity (meters). Symbol shapes correspond to SCOR site locations, and colors correspond to year.

A more interesting pattern emerges when we examine the relationship between *Δds* and annual ablation within the site location clusters. In both Figures 12a and 12b, the triad of points forming the SCOR20 (circles) and SCOR30 (stars) clusters show that 2010 (red point) was markedly different from the previous years. In both of these locations, relative and absolute *Δds* were similar in 2008 and 2009 and local ablation varied only slightly. The year with higher local ablation (2008 at SCOR20, 2009 at SCOR30) experienced slightly higher absolute *Δds* (0.9 m at SCOR20, 0.4 m at SCOR30). At both of these sites, the

local ablation approximately doubled in 2010, but the *Δds* decreased. In this way, our observations suggest that the mid and upper regions of Belcher Glacier behave comparably to land-terminating portions of the GrIS (Sundal and others, 2011), and other Arctic and alpine valley glaciers (Müller and Iken, 1973; Truffer, 2005), where multi-year observations have shown higher annual velocities due to a more effective summer speedup during years with lower than average ablation. Sundal and others (2011) also show that during high-melt years, peak velocities may be higher but the summer speedup is typically shorter in duration and may lead to a quicker fall slow-down.

The cluster of points representing SCOR1 (triangles) shows essentially the opposite pattern for the terminus region: compared to 2008, there was more ablation in 2009, but lower absolute and relative *Δds*, while in 2010 there was substantially more ablation than in either of the previous years, and also much higher *Δds* (~6m greater than in 2008). Again, *Δds* does not linearly scale with ablation, but this pattern does confirm what we have already observed in Section 6.2 regarding factors that drive the inter-annual differences in seasonal flow patterns: the melt season of 2010 produced the highest annual ablation and also strong fluctuations in runoff at a frequency that seems to have kept the subglacial drainage system in a perpetual state of fluctuating pressure.

The most significant thing to note in Figure 3-12c is that the point representing the Deviation *Δds* at SCOR1 in 2008 falls far outside the cluster of the other SCOR1 points. The Deviation *Δds* was actually negative in this year, meaning that the total annual displacement at SCOR1 in 2008 was less than the mean non-summer displacement. By contrast, the Deviation *Δds* at the same site was nearly identical in 2009 and 2010. Because Figure 3-12c shows the annual differences in *Δds* relative to a common inter-annual reference displacement, we can see that the magnitude of the summer speed-up does not necessarily produce proportional changes in the glacier's total displacement at the terminus. Figure 3-11a shows that the difference between the spring and summer velocity at the terminus is relatively consistent between years, and that the spring to summer

speedup is not what drives differences in annual displacement. Rather, this part of the glacier may be exhibiting cycles of velocity change at annual or longer periods, perhaps in response to changes in total annual runoff volume, or perhaps in response to other factors which we have not explored here. The seasonal velocity changes are a higher frequency signal superimposed on these longer term velocity variations.

3.6.4 Factors influencing terminus zone dynamics

Our observations above suggest that the ice dynamics and subglacial hydrologic systems are significantly different between the terminus area, and the mid and upper portions of this glacier. Overall, the mid and upper-glacier regions demonstrate summer velocity variations very similar to those previously observed on land-terminating Arctic and alpine valley glaciers. In these regions, the annual velocity is relatively consistent, and the effective increase in annual displacement due to the summer speedup is greater in years with lower runoff volumes. These observations suggest that the subglacial drainage system undergoes an evolution in drainage efficiency that effectively limits the hydrological forcing of velocity variations. By contrast, in the terminus zone we see an increase in the annual velocity with increased ablation, and an increase in the Δds during summers with high ablation and high runoff variability. This suggests that even though the subglacial drainage system in the terminus region undergoes a seasonal evolution in efficiency, additional factors modulate the subglacial water pressure and rates of basal motion.

We suggest four reasons for the shift in flow dynamics between the terminus (marine) and upper-glacier (alpine) regimes:

1. Lateral friction from valley walls – The mid- and upper- regions of Belcher Glacier flow through a narrow, deep valley. Here, a larger portion of the glacier sole is in contact with the U-shaped valley walls than with the bottom of the valley trough. However, in its lowest 5km, the glacier becomes wider and thinner as it merges with another tributary flow unit from the northwest. As a

result, the surface area of the glacier bed increases, and one side of the glacier is in contact with another moving body of ice rather than a confining rock wall. This suggests that there may be less lateral friction per unit width of the glacier in this region. The lateral shear zones occupy progressively less of the glacier as the width increases, and flow in the center is essentially unaffected by the presence of the valley walls; in this respect, the glacier behaves similarly to an ice shelf (see Figure 12.4 of Paterson (2002)). Therefore, basal friction in the terminus region would become a more important (perhaps the dominant) force resisting flow, and thus hydrologic perturbations to basal friction would have a greater influence on the flow in this region, as opposed to the narrower and more laterally constricted mid- and upper-glacier regions.

2. Bed geometry - A second possible reason for the difference between the two regimes may be the hydrologic effect of the bed being below sea level: if the subglacial hydrologic system is fully connected, its downstream end will be in contact with marine water, and will therefore be at pressure equilibrium (at minimum) with the water-column at the point where conduits exit the glacier at the calving front. Observations of meltwater plumes emerging from the glacier terminus (Milne, 2011) show that subglacial water escapes from the glacier throughout the summer, and that there is communication between the subglacial drainage system and marine water. If subglacial water is escaping conduits open to marine water, then the subglacial water pressure must be greater than the pressure exerted by the depth of water at the channel exit point. This suggests that much of the glacier where the bed is below sea level could have perennially elevated subglacial water pressure, as has been suggested for at a number of other tidewater glaciers (Vieli and others, 2004).

Following the descriptions of Shreve (1972) and Hooke (2000), we calculate the hydraulic potential and potential gradient along the glacier centerline to provide an indication of how the bed geometry influences the subglacial hydrology, and how this might explain some of the differences between the marine and alpine regimes. We use the following equation to approximate

hydraulic potential under the conditions we would expect in the fall: subglacial channels may exist, but are likely not water-filled because runoff has stopped, and thus channel water pressure approaches atmospheric for areas where the bed is above sea level.

Equation:

$$\Phi = Pb + (Pi - Pm)$$

$$= (\rho_w g z) + (\rho_i g H - \rho_w g (h_w))$$

where:

ρ_w and ρ_i are the densities of water and ice, respectively.

g is gravitational acceleration.

z is the bed elevation, and H is the ice thickness.

h_w is the depth of the water column from sea level to the glacier bed.

(h_w is negative where the bed is below sea level, or otherwise zero.)

In this case the local hydraulic potential (Φ) is made up of three components: the potential due to the bed elevation with respect to sea level (Pb), the pressure exerted by the weight of the ice (Pi), and the pressure exerted by the marine water column for areas where the glacier bed lies below sea level (Pm). The hydraulic potential (the red line in Figure 3-13b) demonstrates sensitivity to both the bed and ice surface slope (Figure 3-13a). The local potential is elevated in areas where the bed is below sea level (i.e. between 0-20 km from the terminus), but lower in places where the ice is relatively thin (i.e. between 2.5 – 5 km from the terminus). The first derivative (taken from the up-glacier end of the centerline, to the terminus) gives the gradient of hydraulic potential. A negative gradient occurs in areas where the local potential causes water to flow down-glacier, while a positive gradient identifies areas where reversal in bed-slope may cause local damming and potential storage of subglacial water.

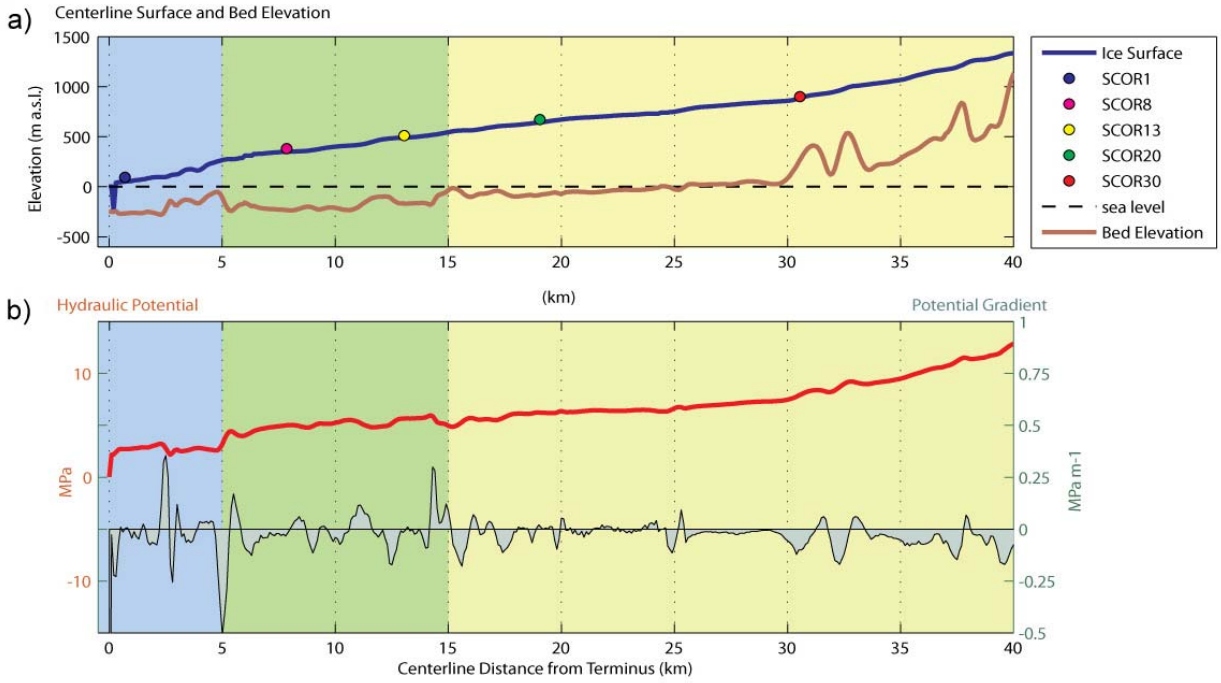

Figure 3-13: a) Elevation profiles of glacier bed (brown line) and surface (blue line). b) Profiles of the local hydraulic potential (red line) and the potential gradient (black line with grey area shading).
In both a) and b), the background shading identifies our proposed dynamic regimes: the marine zone (blue) from 0-5km from the glacier terminus, a transition zone (green) from 5-15km, and the alpine zone (yellow) from 15-40km from the terminus.

Between 0 km and 5 km from the calving margin (the area we have referred to as the terminus zone), ice is thinner than in most other regions of the glacier, and a higher fraction of the ice thickness lies below sea level than above it. Some of the ice in this region, especially that closest to the marine margin, may be at or near flotation (Milne, 2011). Strong variations between negative and positive hydraulic potential gradient in this region indicate that some of the undulations in the bed could present places where water storage could occur (though it should be noted that we are only looking at hydraulic potential along a 1-D flowline, thus ignoring lateral variation). We expect the effective pressure to be very low due to the water depth in relation to the ice thickness, and a contributor to persistently high rates of basal sliding (Vieli and others, 2004).

We consider the section from 5 km to 15 km from the margin to be a transition zone between the terminus zone and the alpine zone, which makes up the remainder of the glacier (from 15 km to >40 km). The ice in the transition zone is still grounded 100-200 m below sea level, but the ice is much thicker, and a larger fraction of the ice depth is above sea level. In the lower part of the alpine zone (15-25 km), a very small fraction of the ice thickness is below sea level, and the remainder of the alpine zone is entirely grounded above sea level. The hydraulic potential in the transition zone is elevated due to the additional pressure exerted by marine water. Multiple variations in the potential gradient throughout this zone indicate locations where basal water storage may occur. We suggest that the effective pressure in the transition zone is perennially lower than in the alpine zone, and that this may be the reason for the difference in the Quiescent period velocities between these two regions. In the transition zone (as seen at SCOR8 and SCOR13 in Figure 3-9c), the Quiescent period velocity of the ice increases towards the terminus, suggesting increased rates of basal sliding due to a gradient in effective pressure, even in the absence of active meltwater drainage. At SCOR20 and SCOR30, by comparison, the Quiescent period velocity does not increase appreciably down-glacier. The hydraulic potential gradient between these sites is predominantly negative, indicating that the bed in this region is likely well drained and there are fewer opportunities for water storage.

3. Bed composition – Previous investigations of the Devon Ice Cap have suggested that glacial-marine sediment at the bed where these glaciers are grounded below sea level may influence the flow dynamics near the termini of the major marine terminating outlet glaciers (Dowdeswell and others, 2004; Burgess and others, 2005). These sediments may have formed during past warmer periods (the Holocene thermal maximum and perhaps the Sangamon interglacial) when the Devon Ice Cap was considerably smaller (Koerner, 1979; Koerner and Fisher, 2002), and the fjords now occupied by outlet glaciers were filled with water. In 2006, bathymetric mapping of the seafloor immediately in front of Belcher Glacier revealed features which are consistent with the presence of a deformable

substrate, including moraines, fluting, and scouring marks (Bell and others, 2006). Given the high water pressure we expect to find at glacier beds in these regions, these sediments may be deformable, and their deformation may contribute to increased rates of basal motion. While Burgess and others (2005) did not specifically suggest this mechanism for Belcher Glacier, it may play a small role in the high and variable rates of ice flow found at the terminus of this glacier.

4. Distribution of sink points - Finally, we suggest that meltwater entry points (moulins and large crevasses that are prone to hydro-fracture) are more densely and evenly distributed in the terminus region of the glacier. The terminus region is highly crevassed, and these crevasses fill with water and drain early in the melt season (Danielson and Sharp, 2013). As ablation rates are very high in this region and local runoff can enter the system at multiple entry points, subglacial water pressure could be elevated over a wide area of the bed. We have suggested that meltwater drainage into these crevasses is responsible for the terminus activation phase ('Phase 2') of the seasonal velocity variation cycle, and that this effect is confined to the lower ~5 km of the glacier. This hypothesis aligns with that of Williamson and others (2008) who monitored multiple QEI tidewater outlet glaciers via repeat optical imagery and observed that those glaciers with heavily crevassed terminus regions and prevalent water-filled crevasses tended to have higher annual near-terminus velocities and exhibit the greatest seasonal velocity fluctuations, whereas those glaciers with minimal terminus crevassing and surfaces efficiently drained via supra-glacial stream networks flowed more slowly and consistently.

In contrast, the mid- and upper-glacier areas have fewer sink points since there are fewer and smaller crevasses in these regions, and moulins are typically separated by several kilometres (Wyatt, 2013). The surface drainage system in these regions is highly developed along linear features, such as flow stripes, and runoff from large areas is consolidated into a few major channels. To illustrate this point, we note the distance between *moulin_C* and *moulin_F* in Figure 3-1. While these are not the only sink-points in this region of the glacier, these have

been identified as the major moulins which drain significant regions of the upper glacier (Duncan, 2011). The surface here is not heavily crevassed, so the surface drainage channels have few potential sink-points. This means that a relatively high volume of surface runoff enters a small number of moulins and very likely a few large subglacial channels. It is likely then, that this water may influence the subglacial water pressure (and potentially basal sliding) over a relatively small fraction of the glacier bed, and only for short periods of time (such as when channels are developing or adjusting to changing meltwater input rates).

3.7 Conclusions

Collecting observations of ice flow velocity, surface meltwater production rates, and surface hydrologic drainage events on a single tidewater glacier in three successive years has allowed us to observe three summer seasons with notably different characteristics in terms of both surface melt and glacier dynamic response to meltwater forcing. Our observations led us to the following four conclusions about the character of the seasonal velocity variations and their impact on annual ice flow at Belcher Glacier:

Each year a distinct seasonal pattern of velocity change occurs at this glacier, which we have broken down into five recognizable phases: the quiescent phase, the terminus activation phase, the spring event, the late-summer hydro-active phase, and the return to quiescence. This cycle of velocity change occurs over a period of 50-60 days during the peak of the melt season (mid-June to mid-August).

Variations in this pattern occur, and affect the timing and the magnitude of the summer speedup. Our observations suggest that the primary drivers of these variations are the thickness of the spring snowpack and the variability of late summer melt. Thicker than average spring snowpack delays the spring event by limiting melt production and slowing the development of supra-glacial drainage. Late summer variability in melt rates, which we infer were driven by synoptic-scale storms and weather patterns at 3-5 and 20-30 day periods, produced more

variability in late summer velocity than a more consistently warm summer with only diurnal variability in air temperature. We suggest that this is due to the time-varying evolution of the subglacial drainage channels, which can evacuate high volumes of water at low pressure under sustained high runoff rates, but may undergo pressure fluctuations while adapting to variable runoff rates.

The summer speedup does not make a large contribution to the total annual ice displacement. As a percentage, the effective change in annual displacement caused by the summer speedup was 5-7% in the upper glacier, 11-13% in the mid-glacier, and 5-8% in the terminus region. In the mid- and upper-glacier regions, these changes were roughly proportional to the annual variations in the summer speedup, as measured by our EVD metric. However, the inter-annual differences in total ice displacement in the terminus region are larger and cannot be explained by variations in the summer speedup alone. Ice in the terminus region seems to undergo velocity fluctuations at annual or longer time-scales, with seasonal variations superimposed on top. These annual scale variations may be a response to the variations in total annual ablation or to changes in the force balance of the terminus region; a longer time series of observations are required to confirm this. However, we have not monitored all aspects of this system, and other possible causes for these longer-term displacement changes may include changes to the back-stress at the glacier terminus due to variations in the sea-ice/mélange breakup, or rates of submarine melting at the ice margin.

Our observations of the flow dynamics of this glacier lead us to conclude that this glacier behaves as a bi-modal system: the mid- and upper-glacier, flowing between deep, confining valley walls, is slow flowing (~60 m a^{-1}), demonstrates little interannual variability in total displacement (7 m a^{-1}), and exhibits seasonal velocity variations similar to those observed on other Arctic and alpine valley glaciers; the terminus region is fast flowing (>200 m a^{-1}), undergoes more interannual displacement variability (>30 m a^{-1}) than the regions up-glacier, and the summer speedup in this region lasts much longer. We suggest that the differences in flow dynamics in the terminus region are due to: 1) decreased

lateral friction from the valley walls, 2) lower effective pressure due to the high fraction of ice below sea level in this region and the increased water pressure caused by the marine water column, 3) the possibility that a deformable bed composed of marine sediments may contribute to higher rates of basal motion near the terminus, and 4) the higher density of meltwater sink points in the terminus region.

3.8 Bibliography

Andersen, M. S., M. Nettles, P. Elósegui, T. B. Larsen, G. S. Hamilton, and L. A. Stearns 2011, Quantitative estimates of velocity sensitivity to surface melt variations at a large Greenland outlet glacier. *Journal of Glaciology*, **Vol. 56**, no. 204, 609-620.

Bartholomaus, T. C., R. S. Anderson and S. P. Anderson 2008. Response of glacier basal motion to transient water storage. *Nature Geoscience* **Vol 1**(Number 1), 33-37.

Bartholomew, I., P. Nienow, D. Mair, A. Hubbard, M. A. King and A. Sole 2010. Seasonal evolution of subglacial drainage and acceleration in a Greenland outlet glacier. *Nature Geoscience* **3**(6), 408-411.

Bartholomew, I., P. Nienow, A. Sole, D. Mair, T. Cowton, S. Palmer and J. Wadham 2011a. Supraglacial forcing of subglacial drainage in the ablation zone of the Greenland ice sheet. *Geophys. Res. Lett.* **38**(8), L08502.

Bartholomew, I. D., P. Nienow, A. Sole, D. Mair, T. Cowton, M. A. King and S. Palmer 2011b. Seasonal variations in Greenland Ice Sheet motion: Inland extent and behaviour at higher elevations. *Earth and Planetary Science Letters* **307**(3-4), 271-278.

Bell, T., D. St. Hilaire, S. Brucker, J. Hughes Clarke, B. Danielson, M. Sharp and L. Tarasov (2006). Seabed mapping at the terminus of Belcher Glacier, Devon Island, Nunavut. *3rd Annual ArcticNet Scientific Meeting*, Victoria, British Columbia, CAN.

Bingham, R. G., P. W. Nienow and M. J. Sharp 2003. Intra-annual and intra-seasonal flow dynamics of a High Arctic polythermal valley glacier. *Annals of Glaciology* **37**(1), 181-188.

Blaszczyk, M., J. Jania and J. O. Hagen 2009. Tidewater glaciers of Svalbard: Recent changes and estimates of calving fluxes. *Polish Polar Research* **30**(2), 85-142.

Boon, S. and M. Sharp 2003. The role of hydrologically-driven ice fracture in drainage system evolution on an Arctic glacier. *Geophysical Research Letters* **30**(18).

Braithwaite, R. J. 1995. Positive degree-day factors for ablation on the Greenland ice sheet studied by energy-balance modelling. *Journal of Glaciology* **41**(137), 153-160.

Burgess, D. O. and M. J. Sharp 2004. Recent changes in areal extent of the Devon Ice Cap, Nunavut, Canada. *Arctic, Antarctic, and Alpine Research* **36**(2), 261-271.

Burgess, D. O., M. J. Sharp, D. W. F. Mair, J. A. Dowdeswell and T. J. Benham 2005. Flow dynamics and iceberg calving rates of Devon Ice Cap, Nunavut, Canada. *Journal of Glaciology* **51**(173), 219-230.

Canada, N. R. (2004) "On-Line Precise Point Positioning Project - How To Use Document " Version 1.1, Natural Resources Canada, Ottawa

Canada, N. R. 2007. CSRS-PPP Accuracy, https://www.nrcan.gc.ca/earth-sciences/geomatics/geodetic-reference-systems/canadian-spatial-reference-system/about-spatial, Natural Resources Canada.

Copland, L., M. J. Sharp and P. W. Nienow 2003. Links between short-term velocity variations and the subglacial hydrology of a predominantly cold polythermal glacier. *Journal of Glaciology* **49**(166), 337-348.

Cowton, T., P. Nienow, A. Sole, J. Wadham, G. Lis, I. Bartholomew, D. Mair and D. Chandler 2013. Evolution of drainage system morphology at a land-terminating Greenlandic outlet glacier. *Journal of Geophysical Research: Earth Surface* **118**, 1-13.

Danielson, B. D. and M. J. Sharp 2013. Development and application of a time-lapse photograph analysis method to investigate the link between tidewater glacier flow variations and supraglacial lake drainage events. *Journal of Glaciology* **59**(214), 287-301.

Das, S. B., I. Joughin, M. D. Behn, I. M. Howat, M. A. King, D. Lizarralde and M. P. Bhatia 2008. Fracture Propagation to the Base of the Greenland Ice Sheet During Supraglacial Lake Drainage. *Science* **320**(5877), 778-781.

Dowdeswell, J. A., R. P. Bassford, M. R. Gorman, M. Williams, A. F. Glazovsky, Y. Y. Macheret, A. P. Shepherd, Y. V. Vasilenko, L. M. Savatyuguin, H. W. Hubberten and H. Miller 2002. Form and flow of the Academy of Sciences Ice Cap, Severnaya Zemlya, Russian High Arctic. *Journal of Geophysical Research-Solid Earth* **107**(B4).

Dowdeswell, J. A., T. J. Benham, M. R. Gorman, D. Burgess and M. J. Sharp 2004. Form and flow of the Devon Island Ice Cap, Canadian Arctic. *Journal of Geophysical Research-Earth Surface* **109**(F2).

Dowdeswell, J. A., T. J. Benham, T. Strozzi and J. O. Hagen 2008. Iceberg calving flux and mass balance of the Austfonna ice cap on Nordaustlandet, Svalbard. *J. Geophys. Res.* **113**(F3), F03022.

Duncan, A. 2011. Spatial and Temporal Variations of the Surface Energy Balance and Ablation on the Belcher Glacier, Devon Island, Nunavut, Canada. (*MSc. Thesis*, University of Alberta.)

Dunse, T., Schuler, T. V., Hagen, J. O., and Reijmer, C. H. 2012. Seasonal speed-up of two outlet glaciers of Austfonna, Svalbard, inferred from continuous GPS measurements. *The Cryosphere* **6**, 453-466.

Forster, R. R., J. E. Box, M. R. van den Broeke, C. Miege, E. W. Burgess, J. H. van Angelen, J. T. M. Lenaerts, L. S. Koenig, J. Paden, C. Lewis, S. P. Gogineni, C. Leuschen and J. R. McConnell 2013. Extensive liquid meltwater storage in firn within the Greenland ice sheet. *Nature Geoscience* doi:10.1038/ngeo2043

Fountain, A. G. and J. S. Walder 1998. Water flow through temperate glaciers. *Reviews of Geophysics* **36**(3), 299-328.

Gardner, A. and M. Sharp 2009. Sensitivity of net mass-balance estimates to near-surface temperature lapse rates when employing the degree-day method to estimate glacier melt. *Annals of Glaciology* **50**, 80-86.

Gardner, A. S., G. Moholdt, J. G. Cogley, B. Wouters, A. A. Arendt, J. Wahr, E. Berthier, R. Hock, W. T. Pfeffer, G. Kaser, S. R. M. Ligtenberg, T. Bolch, M. J. Sharp, J. O. Hagen, M. R. van den Broeke and F. Paul 2013. A Reconciled Estimate of Glacier Contributions to Sea Level Rise: 2003 to 2009. *Science* **340**(6134), 852-857.

Gardner, A. S., G. Moholdt, B. Wouters, G. J. Wolken, D. O. Burgess, M. J. Sharp, J. G. Cogley, C. Braun and C. Labine 2011. Sharply increased mass loss from glaciers and ice caps in the Canadian Arctic Archipelago. *Nature* **473**(7347), 357-360.

Gascon, G., M. Sharp and A. Bush 2013. Changes in melt season characteristics on Devon Ice Cap, Canada, and their association with the Arctic atmospheric circulation. *Annals of Glaciology* **54**(63), 101-110.

Herdes, E., L. Copland, B. Danielson and M. Sharp 2012. Relationships between iceberg plumes and sea-ice conditions on northeast Devon Ice Cap, Nunavut, Canada. *Annals of Glaciology* **53**(60), 1-9.

Herring, T. A., R. W. King and S. C. McClusky 2006. Documentation of the GAMIT GPS Analysis Software (Release 10.3), Massachusetts Institute of Technology.

Hock, R. 2003. Temperature index melt modelling in mountain areas. *Journal of Hydrology* **282**(1), 104-115.

Hoffman, M. J., G. A. Catania, T. A. Neumann, L. C. Andrews and J. A. Rumrill 2011. Links between acceleration, melting, and supraglacial lake drainage of the western Greenland Ice Sheet. *J. Geophys. Res.* **116**(F4), F04035.

Howat, I. M., J. E. Box, Y. Ahn, A. Herrington and E. M. McFadden 2010. Seasonal variability in the dynamics of marine-terminating outlet glaciers in Greenland. *Journal of Glaciology* **56**(198), 601-613.

Iken, A. 1972. Measurements of water pressure in moulins as part of a movement study of the White Glacier, Axel Heiberg Island, Northwest Territories, Canada. *Journal of Glaciology* **11**(61), 53-58.

Iken, A. and R. A. Bindschadler 1986. Combined measurements of subglacial water pressure and surface velocity of Findelengletscher, Switzerland: conclusions about drainage system and sliding mechanism. *Journal of Glaciology* **32**(110), 101-119.

Iken, A., H. Rothlisberger, A. Flotron and W. Haeberli 1983. The uplift of Unteraargletscher at the beginning of the melt season — a consequence of water storage at the bed? *Journal of Glaciology* **29**(101), 28-47.

Jakobsson, M., R. Macnab, L. Mayer, R. Anderson, M. Edwards, J. Hatzky, H. W. Schenke and P. Johnson 2008. An improved bathymetric portrayal of the Arctic Ocean: Implications for ocean modeling and geological, geophysical and oceanographic analyses. *Geophys. Res. Lett.* **35**(7), L07602.

Joughin, I., S. B. Das, M. A. King, B. E. Smith, I. M. Howat and T. Moon 2008. Seasonal speedup along the western flank of the Greenland Ice Sheet. *Science* **320**(5877), 781-783.

King, M. 2004. Rigorous GPS data-processing strategies for glaciological applications. *Journal of Glaciology* **50**, 601-607.

Koerner, R. M. and D. A. Fisher 2002. Ice-core evidence for widespread Arctic glacier retreat in the Last Interglacial and the early Holocene. *Annals of Glaciology* **35**, 19-24.

Koerner, R. M., Fisher, D.A. 1979. Discontinuous flow, ice texture, and dirt content in the basal layers of the Devon Island Ice Cap. *Journal of Glaciology* **23**(89), 209 - 222.

Kouba, J., Heroux, Pierre 2000. GPS Precise Point Positioning using IGS orbit products. G. S. Department of Natural Resources, Canada.

Mair, D., P. Nienow, M. J. Sharp, T. Wohlleben and I. Willis 2002. Influence of subglacial drainage system evolution on glacier surface motion: Haut

Glacier d'Arolla, Switzerland. *Journal of Geophysical Research-Solid Earth* **107**(B8).

McClusky, S. 2010. GAMIT-GLOBK Home Page, http://www-gpsg.mit.edu/~simon/gtgk/.

Milne, H. 2011. Iceberg calving from a Canadian Arctic tidewater glacier. (*MSc. Thesis*, University of Alberta.)

Müller, F. and A. Iken 1973. Velocity fluctuations and water regime of Artic valley glaciers. *Symposium on the Hydrology of Glaciers*. Cambridge, IASH.

Parizek, B. R. and R. B. Alley 2004. Implications of increased Greenland surface melt under global-warming scenarios: ice-sheet simulations. *Quaternary Science Reviews* **23**(9-10), 1013-1027.

Röthlisberger, H. and H. Lang 1987. Glacial Hydrology. In *Glacio-fluvial sediment transfer: an alpine perspective*. A. M. Gurnell and M. J. Clark, *ed.* Chichester, John Wiley and Sons**:** 207-284.

Schoof, C. 2010. Ice-sheet acceleration driven by melt supply variability. *Nature* **468**(7325), 803-806.

Schuenemann, K. C. and J. J. Cassano 2010. Changes in synoptic weather patterns and Greenland precipitation in the 20th and 21st centuries: 2. Analysis of 21st century atmospheric changes using self-organizing maps. *J. Geophys. Res.* **115**(D5), D05108.

Sundal, A. V., A. Shepherd, P. Nienow, E. Hanna, S. Palmer and P. Huybrechts 2011. Melt-induced speed-up of Greenland ice sheet offset by efficient subglacial drainage. *Nature* **469**(7331), 521-524.

Truffer, M. H., W.D.; March, R.S. 2005. Record negative glacier balances and low velocities during the 2004 heatwave in Alaska, USA: implications for the interpretation of observations by Zwally and others in Greenland. *Journal of Glaciology* **51**(175), 663-664.

van der Veen, C. J. 1998. Fracture mechanics approach to penetration of surface crevasses on glaciers. *Cold Regions Science and Technology* **27**(1), 31-47.

van der Veen, C. J. 2007. Fracture propagation as means of rapidly transferring surface meltwater to the base of glaciers. *Geophysical Research Letters* **34**(1), L01501.

Van Wychen, W., L. Copland, L. Gray, D. Burgess, B. Danielson and M. Sharp 2012. Spatial and temporal variation of ice motion and ice flux from

Devon Ice Cap, Nunavut, Canada. *Journal of Glaciology* **58**(210), 657-664.

Vieli, A., M. Funk and H. Blatter 2000. Tidewater glaciers: frontal flow acceleration and basal sliding. *Annals of Glaciology* **31**, 217-221.

Vieli, A., J. Jania, H. Blatter and M. Funk 2004. Short-term velocity variations on Hansbreen, a tidewater glacier in Spitsbergen. *Journal of Glaciology* **50**(170), 389-398.

Weertman, J. 1972. General theory of water flow at the base of a glacier or ice sheet. *Reviews of Geophysics* **10**(1), 287-333.

Williamson, S., M. Sharp, J. Dowdeswell and T. Benham 2008. Iceberg calving rates from northern Ellesmere Island ice caps, Canadian Arctic, 19992003. *Journal of Glaciology* **54**, 391-400.

Willis, I. C. 1995. Intra-annual variations in glacier motion: a review. *Progress in Physical Geography* **19**(1), 61-106.

Wyatt, F. 2013. The spatial structure and temporal development of supraglacial drainage systems, and their influence on the flow dynamics of High Arctic ice caps. (*Doctoral Thesis,* University of Alberta.)

Zwally, H. J., W. Abdalati, T. Herring, K. Larson, J. Saba and K. Steffen 2002. Surface melt-induced acceleration of Greenland ice-sheet flow. *Science* **297**(5579), 218-222.

Chapter Four: Flow Regimes and their relation to velocity variations of four Devon Ice Cap tidewater glaciers**

4.1 Introduction

Our investigations of Belcher Glacier, in Nunavut, Canada, used high-temporal resolution GPS observations at multiple centerline locations to identify episodic, seasonal, and inter-annual variations in the flow of this tidewater glacier. We interpreted the episodic and seasonal velocity variations observed over the 2008 – 2010 period as being caused primarily by hydrologically driven sliding at the ice bed interface, based on coincident observations of ice surface vertical motion, supra-glacial melt, and melt-water drainage events. At the seasonal scale, we concluded that the maximum velocity occurred in the summer, the minimum velocity occurred in the fall or winter, and that, in most cases, the spring velocity approximated the annual average velocity. We also determined that the total annual displacement was highly consistent over three years in the mid- and upper-glacier regions, while a multi-year change in background velocity was occurring in the terminus region.

Climatic and oceanic forcing of glacier flow can vary regionally and have a strong influence on marine outlet glacier dynamics over time (Carr and others, 2013). Based on our observations of Belcher Glacier, seasonal and annual dynamic variations are also influenced by: 1) the fjord geometry, 2) the bed geometry, 3) the bed composition, and 4) the distribution of hydrologic sink points which influence meltwater delivery to the bed and hence the spatial distribution of hydrologically-driven basal sliding. These "glacier-specific factors" (Carr and others, 2013) make it very difficult to make regional estimates or predictions of glacier dynamic response to climatic and oceanic changes.

** A version of this chapter will be submitted for publication to the Journal of Glaciology as: Danielson, B.D., M.J. Sharp, and D.O. Burgess. Flow Regimes and their relation to velocity variations of four Devon Ice Cap tidewater glaciers.

Consequently, we cannot necessarily assume that the patterns of seasonal flow variations and different dynamic regimes observed at Belcher Glacier will be repeated at the other outlet glaciers of the Devon Ice Cap, because each glacier has its own combination of these four factors.

Remote sensing methods, such as satellite radar interferometry, speckle-tracking or optical image correlation, are more appropriate than GPS observations for determining regional-scale ice velocity, because they allow the computation of high spatial-resolution velocity fields with coverage of an entire ice mass. In general terms, these methods determine the ice displacement occurring between two sequential images acquired weeks to months apart, which can be expressed as an average annual velocity. Some methods applied to optical imagery (e.g., gradient correlation, (Haug and others, 2010)) are able to utilize images collected a full year apart, but it can be difficult to acquire suitable images due to darkness during the high latitude winter and frequent cloud cover during summer. Radar imagery bypasses these limitations, potentially yielding more opportunities to collect suitable image pairs, but radar imagery differencing techniques have their own limitations. If there are significant between-image changes in the viewing geometry of the satellites, or large changes to the surface caused by melt, heavy snowfall, drifting, or deformation, then image coherence is lost and displacements cannot be determined. For this reason, image-pairs must be collected over a short time period (on the order of days to weeks) (Van Wychen, 2010; Van Wychen and others, 2012). However, extrapolating these short-interval displacements can potentially over or under estimate the true annual ice velocity, depending upon the timing of image acquisitions and the occurrence of seasonal flow variations. Since one of the most important applications of these velocity field measurements is the estimation of iceberg calving fluxes, there is a strong motivation to ensure their accuracy. Velocity measurements from on-ice GPS stations can be useful in this regard, by providing an indication of when, where, and how much seasonal velocity variability occurs, and how this might affect the relationship between extrapolated estimates and true annual velocity.

The overarching objective of this paper is to extend the scope of our analysis of ice velocity variability to other areas of the Devon Ice Cap from which multi-year GPS observations have been collected. Our specific goals are: 1) to determine whether patterns of seasonal and annual velocity variability similar to those observed on the Belcher Glacier also occur on three other major outlet glaciers of the Devon Ice Cap, 2) to relate our observations of ice velocity variability at different time scales (episodic, seasonal, annual) to the 'Flow Regimes' model that has previously been proposed for this ice cap (Burgess and others, 2005), and 3) to determine whether the Flow Regimes model may be used to relate the knowledge we have gained about seasonal- and annual-scale velocity variability at specific sites to broader regions of the ice cap. We propose that a Flow Regimes map will be helpful for assessing how well short-interval observations represent the mean annual ice velocity. This information could assist with image acquisition planning and error analysis of remote sensing based measurements of ice flow.

4.2 Background

4.2.1 Study Site

The Devon Island Ice Cap covers ~14,000 km^2 and contains ~4,110 km^3 of ice (Burgess and Sharp, 2004). It is among the largest ice caps in the Canadian Arctic. The total mass balance of this ice cap is dominated by the climatic mass balance, which has been predominantly negative since 1960, and increasingly negative over the past decade due to longer and warmer summers (Gardner and others, 2011; Sharp and others, 2011). However, iceberg calving accounted for up to 30% of the total volume loss from the ice cap between 1960 and 1999 (Burgess and others, 2005), which emphasizes the importance of considering the contribution of the dynamic mass loss component to the total mass balance.

Within the last 10 years, airborne radio echo sounding has been used to constrain the three dimensional geometry of the ice cap and its bed (Dowdeswell and others, 2004), and satellite radar and optical imagery have been used to

measure velocity fields over most of the ice surface (Burgess and others, 2005; Van Wychen and others, 2012; Wyatt, 2013). These measurements have led to some important insights into the dynamics of the ice cap. The majority of the ice cap (all of the central dome and the western margin) is grounded above sea level and is very slow flowing (~15 m a^{-1} or less). However, tidewater outlet glaciers drain the interior of the ice cap through deeply incised fjords, and punctuate the northern, eastern, and southern margins. These glaciers flow much faster (up to ~290 m a^{-1}) and their velocities generally increase towards their marine termini, which are grounded below sea level.

This study focuses on four of these glaciers, each draining a different quadrant of the ice cap. The locations of Sverdrup (north-west), Belcher (north-east), Southeast (south-east) and North Croker (south-west) glaciers are shown in Figure 4-1. Of these, Southeast Glacier is somewhat unique, in that its velocity does not increase steadily towards the terminus; it undergoes a complex pattern of velocity changes and may have a history of surge-type behaviour (Burgess and Sharp, 2008; Boon and others, 2010; Van Wychen and others, 2012).

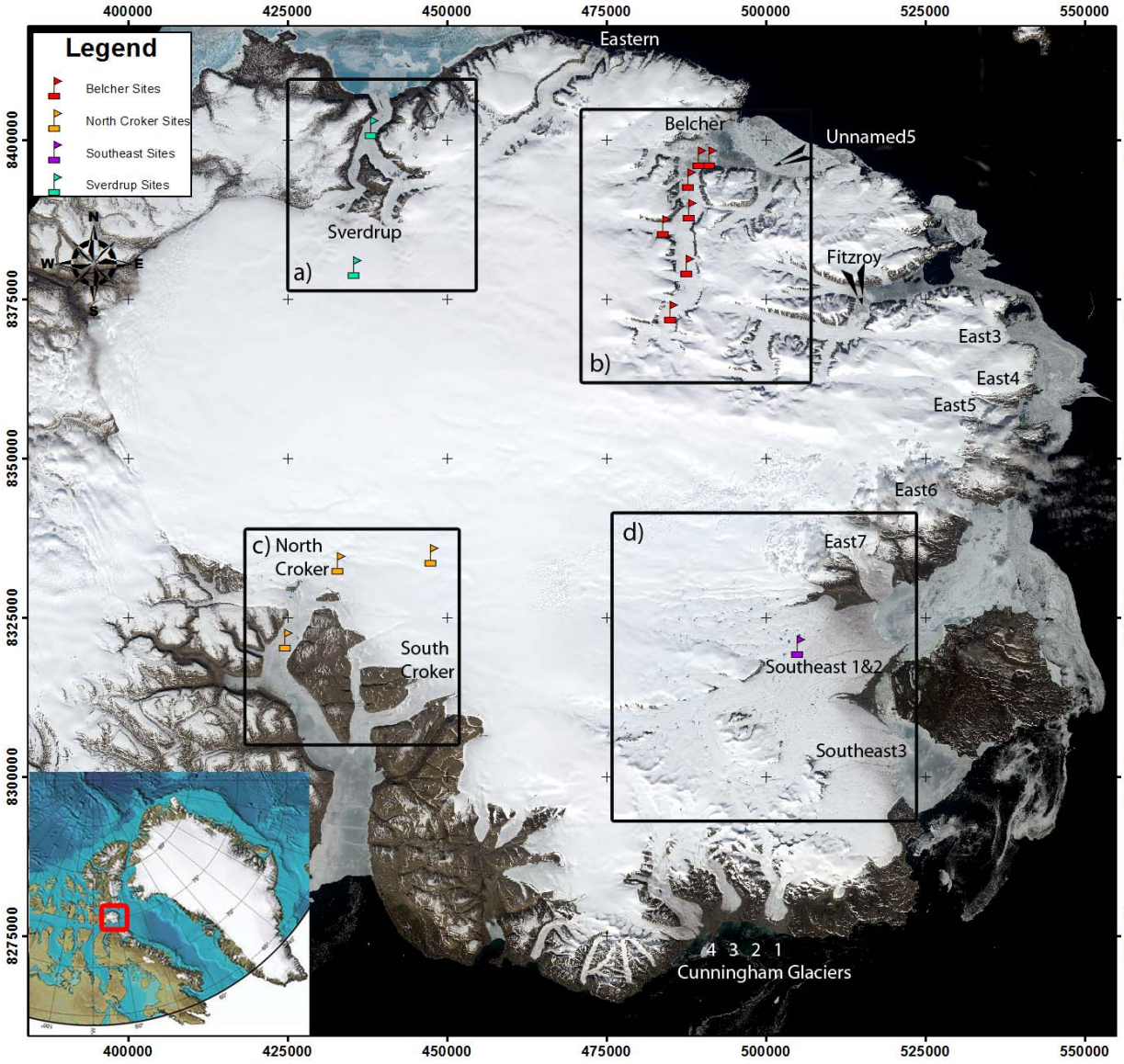

Figure 4-1: Landsat 8 OLI mosaic image (acquired July 2013) of Devon Ice Cap. Black boxes identify the locations of four sub-scenes displayed in Figure 4-3. Grid coordinates are in UTM zone 17X. Inset map shows Devon Island (bounded by red box), which is part of the Canadian Arctic Archipelago. Map selected from the International Bathymetric Chart of the Arctic Ocean (Jakobsson and others, 2008).

4.2.2 Devon Ice Cap Flow Regimes

Burgess and others (2005) identified four distinct "flow regimes" on the Devon Ice Cap using InSAR and speckle-tracking based velocity fields, and ice surface and bed elevation models derived from previous radio echo sounding (Dowdeswell and others, 2004). The authors explored the changing flow dynamics along a number of glacier flow-line transects, based on the relationship between the ice surface velocity to ice thickness ratio (v/h) and the driving stress (τ_d). One significant property of the v/h to τ_d ratio is that its inverse has the same units as viscosity (Pa s), and therefore low(high) ratios of v/h to τ_d represent high(low) 'effective viscosity' of the glacier. Plotting the values of v/h versus τ_d from points along these transects revealed trends indicative of evolution in $v/h : \tau_d$ along glacier flow-lines that implied changes in flow mechanics. Each of the four flow regimes defined represents a different trend or cluster found in the v/h vs. τ_d scatter plot. Threshold values of v/h and τ_d were later imposed to define the approximate cluster domains of each regime and facilitate the production of a raster map of flow regimes over the entire Devon Ice Cap. The key characteristics of each flow regime are summarized below, following Burgess and others (2005).

Flow Regime 1 (FR1) was defined by very low values of v/h ($< 0.075\ a^{-1}$), but no threshold value of τ_d. The limited change in v/h over a wide range of driving stresses was interpreted to suggest that ice in these regions is cold based and frozen to the glacier bed. This regime is characteristic of the high-altitude interior region of the ice cap where flow velocities are very low.

Flow Regime 2 (FR2) is differentiated from FR1 in that values of v/h are higher (typically $> 0.075\ a^{-1}$), v/h is more sensitive to changes in τ_d, and there is generally, though not always, a slightly negative trend between v/h and τ_d. This regime initiates at the heads and continues along the trunks of the main outlet glaciers, where driving stress and rates of shear deformation are typically higher than found in FR1. Burgess and others interpreted the along-flow trends in v/h to τ_d in this region as evidence for a reduction in effective viscosity. The higher

surface velocities observed suggest that basal sliding and enhanced ice deformation occur in these regions, likely because the temperature of the basal ice reaches the pressure melting point. The onset of flow stripes in these regions supports the interpretation that basal motion begins to contribute significantly to surface velocity, as flow stripes are expected to form only where rates of basal sliding are much higher than rates of internal deformation (Gudmundsson and others, 1998).

In Flow Regime 3 (FR3), there is a stronger negative trend between v/h and τ_d as distance increases along a flowline. This seems to occur at threshold values of v/h greater than 0.28 a^{-1} and τ_d greater than 0.075 MPa. The higher values of the v/h to τ_d ratio imply that the effective viscosity of ice in these regions is lower than in FR2. Well developed flow stripes are visible on the surface in regions of FR3. The transition from FR2 to FR3 often coincides with areas of intense crevassing on fast flowing parts of outlet glaciers, suggesting an increase in longitudinal strain rates. Such crevasses provide a high number of potential sink points for surface melt-water, which could then contribute to basal lubrication and higher velocities during the melt season. These combined observations suggest that basal motion (enhanced by the delivery of surface meltwater to the glacier bed) makes a large contribution to surface velocity in FR3.

In Flow Regime 4 (FR4), τ_d is low (<0.075 MPa) with little variance, while values of v/h are high (>0.28 a^{-1}) and vary over a wide range. FR4, inferred to be the result of very low basal friction, is found predominantly near the terminus of only a few fast moving outlet glaciers. Burgess and others (2005) compared this flow regime to the mode of flow described for ice streams, where high velocities under low driving stress conditions are thought to be due to an actively deforming basal sediment layer (Truffer and Echelmeyer, 2003). The observed large range in v/h values in response to very little change in τ_d is strongly indicative of perfectly plastic sediment deformation (Cuffey and Paterson, 2012). This has been taken to mean that the bed in these regions could be composed of unconsolidated sediment with low yield strength dependent on water pressure,

similar to conditions observed at the Trapridge Glacier (Kavanaugh and Clarke, 2006).

4.2.2.1 Expected velocity variability of Flow Regimes

Based on the description of the Flow Regimes above, we would not expect to observe hydrologically driven velocity variations in FR1, because the ice is assumed to be frozen to the bed in these regions. In FR2, Burgess and others (2005) suggested that velocities increased because the basal ice reached the pressure melting point, allowing it to deform more rapidly at a given stress than ice at sub-freezing temperatures, and because basal sliding begins under these conditions. They did not suggest that surface meltwater reached the glacier bed in regions of FR2, so there is no reason to expect seasonal velocity variations forced by temporally varying water inputs to occur. As a result, the impact of seasonal velocity variations on annual ice displacement in these regions is expected to be small or negligible. We do expect to observe episodic and seasonal-scale velocity variations during the melt season in regions of FR3 and FR4, since it was suggested that surface melt-water could potentially drain into the many crevasses in these regions (Clason and others, 2012), thereby perturbing sub-glacial water pressures and facilitating increased basal sliding.

4.3 Description of Datasets

4.3.1 Ice Velocity via In situ GPS

Observations of ice motion were collected using GPS instruments since from 2008 at six locations on the Belcher Glacier (deployed and operated by the University of Alberta), and from May 2009 at one location on each of the other outlet glaciers (deployed and operated by the Geologic Survey of Canada). Additional survey locations were added as equipment became available. The four month period of near or total darkness makes it impossible to operate these systems continuously year-round without measurement gaps, without significant investment in batteries and solar/wind charging capability.

We employed a variety of observational strategies, each of which involved a trade-off between temporal resolution and operational duration. On Belcher Glacier, we operated some of the GPS systems continuously (15 second sampling) throughout the summer months to produce the high-temporal resolution measurements required for observing short-term dynamic changes (as described in Chapters 2 and 3). We switched these stations to a lower and intermittent sampling rate of 4 sessions x 60 minutes per day, to conserve power for winter deployment or during years when we were unable to make multiple maintenance visits. All of the non-Belcher sites employed a 1 session x 90 minutes per day sampling strategy. This produced a sparser time series of measurements, but allowed some stations to operate through nearly the entire winter by conserving more power compared to the other sampling rates. A summary of the operational coverage and sampling duty cycle of each GPS station can be found in Figure 4-2. The locations of each GPS station are shown in Figure 4-1 and Figure 4-3.

For the purpose of keeping the data processing consistent, we have segmented any continuous observations into 60 minute long files. All of our raw 60 and 90 minute GPS data files were post-processed using the segmented-static Precise Point Positioning approach described in Chapter 3. This processing resulted in one position estimate per input file, with an estimated uncertainty of ±0.10 m for 2D horizontal positions, and ±0.165 m for 2D horizontal displacements (used in velocity calculations).

Here we present the collected velocity data from all Belcher stations, as well as all available data from the other three outlet glaciers. In total, there are 13 different GPS stations, and ~1 to 4 years of observations per station. In Appendix A we include the plots of horizontal velocity, cumulative vertical displacement, and the plan-view motion trajectory for each station.

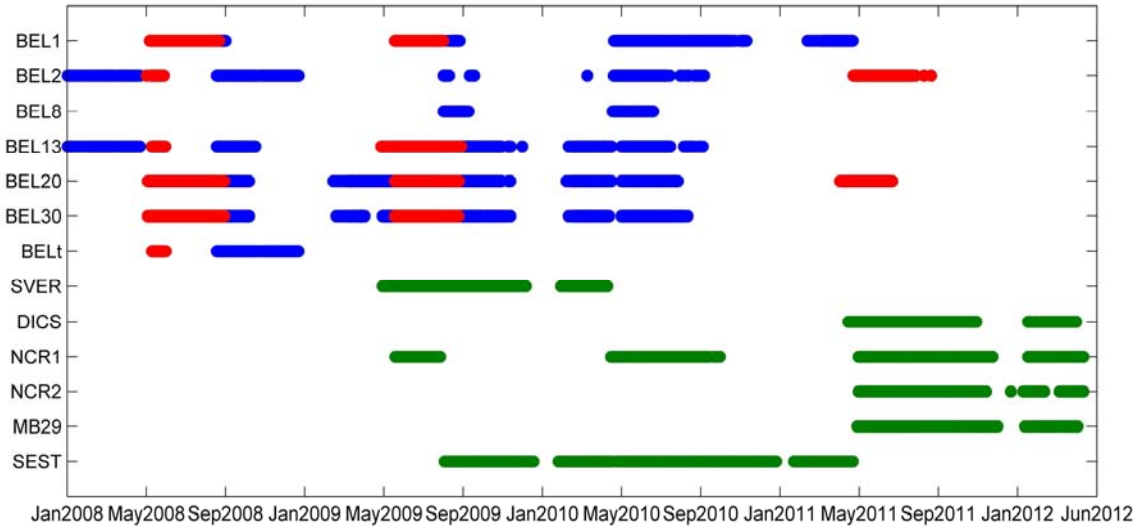

Figure 4-2: Summary of GPS station occupation. Colors represent the sampling rate of each time series: Green: 1 point / 24 hours, Blue: 1 point / 6 hours, Red: 1 point / 1 hour.

4.3.2 Ice Surface and Bed Elevation

In April 2000, staff from the Scott Polar Research Institute (SPRI) used an airborne 100MHz radar instrument to measure the ice surface and bed elevations of the Devon Ice Cap (Dowdeswell and others, 2004). Radar transects were flown in a 10 km grid pattern over the ice cap, and down the centerlines of several significant outlet glaciers.

Digital Elevation Models (DEM) of 1 km cell size were produced for the ice cap surface and bed. The vertical accuracy of the original radar measurements was ±10 m, however the elevation model created by interpolating these flight-line measurements over a wide area and over complex terrain would result in significantly higher elevation errors for many areas of the ice cap. We use these data mainly for the purpose of identifying the regions where our glaciers of interest are grounded below sea level. These regions, found at the terminus of each outlet glacier, are marked by contour lines (at 50 m depth below sea level increments) in Figure 4-3.

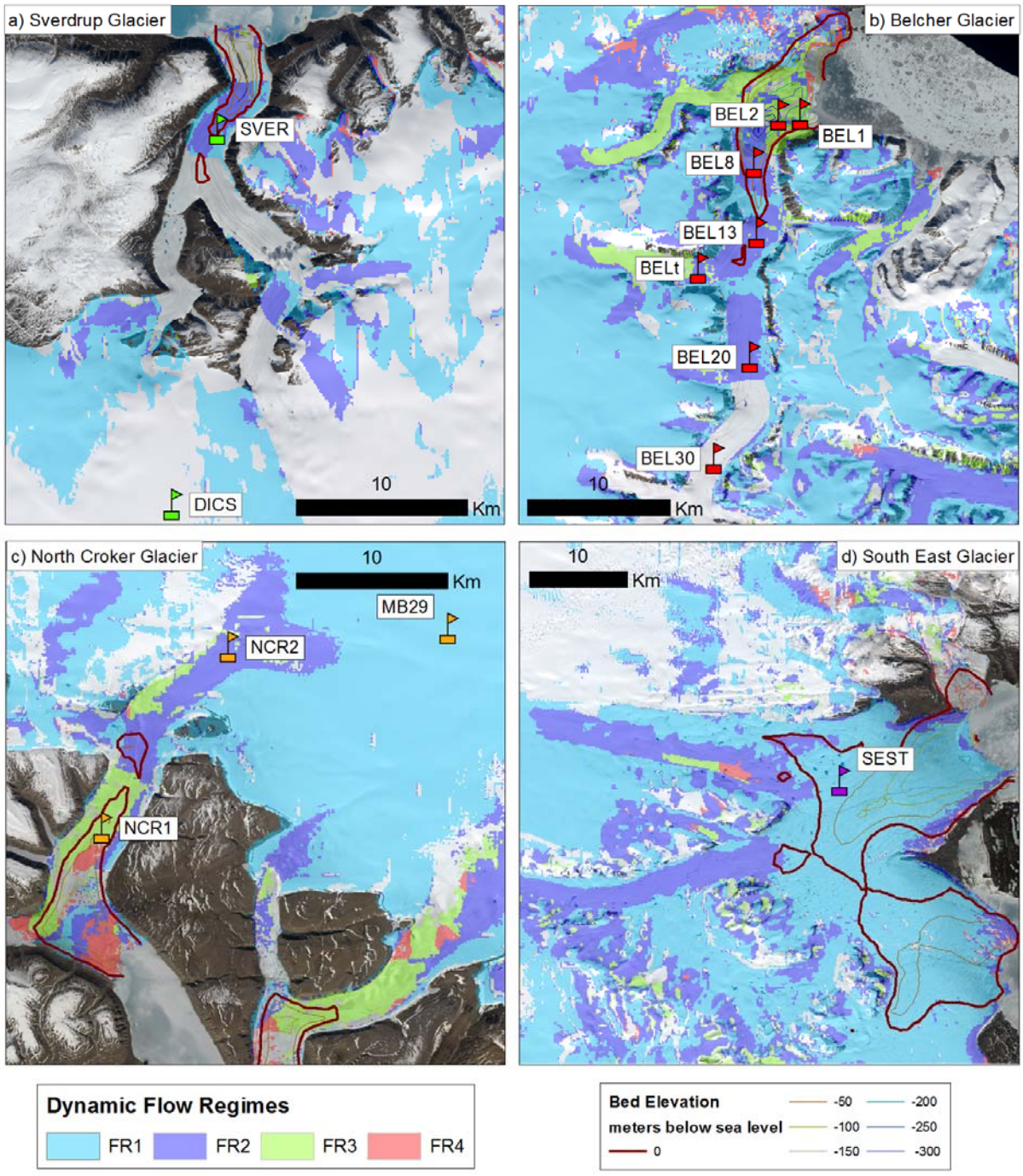

Figure 4-3: Four Devon Ice Cap outlet glaciers: a) Sverdrup, b) Belcher, c) North Croker, and d) Southeast. Each glacier is shown in the same Landsat 8 OLI scene as Figure 4-1, overlain with the Flow Regimes map from Burgess and others (2005). The Flow Regimes map contains gaps where measurements of ice velocity, thickness, or both were missing. All GPS stations used in this study are identified with coloured flag symbols. Contour lines identify the depths at which the glacier beds are grounded below sea level.

4.3.3 Dynamic Flow Regimes Map

Burgess and others, (2005) estimated the parameters v/h and τ_d for most regions of the ice cap using their ice surface velocities based on InSAR, and ice thickness estimates based on the SPRI radar DEM; threshold values of these parameters (discussed above) were then used to produce a raster map of the distribution of Flow Regimes across the Devon Ice Cap. The errors in the underlying datasets propagate into the Flow Regimes map, and uncertainty in the values of v or h could strongly impact raster pixel classification. For instance, SAR interferometry yields look direction surface velocities that are then resolved into flow direction velocities using a surface elevation model that contains its own significant errors, and the interpolation of ice thickness data from a grid of radar flight-lines means that some regions of the ice thickness DEM also contain significant errors. This suggests that interpretation of the Flow Regimes map should be made with caution, especially in regions of steep and/or complex topography where velocity and ice thickness errors are likely to be highest (e.g., the Cunningham Mountains region on the southern edge of the ice cap). Areas of the map that show transitions between multiple flow regimes over very small areas (i.e., within the space of a few pixels) were treated with scepticism. However, the map should reliably describe the dynamics of regions where larger patterns of Flow Regimes occur on less topographically-complex parts of the ice cap or on the major outlet glaciers where radar flight-lines likely yielded good ice thickness measurements.

In Figure 4-3 we have overlain this map on a Landsat8 image of the Devon Ice Cap to show the distribution of Flow Regimes on the four glaciers we are examining here, and to identify the regimes in which our GPS stations were located. In a few cases where there are gaps in the map, we use the classification thresholds defined by Burgess and others (2005) to help us determine the appropriate FR classification for our GPS sites.

4.4 Observations

The velocity observations from our GPS stations are discontinuous and not always overlapping in time. In the worst cases (BEL8 and BELt) we have less than one full year of data. In the best cases (BEL1, NCR1, etc.), we have up to three years of measurements, including the full summer period, but are missing all of the winter and most of the late fall / early spring.

In Chapters 2 and 3, we focused on describing specific acceleration events or patterns of velocity change that could be linked to observed drainage events or changes in surface melt rates and drainage morphology. Here, however, we lack detailed coincident observations of surface melt or drainage events for most of our GPS sites. Furthermore, the velocity measurements at the North Croker, Sverdrup, and Southeast glaciers are 24 hour averages, so we avoid trying to identify the potential drivers behind any hourly- to daily-scale 'episodic' velocity variations. Instead, we focus here on broader patterns of seasonal variability.

4.4.1 Belcher Glacier

4.4.1.1 Flow Regimes

Comparison of the Flow Regimes map with the location of our GPS stations (Figure 4-3b) reveals that, of the seven GPS stations on Belcher Glacier, none were positioned on ice classified as FR1 or FR4. Only a few pixels of FR4 are found on the very edge of the calving terminus, but generally Belcher Glacier does not seem to have any significant regions characterized by this flow regime. The lower ~5 km of the glacier were classified as FR3, and GPS stations BEL1 and BEL2 are in this zone. With the exception of BEL30, the remaining Belcher GPS stations were positioned on ice classified as FR2.

The upper-glacier region around BEL30, (30 km from the glacier terminus) lacks a flow regime classification because Burgess and others (2005) were missing ice thickness data for this region. However, additional ice thickness measurements were collected along the glacier centerline in 2005 by NASA as part of the IceBridge mission (this dataset was presented in Chapter 3). Based on

these measurements, the ice thickness in the vicinity of BEL30 is 317 ±10 m. Annual mean velocity measured by the BEL30 station was 55.1 ±0.165 m a^{-1}, and therefore v/h = 0.174 a^{-1}. This is greater than 0.075 a^{-1} and less than 0.28 a^{-1}, meeting the criteria of Burgess and others (2005) to be classified as FR2.

4.4.1.2 Seasonal Flow Characteristics

The summer speedup was a consistent feature of all of the Belcher velocity time series (except BELt, which failed to record during the 2008 summer). From BEL30 all the way down to BEL1, the onset of the summer speedup can be seen as a rapid rise from the background spring velocity up to the annual maximum velocity during what is often referred to as the 'spring event' (Iken and others, 1983; Röthlisberger and Lang, 1987). This was followed by a period of highly variable flow, incorporating multiple acceleration/deceleration cycles. The series of these cycles that occur each year forms a pattern that is unique to that summer, and the strongest elements of the annual pattern of velocity variability can be observed at each GPS station along the centerline. For example, in the Appendix, see how the ‘twin-peak’ pattern during the 2008 summer is repeated at BEL30, BEL20, and BEL1 (Figures A11, A9, A1).

In the FR2 zone, at stations BEL30, BEL20, and to some extent BEL8, we observe vertical displacement of the ice surface coincident with the spring event and other acceleration events during the summer period. Upwards vertical motion coinciding with rapid horizontal acceleration at these sites was discussed in detail in Chapter 3. These events were interpreted to be a result of ice-bed separation in response to increased water pressure at the bed.

The velocity records from the five GPS stations in FR2 demonstrated the following common features: mean spring velocity was within ±4% of the annual velocity; the annual minimum velocity occurred in the fall and ice flow slowly accelerated throughout the winter and into the spring; the mean summer velocity was 35-55% faster than the annual mean.

4.4.1.3 Annual Flow Characteristics

In the cases where we had GPS stations in the FR2 zone of Belcher Glacier operating for multiple years in the same location (BEL30, BEL20, and BEL13), we found the annual mean velocity to be highly consistent. Annual velocities at FR2 stations ranged in value from 55 to 107 m a^{-1}. There was a spatial trend towards increasing velocity in the down-glacier direction, though BEL13 was an exception to this trend. BEL13 was positioned near the top of an ice-fall, and the surface slope in this region is much steeper (and driving stresses higher) than at any of the other sites in this zone of the glacier. Consequently, BEL13 is flowing slightly faster than BEL8.

In the FR3 region near the glacier terminus, the annual mean velocity, and the maximum velocity recorded during the summer, was far higher than the equivalent velocities in the other regions of the glacier. At BEL2, spring velocity was also within 4% of the annual velocity, but the fall/winter velocity was 8% slower than the annual mean. The summer velocity at BEL2 was the highest of all the Belcher stations, in terms of both magnitude and percentage of the annual velocity. BEL1 had the highest annual velocity (228 m a^{-1}), and showed the most inter-annual variability in velocity (a mean increase of 38 m a^{-1} over 3 years). Because of this long-term acceleration, the 3-year mean spring velocity was lower than the mean fall/winter velocity, and suggests that the spring velocity underestimates the annual velocity by 13%. However, in 2010 it appears the acceleration trend may have stopped, since the fall velocity was slightly lower than the spring, and the 2010 and 2011 spring velocities were nearly equal. When the seasonal velocities were recalculated based exclusively on 2010, the spring mean was again within 4% of the annual velocity.

4.4.2 North Croker Glacier

4.4.2.1 Flow Regimes

The lower ~16 km of the North Croker Glacier is grounded below sea level. Our GPS at NCR1 was situated on a zone of FR3 ice grounded below sea level,

while NCR2 was located on FR2 ice with its bed above sea level. MB29 was located in a sheet-flow region of the ice cap characterized by FR1, and the ice-bed in this region is ~600 m a.s.l.

4.4.2.2 Seasonal Flow Characteristics

The ice at MB29 demonstrated no seasonal velocity variability. MB29 is in the ablation zone, just below the superimposed ice zone. In this region of the ice cap, lakes and streams form on the surface, but most water runs off down slope, or freezes in place (Wyatt, 2013). There is little evidence of meltwater penetration via crevasses or moulins in this region.

Both NCR1 and NCR2 underwent large velocity variations during the late-June through August period of 2011. Figure 4-4 shows that short-term velocity variations during the summer were common between NCR1 and NCR2. The air temperature time series shown in Figure 4-4c was recorded at a site ~1000 m above sea level, at a location 5 km south of MB29 and 15 km east of NCR2. This temperature record provides a good indication of when surface melt would have occurred at the NCR2 site, but the temperature at NCR1 (at 400 m.a.s.l.) was probably warmer and the melt season longer.

The coincident air temperature time series reveals that the periods of enhanced summer flow relate to periods of positive air temperatures, and that variations in the air temperature at multi-day scales appear to coincide with variations in ice flow. This suggests that the ice flow variations are related to variations in meltwater production and drainage, similar to what was observed on the Belcher Glacier (Chapter 3).

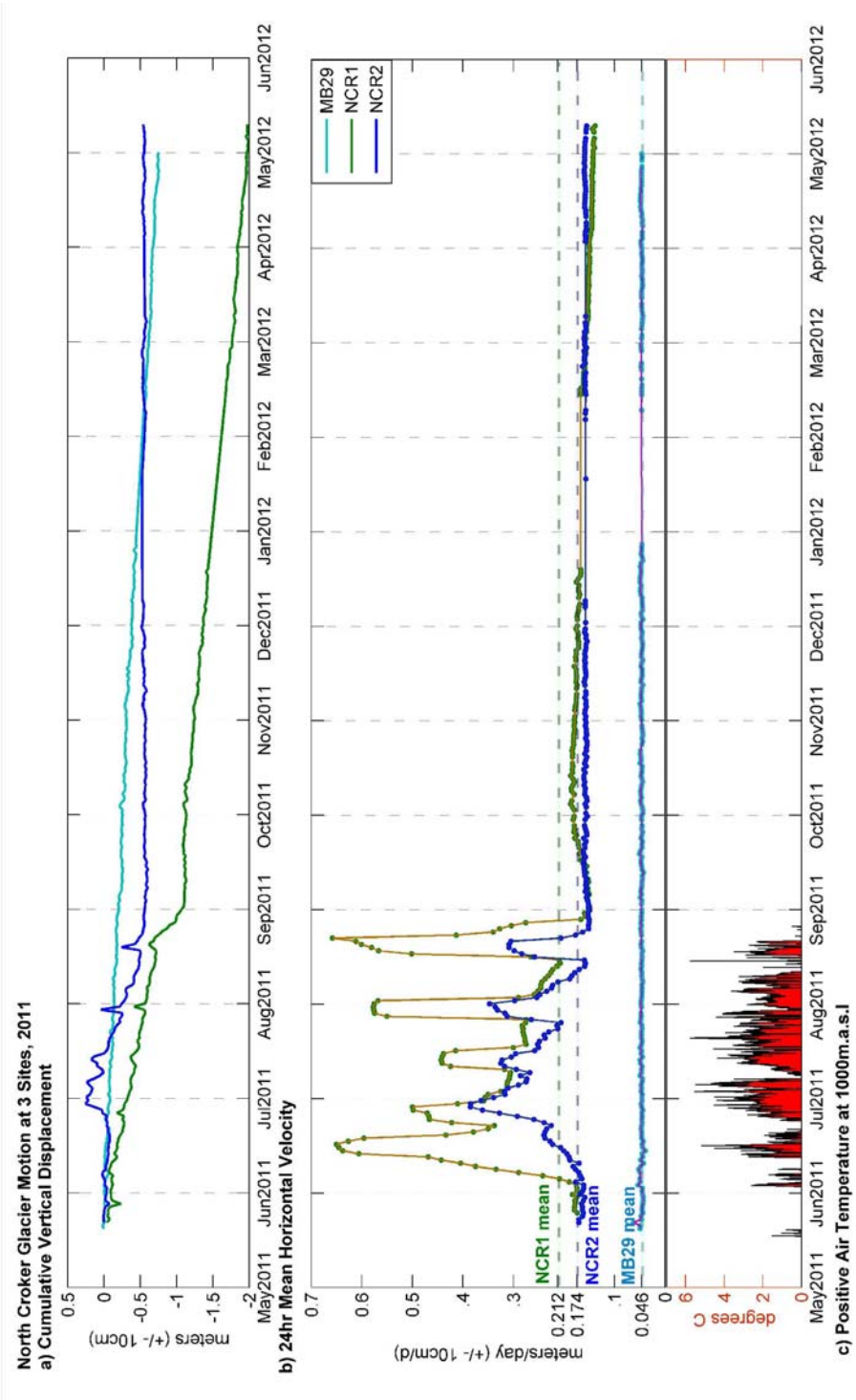

Figure 4-4: Ice motion at 3 Sites on the North Croker Glacier, May 2011 to May 2012: a) cumulative vertical displacement (Note: does not include surface ablation or accumulation); b) Horizontal ice velocity MB29 (Light blue, Flow Regime 1), NCR2 (Dark blue, Flow Regime 2), and NCR1 (Green, Flow Regime 3); c) Positive Air Temperature at ~1000m.a.s.l.

4.4.2.3 Annual Flow Characteristics

The velocity estimates at NCR1 (shown in Figure A17) demonstrate that the high-magnitude and short time-scale velocity variability that occurred in this region each summer (FR3) was superimposed on a long-term deceleration. The long-term trend in the background velocity can be observed by examining the spring pre-speedup velocity and, where available, the fall and winter velocity. On June 1, 2009, the spring velocity was 117.9 m a^{-1}, and this gradually decreased to 104.8 m a^{-1} by June 1 of 2010, 64.3 m a^{-1} by June 1 of 2011, and 50.4 m a^{-1} by May 8 of 2012. Therefore this region of the glacier was undergoing a multi-year change in velocity of -22.5 m a^{-2}, with the summer speedup superimposed on this trend.

4.4.3 Sverdrup Glacier

4.4.3.1 Flow Regimes

The DICS station was positioned in the upper region of the Sverdrup Glacier drainage basin. Ice from this location drains into the Sverdrup valley, but is clearly part of the "sheet-flow" region of the ice cap. Based on ice velocity and thickness at the DICS site, $v/h = 0.010$ a^{-1}, which suggests this site should be classified as FR1.

Significant sections of the Flow Regimes map are blank for the main trunk of the Sverdrup glacier, but it appears that a wide channel down the glacier centerline is predominantly characterized by FR2, with narrow zones of FR1 along the valley margins. This indicates that there are wide shear zones along the lateral margins of this glacier, and only the ice in the center channel appears to flow with some contribution from basal sliding. The SVER station was positioned on the glacier centerline, in the FR2 zone. This region of the glacier (the lower 7-10 km) is also grounded below sea level.

Very small patches (a few pixels) of FR3 and FR4 are found at the very edge of the glacier terminus. In contrast to the Belcher or North Croker glaciers,

the Sverdrup has only a narrow band of crevassed ice at its terminus, and this is the only area where fast ice flow is likely to occur on this glacier.

4.4.3.2 Seasonal Flow Characteristics

Ice velocity at DICS is extremely low (~3 m a^{-1}) and constant year-round. There is no discernible increase in flow velocity during the summer, or significant vertical ice motion.

We have approximately one year (2009) of GPS measurements from the SVER station. The ice velocity on the main trunk of the Sverdrup glacier is highly consistent in the spring, fall, and winter. Mean annual velocity was ~25 m a^{-1}, the spring velocity was within 5% of the annual mean, and the magnitude of the fall slow-down was minimal (~3 m a^{-1} below spring). Significantly faster flow occurs for a brief period in the summer. In July the horizontal velocity rapidly increased by ~300% above the spring background velocity, coincident with a 50 cm rise in ice surface elevation. This fast-flow event lasted 20 days, and was followed by a much shorter (9 day) fast-flow event of much lower magnitude in early August, before ice flow returned to a slower fall/winter rate by late August.

4.4.4 South-East Glacier

4.4.4.1 Flow Regime

A large region of the lower part of this glacier is grounded below sea level (up to 22km from the terminus), and much of the wide calving terminus is grounded between 100-200 m below sea level. Our GPS site SEST is on ice that is grounded just slightly below sea level.

According to the Flow Regimes map, the region in which SEST was installed is classified as FR1; however we argue that this region should be reclassified as FR2. The velocity calculated by Burgess and others (2005) shows that the region around the SEST site and extending to the glacier terminus was moving ~10 m a^{-1} in 1996. The GPS based measurements from 2009 to 2011 shows that the velocity at SEST has increased to ~39 m a^{-1}, and ice thickness in

this region is ~300m. Therefore $v/h = 0.13133\ a^{-1}$, which means this region now meets the classification criterion for FR2.

Our observation of a four-fold increase in velocity here is consistent with several recent studies which have shown evidence that this glacier is undergoing a long, slow surge. Van Wychen and others (2012) compared their surface velocities to those determined by Burgess and others (2005), to reveal a long-term pattern of velocity change at the Southeast2 Glacier (the northern half of the Southeast1&2 complex). Specifically, they noted a deceleration near the glacier head, and a down-glacier migration of fast flow. Assessments of long-term thickness changes of this glacier show that the lower regions of this fast flow migration (in the vicinity of our SEST site) were experiencing rates of thickening on the order of 0.5 m a^{-1} (G.Moholdt, pers. comms 2009; Burgess and Sharp, 2008). Furthermore, surface morphology features consistent with a surge-type glacier (including looped moraines and degraded flow stripes) have also been observed in Landsat7 imagery (Burgess and Sharp, 2008; Boon and others, 2010).

If Southeast Glacier is a surge type glacier, then FR1 classification is likely not the best descriptor of the lower regions of this glacier. Most areas of FR1 are in low accumulation, low slope regions of the ice cap interior, where ice is likely frozen to the bed and flow speeds are highly stable over time. The lower regions of Southeast Glacier, likely the stagnating remains of a surge lobe, were classified as FR1 based on the low surface slope and low flow velocities that were observed at the time. However these characteristics are atypical of ice cap marginal areas, and are the result of the unsteady flow of this lobe of ice over time. The time-varying dynamics of this region might warrant a separate flow regime classification.

4.4.4.2 Seasonal Flow Characteristics

There is a clearly defined summer speedup at SEST, and at the peak of the spring-event we recorded a velocity ~200% higher than the background velocity. The mean summer velocity was 59% higher than the annual mean. The mean spring velocity was just slightly slower than the mean fall velocity, and these

seasonal means were 15% and 9% lower, respectively, than the annual mean. In contrast to most of the other FR2 sites we have observed, the mean spring velocity would therefore not be a suitable estimate (±5%) of the annual mean.

There are two interesting features in the vertical motion time-series: 1) there was upwards vertical motion coincident with the rapid increase of horizontal velocity during the spring-event, which has been observed at several other locations discussed above, but there was no lowering of the surface corresponding to the decrease in velocity later in the summer. The ice surface remained elevated. 2) The long-term upwards trend of the ice surface, which occurred even though the surface slope and the bed slope in this region trend downwards in the direction of flow.

Both of these observations of surface uplift are consistent with the rates of thickening previously observed in this region (G.Moholdt, pers. comms 2009; Burgess and Sharp, 2008). This further confirms that a long-term build-up of mass is occurring in this region in response to a down-glacier migration of fast ice flow.

4.4.5 Seasonal and Annual Velocity Comparisons

We used all available data to estimate the mean seasonal and mean annual velocity at each GPS site. We took the mean of all velocity measurements in May and early June (up to but excluding a 'spring event' if one was discernable) as an estimate of spring velocity, July and August for the summer velocity, and any velocity measurements available from September through January as the Fall/Winter velocity. The annual velocity was determined by finding the displacement between two position measurements as close as possible to one calendar year apart, and divided by the intervening time (if possible, we repeated this multiple times and found the multi-year mean annual velocity). This was checked against a time-weighted mean of the combined seasonal velocities. These two measures of annual velocity usually agreed within ±1 m a^{-1}, unless there was significant inter-annual velocity change (i.e. at BEL1 and NCR1). Each

seasonal mean velocity was then expressed as a percentage of the annual velocity. These results are summarized in Table 4-1.

Table 4-1: Summary of the Total Annual Displacement and mean Seasonal Velocities at each glacier site. Seasonal velocities were determined as the mean of all available data from: May and June (Spring), July and August (Summer) and September to December (Fall/Winter). The numbers in the far right column indicate how many years of data were used for determining the annual and seasonal mean velocities. The # symbol indicates that insufficient data was available to make a complete estimate (see Appendix A).

Glacier	FR	Mean Annual Velocity (m/yr)	Mean Spring (m/yr)	% of Annual	Mean Summer (m/yr)	% of Annual	Mean Fall/ Winter (m/yr)	% of Annual	# of years
Belcher									
BEL1	3	228.3	197.5	87%	307.2	135%	222.7	98%	3
BEL1 (2010)	3	238.7	228.5	96%	325.0	136%	219.6	92%	1
BEL2	3	199.6	208.3	104%	336.0	168%	173.1	87%	2
BEL8	2	96.4	99.9	104%	148.1	154%	82.5	86%	#
BEL13	2	107.2	109.5	102%	144.5	135%	94.4	88%	2
BELt	2	68.9	71.1	103%			63.9	93%	#
BEL20	2	61.3	63.3	103%	95.8	156%	51.3	84%	3
BEL30	2	55.1	53.5	97%	74.9	136%	51.2	93%	3
Sverdrup									
SVER	2	24.8	23.5	95%	46.5	188%	20.8	84%	1
DICS	1	3.4	3.4	102%	3.4	103%	3.3	99%	1
North Croker									
NCR1	3	110.7	101.1	91%	185.6	168%	62.8	57%	3
NCR1 (2011)	3	77.4	64.6	83%	142.0	183%	64.5	83%	1
NCR2	2	63.4	58.2	92%	93.3	147%	57.3	90%	1
MB29	1	17.0	16.8	99%	17.0	100%	17.0	100%	1
Southeast									
SEST	2	39.8	33.6	84%	63.2	159%	35.4	89%	1

Because BEL1 and NCR1 in the FR3 zone demonstrate multi-year velocity changes, the seasonal velocities based on 3-year means may not be the best representation of how well the spring or fall/winter velocities relate to the annual mean velocity. Therefore we also calculated the seasonal means based on a single year (2010 and 2011 respectively) for these two sites.

4.5 Discussion

4.5.1 Seasonal and Annual patterns of flow variability

Our observations show that all four of the major outlet glaciers exhibit a pattern of seasonal velocity variations, similar to those described previously for Belcher Glacier. The pattern we recognized there included the following phases: 1) Quiescence, 2) Terminus Zone Activation, 3) Spring Event, 4) Hydro-Active, 5) return to Quiescence.

The Spring Event and Hydro-Active phases are clearly observed at the Sverdrup, Southeast, and North Croker glaciers. However, at these glaciers we have not observed the Terminus Zone Activation phase, which was described in Chapter 3 as a gradual acceleration over 10-20 days prior to the spring-event. At Belcher Glacier, this phase only occurred within 1 to 2 kilometres of the glacier terminus, and none of our measurement sites on the other three glaciers were in similar locations.

4.5.2 The relationship between Flow Regimes and velocity variability

In Table 4-2 we summarize our observations of the seasonal and annual velocity variability characteristics from each of the GPS records, and associated these with the flow regime for each GPS site. Also included are some observations of the local ice characteristics at these sites.

The key associations between flow regimes and velocity variability are:

FR1 does not exhibit seasonal or annual velocity variability;

FR2 undergoes seasonal velocity variability but inter-annual variability is less likely; and

FR3 exhibits both seasonal and interannual variability.

Table 4-2: Qualitative comparison of seasonal and annual velocity variability, and other distinguishing characteristics, of the four flow regimes.

FLOW REGIME	1	1	2	2	2	2	2	2	2	2	3	3	3	4
GPS Station	DICS	MB29	SEST	SVER	NCR2	BEL8	BEL13	BELt	BEL20	BEL30	BEL1	BEL2	NCR1	N/A
Summer Speedup?	N	N	Y	Y	Y	Y	Y	--	Y	Y	Y	Y	Y	
Vertical motion with horizontal acceleration?	N	N	Y	Y	Y	Y	N	--	Y	Y	N	N	Y	
Fall Slowdown? (Fall < Spring Velocity)	N	N	N	Y	Y	Y	Y	Y	Y	Y	N *	Y	Y	
Spring Velocity +/- 5% of Annual Mean Velocity?	Y	Y	N	Y	N	Y	Y	Y	Y	Y	N *	Y	N	
Fall/Winter Velocity 10-15% lower than Annual Mean Velocity?	N	N	Y	Y	Y	Y	Y	N	Y	N	N	Y	Y	
Inter-annual Displacement Variability	N **	N **	--	--	--	--	N	--	N	N	Y	Y	Y	
On plateau ice?	Y	Y	N	N	N	N	N	N	N	N	N	N	N	
High Crevasse Density?	N	N	N	N	N	N	N	N	N	N	Y	Y	Y	
Bed below sea level?	N	N	Y	Y	N	Y	**Y** ***	N	N ***	N	Y	Y	Y	

* Fall was faster than spring due to multi-year trend
** Assumed, based on 1year of measurements
*** Bed very close to 0 m a.s.l.
-- Not enough data available to determine

All of our observations in FR2 locations show that these regions exhibit a 35-90% speedup during the summer, and with the exception of BEL13, discrete acceleration events often associated with vertical motion of the ice. In Chapters 2 and 3, we showed that some of these events were linked to observed lake drainage events or meltwater drainage via moulins in the FR2 regions of the Belcher. Wyatt (2013) mapped meltwater sink points throughout FR2 regions on the Devon Ice Cap, and suggests that these form potential pathways for surface meltwater to reach the bed. Predictive modelling of moulin formation and meltwater drainage throughout the Croker Bay drainage basin has also indicated that surface to bed drainage of meltwater is highly likely throughout FR2 regions

(Clason and others, 2012). Combined, this strongly supports the idea that basal sliding in FR2 is due not only to ice reaching the pressure melting point, but that localized dislocation of the ice-bed interface may occur in response to temporally varying water inputs.

Our observations of FR3, at BEL1, NCR1, and to a lesser extent BEL2, show that the velocity variability during summer is superimposed on longer term trends of velocity change. The 3-year background trend at BEL1 was an increase of 12.6m a^{-2}, while at NCR1 there was a decrease of 22.5 m a^{-2}. The duration of our GPS-based observations of these glaciers is too short to identify the drivers of these trends and their time-scales, or to determine whether these are unidirectional, cyclical, or random changes. But considering that the defining trend of FR3 is a highly sensitive, inverse relationship between v/h and τ_d, we might anticipate large changes in long-term velocity driven by relatively small perturbations to driving stress. Since changes to ice thickness and surface slope relate directly to driving stress, we speculate that even changes in surface mass balance gradients along the glacier profile could potentially drive modest multi-year velocity changes.

4.5.3 Flow Regime 4

Regions of FR4 ice are difficult to access and instrument, and we have no GPS observations from these regions. However, we can use existing observations of these regions to develop answers to our remaining questions about FR4:
1) Why do extensive regions of FR4 exist at the termini of some outlet glaciers, and not others? 2) What degree of inter-annual flow variability can be expected at glacier termini exhibiting FR4?

4.5.3.1 Bed Composition

Burgess and others (2005) suggested that FR4 likely occurs near the terminus of glaciers underlain by a sedimentary till layer which could deform as a perfectly plastic medium, even under the low driving stresses characteristic of

these areas, and thus contribute to high rates of basal motion. Earlier work on the Devon Ice Cap suggested that the beds of marine terminating glaciers grounded below current sea level were likely composed of glacio-marine sediments deposited in the late Quaternary (or earlier inter-glacial periods) when the Devon Ice Cap had receded and sea levels were higher (Dowdeswell and others, 2004). However, most of the major outlet glaciers have beds grounded below sea level (see Figure 4-3), but of these, only the North and South Croker exhibit FR4 at their termini. How can this discrepancy be explained?

There is evidence that both North and South Croker Glaciers may be underlain by bed material of very different composition to that underlying Belcher and Sverdrup Glaciers, which may help explain why large regions of FR4 are observed at the termini of the former glaciers but not the latter. The western side of Devon Island is characterized by light coloured sedimentary rock, which overlaps the much darker metamorphic basement rock exposed on the eastern side of the island (Figure 4-5). The lighter coloured sedimentary rock is limestone or dolomite of Cambrian and Ordovician age (Frisch, 1984). This formation terminates ~30km east of Croker Bay on southern Devon Island, and near Truelove Lowlands on the northern shore, which is ~30 km west of Sverdrup Glacier.

The cliffs forming the fjord walls of North and South Croker glaciers are composed primarily of this horizontally bedded, light coloured rock. Large talus slopes form along these cliffs, indicating that the material has undergone considerable weathering and fragmentation (Figure 4-6a). The weathered rock on the plateaus surrounding North and South Croker glaciers is broken down to gravels and smaller particles (Figure 4-6d). It is possible that the Croker glaciers are underlain by unlithified debris eroded from the highly weathered rock in this region. This could provide a deep till bed that may be susceptible to deformation.

Figure 4-5: Truelove Lowlands (camp in foreground) is a site ~30 km to the west of the Sverdrup Glacier and ~15km north of the Devon Ice Cap margin. The on-lap of lighter coloured sedimentary rock atop darker basement rock can be seen in the hills in the background.

Conversely, the fjord walls containing Sverdrup and Belcher Glaciers are composed of gneisses and metamorphosed granite of Archean age (Frisch, 1984). Talus slopes along these cliffs are much smaller or non-existent (Figure 4-6b and 6c), and are composed of much larger fragments, indicating that this material does not break down as easily as the sedimentary rock in the Croker Bay region. Debris found in the medial moraines on Belcher Glacier (Figure 4-6e) ranges from coarse gravel to car-sized boulders, and the weathered rocks on the surrounding cliff tops are predominantly large boulders (Figure 4-6f). We therefore consider it much less likely that Belcher and Sverdrup Glaciers are underlain by deep till layers originating from the local bedrock. This leads us to hypothesize that the availability and composition of basal till sourced from the local rock may play as important a role as the existence of glacio-marine

sedimentary deposits in creating the conditions required for FR4 to occur at a given glacier.

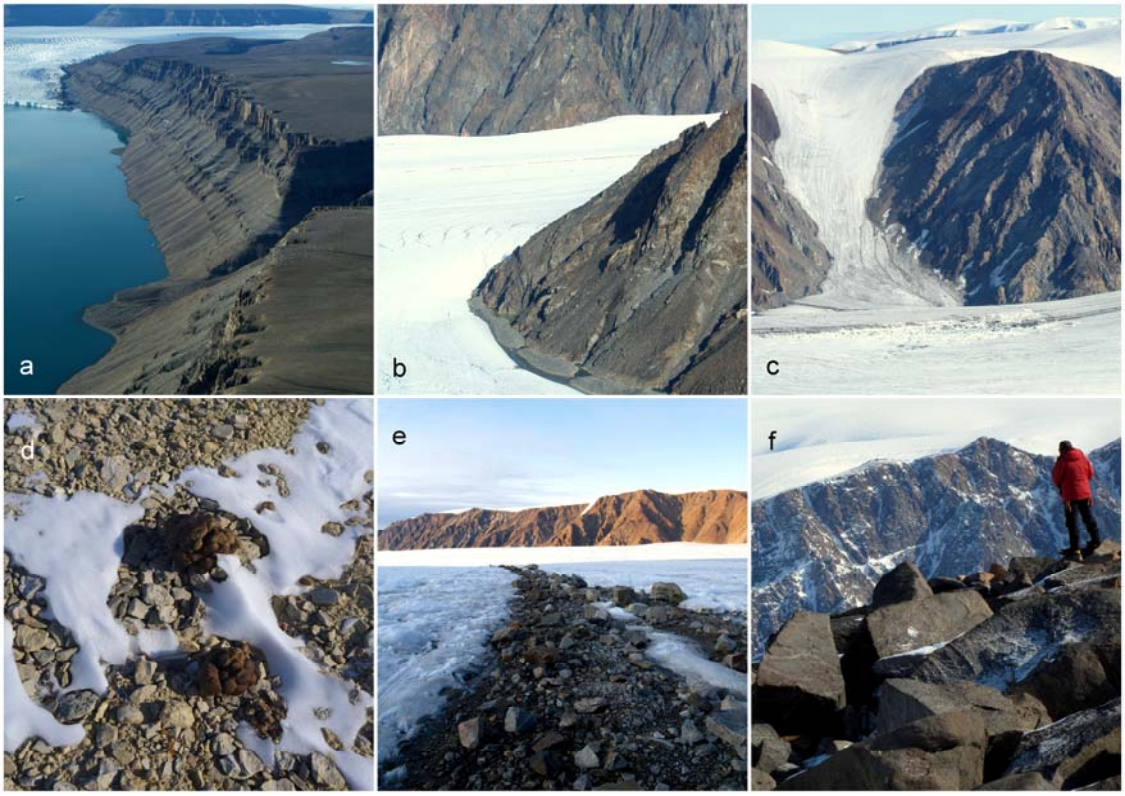

Figure 4-6: Field photographs demonstrating the differences in rock types in the vicinity of the Croker, Sverdrup, and Belcher Glaciers:
a) Large talus slopes exist along the fjord walls in the Croker Bay region, but the metamorphic rocks in the (b) Sverdrup and (c) Belcher regions are more resistant to weathering and fragmentation. d) Gravels and much finer particles are common among the weathered material on the cliff tops in the Croker Bay region (Muskox dung for scale). e) Medial moraine debris on Belcher Glacier ranges from large gravel to boulders. f) Weathered rocks on cliff tops surrounding the Belcher are predominantly large boulders (second author for scale).

4.5.3.2 Inter-annual Flow Variability

To get an indication of the degree of inter-annual velocity variation that might occur in FR4 regions of glacier termini, we examined all of the large to medium sized outlet glaciers for which previous velocity field measurements are available. Table 4-3 summarizes the comparisons of terminus-area velocities measured by Burgess and others (2005) and Van Wychen and others (2012)

(referred to as 1996 vs 2009 velocities, based on the approximate dates of data collection used in those studies). Van Wychen and others (2012) argue that some of the difference between ice surface velocity from their study vs the Burgess and others (2005) study may be due to differences in either methodology (InSAR vs. speckle-tracking) or measurement period (spring vs. fall), but that most of the observed velocity changes are likely due to real changes in ice dynamics that occurred over the ~15 year time interval between the two sets of measurements.

The dramatic velocity changes exhibited by East and Cunningham Glaciers over this ~15 year period suggest that all of these smaller outlet glaciers are capable of switching between fast and slow phases of flow. The eastern tidewater glaciers (East3-6) appear to undergo velocity fluctuations of -50% to +100% (halving or doubling flow speed). The land-terminating Cunningham glaciers are slower flowing in general, but exhibit similar relative magnitudes of velocity change (-50% to >+100%). Of these, only Cunningham 3 Glacier (referred to as Cunningham West on some maps) has previously been identified as a surge-type glacier based on its surface morphology (Copland and others, 2003). We also identified looped moraines, a characteristic surge-type surface feature (Copland and others, 2003), on Cunningham 4 Glacier in a Landsat8 OLI image (4 July 2013), which provides evidence in addition to its flow speed changes that this may also be a surge-type glacier. Furthermore, all of these glaciers show, to varying degrees, evidence of Quaternary age till deposits along their margins (Dyke, 2001), indicating that they may be underlain by sedimentary material susceptible to deformation.

Table 4-3: Approximate terminus area velocity changes at all large to medium sized outlet glaciers of the Devon Ice Cap.

Outlet Glacier Name	FR4 Present?	Approximate Terminus Velocity Change 1996 vs 2009	Notes
Sverdrup	N/A	N/A	No velocity or FR classification available from Burgess and others (2005)
Eastern	N/A**	N/A	
Fitzroy	N/A**	N/A	
Belcher	No	-75 to -100 m/yr	These changes likely due to differences in velocity measurement methods and seasonal velocity variability.
Unnamed5	No*	-10 to +10 m/yr	little to no change
East3	Yes	-25 to -50 m/yr	~50% decrease
East4	Yes	+50 to +75 m/yr	~100% increase
East5	No	>+100 m/yr	>100% increase in lower regions, 50% decrease in upper
East6	Yes	-25 to -50 m/yr	~50% decrease
East7	Yes*	N/A	scant velocity data from 1996
Southeast1&2	Yes	+25 to +50 m/yr	~100% increases; complex pattern of changes; FR4 region ~20km upglacier
Southeast3	No	-10 to +10 m/yr	little to no change
Cunningham 1	Yes	-50 to -75 m/yr	~10x decrease
Cunningham 2	Yes*	N/A	scant velocity data from 1996
Cunningham 3	Yes	-100 to +100 m/yr	~50% decreases to 200% increases; complex pattern of large localized changes
Cunningham 4	No	+25 to +50 m/yr	~100% increase in lower regions, 50% decrease in upper regions
South Croker	Yes	+100 m/yr	~50-100% increase at terminus, but slow-down on main trunk
North Croker	Yes	mixed: -25 to +100 m/yr	complex velocity patterns; partially due to differences in velocity measurement methods

* Scant data from 1996 made determination of FR4 difficult.
** No velocity or FR classification available from Burgess and others (2005)

Additional observations of inter-annual velocity variations include those made by Wyatt (2013), who calculated the annual velocity anomalies over the period 1999-2008 for the North and South Croker glacier terminus regions (both FR4), and showed that both glaciers underwent a nearly-sinusoidal cycle of velocity change over the 9-year period. This is in contrast to the relatively irregular velocity changes exhibited by Belcher and Fitzroy Glaciers over the same time period.

4.5.3.3 Surge-like behaviour in Flow Regime 4

The above observations show that Devon Island outlet glacier termini, especially those classified as FR4, can exhibit large, and in some cases, cyclical multi-year velocity variations. While these velocity variations may not fit the typical surge-type glacier flow pattern (decades of slow quiescent-phase flow, followed by months to years of flow 10-1000 times faster (Murray and others, 2003)) there are similarities between FR4 glaciers on Devon Island and some of the surge-type glaciers identified on Svalbard. In contrast with the abrupt and dramatic surges observed on some Alaskan glaciers (notably Variegated Glacier (Kamb and others, 1985)), typical surge cycles observed on Svalbard glaciers are longer, slower, and have lower amplitude velocity variations (Murray and others, 2003). The surge currently taking place on Southeast Glacier bears similarity to the description of the 10+ year long active phases on some Svalbard glaciers (Dowdeswell and others, 1991). Svalbard surge-type glaciers tend to have polythermal regimes (Jiskoot and others, 2000; Murray and others, 2003), and likewise, Devon outlet glaciers with flow regimes 2, 3, and 4 are inferred to have basal ice at the pressure melting point and/or periodically have meltwater at their beds. Finally, Svalbard surge-type glaciers tend to overlie sedimentary bedrock, and have beds composed of fine-grained till (Hamilton and Dowdeswell, 1996; Jiskoot and others, 2000). As we have shown, there seems to be a similar tendency with FR4 glaciers on Devon.

While these similarities do not conclusively identify any glaciers as surge-type, we do suggest that FR4 classification is at least a good indication that a glacier may demonstrate surge-like behaviour. The observation of FR4 regions switching between states of high or low surface velocities fits well with the interpretation that these regions have beds composed of unconsolidated sediment, capable of undergoing perfectly plastic deformation, which may contribute to high rates of basal motion. Below a critical value of driving stress and/or subglacial water pressure, no deformation will occur; above these critical values, rapid rates of deformation can occur, independent of additional driving stress

(Kavanaugh and Clarke, 2006). Therefore the fast-flow/slow-flow states of these regions could potentially be switched by minor changes in ice thickness, surface slope, or subglacial water pressure.

This has implications for the interpretation of FR1 at the termini of outlet glaciers. Some of the glaciers listed in Table 4-3 (East5, East7, lower regions of SouthEast2) may have been classified as FR1 instead of FR4 near their termini by Burgess and others (2005) because they were in a slow phase during the measurement period of that study and exhibited very low surface velocities (and low driving stresses). This would almost certainly change if the flow regime classification were repeated during the 'active phase' of these glaciers (i.e. in 2009 for East5).

4.5.4 Predictions of Annual Displacement Uncertainty

Our final goal for this paper was to identify how to determine the most appropriate estimate of a glacier's annual velocity, using short-interval displacement measurements. To cite a specific example of where this might be applicable, we refer to the work of Van Wychen and others (2012). In that study, a speckle-tracking technique was applied to co-registered pairs of RADARSAT-2 images to determine the ice surface displacement that occurred over the 24 day period between image acquisitions. The imagery was acquired during the month of March. If these results were used to estimate the annual ice flux at the termini of tidewater calving glaciers, would the velocity measured in March over- or under-estimate the mean annual velocity – and by how much?

We propose that knowledge of the type of Flow Regime found at the terminus of a tidewater outlet glacier may help those using remote sensing methods of velocity measurement to refine their error analysis for annual terminus velocity. Using the data assembled in Table 4-1, we estimate how closely velocity measurements made during the spring, summer, or fall/winter periods approximate the annual mean velocity. These results are summarized by Flow Regime in Table 4-4.

Table 4-4: Recommendations for estimating annual glacier velocity in each Flow Regime, based on short-interval measurements collected in different seasonal periods. Seasonal periods correspond to the following months: Spring: May and early June; Summer: late June through August; Fall/Winter: September through April.

Flow Regime	Over (+) or under (-) estimate of annual velocity (mean ± standard deviation)		Recommendation for estimate of annual velocity at glacier terminus with this Flow Regime
FR1	Spring	+0.5% ± 2.3%	Short-interval velocity of any period is a reasonable estimate of annual. Seasonal or annual variability is unlikely. (see caveat below)
	Summer	+1.6% ± 1.7%	
	Fall/Winter	-0.5% ± 1.0%	
FR2	Spring	-2.5% ± 6.9%	Spring velocity +5% to -15% of annual. Fall/winter velocity will underestimate annual by ~10-15%.
	Summer	+53.4% ± 17.8%	
	Fall/Winter	-11.7% ± 3.7%	
FR3	Spring	-5.5% ± 10.5%	Spring velocity +5% to -15% of annual. Fall/winter velocity will underestimate annual by ~10-15%.
	Summer	+62.6% ± 24.1%	
	Fall/Winter	-12.7% ± 4.4%	
FR4			Fall/winter velocity likely to underestimate annual by at least 15%, but this recommendation is based on inference and not supported by direct measurements.

In Flow Regimes 2 and 3, the summer months are the least ideal for acquiring short-interval measurements of velocity due to the high likelihood of overestimating the annual velocity by a large margin. Fall estimates appear to consistently underestimate the annual velocity, within a small range of values. Spring estimates may on average be more accurate, but less precise on a per measurement basis. The high standard deviation of spring estimates reflects the higher potential for velocity variability in spring vs. fall, which translates to an annual velocity estimate with higher uncertainty. Based on the above, our general recommendation is to use short-interval measurements collected during the fall/winter period, and account for a 10-15% under-estimate of annual velocity in FR2 and FR3 regions. Though we lack direct observations of FR4, we suggest that the fall/winter period would also be the most consistent period in which to measure the background velocity of these regions. We speculate that the background velocity underestimates the annual mean velocity by at least 15% in

FR4. Installation of GPS systems in the FR4 zones of the North and South Croker glaciers could verify this hypothesis.

Care should be taken in the interpretation of velocities from the terminus region of any outlet glacier classified as FR4 or FR1. The FR1 classification was intended to describe the interior "sheet-flow" regions of the ice cap. In the interior regions, there is likely to be very little inter-annual change in velocity. However, at the terminus of an outlet glacier (such as Southeast Glacier), FR1 classification may potentially identify a glacier in a slow-flow state, capable of switching to a fast-flow state. Therefore, if velocities higher than ~20 m a^{-1} are measured at such a site, its current flow regime classification should be revaluated.

4.6 Conclusions

Our GPS measurements from 13 different sites on the Devon Ice Cap confirm that the Flow Regimes classification map of Burgess and others (2005) adequately identifies regions of the ice cap most likely to incorporate hydrologically driven basal motion as a component of ice surface velocity. We show here that this also helps to indicate areas of the ice cap exhibiting seasonal and inter-annual flow variability, which must be taken into account in the derivation of regional calving flux estimates.

In FR1, ice is slow flowing, and is unlikely to exhibit seasonal or inter-annual changes in velocity. The exception to this is where FR1 is found downstream of faster flowing regions of outlet glaciers, which may indicate the ice is in a slow-flow quiescent state, which could change over multi-year time-scales. Both FR2 and FR3 regions exhibit cycles of seasonal velocity variability, where summer flow speeds are significantly higher (35-90%) than spring, fall, or winter velocities. Within the scope of our GPS observations, we have not observed inter-annual changes in mean velocity in FR2 zones. However we have observed multi-year trends in the background velocity in FR3 zones. Because of the relationship between strain rate (v/h) and driving stress (τ_d) in FR3, these

regions are highly sensitive to variations in basal friction and perhaps also to longer-term perturbations of ice thickness and surface slope. Though we have not directly measured the velocity of ice classified as FR4 using GPS, we speculate, based on the behaviour of adjacent FR3 regions and the interpretation that FR4 regions overlie deformable bed material, that these regions exhibit more extreme variations in seasonal and annual velocities when subjected to the same perturbations. Comparisons between velocity measurements made in previous studies (Burgess and others, 2005; Van Wychen and others, 2012) confirm that large changes in annual velocity occur in FR4 zones. FR4 classification may indicate that a glacier is likely to exhibit surge-like behaviour.

The most reliable way to estimate the mean annual velocity using short-interval displacement measurements is to collect measurements during the fall/winter period (i.e., September through April), and anticipate that this measurement is an accurate estimate for FR1, but 10-15% below the mean annual velocity in FR2 and FR3. For FR4, we speculate that a fall/winter measurement underestimates the annual velocity by at least 15%, but we do not have direct observations to support this statement. Calving fluxes computed using the adjusted mean annual velocities would be larger by approximately the same magnitude (10-15%). The result would be more-negative dynamic mass losses for glacier-specific or regional mass balance estimates.

At other Arctic ice cap locations where velocity and ice thickness measurements are available, Flow Regime distribution could be determined based on the same ice-dynamic criteria used by Burgess and others (2005). Doing so will assist with the interpretation of short-interval velocity measurements made in the interests of calculating calving fluxes from tidewater glaciers.

Bibliography

Boon, S., D. Burgess, R. M. Koerner and M. J. Sharp 2010. Forty-seven Years of Research on the Devon Island Ice Cap, Arctic Canada. *Arctic* **63**(1), 13-29.

Burgess, D. O. and M. J. Sharp 2004. Recent Changes in Areal Extent of the Devon Ice Cap, Nunavut, Canada. *Arctic, Antarctic, and Alpine Research* **36**(2), 261-271.

Burgess, D. O. and M. J. Sharp 2008. Recent changes in the thickness of the Devon Island ice cap, Nunavut, Arctic Canada. *Journal of Geophysical Research* **113**(B07204).

Burgess, D. O., M. J. Sharp, D. W. F. Mair, J. A. Dowdeswell and T. J. Benham 2005. Flow dynamics and iceberg calving rates of Devon Ice Cap, Nunavut, Canada. *Journal of Glaciology* **51**(173), 219-230.

Carr, J. R., C. R. Stokes and A. Vieli 2013. Recent progress in understanding marine-terminating Arctic outlet glacier response to climatic and oceanic forcing: Twenty years of rapid change. *Progress in Physical Geography* **37**(4), 436-467.

Clason, C., D. W. F. Mair, D. O. Burgess and P. W. Nienow 2012. Modelling the delivery of supraglacial meltwater to the ice/bed interface : application to southwest Devon Ice Cap, Nunavut, Canada. *Journal of Glaciology* **58**(208), 361-374.

Cuffey, K. and W. S. B. Paterson 2012. *The physics of glaciers*. Burlington, MA, Academic Press.

Dowdeswell, J. A., G. S. Hamilton and J. O. Hagen 1991. The Duration of the Active Phase on Surge-Type Glaciers - Contrasts between Svalbard and Other Regions. *Journal of Glaciology* **37**(127), 388-400.

Dowdeswell, J. A., T. J. Benham, M. R. Gorman, D. Burgess and M. J. Sharp 2004. Form and flow of the Devon Island Ice Cap, Canadian Arctic. *Journal of Geophysical Research-Earth Surface* **109**(F2).

Frisch, T. 1984. Geology, Devon Ice Cap, District of Franklin, Northwest Territories. Geological Survey of Canada, "A" Series Map. Sherbrooke, Quebec, Geological Survey of Canada**:** Map 1574A.

Gardner, A. S., G. Moholdt, B. Wouters, G. J. Wolken, D. O. Burgess, M. J. Sharp, J. G. Cogley, C. Braun and C. Labine 2011. Sharply increased mass

loss from glaciers and ice caps in the Canadian Arctic Archipelago. *Nature* **473**(7347), 357-360.

Gudmundsson, G. H., C. F. Raymond and R. Bindschadler 1998. The origin and longevity of flow stripes on Antarctic ice streams. *Annals of Glaciology* **27**, 142-152.

Hamilton, G. S. and J. A. Dowdeswell 1996. Controls on glacier surging in Svalbard. *Journal of Glaciology* **42**(140), 157-168.

Haug, T., A. Kaab and P. Skvarca 2010. Monitoring ice shelf velocities from repeat MODIS and Landsat data – a method study on the Larsen C ice shelf, Antarctic Peninsula, and 10 other ice shelves around Antarctica. *The Cryosphere* **4**, 161-178.

Iken, A., H. Rothlisberger, A. Flotron and W. Haeberli 1983. The uplift of Unteraargletscher at the beginning of the melt season — a consequence of water storage at the bed? *Journal of Glaciology* **29**(101), 28-47.

Jakobsson, M., R. Macnab, L. Mayer, R. Anderson, M. Edwards, J. Hatzky, H. W. Schenke and P. Johnson 2008. An improved bathymetric portrayal of the Arctic Ocean: Implications for ocean modeling and geological, geophysical and oceanographic analyses. *Geophysical Research Letters* **35**(7), L07602.

Jiskoot, H., T. Murray and P. Boyle 2000. Controls on the distribution of surge-type glaciers in Svalbard. *Journal of Glaciology* **46**(154), 412-423.

Kamb, B., C. F. Raymond, W. D. Harrison, H. Engelhardt, K. A. Echelmeyer, N. Humphrey, M. M. Brugman and T. Pfeffer 1985. Glacier Surge Mechanism - 1982-1983 Surge of Variegated Glacier, Alaska. *Science* **227**(4686), 469-479.

Kavanaugh, J. L. and G. K. C. Clarke 2006. Discrimination of the flow law for subglacial sediment using in situ measurements and an interpretation model. *Journal of Geophysical Research: Earth Surface* **111**(F1), F01002.

Murray, T., T. Strozzi, A. Luckman, H. Jiskoot and P. Christakos 2003. Is there a single surge mechanism? Contrasts in dynamics between glacier surges in Svalbard and other regions. *Journal of Geophysical Research-Solid Earth* **108**(B5).

Röthlisberger, H. and H. Lang 1987. Glacial Hydrology. In *Glacio-fluvial sediment transfer: an alpine perspective*. A. M. Gurnell and M. J. Clark, *ed.* Chichester, John Wiley and Sons**:** 207-284.

Sharp, M., D. O. Burgess, J. G. Cogley, M. Ecclestone, C. Labine and G. J. Wolken 2011. Extreme melt on Canada's Arctic ice caps in the 21st century. *Geophys. Res. Lett.* **38**(11), L11501.

Truffer, M. and K. A. Echelmeyer 2003. Of isbrae and ice streams. *Annals of Glaciology* **36**, 66-72.

Van Wychen, W. 2010. Spatial and Temporal Variations in Ice Motion, Belcher Glacier, Devon Island, Nunavut, Canada. (*MSc. Thesis,* University of Ottawa.)

Van Wychen, W., L. Copland, L. Gray, D. Burgess, B. Danielson and M. Sharp 2012. Spatial and temporal variation of ice motion and ice flux from Devon Ice Cap, Nunavut, Canada. *Journal of Glaciology* **58**(210), 657-664.

Wyatt, F. 2013. The spatial structure and temporal development of supraglacial drainage systems, and their influence on the flow dynamics of High Arctic ice caps. (*Doctoral Thesis*, University of Alberta.)

Chapter Five: Concluding Remarks

Much attention over the last decade has been spent on the question of whether increased surface melting will drive wide-scale acceleration of glacier ice, especially after observations from near the equilibrium line of the Greenland ice sheet demonstrated a correspondence between meltwater drainage and increases in surface velocity (Zwally and others, 2002). This idea gained some traction (Parizek and Alley, 2004), and was in fact one of the early factors motivating this study, but more recently the picture has evolved and a simple relationship of increased melt driving faster ice flow does not seem likely. The modelling work by Schoof (2010) demonstrates that high rates of meltwater delivery to the subglacial drainage system force the system to rapidly evolve in efficiency, leading to a decrease in water pressure and quick end to transient fast-flow. Alternatively, enhanced basal sliding can be driven by high variability in both the rate and total volume of meltwater delivery to the bed, which forces the subglacial drainage system into a constant state of adaptation, leading to effective pressure changes that facilitate accelerated sliding (Bartholomaus and others, 2008; Schoof, 2010). Field and remote sensing observations at a number of glaciers, including ours, are consistent with these findings.

This study set out to determine whether spatial and temporal variations in the delivery of surface meltwater to a glacier's basal drainage system can drive variations in glacier velocity at different time scales. This issue is particularly pertinent considering the recent observations of longer, warmer summers (Sharp and others, 2011), changes in synoptic scale weather patterns (Gascon and others, 2013), and higher volumes of glacier meltwater runoff (Gardner and others, 2011) in the Canadian Queen Elizabeth Islands. Specific questions that we sought to answer included:

1. Do individual supra-glacial drainage events have a measurable impact on tidewater glacier flow velocity? How do these events contribute to the overall

pattern of seasonal velocity variability, and do they have a quantifiable impact on total seasonal/annual displacement?

2. Is there a pattern of seasonal velocity variability that is consistent over multiple years? Is there interannual variability in this pattern that can be explained by differences in melt season characteristics, the seasonal evolution of the surface drainage system, or the occurrence of distinct meltwater drainage events?

3. Do hydrologically-driven seasonal variations in velocity significantly affect the estimation of annual mean velocity extrapolated from short-term measurements?

Our observations of Belcher Glacier during the 2009 summer demonstrated that individual meltwater drainage events, such as the rapid drainage of supra-glacial lakes or water-filled crevasses, appear to drive rapid responses in glacier velocity. However, even the largest of the fast lake drainage events observed (on the order of 10^6 m^3 in <48 hours) produced very short-duration ice acceleration events. Combined, the total additional displacement of Belcher Glacier terminus caused by the lake drainage events observed in 2009 amounted to <1% of the total annual ice displacement. Likely of greater importance is that some of these drainage events, especially the drainage of water-filled crevasses, establish the surface to subglacial hydrologic connections into which surface meltwater can flow throughout the remainder of the melt season.

A cycle of seasonal velocity changes occurs in response to the 50-60 day melt season on Belcher Glacier each year, and we identified a sequence of phases in this cycle which consist of: the quiescent (winter velocity) phase, the gradual speedup in the terminus zone near the beginning of the melt season, the spring event phase which occurs glacier-wide, the late-summer 'hydro-active' phase, and the gradual return to quiescence at the end of the melt season. Inter-annual variations to this pattern are largely be explained by two factors which influence the drainage of surface runoff to the glacier bed.

The first factor is the thickness of the spring snowpack, which exerts a strong control on the evolution of the surface drainage system early in the melt season. Thicker spring snowpack retards the surface melt rate for a longer fraction of the summer by delaying the exposure of the low albedo ice surface, it delayed the runoff of meltwater by acting as a storage medium, and it delayed the development of drainage channels and the opening of meltwater sink points. For years with exceptionally thick spring snowpack, this resulted in a delay of the spring event, and reduced the time available for the hydro-active phase of the seasonal cycle to occur.

The second factor was the amount of variability in late summer meltwater production. Years that included mid-summer snow storms or synoptic scale weather patterns that caused strong variations in melt at multi-day time scales also produced more variability in velocity during the hydro-active phase of the seasonal cycle than a monotonically warm summer with little variability in melt rates. As described above, this was inferred to be due to the time-varying evolution of the subglacial drainage channels, which can evacuate high volumes of water at low pressure under sustained high runoff rates, but while adapting to variable runoff rates the pressure in these large channels may increase and drive water out into distributed water-filled cavities which causes basal sliding rates to increase (Iken and Bindschadler, 1986; Bartholomaus and others, 2008; Schoof, 2010).

During the latter half of the 2000-2010 decade, an increase in the frequency of 3-5 day long surface low-pressure systems was observed in August (Gascon and others, 2013). The timing and frequent occurrence of these low-pressure systems (and associated changes in net longwave radiation) identified by Gascon and others (2013) help to explain the 3-5 day variability in melt which we observed on Belcher Glacier in August 2010. Since a northward shift in the North Atlantic storm track favourable to the continuation of this trend is predicted for 21st century (Schuenemann and Cassano, 2010) we might expect to continue to see long melt seasons with highly variable late-summer melt patterns similar to

2010. This is one trend that might drive a modest increase in seasonal glacier flow enhancement.

To determine whether the summer speedup makes a significant contribution to the mean annual velocity, we estimated the effective change in annual displacement attributable to the summer speedup (Δds). This was calculated as the difference between the surveyed total annual displacement and the hypothetical displacement that would occur if the ice moved without any seasonal hydrological forcing. The relative displacement change as a percentage of the total annual displacement was 5-7% in the upper glacier, 11-13% in the mid-glacier, and 5-8% in the terminus region. Inter-annual differences in the seasonal velocity cycle therefore caused only 2-3% changes in annual ice displacement over three years. The summer speedup does not make a large contribution to the total annual ice displacement because of the short duration of the summer melt season relative to the remainder of the year during which flow speeds are lower. In some cases, the high summer velocities are offset by a period of slower than background velocity immediately following the end of the melt season. The Δds observed at Belcher Glacier is of a similar magnitude to the effect of seasonal variations on the annual displacement of a number of tidewater outlet glaciers on the western margins of the Greenland ice sheet (Joughin and others, 2008; Sole and others, 2011).

In Chapter 3 we described Belcher Glacier as a bi-modal system, based on the dynamic differences observed between the terminus zone and the mid- and upper-glacier regions. The division between these zones, roughly 5 km up-glacier from the calving terminus, was defined by three features: down-glacier of this point is the distinct onset of extensive surface crevassing, a strong transition to much higher annual mean velocity, and the transition to where a larger fraction of the ice thickness lies below rather than above mean sea level. In the mid- and upper-glacier, the annual mean velocity was relatively consistent, and the effective increase in annual displacement due to the summer speedup (Δds) was greater in years with lower runoff volumes. These observations suggest that the

subglacial drainage system undergoes an evolution in drainage efficiency that effectively limits the hydrological forcing of velocity variations. There was a reverse trend in the terminus zone - an increase in the Δds during summers with greater ablation and high runoff variability, and inter-annual changes in the mean velocity. Several potential reasons were suggested for the shift in flow dynamics between these two regions, but one of these relates directly to results of Chapter 2, which demonstrated critical differences in the types of surface drainage events that occur in these regions.

In the mid- and upper-glacier regions, extensive surface drainage channels develop along linear features such as flow stripes and medial moraines (Wyatt, 2013), routing high volumes of water produced over large fractions of the glacier area into a small number of sink points (moulins, or lakes which eventually drain). Previous observations and modelling studies (Fountain and Walder, 1998; Schoof, 2010) indicate that these are the conditions under which a subglacial drainage system composed of a small number of highly efficient channels is likely to develop. The development of such a system in the mid- and upper-glacier regions provides an explanation for why the lake drainage events that occurred in mid-summer produced only brief high-velocity events, and also explains why ice velocity progressively decreases in the late melt season, despite continued inputs of surface runoff into moulins.

In the terminus zone (the lower 5 km of the glacier), where there is a high density of large, deep crevasses distributed across most of the glacier width, large lakes tended not to form and the extensive crevassing interrupts the development of a supra-glacial stream network. The lower elevation and perennially thin snowpack contribute to the slightly earlier onset of meltwater ponding in this region, as opposed to up-glacier regions. Meltwater collecting in and draining through these crevasses (the earliest drainage events observed) may therefore contribute to elevating subglacial water pressure across a wide region of the glacier bed in the terminus zone. Because relatively low volumes of water drain into each of these widely distributed sink points, it is feasible that an efficient,

highly channelized drainage system might take much longer to develop in many parts of this zone. This structural difference in the surface drainage system is likely one of the main reasons why the summer speedup occurred earlier, lasted longer, and maintained relatively high mean velocities throughout the summer in the terminus region. These observations are supported by a recent examination of the relationship between glacier dynamics and differences in the structure of surface hydrologic drainage of the entire Devon Ice Cap (Wyatt, 2013), which showed that ice velocity and velocity variability increase in regions with a higher density and distribution of meltwater sink-points.

In Chapter 4, observations of glacier velocity variability were compared to the flow regimes model proposed by Burgess and others (2005), which characterizes the changes in dynamics along a glacier flowline as a progression of four possible flow regimes (FR1 – FR4). Our GPS measurements from 13 different sites on four outlet glaciers of the Devon Ice Cap confirmed that the map of these flow regimes adequately identified regions where basal sliding likely contributes to glacier flow (i.e., all regions except FR1), and thus the identification of areas of the ice cap that might be subject to hydrologically driven changes in flow dynamics. Wyatt (2013) showed that inter-annual velocity variability increased with progression through FR1 to FR4. This study confirms that result, and adds that these flow regimes exhibit progressively higher degrees of shorter-term and seasonal flow variability as well. FR1 showed no velocity variability at any time-scale, which is consistent with the interpretation that hydrologically driven basal sliding does not occur in this regime (Burgess and others, 2005). FR2 and FR3 both exhibited short-term and seasonal scale variability, and in FR3 we observed multi-year trends in annual mean velocity as well. We lacked GPS observations of any FR4 regions on Devon Ice Cap glaciers, and were therefore unable to assess the seasonal-scale variability of these regions. However, a review of previously published velocity observations on the Devon Ice Cap (Burgess and others, 2005; Van Wychen and others, 2012; Wyatt, 2013) suggested that glaciers which included regions of FR4 may demonstrate

large variations in inter-annual velocity, in some cases similar to surge-type glaciers.

The inter-annual velocity changes observed in FR3 and FR4 are significant because these regimes are characteristic of the terminus regions of the largest and fastest flowing tidewater glaciers of the Devon Ice Cap, indicating that these glaciers have the potential for significant variations in iceberg calving rates over multi-year time scales. The relationship between strain rate and driving stress in FR3 suggests that the velocity in these regions is highly sensitive to small changes in basal friction and perhaps even changes in ice thickness or surface slope at multi-year time scales. In FR4 regions, where plastic deformation of the glacier bed may contribute to surface velocity, a minor decrease in driving stress below a critical threshold or a change in subglacial water storage could potentially cause a switch between fast- and slow-flow states. Much longer time-series of velocity measurements of these glaciers are required to determine the potential magnitude of velocity change, and whether these long-term changes are cyclical or correlated with variations in any external driving processes. However, since these glacier regions may be poised to respond to very subtle perturbations of driving stress, it may be extremely difficult to identify any obvious external processes that trigger these long-term changes in velocity and rates of calving flux. For instance, inter-annual variations in surface mass balance gradients might be sufficient to drive velocity variations in these regions. Or there might be an unknown hydrologically driven explanation for these changes,

A very recently published study, which used velocity observations of 160 glaciers throughout Alaska between 2006 and 2011, shows evidence that wintertime glacier velocity is inversely related to the amount of melt that occurred in the previous summer (Burgess and others, 2013). The authors argue that anomalously high summer melt results in a reduction in the amount of water stored subglacially through winter, reducing rates of winter sliding velocity. While this hypothesis certainly seems plausible, it suggests the likelihood of regional synchronicity in inter-annual glacier velocity variations, making it

somewhat difficult to reconcile with this study's observations of three-year velocity trends of opposing sign at Belcher and North Croker Glaciers. However it would be worthwhile exploring this hypothesis further using a larger and longer-term collection of annual velocity observations from Canadian Arctic glaciers.

Chapter 4 attempted to provide an answer to the question that motivated this study: Do hydrologically-driven seasonal variations in velocity significantly affect the estimation of annual mean velocity extrapolated from short-term measurements? The answer is: yes, extrapolating short-term measurements of ice displacement to annual velocities will introduce a bias, the direction and magnitude of which depends on when the short-term measurement was made. Knowledge of the type of Flow Regime found at the terminus of a tidewater outlet glacier may help other researchers using remote sensing methods of velocity measurement to refine their error analysis for annual terminus velocity and calving flux computation. Table 4-4 demonstrated how closely short-term velocity measurements made during the spring, summer, or fall/winter periods would approximate the annual mean velocity of ice in different flow regimes. The most reliable way to estimate the mean annual velocity using short-interval displacement measurements is to collect measurements during the fall/winter period (September through April), and anticipate that this measurement will be an accurate estimate for FR1, but 10-15% below the mean annual velocity in FR2 and FR3. For FR4, we could only speculate that a fall/winter measurement would underestimate the annual velocity by at least 15%, due to a lack of GPS observations.

This answer may not be definitive, but at least provide a guideline for how to account for seasonal velocity variations when using short-duration displacement measurements based on image differencing techniques, and may also allow researchers to make an informed decision when selecting imagery for use.

5.1 Outlook and recommendations for future work

Many of the field observations used in this research project were acquired as part of the International Polar Year Glaciodyn project, the goal of which was to investigate the dynamics of Arctic glaciers, their response to future climate change scenarios, and their contributions to sea level rise. One of the aims of the Glaciodyn project was to develop a coupled glacier hydrology-dynamics-calving model that would be capable of assimilating a wide range of field measurement data to determine the dynamic response of tidewater glaciers to hydrologic and climatic drivers. A general model of this system was produced (Pimentel and Flowers, 2010; Pimentel and others, 2010) that is capable of simulating various different glacier geometries and boundary conditions. Remote sensing and field measurements collected by many members of the Glaciodyn project team were required to constrain the glacier geometry and define the climatic, mass balance, and hydrologic inputs necessary to represent the Belcher Glacier system in this model (Sylvestre, 2009; Van Wychen, 2010; Duncan, 2011; Milne, 2011; Herdes and others, 2012; Wyatt, 2013). Our observations of surface meltwater drainage events, sink point locations and meteorological observations have helped to define some of the required hydrologic input data, and our observations of the spatial and temporal variability of ice surface velocity have helped to define constraints and validation for ice flow velocity fields generated by the model. In this way the work presented in this thesis makes a contribution towards developing more accurate predictions of glacier dynamic response to climate and contribution to future sea level rise.

The practical application of the results of this thesis involves using the recommendations given above to account for seasonal velocity variability when measuring tidewater glacier terminus velocity using image differencing or correlation techniques. Doing so requires the use of a flow regimes map for the ice cap of interest. Currently, a flow regimes classification has only been performed for the Devon Ice Cap, and it was based on ice velocity measurements

from 1995. Therefore a recommendation for future work is to use updated ice velocity fields to a) regenerate the Flow Regimes map for the Devon Ice Cap, and b) apply the Flow Regimes classification to other ice caps in the Canadian Arctic. Since updated velocity measurements are now available for the Devon Ice Cap, it would be beneficial to regenerate the Flow Regimes map to fill in the gaps in the original map. A comparison between the two maps may reveal significant dynamic changes on some of the outlet glaciers. For other Arctic ice caps, the process of defining flow regimes based on the same ice-dynamic criteria used by Burgess and others (2005) should be possible, with some minor tuning of the necessary thresholds. This would be a useful exercise as the resulting classification map will provide meaningful information about ice dynamics, useful for analyzing ongoing velocity observations of High Arctic ice caps. The limiting factor will be the availability of surface and bedrock DEMs for some of these regions.

Velocity measurements of all of the major tidewater glaciers in the Queen Elizabeth Islands have been made at least once via remote sensing methods, and in some cases repeat measurements have indicated that several of these glaciers may exhibit large inter-annual changes that make a significant impact on regional calving flux (Short and Gray, 2005; Williamson and others, 2008; Van Wychen and others, 2012). A Flow Regimes map covering all of the ice caps in the Queen Elizabeth Islands would help to identify, via classification of FR3 and FR4 zones, other glaciers which might undergo large changes in dynamics over time, and should therefore be the targets of frequent monitoring.

Bibliography

Bartholomaus, T. C., R. S. Anderson and S. P. Anderson 2008. Response of glacier basal motion to transient water storage. *Nature Geoscience* **Vol 1**(Number 1), 33-37.

Burgess, D. O., M. J. Sharp, D. W. F. Mair, J. A. Dowdeswell and T. J. Benham 2005. Flow dynamics and iceberg calving rates of Devon Ice Cap, Nunavut, Canada. *Journal of Glaciology* **51**(173), 219-230.

Burgess, E. W., C. F. Larsen and R. R. Forster 2013. Summer melt regulates winter glacier flow speeds throughout Alaska. *Geophysical Research Letters* doi: 10.1002/2013GL058228.

Duncan, A. 2011. Spatial and Temporal Variations of the Surface Energy Balance and Ablation on the Belcher Glacier, Devon Island, Nunavut, Canada. (*MSc. Thesis*, University of Alberta.)

Fountain, A. G. and J. S. Walder 1998. Water flow through temperate glaciers. *Reviews of Geophysics* **36**(3), 299-328.

Gardner, A. S., G. Moholdt, B. Wouters, G. J. Wolken, D. O. Burgess, M. J. Sharp, J. G. Cogley, C. Braun and C. Labine 2011. Sharply increased mass loss from glaciers and ice caps in the Canadian Arctic Archipelago. *Nature* **473**(7347), 357-360.

Gascon, G., M. Sharp and A. Bush 2013. Changes in melt season characteristics on Devon Ice Cap, Canada, and their association with the Arctic atmospheric circulation. *Annals of Glaciology* **54**(63), 101-110.

Herdes, E., L. Copland, B. Danielson and M. Sharp 2012. Relationships between iceberg plumes and sea-ice conditions on northeast Devon Ice Cap, Nunavut, Canada. *Annals of Glaciology* **53**(60).

Iken, A. and R. A. Bindschadler 1986. Combined measurements of subglacial water pressure and surface velocity of Findelengletscher, Switzerland: conclusions about drainage system and sliding mechanism. *Journal of Glaciology* **32**(110), 101-119.

Joughin, I., S. B. Das, M. A. King, B. E. Smith, I. M. Howat and T. Moon 2008. Seasonal Speedup Along the Western Flank of the Greenland Ice Sheet. *Science* **320**(5877), 781-783.

Milne, H. 2011. Iceberg calving from a Canadian Arctic tidewater glacier. (*MSc. Thesis*, University of Alberta.)

Parizek, B. R. and R. B. Alley 2004. Implications of increased Greenland surface melt under global-warming scenarios: ice-sheet simulations. *Quaternary Science Reviews* **23**(9-10), 1013-1027.

Pimentel, S. and G. E. Flowers 2010. A numerical study of hydrologically driven glacier dynamics and subglacial flooding. *Proceedings of the Royal Society A* **467**, 537-558.

Pimentel, S., G. E. Flowers and C. G. Schoof 2010. A hydrologically coupled higher-order flow-band model of ice dynamics with a Coulomb friction sliding law. *Journal of Geophysical Research: Earth Surface* **115**(F4), F04023.

Schoof, C. 2010. Ice-sheet acceleration driven by melt supply variability. *Nature* **468**(7325), 803-806.

Schuenemann, K. C. and J. J. Cassano 2010. Changes in synoptic weather patterns and Greenland precipitation in the 20th and 21st centuries: 2. Analysis of 21st century atmospheric changes using self-organizing maps. *J. Geophys. Res.* **115**(D5), D05108.

Sharp, M., D. O. Burgess, J. G. Cogley, M. Ecclestone, C. Labine and G. J. Wolken 2011. Extreme melt on Canada's Arctic ice caps in the 21st century. *Geophys. Res. Lett.* **38**(11), L11501.

Short, N. H. and A. L. Gray 2005. Glacier dynamics in the Canadian High Arctic from RADARSAT-1 speckle tracking. *Canadian Journal of Remote Sensing* **31**(3), 225-239.

Sole, A. J., D. W. F. Mair, P. W. Nienow, I. D. Bartholomew, M. A. King, M. J. Burke and I. Joughin 2011. Seasonal speedup of a Greenland marine-terminating outlet glacier forced by surface melt–induced changes in subglacial hydrology. *J. Geophys. Res.* **116**(F3), F03014.

Sylvestre, T. 2009. Spatial Patterns of Snow Accumulation across the Belcher Glacier Basin, Devon Island, Nunavut, Canada. (*MSc. Thesis*, University of Ottawa.)

Van Wychen, W. 2010. Spatial and Temporal Variations in Ice Motion, Belcher Glacier, Devon Island, Nunavut, Canada. (*MSc. Thesis*, University of Ottawa.)

Van Wychen, W., L. Copland, L. Gray, D. Burgess, B. Danielson and M. Sharp 2012. Spatial and temporal variation of ice motion and ice flux from

Devon Ice Cap, Nunavut, Canada. *Journal of Glaciology* **58**(210), 657-664.

Williamson, S., M. Sharp, J. Dowdeswell and T. Benham 2008. Iceberg calving rates from northern Ellesmere Island ice caps, Canadian Arctic, 1999-2003. *Journal of Glaciology* **54**, 391-400.

Wyatt, F. 2013. The spatial structure and temporal development of supraglacial drainage systems, and their influence on the flow dynamics of High Arctic ice caps. (*PhD. Thesis*, University of Alberta.)

Zwally, H. J., W. Abdalati, T. Herring, K. Larson, J. Saba and K. Steffen 2002. Surface melt-induced acceleration of Greenland ice-sheet flow. *Science* **297**(5579), 218-222.

APPENDIX A: GLACIER MOTION TIME-SERIES

A.1. Overview

The figures in this Appendix show the processed results of GPS observations collected between 2008 and 2012 on four tidewater outlet glaciers of the Devon Island Ice Cap: the Belcher Glacier, Sverdrup Glacier, North Croker Glacier, and Southeast Glacier. The figures include the time-series of horizontal and vertical ice surface motion measured at each GPS station, as well as the plan-view of horizontal displacement of each station over its operational period. The graph below shows the time period that each GPS station was in operation. The order in which stations are listed in the graph is the same order the corresponding figures appear in this Appendix. The location of each GPS station is shown in Figure 4-1.

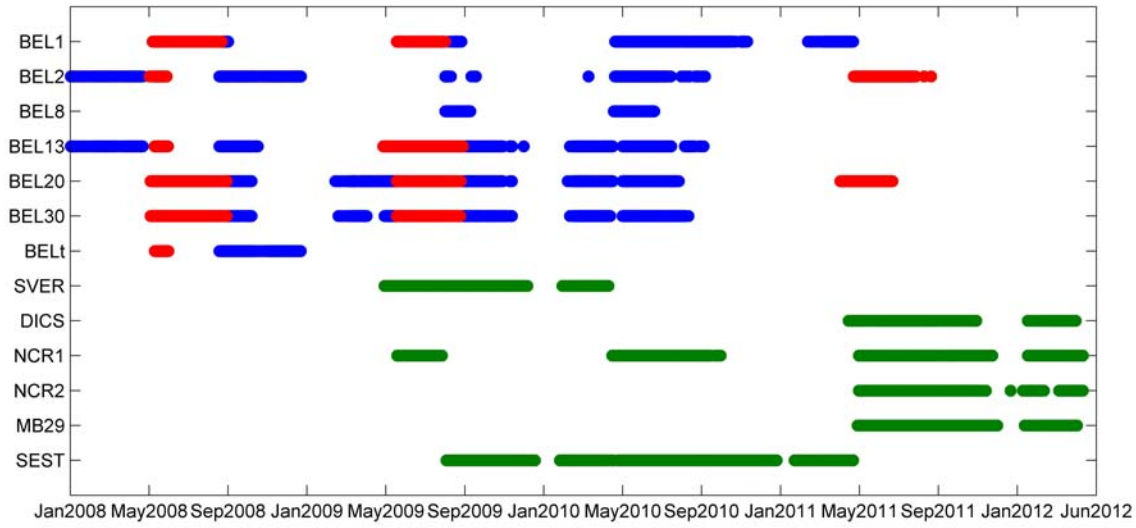

Summary of GPS station occupation. Colors represent the sampling rate of each time series: Green: 1 point / 24 hours, Blue: 1 point / 6 hours, Red: 1 point / 1 hour

A.2. Belcher Glacier

Figure A1: Time-series of Cumulative Vertical Displacement (*top*), and Horizontal Velocity (*bottom*). The dotted horizontal line represents the annual mean velocity recorded at BEL1.

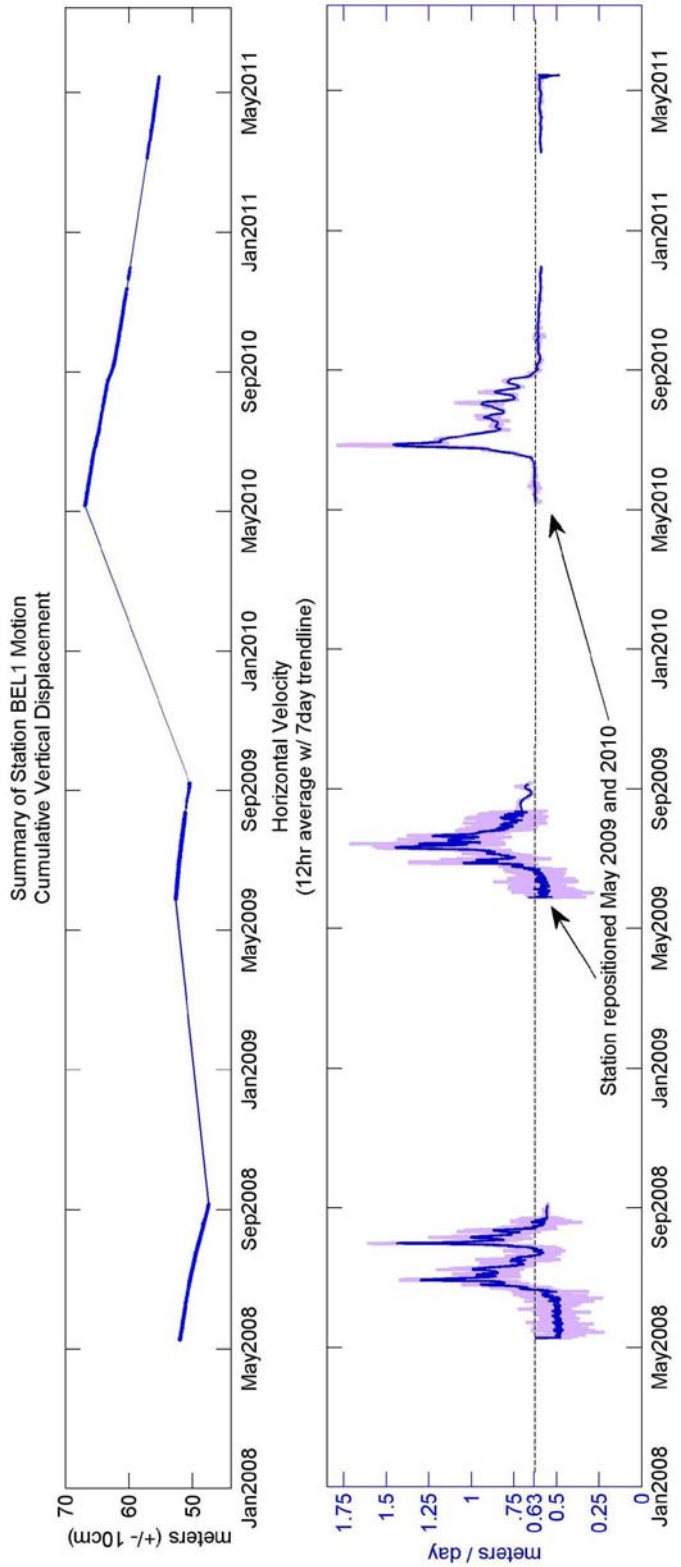

Figure A2: Plan-view of BEL1 station motion

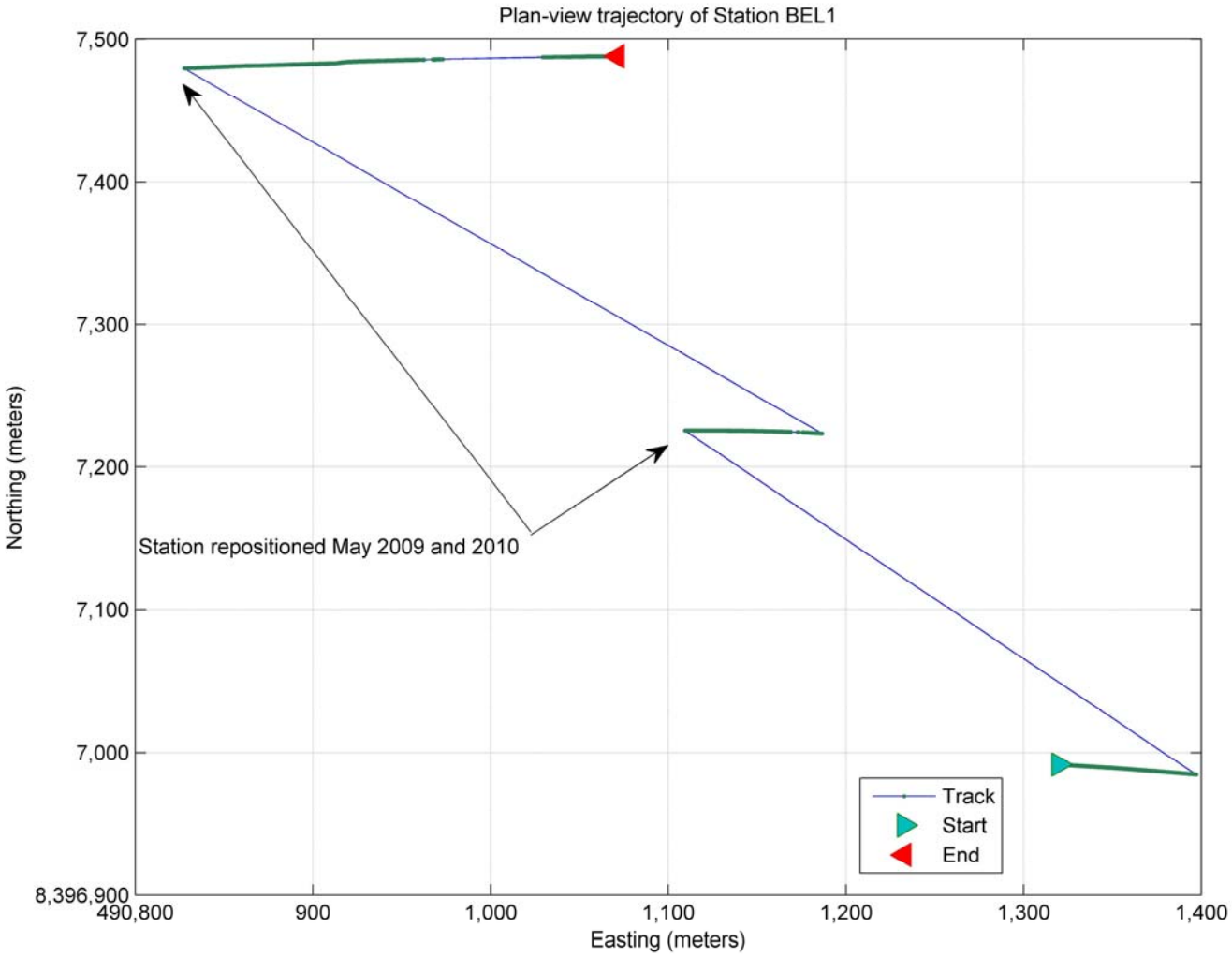

Figure A3: Time-series of Cumulative Vertical Displacement (*top*), and Horizontal Velocity (*bottom*). The dotted horizontal line represents the annual mean velocity recorded at BEL2.

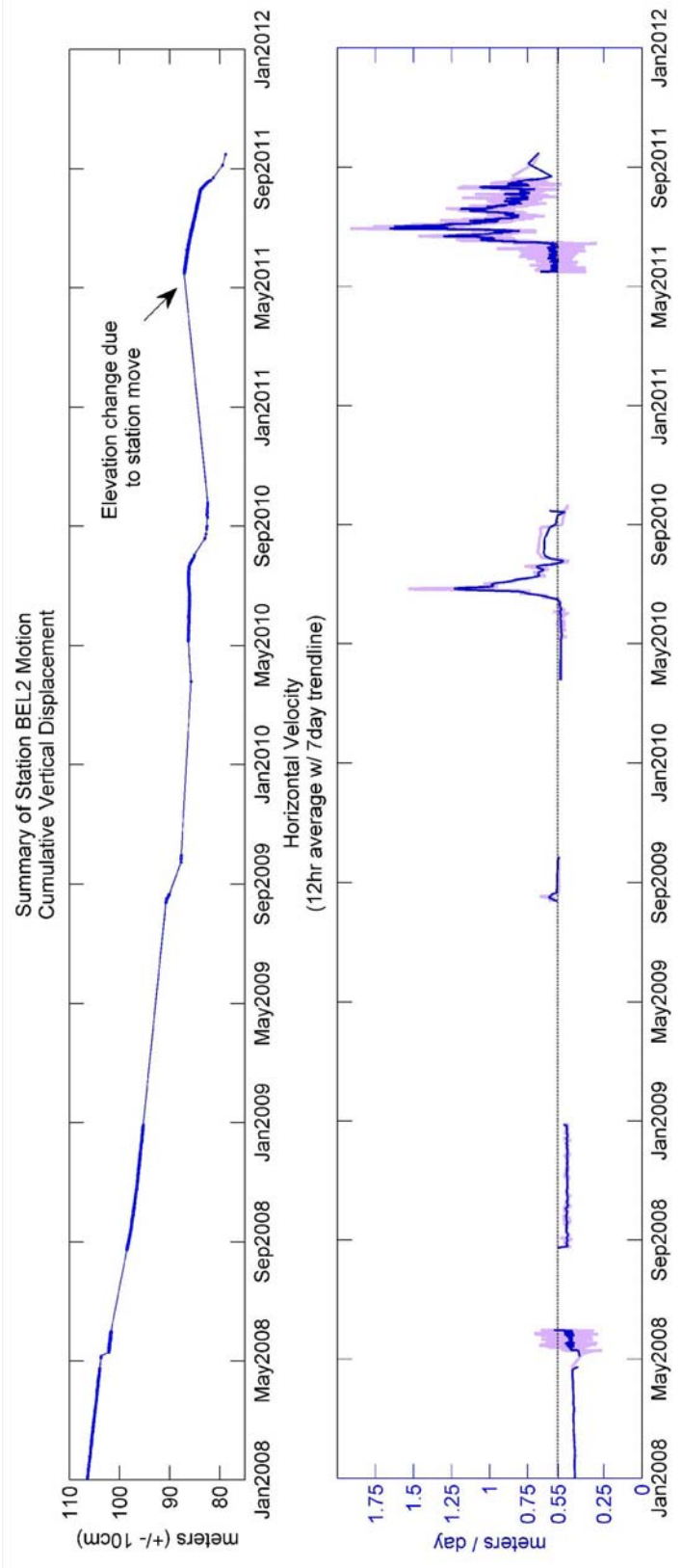

Figure A4: Plan-view of BEL2 station motion

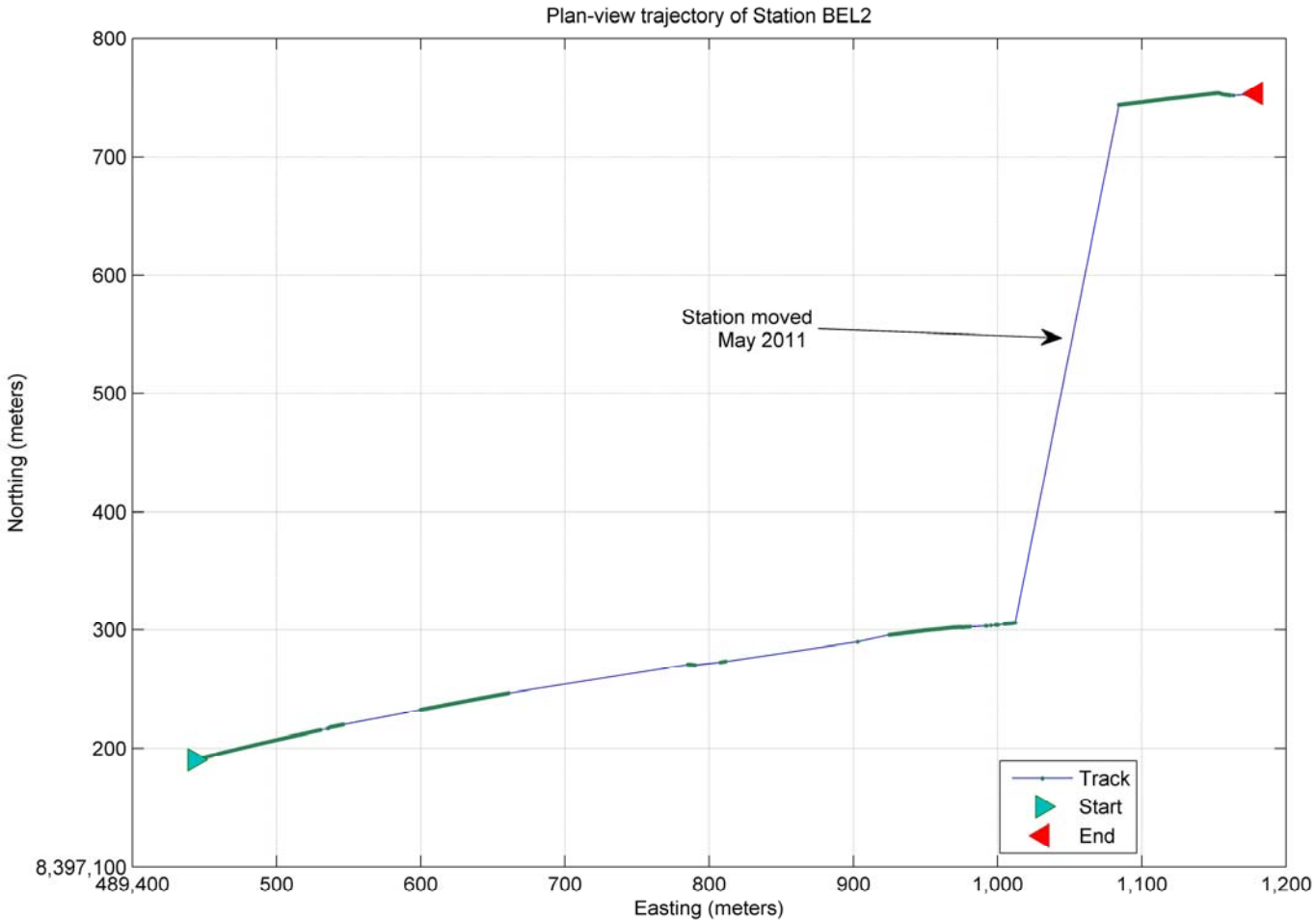

Figure A5: Time-series of Cumulative Vertical Displacement (*top*), and Horizontal Velocity (*bottom*). The dotted horizontal line represents the annual mean velocity recorded at BEL8.

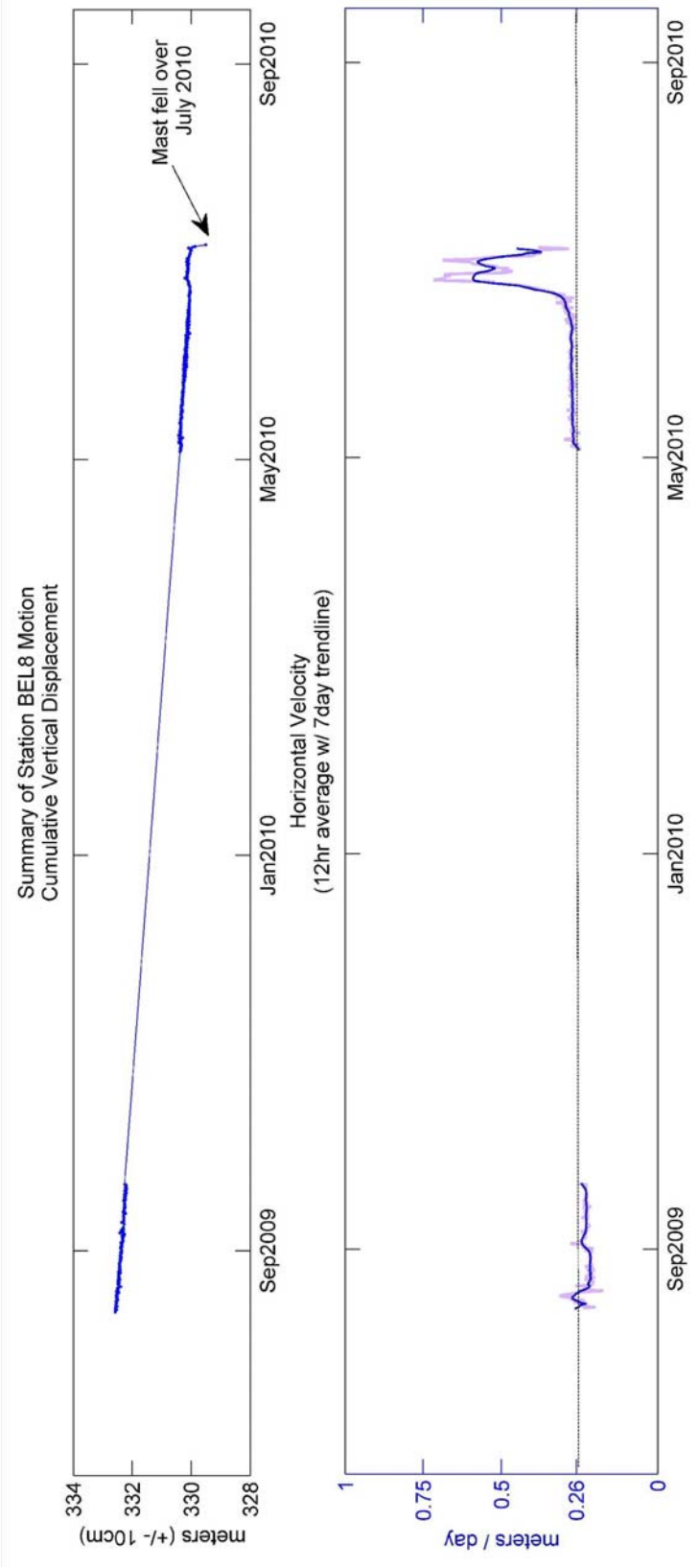

Figure A6: Plan-view of BEL8 station motion

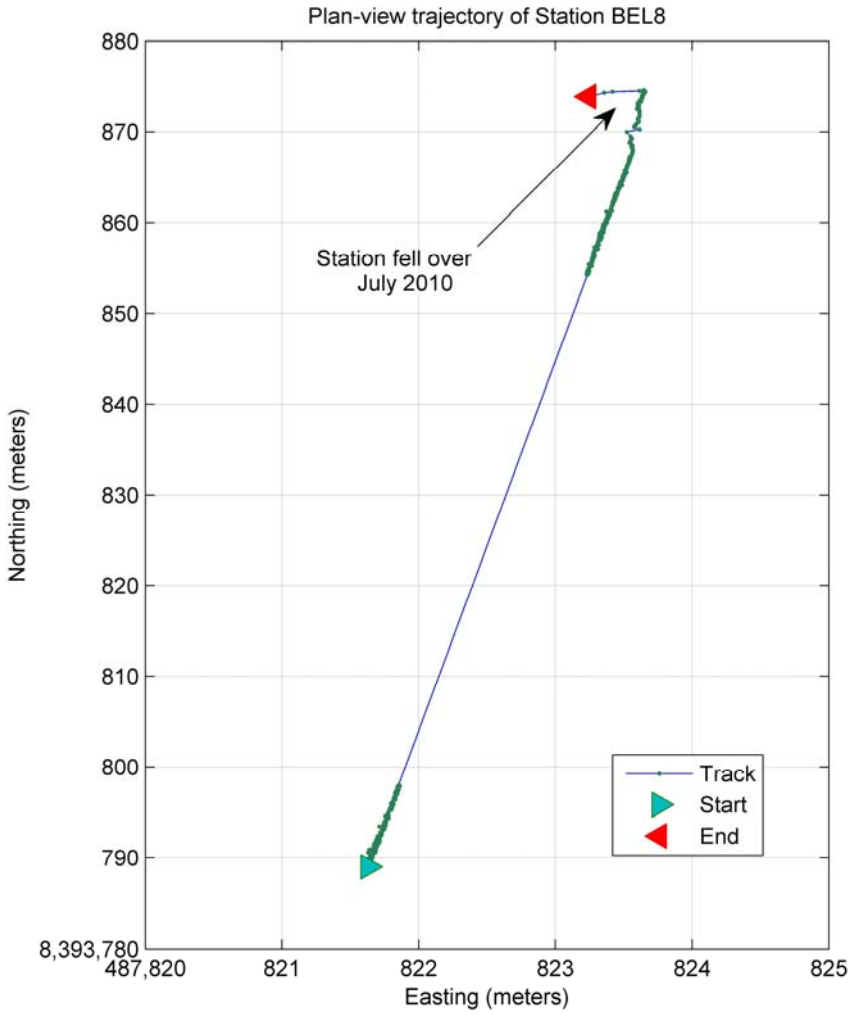

Figure A7: Time-series of Cumulative Vertical Displacement (*top*), and Horizontal Velocity (*bottom*). The dotted horizontal line represents the annual mean velocity recorded at BEL13.

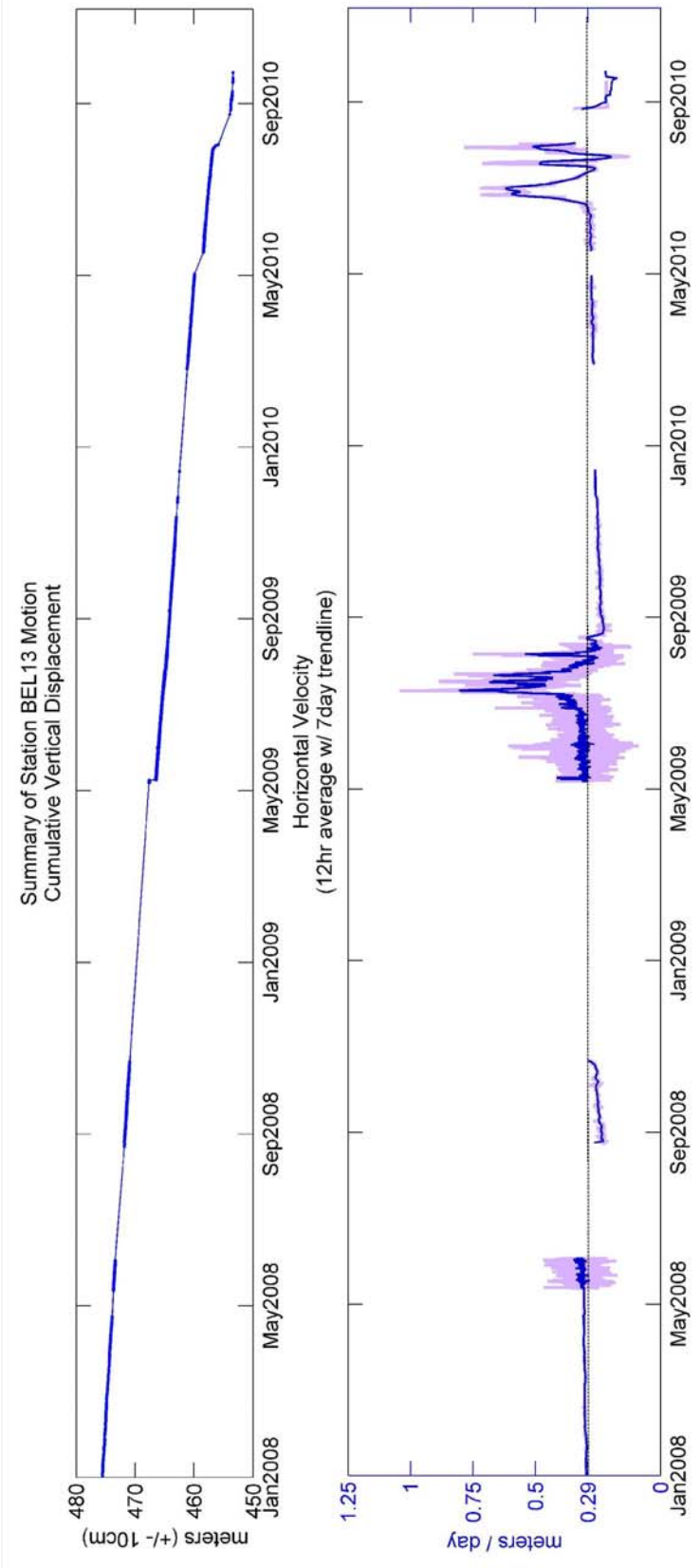

Figure A8: Plan-view of BEL13 station motion

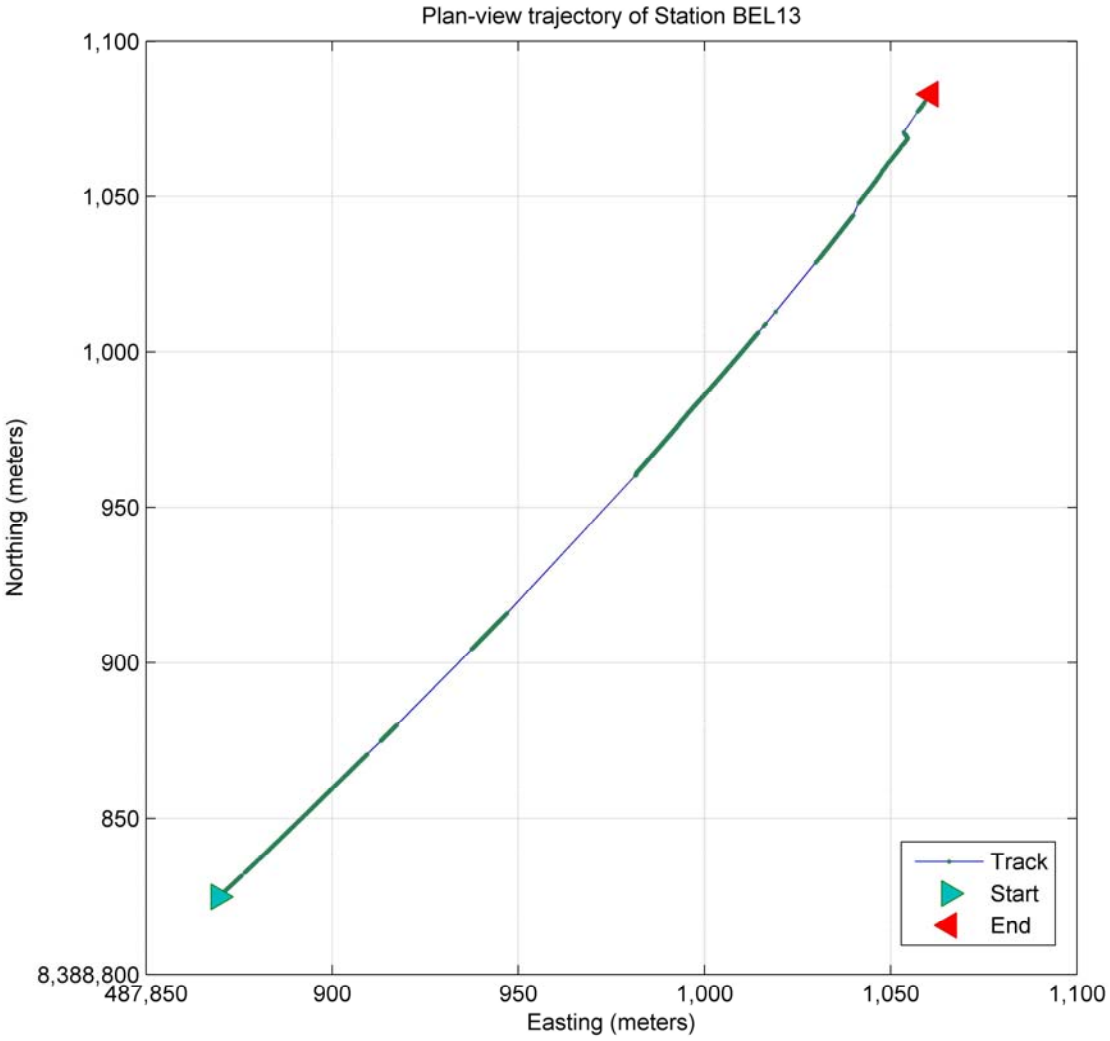

Figure A9: Time-series of Cumulative Vertical Displacement (*top*), and Horizontal Velocity (*bottom*). The dotted horizontal line represents the annual mean velocity recorded at BEL20.

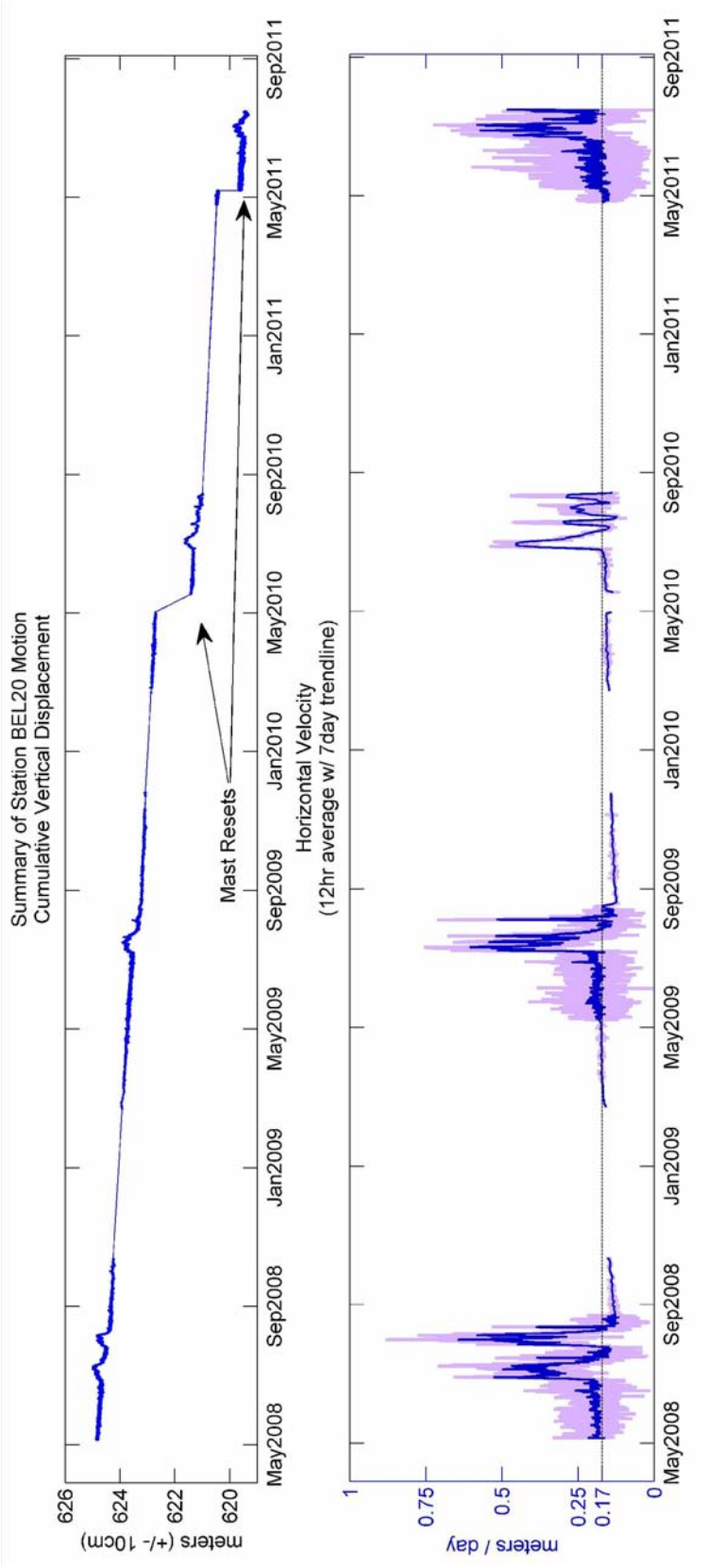

Figure A10: Plan-view of BEL20 station motion

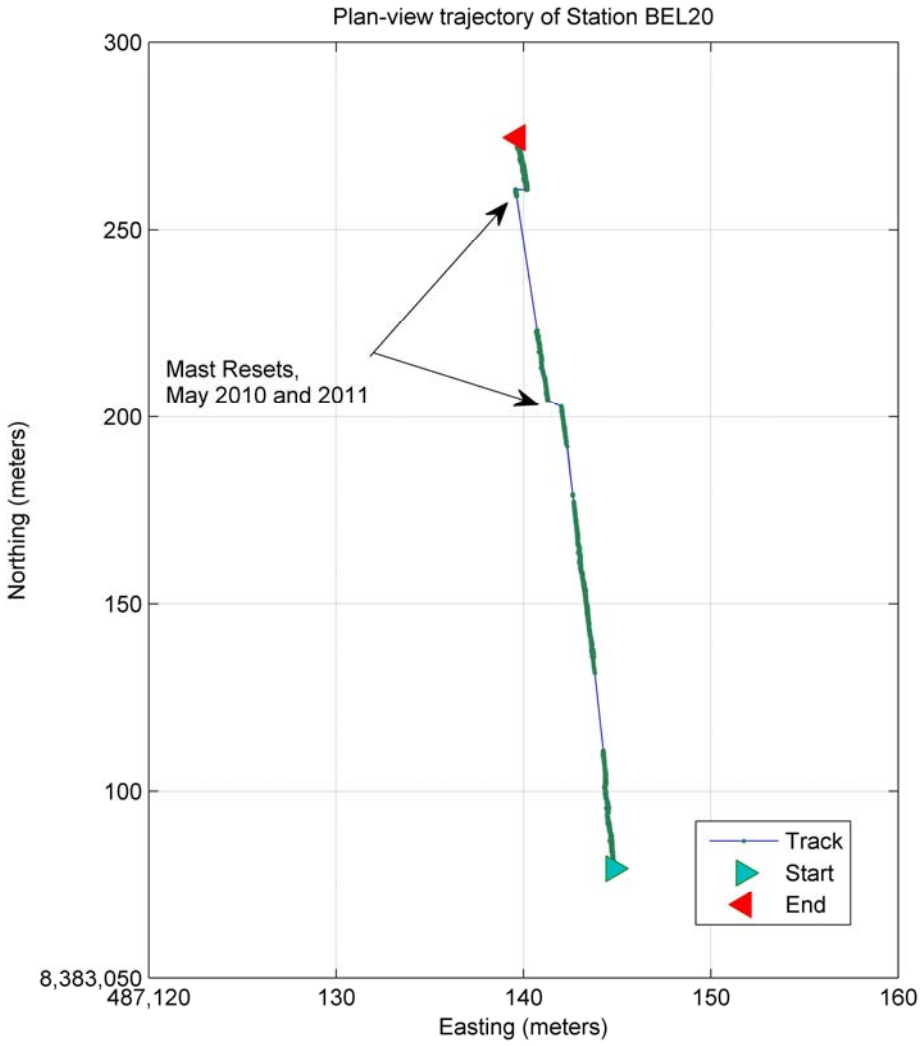

Figure A11: Time-series of Cumulative Vertical Displacement (*top*), and Horizontal Velocity (*bottom*). The dotted horizontal line represents the annual mean velocity recorded at BEL30.

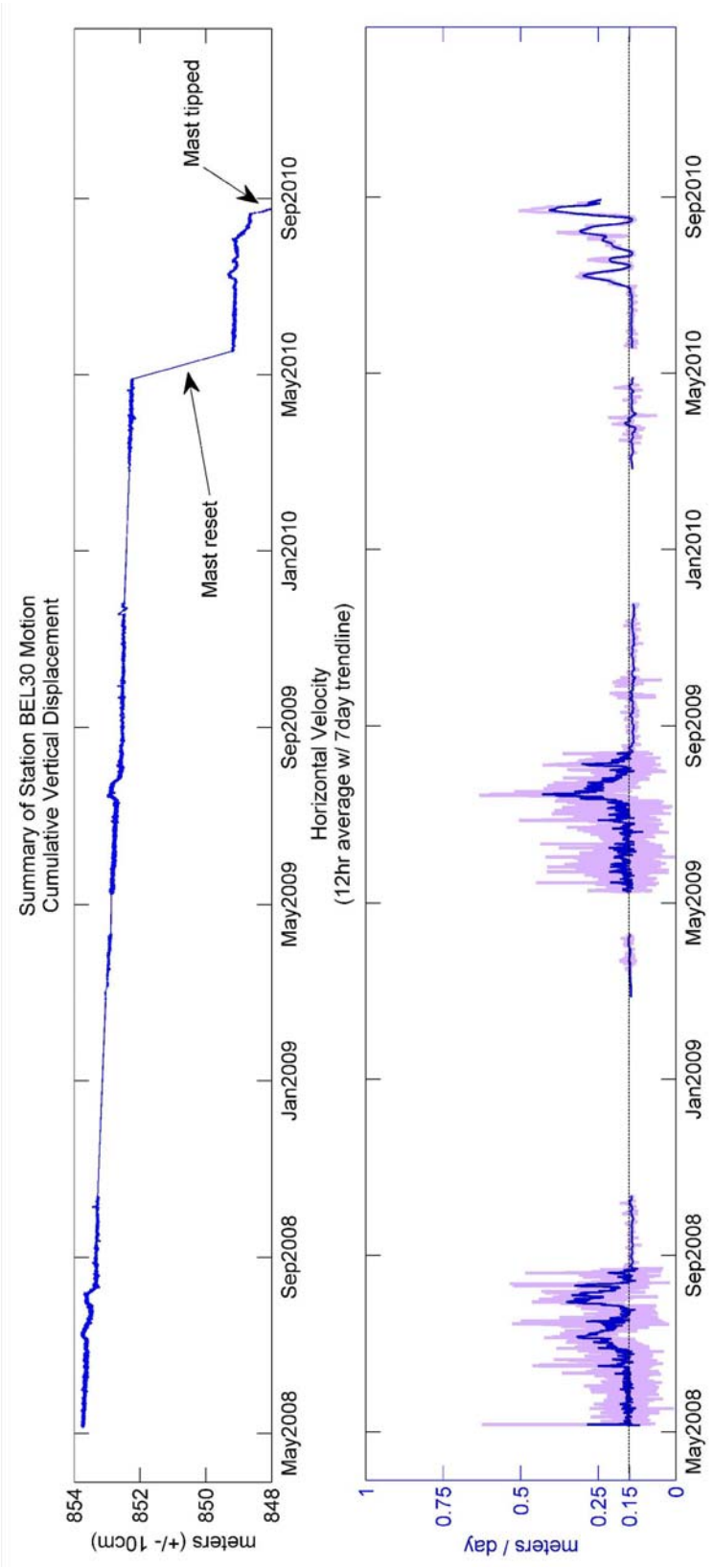

Figure A12: Plan-view of BEL30 station motion

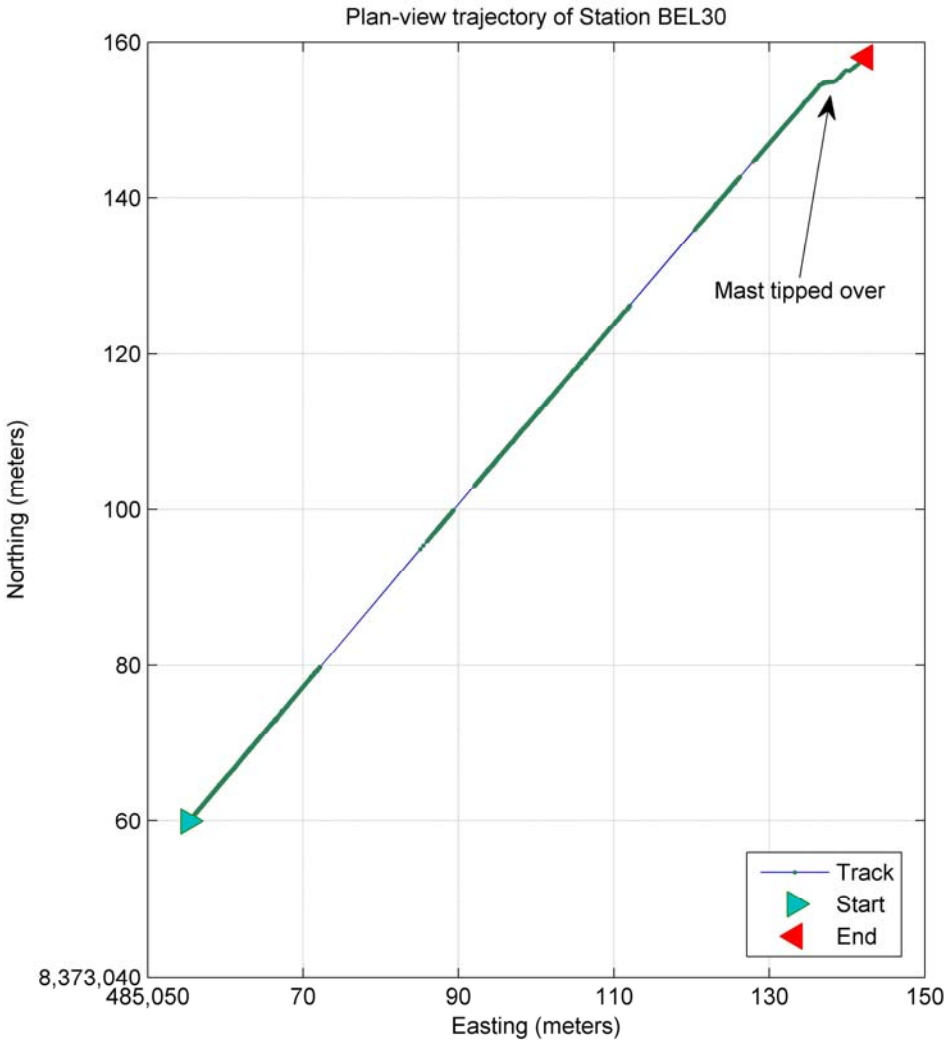

Figure A13: Time-series of Cumulative Vertical Displacement (*top*), and Horizontal Velocity (*bottom*). The dotted horizontal line represents the annual mean velocity recorded at BELt.

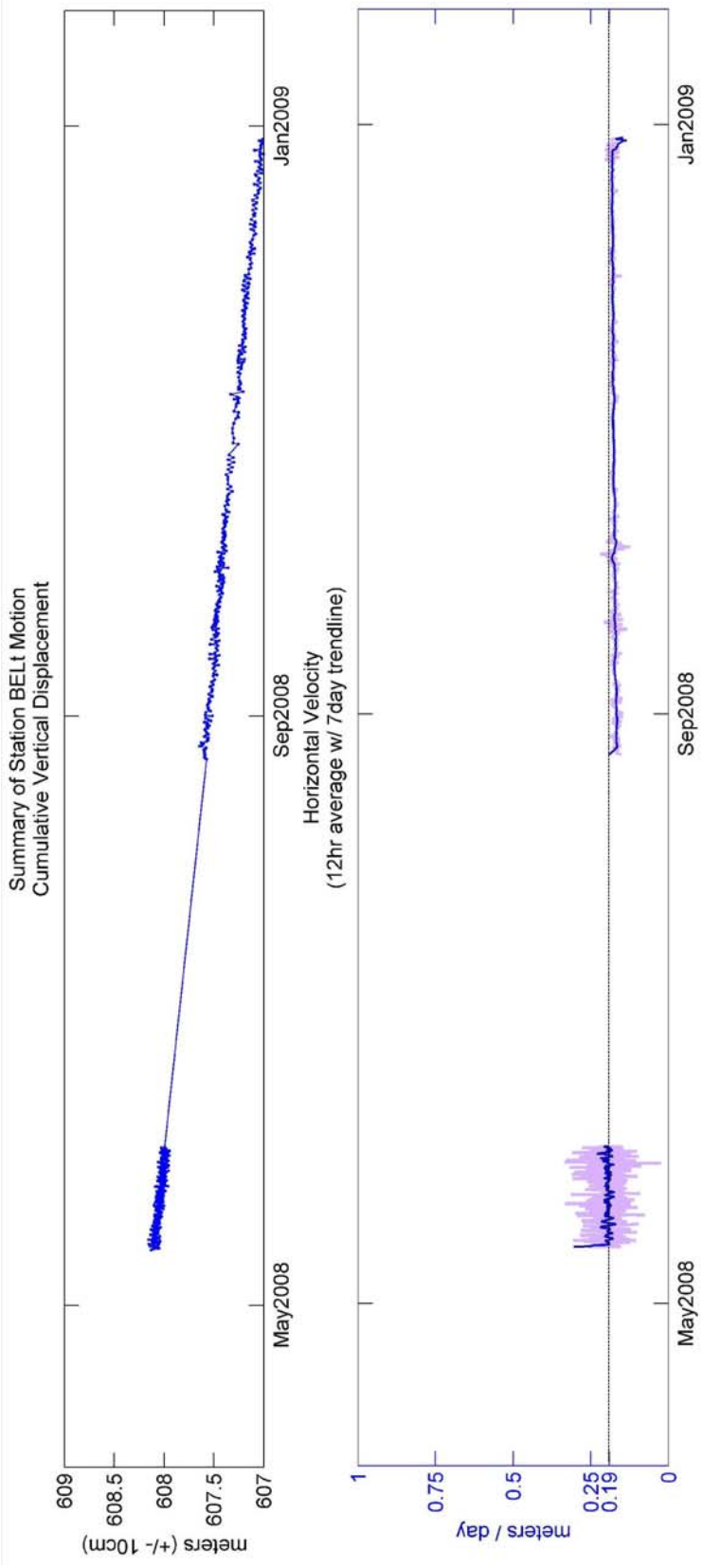

Figure A14: Plan-view of BELt station motion

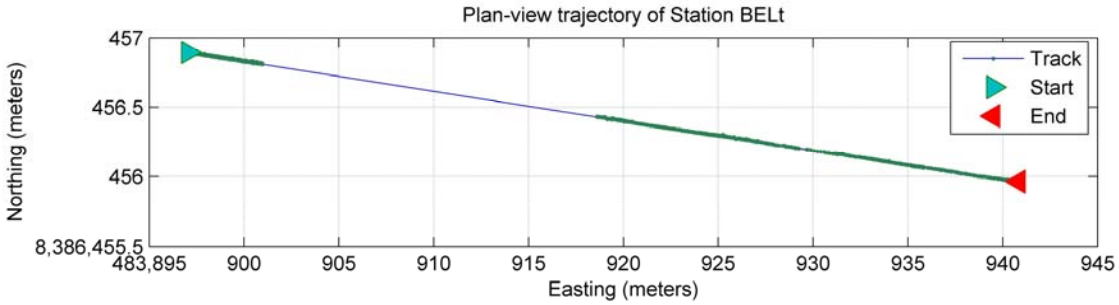

A.3. Sverdrup Glacier

Figure A15: Time-series of Cumulative Vertical Displacement (*top*), and Horizontal Velocity (*bottom*). The dotted horizontal line represents the annual mean velocity recorded at SVER.

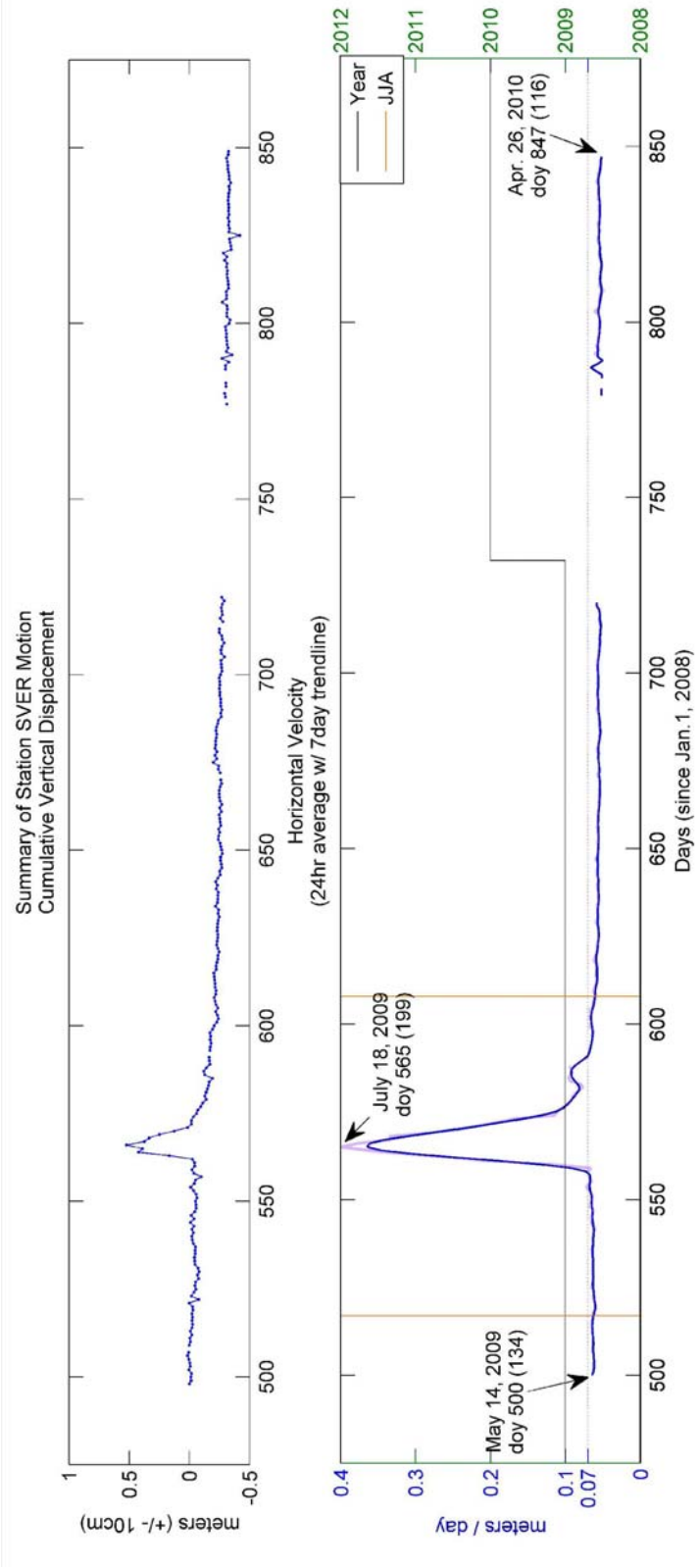

Figure A16: Plan-view of SVER station motion

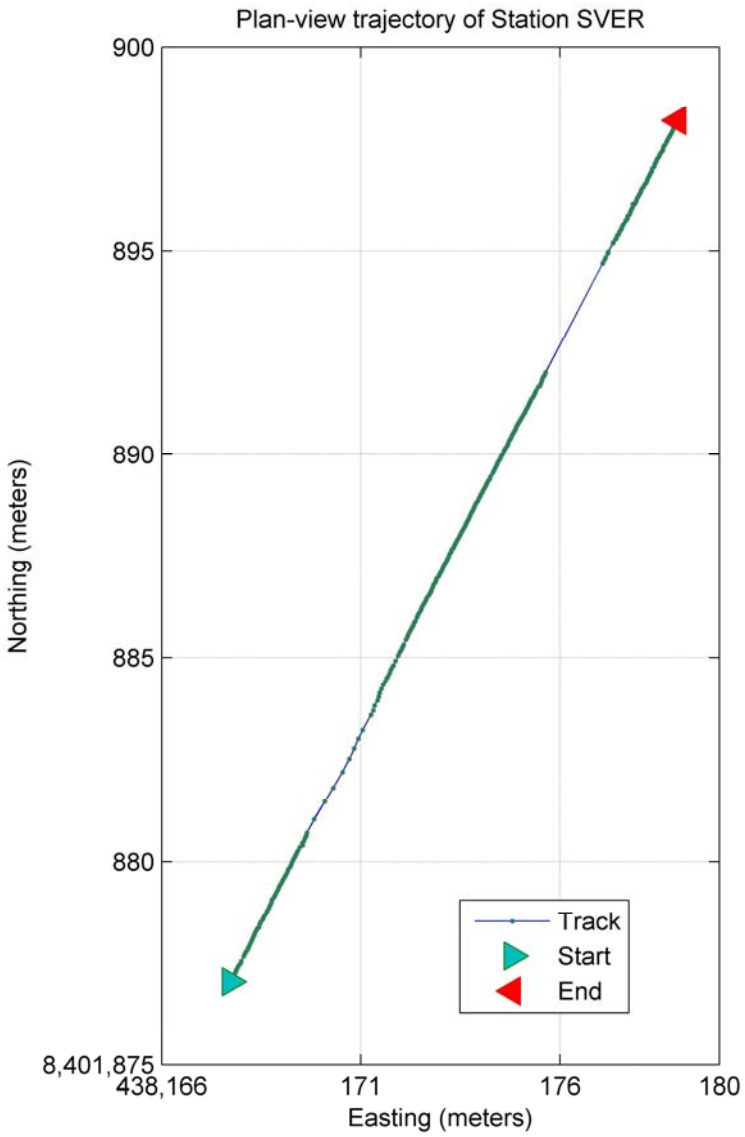

Figure A17: Time-series of Cumulative Vertical Displacement (*top*), and Horizontal Velocity (*bottom*). The dotted horizontal line represents the annual mean velocity recorded at DICS.

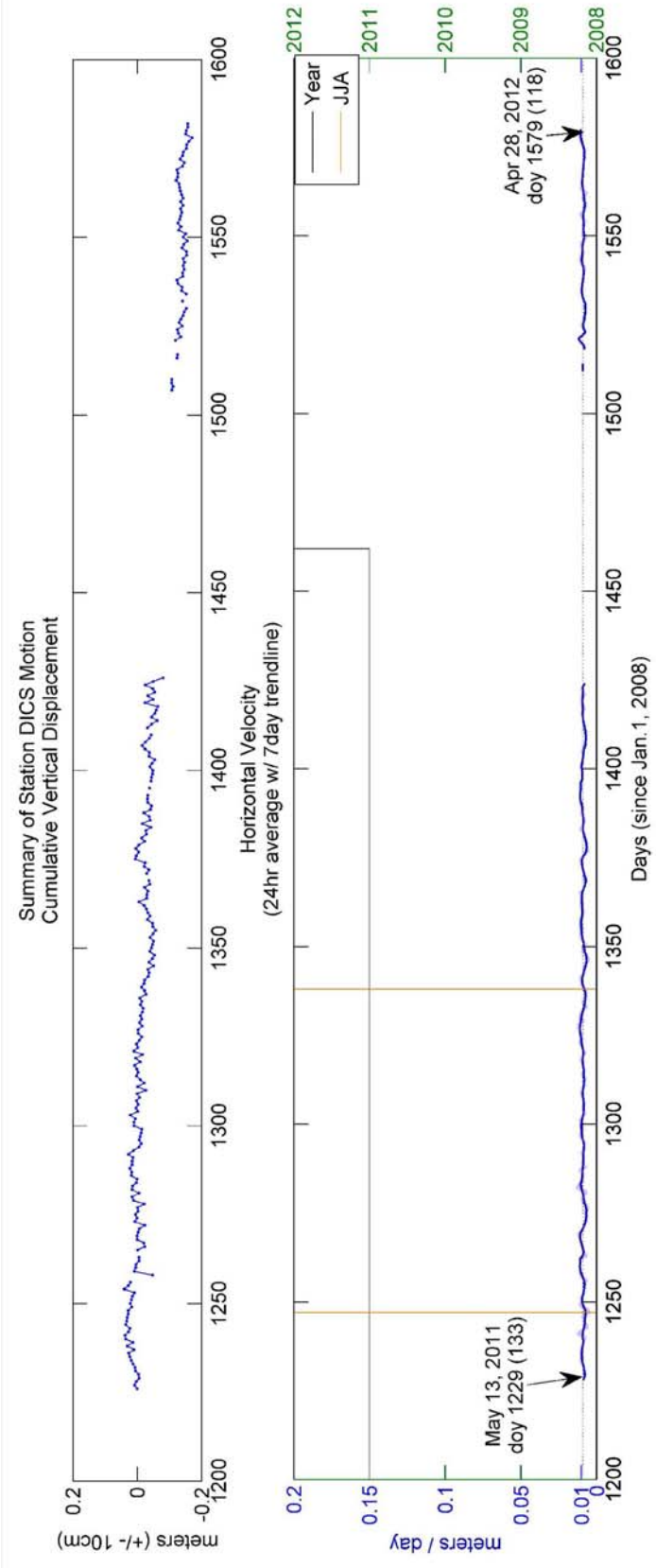

Figure A18: Plan-view of DICS station motion

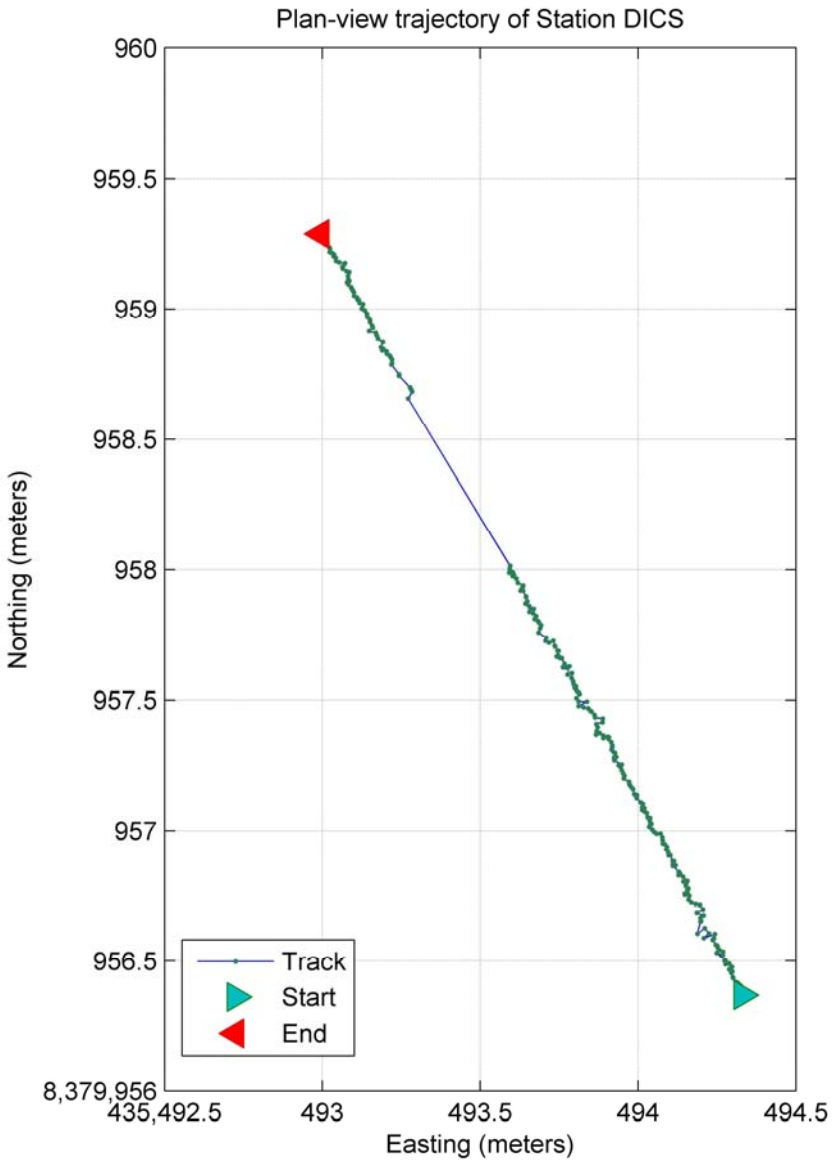

A.4. North Croker Glacier

Figure A19: Time-series of Cumulative Vertical Displacement (*top*), and Horizontal Velocity (*bottom*). The dotted horizontal line represents the annual mean velocity recorded at NCR1.

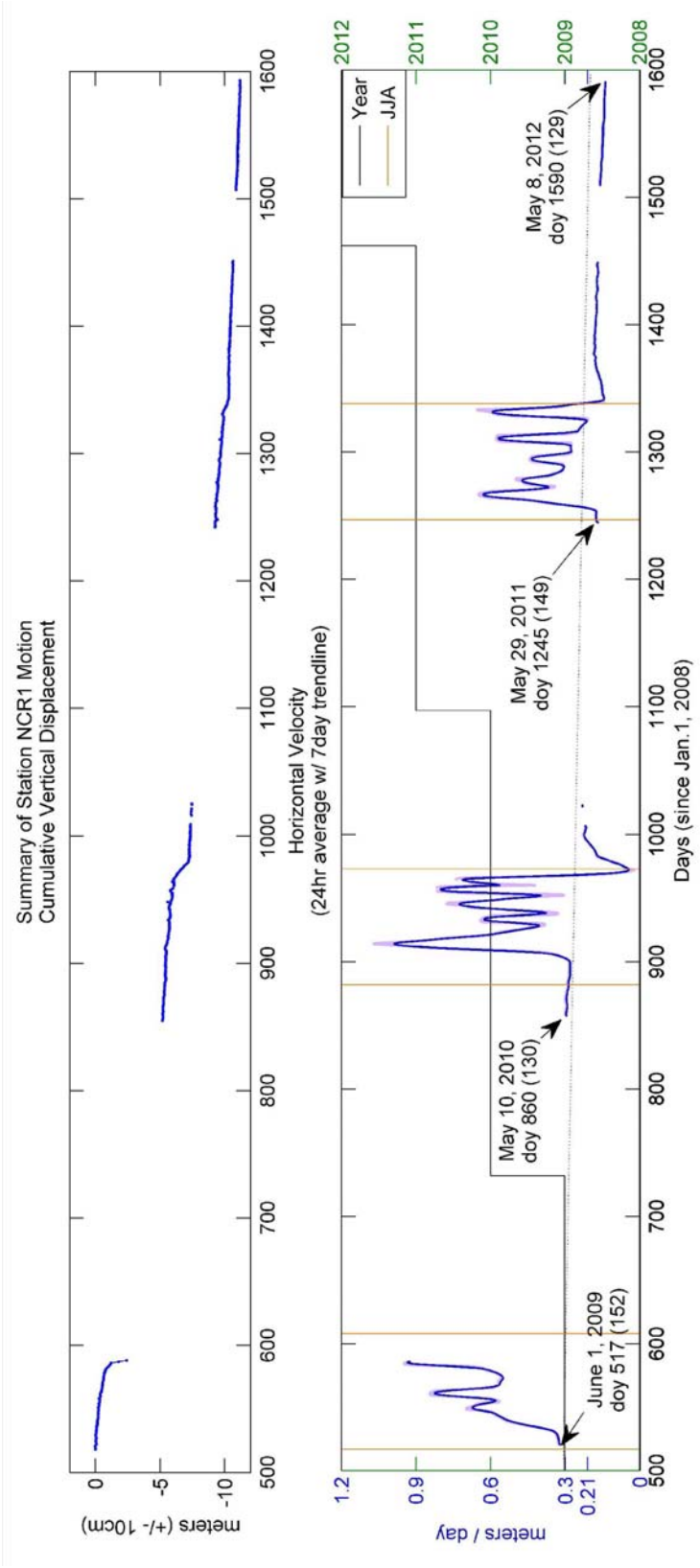

Figure A20: Plan-view of NCR1 station motion

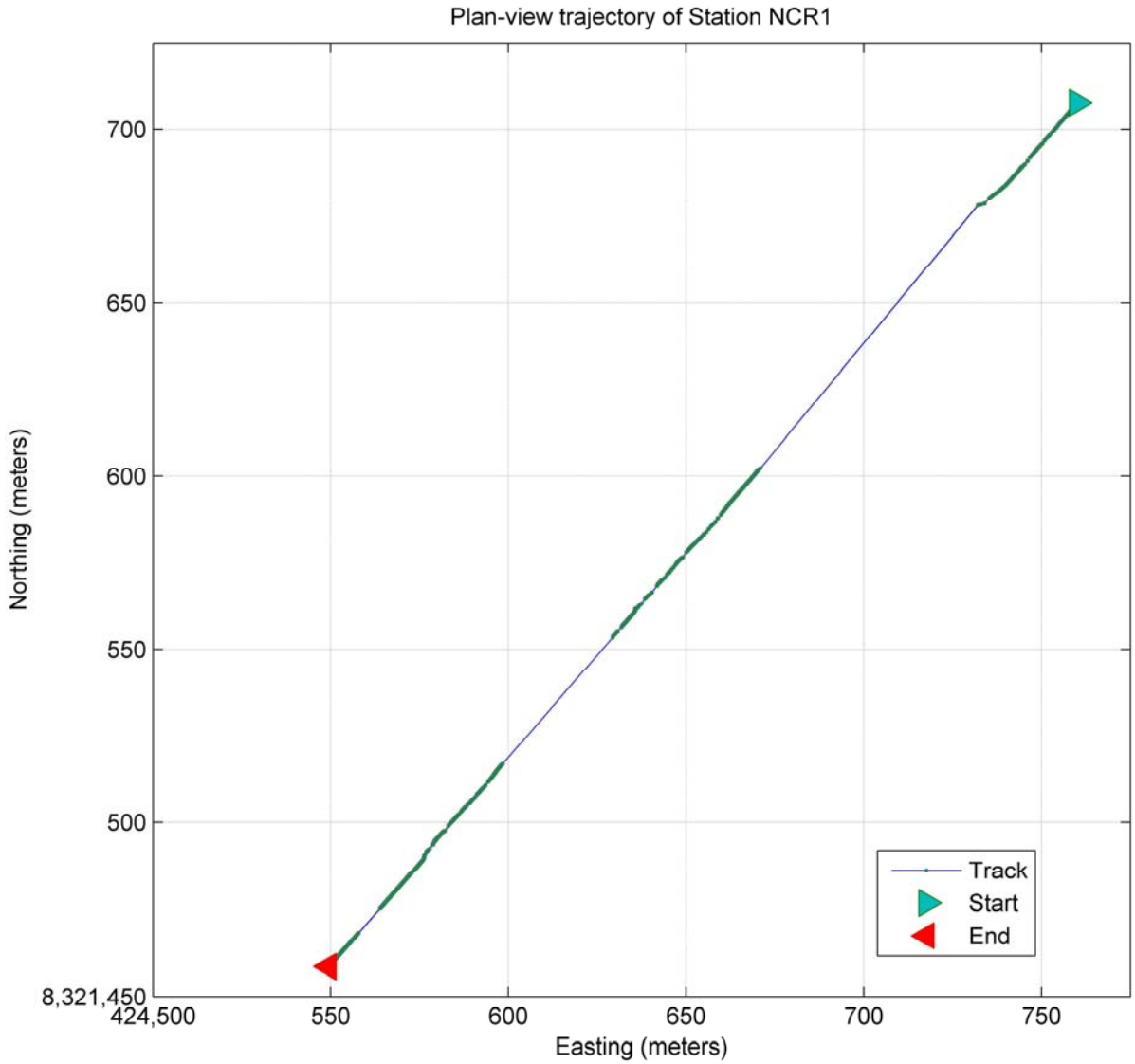

Figure A21: Time-series of Cumulative Vertical Displacement (*top*), and Horizontal Velocity (*bottom*). The dotted horizontal line represents the annual mean velocity recorded at NCR2.

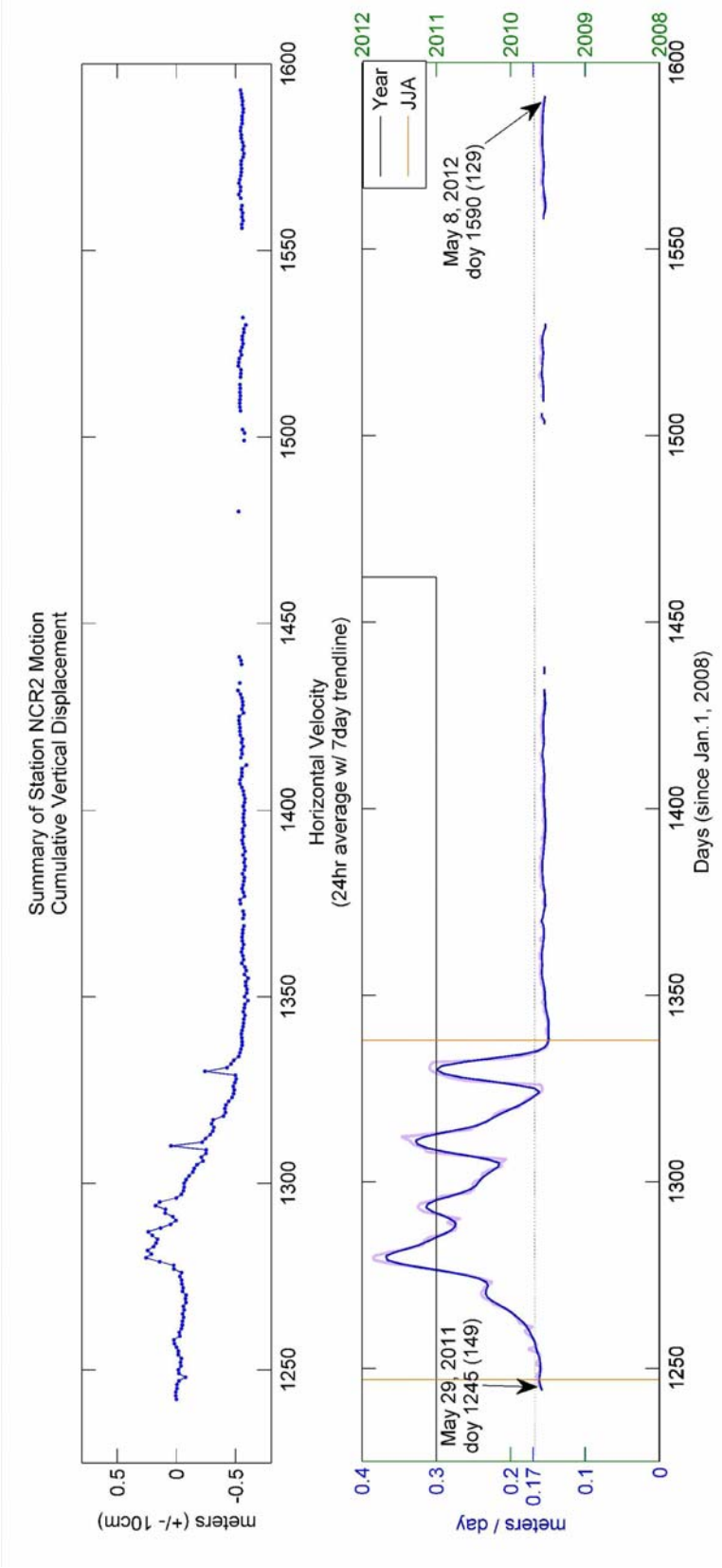

Figure A22: Plan-view of NCR2 station motion

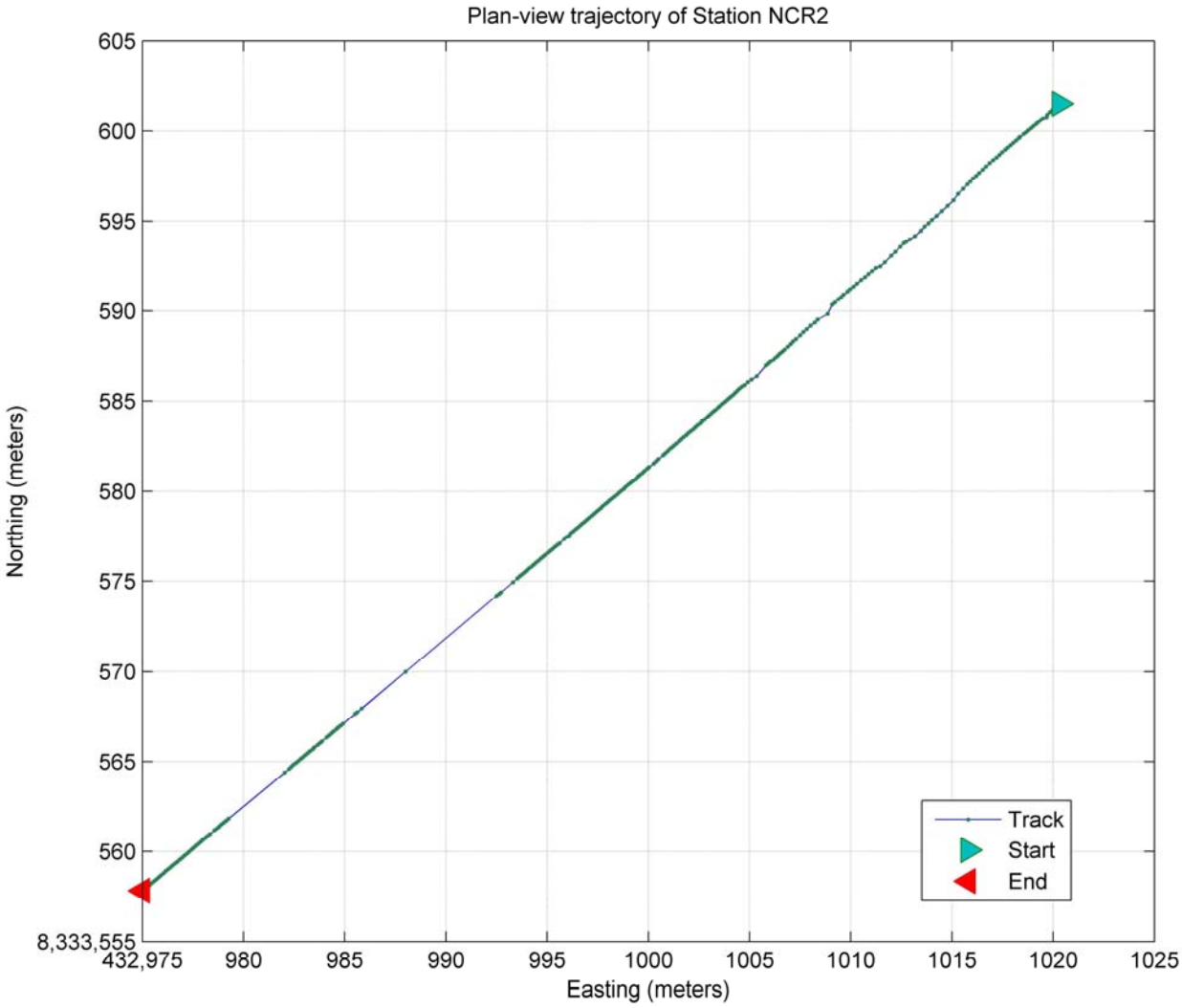

Figure A23: Time-series of Cumulative Vertical Displacement (*top*), and Horizontal Velocity (*bottom*). The dotted horizontal line represents the annual mean velocity recorded at MB29.

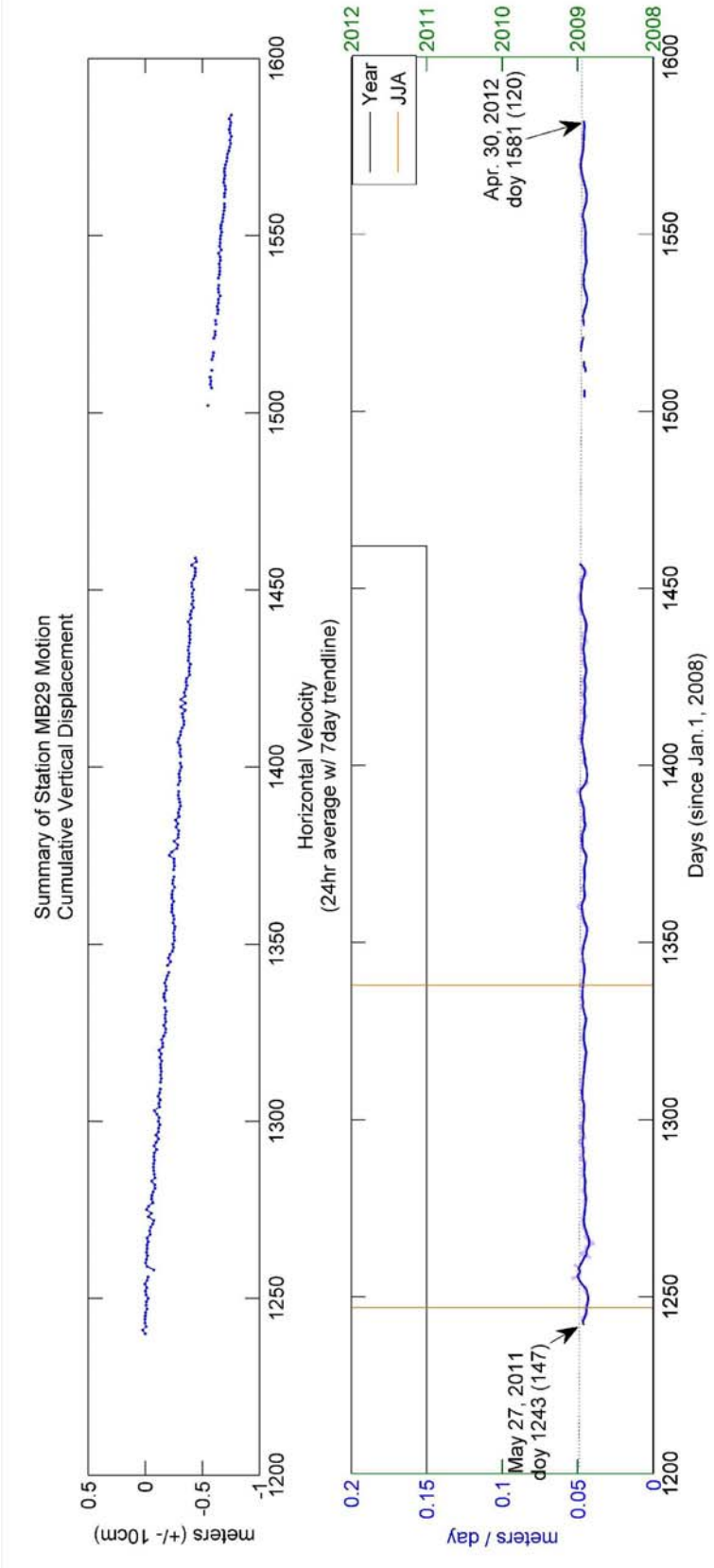

Figure A24: Plan-view of MB29 station motion

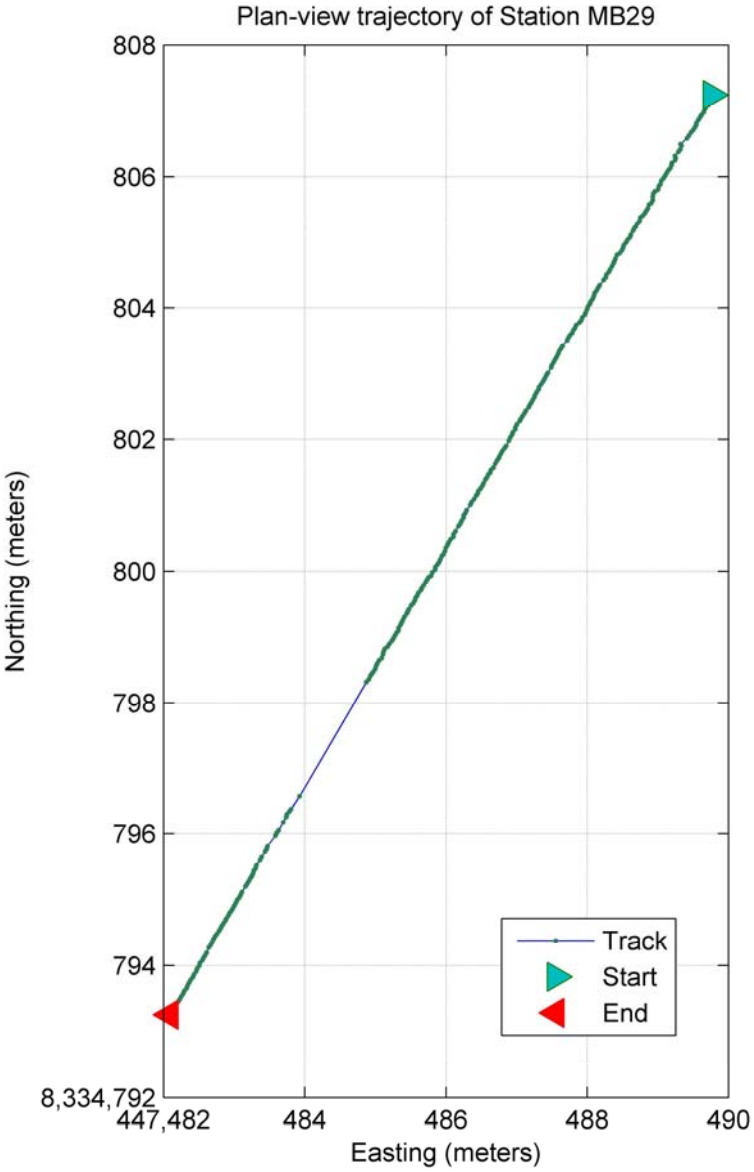

A.5. Southeast Glacier

Figure A25: Time-series of Cumulative Vertical Displacement (*top*), and Horizontal Velocity (*bottom*). The dotted horizontal line represents the annual mean velocity recorded at SEST.

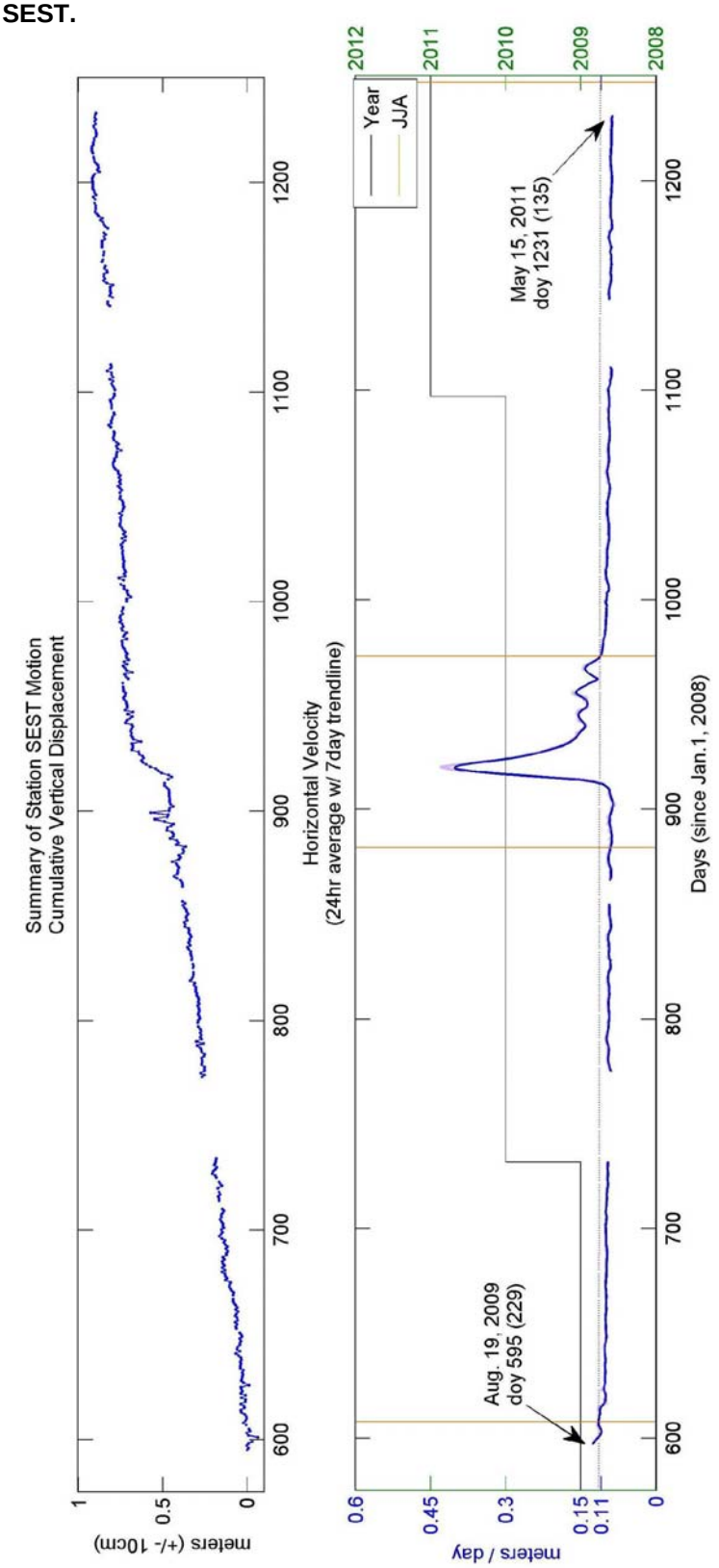

Figure A26: Plan-view of SEST station motion